LNGS/EXP-02/02
May 2002

INFN

Laboratori Nazionali del Gran Sasso

Annual Report 2001

The Gran Sasso National Laboratory

The Gran Sasso National Laboratory (LNGS) is one of four INFN national laboratories. It is the largest underground laboratory in the world for experiments in particle and nuclear astrophysics and it is used as a worldwide facility by scientists (presently 748 in number) from 22 countries.
Its location is between the towns of L'Aquila and Teramo, about 120 km from Rome. The underground facilities are located on a side of the ten kilometres long freeway tunnel crossing the Gran Sasso Mountain. They consist of three large experimental halls, each about 100 m long, 20 m wide and 15 m high and service tunnels for a total volume of about 180,000 cubic metres. The average 1400 m rock coverage gives a reduction factor of one million in the cosmic ray flux; moreover the neutron flux is thousand times less than on the surface, thanks to the smallness of the Uranium and Thorium content of the dolomite rocks of the mountain.
The extensive air shower experiment (EAS-TOP) at Campo Imperatore completed its data collecting runs in May 2000 and the facility has been decommissioned during the summer. The analysis of the data is still in progress.
The mission of the Laboratory is to host experiments that require a low background environment in the field of astroparticle physics and nuclear astrophysics.
The Laboratory hosts experiments in other disciplines too, mainly geology and biology that can profit of its characteristics and of its infrastructures.
Main research topics of the present program are: neutrino physics with neutrinos naturally produced in the Sun, in the Earth atmosphere, in a Supernova and neutrino oscillations with a beam from CERN (CNGS program), search for neutrino mass in neutrino less double beta decays, dark matter search, nuclear reactions of astrophysical interest, high energy cosmic rays and search for exotics (monopoles, wimps, etc.).
Solar neutrino physics is one of the main research sector of the laboratory. The GALLEX experiment, completed in 1997, has given fundamental results in particle physics and astrophysics, showing a relevant deficit in the solar neutrino flux at low energy. It is extremely difficult now, after the GALLEX results, to avoid the conclusion that neutrinos oscillate, and as a consequence have non-zero masses. If confirmed, this will be the first evidence of physics beyond the standard theory. GNO has improved the technique to continue the research for a long period, gradually improving the resolution. The data of the first two data collection periods have been published, reducing the systematic uncertainty to 5.4%.
The results of GALLEX and of the other solar neutrino experiments in the world (Homestake, Kamiokande and Superkamiokande, SAGE and SNO) indicate that the flux of electron-neutrino from the Be chain might be substantially different from the predictions

of the theory and, as a consequence, particularly sensitive to new physics. Borexino is dedicated mainly to the measure of the Be line component of the solar neutrino spectrum. In the year 2001 the construction of the main detector and of its ancillary facilities has been almost completed, the test facility CTF has been used for a series of tests. The beginning of the filling of the detector is now foreseen for the middle of the year 2002. The rigorous analysis of the safety issues has continued. A full HAZOP analysis has been accomplished both for the plants and for the procedures.
LENS is a proposal for a real time, flavour sensitive experiment sensitive down to the fusion neutrinos, aiming to a final clarification of the solar neutrino problem and to the measurement of the oscillation parameters. A series of R&D studies have been performed. Major breakthroughs allow now to design the experiment.
The solar models are based on data and extrapolations; in particular the thermonuclear cross sections of the involved reactions are not measured in the relevant energy range but rather extrapolated from higher energies.
The direct measurements are made very difficult by the very low values of the cross sections. A pilot experiment, using a 50 kV accelerator, LUNA, was designed primarily to study the reaction 3He(3He,2p)4He in the energy relevant for the reactions in the sun. The new 400 kV accelerator, installed in 2000 (LUNA2), has been tested finding excellent resolution and stability. During 2001, at the 50 kV facility the D(p,γ)^{3}He reaction has been investigated down to 2.5 keV, at the 400 keV facility the study of the reaction ^{14}N(p,γ)^{16}O has started.
Elementary particles are different from their antiparticles because their charges - not only the electric one, but all of them - are opposite. The standard model assumes that neutrinos have only one charge, the lepton number. But, if this charge is not conserved, neutrinos and antineutrinos can be two states of the same particle. In this case well-specified nuclides would decay through the neutrino-less double beta channel. The Laboratory hosts experiments searching for these very rare decays, employing different and complementary techniques.
The Heidelberg-Moscow experiment with a sensitive mass of 11 kg of enriched ^{76}Ge is the most sensitive experiment in the world. It took regularly data during 2001. Recently, Klapdor-Kleigrothaus and collaborators have claimed to have indeed observed the decay ^{76} Ge $\longrightarrow^{76}$ Se + 2 e^-. If confirmed this would be a revolutionary discovery, but caution is mandatory, due to the extremely difficult nature of the experiment. Criticism to the statistical analysis employed by the author to extract the signal has been also published.
The second most sensitive experiment on a different isotope in the world is MIBETA that employs an array of 20 thermal detectors, based on TeO_2 crystals (340 g natural tellurium each). During 2001 the set-up was dismounted and remounted after accurate polishing of the surfaces, obtaining a reduction of the background rate by a factor two. CUORICINO uses larger TeO_2 bolometers (750 g natural tellurium each). The R&D continued mainly to fix the final detector structure. When completed it will consist of 100 bolometers, a sensitive mass almost an order of magnitude larger than MIBETA. From astronomical observations, we know that about 80% of the matter in the Universe is non baryonic, meaning that is not made of nuclei and electrons as normal matter. It is called dark matter, because it does not emit light, and its nature is unknown. Probably, its constituents are not yet discovered elementary particles that interact only very weakly with the rest

(they are called WIMPs). They are around us, invisible, waiting to be discovered. The search for WIMPs is very difficult and requires a very low background environment and the development of advanced background reduction techniques. The search is going on in many experiments worldwide. At Gran Sasso three experiments, using different techniques, are active.

DAMA employs NaI crystals to detect the WIMPs by means of the flash of light produced in the detector by an Iodine nucleus recoiling after having been hit by a WIMP, a very rare phenomenon. To distinguish these events from the background, DAMA searches for an annual modulation of the rate, a behaviour that has several aspects that are peculiar of the searched effect and not of the main backgrounds. With its about 100 kg sensitive mass DAMA is the most sensitive experiment world wide. Data corresponding to a two-year continuous run (4-years overall) have been published in January 2000. They show evidence of the annual modulation signal, with all the expected characteristics. Data on further two and half years period have been collected by the end of year 2001. The run will come to an end by summer 2002, when the set up will be dismounted and a new one (LIBRA) with 250 kg sensitive mass assembled.

CRESST searches for WIMPs with a cryogenic technique, looking for a, very tiny, temperature increase in the detector, due to the energy deposited by nuclei hit by the WIMPs. To this aim the detector is kept at a very low temperature, 15 mK. Measurements foreseen for the phase 1 were finished in March 2001, meeting the milestones of this phase. The second phase of the experiment was then approved to run till 2005. The experiment was requested by the management to move from hall B to hall A to free the space for one of the experiments on the CNGS. The move was completed by the end of 2001 as scheduled.

The Heidelberg Dark Matter Search (HDMS) uses a special configuration of Ge detectors to search for WIMPs, namely a crystal were the WIMP interaction takes place, fully surrounded by a second crystal that acts as an active screen from the background. After one year of running, the inner detector has been replaced with an enriched ^{73}Ge crystal, starting data taking with reduced background in August 2000.

The GENIUS project proposes the use of one ton enriched Germanium with a strong reduction of the background for dark matter searches, double beta decay and other searches. As a first step, the small test facility GENIUS-TF with 40 kg of natural Germanium operated in liquid Nitrogen is under installation.

MACRO was a very large multi-purpose experiment, which continuously collected data for several years. The experiment completed its extremely successful life in December 2000. The final analysis has been performed producing results on atmospheric neutrino oscillations, high-energy neutrino astronomy, searches for WIMPs, search for low energy stellar gravitational collapse neutrinos, stringent upper limits on magnetic monopoles flux and primary cosmic rays composition.

LVD has completed the construction of the apparatus with a sensitive mass of 1000 t and improved its efficiency with an up time in 2001 of 99.7%. The experiment would collect a few hundred events from a supernova explosion in the centre of the Galaxy.

One of the major commitments of the Gran Sasso laboratory in the next decennium will be the search of tau neutrino appearance and related topics on an artificial neutrino beam being built at CERN in Geneva, the CERN Neutrinos to Gran Sasso (CNGS) project. The beam will be directed through the Earth crust to two detector located in Gran Sasso

at 732 km distance. Beam and experiments are foreseen to be ready in 2005.
ICARUS is a general-purpose detector, with a broad physics programme, not limited to the CNGS project. It was proposed in 1985 based on the novel concept of the liquid Argon time-projection chamber. A first important step was the construction of a 3 t prototype that was used for the necessary R&D program, completed in 1993. The following years have been spent to develop the techniques suitable for industrial production of large-scale detectors. A first 600 t module, proposed in 1995 and approved and funded in 1996, has been successfully operated in Pavia in the summer 2001. The proposal of a larger detector system composed of a number of similar modules has been submitted.
Tau neutrinos resulting from oscillations of the muon neutrino of the beam will be searched by OPERA looking for the tau leptons they produce. This search requires both micrometer scale resolution, obtained with modern emulsion techniques and large sensitive mass (2000 t) obtained with Pb sheets interleaved by emulsion layers. During 2001 the OPERA proposal, approved by the INFN and by CERN, was defined in it must important aspects.
GIGS is a laser interferometer for geophysical purposes operating since 1994. The main results obtained so far are: 1) the recording of co-seismic steps during local earthquakes in 1994, 2) the recording of swarms of slow earthquakes, more than 180 in total, after 1997. A new scale law between the seismic moment and the rise time of the slow quakes has been established. A very interesting statistical, not causal, correlation between slow and normal quake sequences has been observed. During 1999 the group further analysed the 1997 data; till October 1999 the spectrometer worked in an equal arm configuration. In 1999 a new interferometer was built and from October 1999 two independent interferometers are at work.
The PULEX-2 is a biology experiment exploits the unique low radiation characteristics of the Laboratory. Mammalian cells were cultured in parallel at LNGS underground laboratory, were a cell culture facility has been set up on purpose, and at the ISS in Rome, in the presence of standard background.
During 2001 the Gran Sasso laboratory became one of the large European infrastructures as a "Low background facility for Particle Physics, Astrophysics, Nuclear Physics and Biology" (HPRI - CT- 2001-00149) in the action "Access to Research Infrastructures". This EU activity aims to maximise the impact of research infrastructures, facilities that provide essential services to Europe's research community in industry and academia.
All the services and the personnel of the lab have been engaged in the planning within sight of the next phases of activity ranging from the decommissioning of some large experiments, to the preparation of the infrastructures needed for the next experiments and to the rigorous definition of the safety rules, procedures and infrastructures.
Another European contract (HPRP-CT-2001-00018), prepared and run in collaboration with the large European particle laboratories, CERN and DESY, aims to evaluate the effectiveness of their outreach actions.
The geographical location (inside the National Park of Gran Sasso - Monti della Laga) and the special operating conditions (underground, near a highway tunnel and in close proximity to water basins) demand that special attention is paid to the safety and environmental aspects of their activities.
We have introduced also an Environmental Management System (EMS) complying with the UNI - EN - ISO 14001 standard, in order to make the organisation more modern and

efficient, to assure the conformity to current laws, and to achieve a continuous improvement of the environment performance.
The system is verified by an independent auditing authority, which constantly checks the conformity to the standard, in order to assure the management, and all the various involved parties (local authorities, citizens, members of the staff, collaborators and research institutes) of the adequacy of the Environmental Policy, the operating conditions, procedures, and checks.

Gran Sasso, April 2002.

The Director of the Laboratory
Prof. Alessandro Bettini

Contents

BOREXINO. Solar Neutrino Physics

H. Back[n], M. Balata[b], A. de Bari[e], T. Beau[o], A. de Bellefon[o], G. Bellini[a], J. Benziger[c], S. Bonetti[a], A. Brigatti[a], C. Buck[j], B. Caccianiga[a], L. Cadonati[d], F.P. Calaprice[d], G. Cecchet,[e], M. Chen,[r], O. Dadoun[o], D. Dangelo[h], A. Derbin[m], M. Deutsch[f], A. Di Credico[b], G. Di Pietro[a], F. Elisei[g], A. Etenko[s], F. von Feilitzsch[h], R. Fernholz[d], R. Ford[b], D. Franco[a], B. Freudiger[j], C. Galbiati[d], F. Gatti[i], S. Gazzana[b], V. Gehman[n], M.G. Giammarchi[a], D. Giugni[a], A. Goretti[b], C. Grieb[h], E. de Haas[d], C. Hagner[n], W. Hampel[j], J. Handt[j], B. Harding[d], F.X. Hartmann[j], R. von Hentig[h], G. Heusser[j], M. Hissmann[j], M. Hult[p], A. Ianni,[b], A.M. Ianni[d], H. de Kerret[o], S. Kidner[d], J. Kiko[j], T. Kirsten[j], G. Korga[a], Y. Kozlov[s], G. Korschinek[h], D. Kryn[o], V. Lagomarsino[i], M. Laubenstein[b], C. Lendvai[h], E. Litvinovich[s], F. Loeser[d], P. Lombardi[a], I. Machulin[s], S. Malvezzi[a], I. Manno[k], J. Maneira[r], D. Manuzio[i], G. Manuzio[i], A. Martemianov[b], F. Masetti[g], U. Mazzucato[g], K. McCarty[d], E. Meroni[a], L. Miramonti[a], B. Moffat,[r], M.E. Monzani[a], P. Musico[i], H. Neder[j], M. Neff[h], L. Niedermeier[h], S. Nisi[b], L. Oberauer[h], M. Obolensky[o], M. Orsini[b], F. Ortica[g], M. Pallavicini[i], L. Papp[a], S. Parmeggiano[a], R. Parsells[d], L. Perasso[a], A. Perotti[e], A. Pocar[d], R.S. Raghavan[l], G. Ranucci[a], W. Rau[j], A. Razeto[i], E. Resconi[i], A. Sabelnikov[a], P. Saggese[a], C. Salvo,[i], S. Schönert[j], H. Seidl[h], T. Shutt[d], M. Skorokhvatov[s], H. Simgen[j], O. Smirnov[m], A. Sonnenschein[d], A. Sotnikov[m], S. Sukhotin[s], V. Tarasenkov[s], R. Tartaglia,[b], G. Testera[i], D. Vignaud[o], B. Vogelaar[n], V. Vyrodov[s], A. Wingler[h], W. Wojcik[q], Y. Zakharov[j], O. Zaimidoroga[m], G. Zuzel[q]

[a]Dip. di Fisica dell'Università and Infn Milano - Italy
[b]Laboratori Nazionali del Gras Sasso, Assergi (Aq) - Italy
[c]Dep.t of Chemical Engineering, Princeton University - NJ USA
[d]Dep.t of Physics, Princeton University - NJ USA
[e]Dip. di Fisica dell'Università and Infn Pavia - Italy
[f]Dep.t of Physics, Massachusetts Institute of Technology - MA USA
[g]Dip. di Chimica dell'Università and Infn Perugia - Italy
[h]Technische Universität München - Germany
[i]Dip. di Fisica dell'Università and Infn Genova - Italy
[j]Max Planck Inst. für Kernphysik, Heidelberg - Germany
[k]KFKI-RMKI Research Institute for Particle & Nuclear Physics, Budapest - Hungary
[l]Bell Laboratories, Lucent Technologies, Murray Hill - NJ USA
[m]J.I.N.R. Dubna - Russia
[n]Dep.t of Physics, Virginia Polytechnic Institute - VA USA
[o]Laboratoire de Physique Corpusculaire et Cosmologie, Paris - France
[p]I.R.M.M. - EURATOM, Geel - Belgium
[q]Institute of Physics, Jagellonian University, Kracov - Poland
[r]Dept. of Physics, Queen's University, Ontario - Canada
[s]RRC Kurchatov Institute, Moscow - Russia

Abstract

The Borexino construction is getting at its final stage . This report summarizes the present status of the installation of the detector in the LNGS and the main operations achieved during 2001; the expected potential of Borexino in the present scenario of the neutrino oscillations physics is briefly reminded .

1 The experiment: goals and achievements

Borexino is the first experiment planned to measure in real time the reactions induced by the low energy (hundreds of KeV) solar neutrinos. The main experimental goal is the study of the 0.862 MeV ^{7}Be solar neutrino line through the detection of the ν-e scattering. The measurement of the event rate induced by neutrinos originated by this source is still now a key point both from the point of view of the standard solar model confirmation (the apparent lack of the flux of ^{7}Be ν was a tricky problem originated by the comparison of different experimental results) and in the experimental proof of the neutrino flavor oscillations hypothesis (the possible region of the characteristic parameters, suggested by the present experiments, has to be definitively fixed).

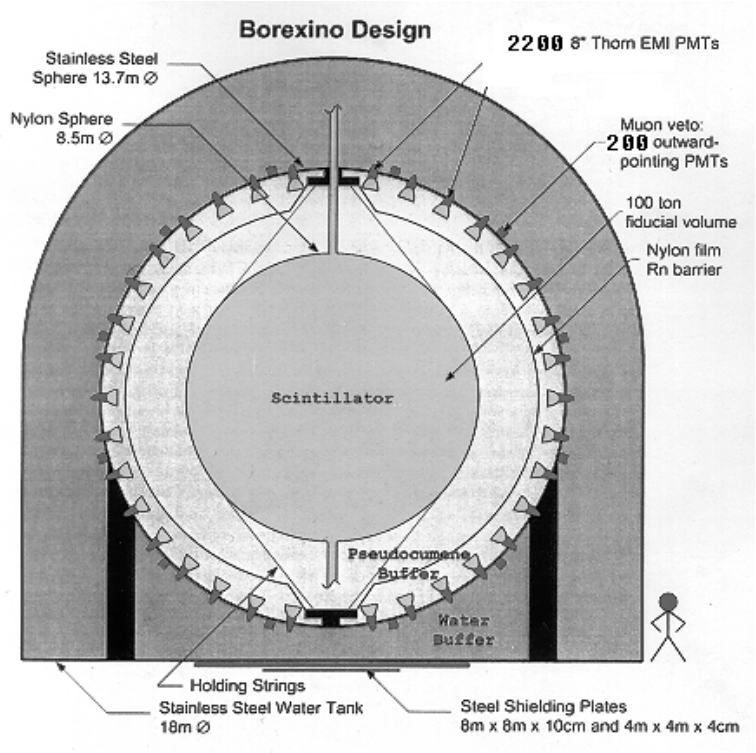

Figure 1: Schematic view of the Borexino detector.

In the detectable ^{7}Be ν elastic scattering, the maximum energy of the recoiling electron is 664 KeV and a reasonable experimental threshold is assumed at 250 KeV, (corresponding to a ν energy of about 400 KeV). This low energy region, envisaged by the experiment,

is completely overlapping with that one of the natural radioactivity products of disintegration, which are present in any environment and in any material: this is the main problem that the Borexino project had to face.

As a consequence an intense R&D program has been carried out in the last ten years to develop methods for selecting very low radioactivity materials or to purify them. An effort in this field has matched an equally hard research in the field of the detection systems and measurements of ultralow radioactivity levels.

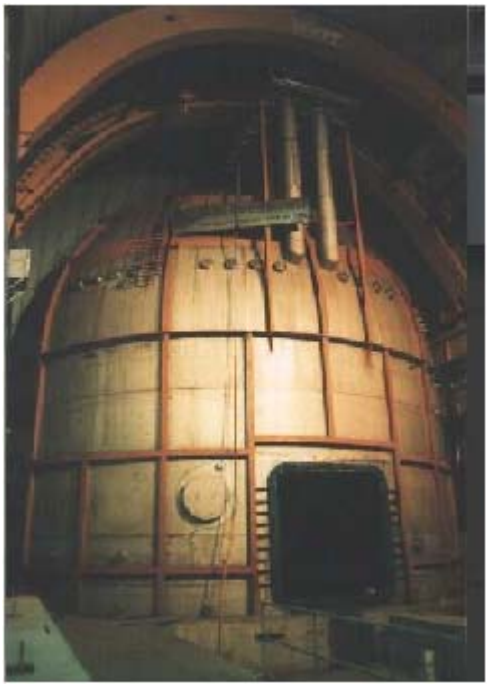

Figure 2: The Water Tank

Deep developments have been attained in the purification methods of liquid aromatic compounds, as distillation, water extraction, stripping with ultrapure N_2, solid gel column (Si gel, Al gel). Moreover, the Borexino Collaboration developed new detectors and new methods for the measurements of ultra-low radioactivity, in addition to use the more classic systems. In particular, a detector at ton level, the Counting Test Facility (CTF), has been constructed on purpose and installed in the underground Laboratory at Gran Sasso. In all these fields many records have been achieved, and the results obtained satisfied the mandatory step previously fixed in order to assure the feasibility of Borexino. Many of the radiopurity goals had been obtained using plants constructed and installed for the CTF, and consequently adopted in the Borexino auxiliary plants; some other results have been achieved in the Borexino plants, already installed and tested.

The CTF was in addition an important bench mark for testing and studying various solutions for the Borexino detector [1] [2] [3] [4]. It is now running again after an upgrading campaign.

2 The Detector

Borexino (fig. 1) is an unsegmented liquid detector featuring 300 tons of well shielded ultrapure scintillator viewed by 2200 photomultipliers . The detector core is a transparent spherical vessel (Nylon inner vessel, 100μm thick), 8.5 m of diameter, filled with 300 tons of liquid scintillator and surrounded by 1000 tons of high-purity buffer liquid. The scintillator mixture is PC and PPO (1.5 g/l) as a fluor, the buffer liquid is pure PC (with the addition of the light quencher DMP). The photomultipliers are supported by the stainless steel sphere (SSS), which also separates the inner part of the detector from the external shielding, provided by 2400 tons of pure water (water buffer). An additional containment vessel (Nylon film radon barrier) is interposed between the scintillator Nylon sphere and the photomultipliers, with the goal of reducing radon diffusion towards the internal part of the detector.

Figure 3: The stailess steel sphere as seen from the water tank

The outer water shield, contained in the Water Tank (WT) is instrumented with 200 outward-pointing photomultipliers serving as a veto for penetrating muons, the only significant remaining cosmic ray background at the Gran Sasso depth (about 3800 meters of water equivalent). Inside the stainless steel sphere , 1800 photomultipliers are equipped with light concentrators so that they can see light coming only from the Nylon Sphere region, while the remaining 400 PMT's are sensitive to light originated in the whole volume of the SSS. This design greatly increases the capability of the system to identify muons crossing the PC buffer but not the scintillator. The Borexino design is based on the concept of a graded shield of progressively lower intrinsic radioactivity as one

approaches the sensitive volume of the detector; this culminates in the use of 200 tons of the low background scintillator to shield the 100 tons innermost Fiducial Volume. In these conditions, the ultimate background will be dominated by the intrinsic contamination of the scintillator, while all backgrounds from the construction materials and external shieldings are almost negligible compared to the signal. Borexino also features several external systems and plants conceived to purify water, nitrogen and scintillator, and clean rooms to keep clean conditions during the installation of the detector .

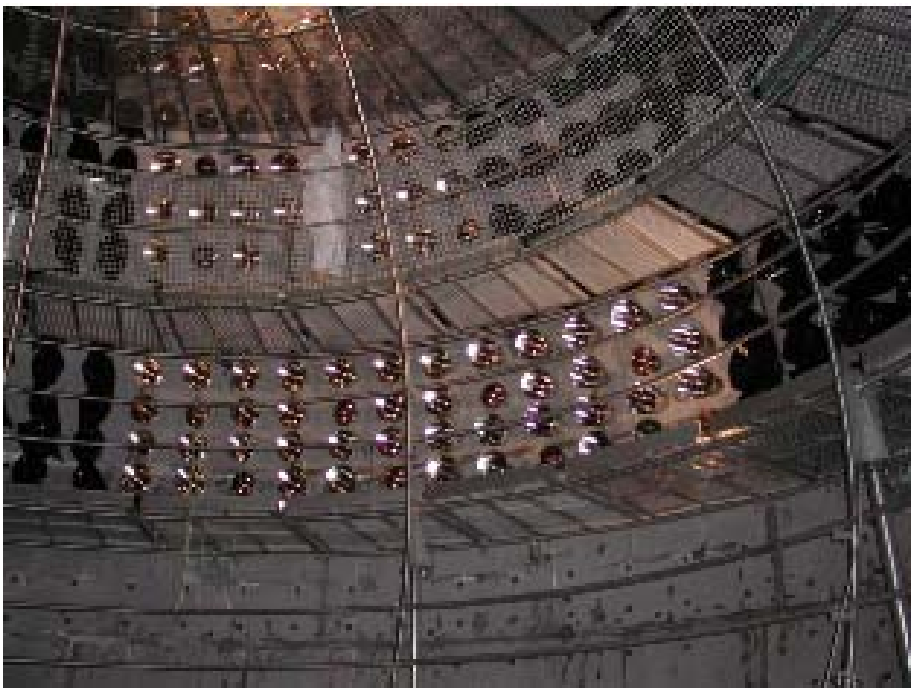

Figure 4: The photomultipliers, during the installation

3 Status of the Experiment

The completion of Borexino has now reached its final stage.

The installation of the structural part of the detector (water tank, stainless-steel sphere) (fig. 2,3) has been completed , and service systems (as air control in the sphere, clean-rooms, etc.) are running in standard conditions.

All cables have been positioned from the PMTs to the electronics Front-End . The phototubes (manifactured by ETL with a special glass of low radioactivity) have been completely assembled , sealed, coupled with the optical concentrators, and finally tested ; the installation of about 95% of them has been performed at the expected rate of 300 PMTs/month : for technical reasons, the last 5%will be mounted on the SSS after the Nylon vessels insertion. A new material, of very low contamination, has been selected for the manifacturing of the lastly procured 1000 concentrators. (fig. 4)

The detector calibrations will be performed by different systems: continous monitoring of the PMTs by means of a system of optical fibers guiding a laser light; tests with various radio-sources within the inner vessel, systematic tests of the optical properties of the buffer PC via laser light. The equipments for the calibrations are practically ready : the optical fibers have been installed concurrently with the PMTs, and different tests have been made at the final stage of this mounting.

The read-out electronics, already completed and installed in the Counting Room during the previous year, is now in tuning phase . During the year 2001 a large part of the hardware/software integration has been performed and also some preliminary joint test of the electronic/PMTs has been carried out. In the DAQ system, the analyzer code, the Data Base structure and a graphical command interface are almost completed.

The selection of the kind of Nylon to be used in the vessels (inner containment vessel and radon barrier) manifacturing has required a big effort. A sistematic check of the mechanical, optical, chemical quality of different kinds of this material, and particularly careful measurements of the Rn emanation from thin layers of various samples, was carried out. The costruction of these vessels has been completed inside a large clean room . Special care has been devoted to the leak check of these vessels before their shipment to LNGS, scheduled on march 2002 (fig. 5) .

Figure 5: The nylon vessels, mounted for a pressure test

The auxiliary plants are in a good stage of completion:

the Storage Area, already installed, has been throughly cleaned and leak-checked, and now is partially in operation for CTF3;

the solid Si-gel column and the scintillator handling for CTF and for Borexino is running (Module 0): the final column is expected in few months;

the distillation, water extraction, N_2 stripping systems have been built and are almost ready for operations;

the interconnection among the various purification systems, Storage Area, Borexino and CTF detectors has been installed and cleaned;

the filling stations systems are under construction and part of them has been installed;

the PPO and DMP handling systems are almost finalized;

the N_2 distribution plant, both for the normal Nitrogen and for high purity line (less than $1\mu Bq/m^3$) are normally functioning;

in addition the exaust system has been completed .

The supplier of the scintillator solvent Pseudocumene (PC) is Enichem, which produces it at Sarroch (Sardinia). The procurement of this PC has started in 2001. A special loading station, constructed on site, and four high quality shipping tanks are used for this purpose. The optical properties of the PC are tested in Sarroch each time, before its loading and delivering to Gran Sasso.

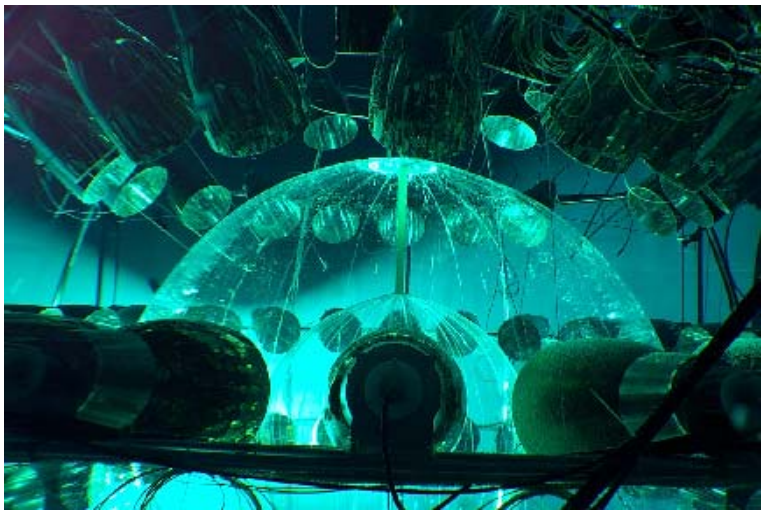

Figure 6: Inside CTF : during the filling

The PPO has been already procured and stored underground and the producer of the DMP quencher has been selected.

The offline codes cover a full simulation of the signal and background events, the tracking and reconstruction of them. Their origin are the codes already developed for the CTF1 data analysis, that are working since few years. A continuous activity of upgrading and development has been performed in their various aspects. The analysis of the CTF3 data can offer the possibility of testing parts of the new performance and reliability of these codes, explicitly developed for CTF. For the event tracking, the code Geant4, developed by CERN, has been adapted both to the CTF3 and Borexino needs. The organisation of the storage, handling, distribution and analysis of the data that will be collected during the Borexino running is in progress .

The upgraded version of CTF (CTF3), has been running since few months (fig. 6) The program of the measurements is fixed as follows: any batch of scintillator, as received

from Sarroch, will be tested; separate tests will follow after storage and circulation in the Storage Area, and after handling in the purification systems. Consequently, the Borexino inner vessel will be filled with a scintillator tested at the requested radiopurity level.

Since the beginning of the project realization, the Borexino Collaboration has faced the safety matter in all its aspects with great rigour. In this frame, all the plants have been analyzed for their intrinsic safety and are equipped with various fire estinguishing plants and alarms. A full HAZOP analysis has been accomplished for the plants and for the procedures adopted in the various operations.

The final filling of Borexino is scheduled in the summer 2002, and the starting run by the end of 2002.

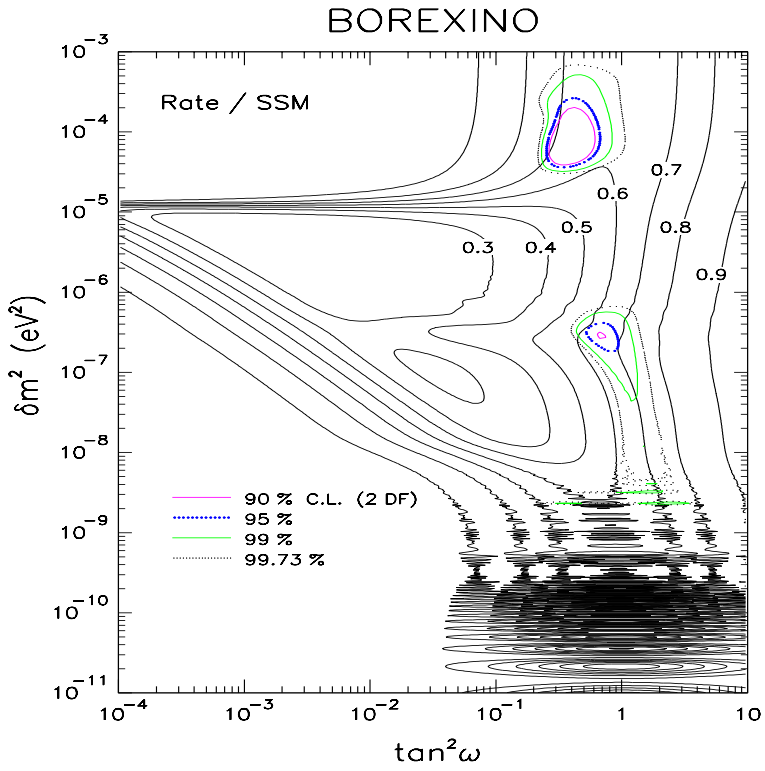

Figure 7: Allowed regions in the Δm^2-$\tan^2\omega$ parameter space for the LMA and LOW solutions: the Borexino rate fits

4 Solar neutrino physics: potential of Borexino

The evidence for an active, non-electronic ν component in the samples of the solar neutrino reactions, detected both by SKamiokande and SNO experiments, and the combination of all the results obtained until now, strongly favours the LMA (Large Mixing Angle) and LOW (Low probability, Low mass) regions for the $\tan^2\omega$ and δm^2 parameter of the ν-oscillation model .

The rates expected in Borexino are respectively 30 counts/day in the LMA solution, and 23 events/day in the LOW solution, to be compared to an expected background of

roughly 15 events/day . These values refer to the energy of electron scattered by ^{7}Be ν ranging from .25 to .8 MeV, which is the experimental range where the neutrinos coming from ^{7}Be source are detectable in Borexino, and to the 100 ton Fiducial Volume region (fig. 7). The good capacity of Borexino of detecting seasonal variations is overall important to tag the solar origin of the detected neutrinos : their flux variation due to the eccentricity of the Earth orbit is about 7%, with a typical $1/R^2$ behaviour (the Borexino sensitivity to this effect is 5 σ of C.L. in 3 years of data taking).

Moreover, an additional seasonal variation should be dramatically exhibited by Borexino in the Vacuum Oscillation hypothesis: the lack of this effect should strenghten the cancellation of this solution, as it is now disfavoured.

Borexino will offer a very good sensitivity to the Day/Nigth difference in the event rates, effect which is enhanced in the LOW solution just in the ^{7}Be ν energy region (fig.8).

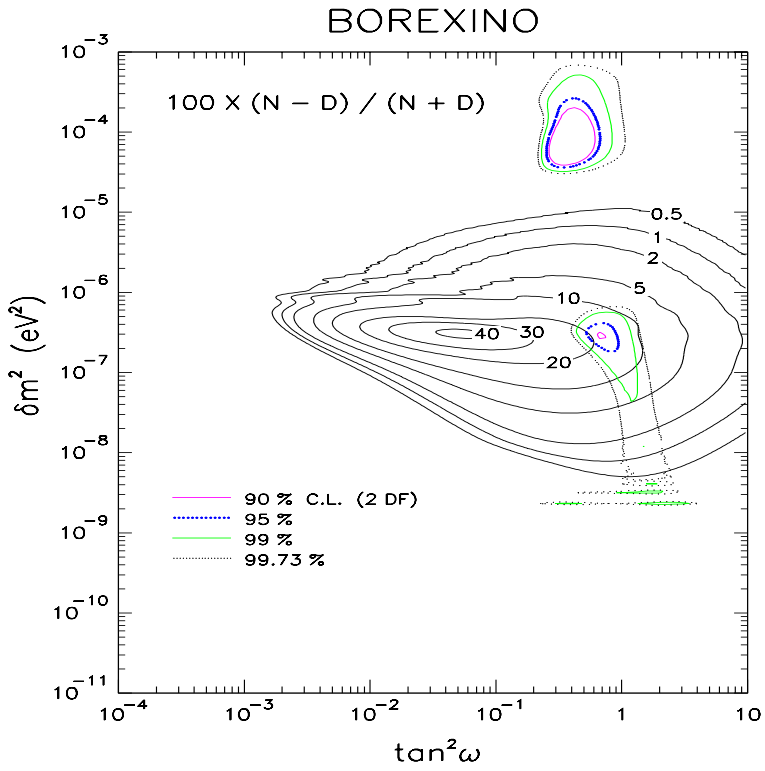

Figure 8: Day-night effect expected in Borexino (LOW solution)

Finally, the direct measurement of the reactions induced by neutrinos arisen in the ^{7}Be source inside the Sun will be the unique last tessera needed to close the Standard Solar Model experimental proof.

5 List of publications

1. G. Alimonti et al. *Science and Technology of Borexino: a real time detector for low energy solar neutrinos.*

Astroparticle Physics , 16 (2001) 205 .

2. G. Bellini et al. *High sensitivity double β decay study of ^{116}Cd and ^{100}Mo with the Borexino counting test facility (CAMEO project).*

   European Physical Journal C19 (2001) 43 .

3. C.Arpesella et al. *Measurements of extremely low radioactivity levels in Borexino.*

   Hep-ex/0109031 , in publication on Astroparticle Physics

4. H.O.Back et al. *Search for electron decay mode $\nu_e \rightarrow \gamma + \nu_e$ with prototype of Borexino detector.*

   in publication on Phys. Lett.

6 List of Presentations given during year 2001

1. *Borexino: a real time detector for low energy solar neutrinos.* B.Caccianiga - Frontiers in Contemporary Physics II, Nashville (USA), 5-10 March 2001

2. *Progress in measurements of radon background at the solar neutrino experiment Borexino.* B.Freudiger - DPG Spring Conference, Bonn (Germany), March 2001

3. *Measurement of ^{226}Ra in Nylon and the consequences for the background of Borexino.* H.Simgen - DPG Spring Conference, Bonn (Germany), March 2001

4. *Status report of Borexino.* H.Neder - 11th International School on Particles and Cosmology, Kabardino Balkaria,Baksan (Russia), April 2001

5. *Radon background in the Borexino solar neutrino experiment.* H.Simgen - 11th International School on Particles and Cosmology, Kabardino Balkaria,Baksan (Russia), April 2001

6. *Borexino.* G. Ranucci - Neutrino Oscillations in Venice, Venezia (Italy), 24-26 July 2001

7. *Sub-MeV solar neutrino detection in Borexino experiment.* M.E.Monzani - International School of Nuclear Physics, Erice (Italy), 18-26 September 2001

8. *Rn/Ra assay in water.* H.Simgen - International School of Nuclear Physics, Erice (Italy), 18-26 September 2001

9. *Rn measurements for the solar neutrino experiment Borexino.* B.Freudiger - International School of Nuclear Physics, Erice (Italy), 18-26 September 2001

10. *Borexino: a status report.* T.Shutt - TAUP Conference,LNGS (Italy), 8-12 September 2001

11. *Future experiments on solar neutrinos.* S.Bonetti - SIF Conference, Milano (Italy), 24-29 September 2001

12. *The Cameo double β decay Proposal.* M.Giammarchi - Conference on Underground Science, Lead, SouthDakota (USA), 4-7 October 2001

References

[1] G. Alimonti et al. (Borexino Collaboration). A Large Scale Low Background Liquid Scintillation Detector: the Counting Test Facility at Gran Sasso, Nuclear Instruments and Methods, A406 (1998) 411.

[2] G. Alimonti et al. (Borexino Collaboration). Ultralow background measurements in a large volume underground detector, Astroparticle Physics, 8 (1998) 141.

[3] G. Alimonti et al. (Borexino Collaboration). Measurements of the ^{14}C abundance in a low-background liquid scintillator, Phys. Lett. B, 422 (1998) 349.

[4] G. Alimonti et al. (Borexino Collaboration). Light propagation in a large volume liquid scintillator. Nuclear Instr. and Methods A 440 (2000) 360.

CRESST/CRESST2. Dark Matter Search

M. Altmann[a], G. Angloher[a], M. Bruckmayer[a], C. Bucci[d], S. Cooper[c], C. Cozzini[a], F. von Feilitzsch[b], T. Frank[a], D. Hauff[a], T. Jagemann[b], J. Jochum[b], R. Keeling[c], H. Kraus[c], J. Macallister[c], F. Pröbst[a], Y. Ramachers[c], J. Schnagl[b], W. Seidel[a*], M. Stark[b], L. Stodolsky[a], H. Wulandari[b]

[a] Max–Planck–Institut für Physik,
Werner Heisenberg Institut,
Föhringer Ring 6, D-80805 Munich, Germany
[b] Technische Universität München,
Physik Department E15, D-85748 Garching, Germany
[c] Oxford University, NAPL, Keble Road, Oxford OX1 3RH, UK
[d] Laboratori Nazionali del Gran Sasso, INFN, 67010 Assergi (AQ), Italy
[*] Spokesman of the collaboration

Abstract

We present the status as of 2001 for the CRESST (Cryogenic Rare Event Search using Superconducting Thermometers) experiment for the direct detection of WIMP dark matter. Measurements for the Phase I of CRESST were finished in March 2001. We met the projected milestones for phase I of CRESST and have been approved at the scientific committee meeting of March 2001 for the second phase of CRESST, up to the year 2005. The move of the experiment from Hall B to Hall A requested by the management was finished on time at the end of 2001.

1 Introduction

The goal of the CRESST project is the direct detection of elementary particle dark matter and the elucidation of its nature. The search for Dark Matter and the understanding of its nature remains one of the central and most fascinating problems of our time in physics, astronomy and cosmology. There is strong evidence for it on all scales, ranging from dwarf galaxies, through spiral galaxies like our own, to large scale structures [1].

Particle physics provides some well motivated candidates of which the lightest supersymmetric particle (LSP) is the favourite one. The extension of the standard model of elementary particles physics to the minimal supersymmetric standard model (MSSM) offers the LSP as a Dark Matter candidate in the form of a neutralino. It is a superposition of neutral particles arising in the theory, fulfilling all necessary requirements like e.g. stability and weak interaction cross sections with 'ordinary' baryonic matter. Indeed, supersymmetric models contain many parameters and many assumptions and by relaxing few simplifying assumptions one can find candidates for particle dark matter in a wide mass range [2]. Generically, particle dark matter candidates, being neutral, stable and weakly interacting, are called WIMPs (weakly interacting massive particles) and are to be distinguished from proposals involving very light quanta such as axions. WIMPs are expected to interact with baryonic matter by elastic scattering on nuclei and all direct detection experiments have focused on this possibility.

Conventional methods for direct detection rely on the ionization or scintillation caused by the recoiling nucleus. This leads to certain limitations connected with the relatively high energy involved in producing an ionization and with the sharply decreasing efficiency of ionization by slow nuclei. Cryogenic detectors use much lower energy excitations, such as phonons, and while conventional methods are probably close to their limits, cryogenic technology can still make great improvements. Since the principal physical effect of a WIMP nuclear recoil is the generation of phonons, cryogenic calorimeters are well suited for WIMP detection.

The detectors developed by the CRESST collaboration consist of a dielectric target–crystal with a small superconducting film evaporated onto the surface. When this film is held at a temperature in the middle of its superconducting-to-normal conducting phase transition, it functions as a highly sensitive thermometer. The detectors presently employed in Gran Sasso use tungsten films and sapphire absorbers, running at a temperature of 15 mK [3, 4]. The technique can also be applied to a variety of other materials [5]. The small change in temperature of the superconducting film resulting from an energy deposit in the target leads to a relatively large change in the film's resistance. This change in resistance is then measured with a SQUID.

2 Status of CRESST

At the end of 2000 and subsequently in the first months of 2001 we conducted several test measurements to examine possible systematic uncertainties of the setup before the final data analysis. Results for the first phase of CRESST were obtained and published at that time. In the following we summarise these results and finally report briefly about the move of the experiment and the current status of CRESST as of the end of 2001.

2.1 CRESST detectors

An example of a detector used for CRESST I can be inspected in Fig. 1. The detector used for dark matter limits had a tungsten thermometer of size 3mm×5mm. The electrical and thermal connections are shown in Fig. 1. Thermal contact between the holder and the

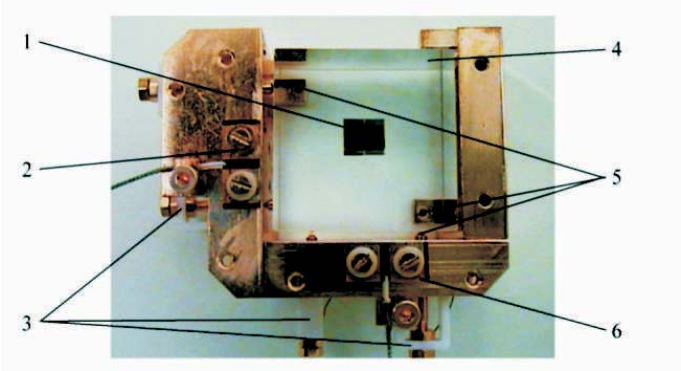

Figure 1: Picture of a sapphire 262g crystal. (1) Tungsten thermometer, (2) holder pads with screw contacts for connecting to the heater circuit, (3) plastic springs, (4) sapphire crystal, (5) sapphire balls, (6) holder pads with screw contacts for connecting to the SQUID read–out circuit.

detector was provided by gold wires of 25μm diameter bonded to the copper holder and to a gold contact pad in the middle of the tungsten thermometer. The copper holder was thermally connected via the cold finger to the mixing chamber of the dilution refrigerator, which was stabilised to a temperature of 6 mK. The electrical connection to the detector was made by superconducting aluminium wires bonded to aluminium pads on each end of the thermometer and to isolated contact pads on the holder. To avoid radioactive solder joints, the superconducting wires from there to the external readout circuit were screwed to the contact pads. The thermometer resistance is measured by passing a constant current I_0 through the readout circuit, in which the thermometer is in parallel to a small resistor and the input coil of a DC–SQUID. A rise in the thermometer resistance is then measured via the current rise through the SQUID input coil.

In a separate circuit, a heater to control the temperature of the detector is provided by a 5mm long, 25μm diameter gold wire which is bonded to the gold pad in the centre of the tungsten thermometer and to two small aluminium contact pads on the sapphire crystal on either side of the thermometer. External connections to the two small aluminium pads are used to apply a controlled voltage across this gold wire. The thermometer temperature is kept constant between pulses by using the baseline of the SQUID output voltage as the temperature indicator and then regulating the voltage to the heater using a proportional integral algorithm. The heater was also used to inject short heat pulses to monitor the long-term stability of the energy calibration and for measuring the trigger efficiency close to threshold.

For the actual data taking we monitored the detectors by injecting a heater pulse every 30 s during measurement as well as calibrations runs. The height of the pulses was varied in order to cover the whole dynamic range, with many pulses in the low-energy region. Therefore we obtain a monitor of the stability of the detectors, an extrapolation of the energy calibration over the whole dynamic range and a measure of the trigger efficiency as a function of the deposited energy.

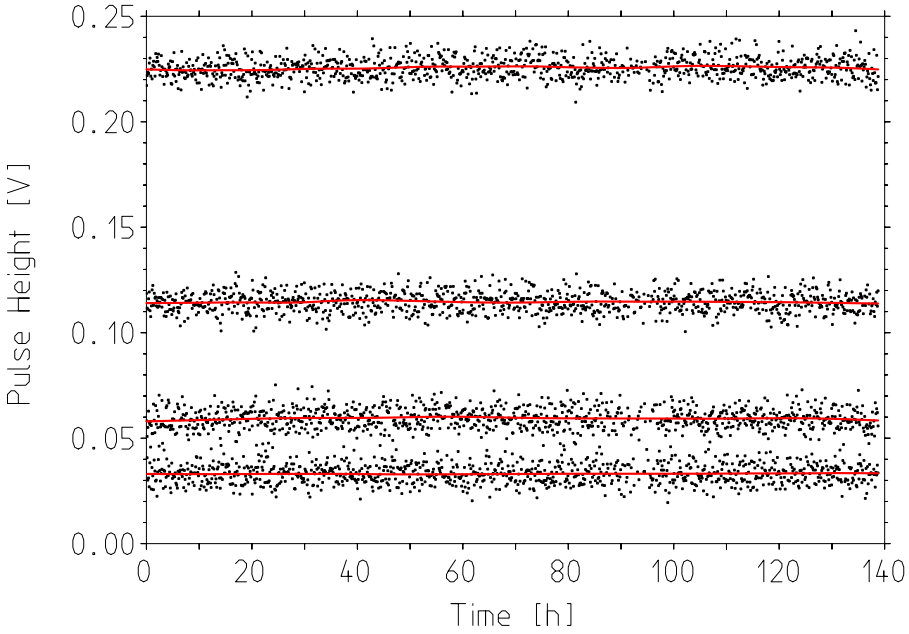

Figure 2: The measured pulse-height of detector #8 as a function of time during the dark matter run for the heater pulses of energy 0.58, 1.04, 2.04 and 4.08 keV. The detector is seen to be stable to within the resolution. The fitted lines were used to calculate the response function at the time of event pulses.

2.2 Measurements and results

The individual detectors varied in their response, with detector #8 (numbered by order of fabrication) having the lowest threshold and thus giving the best dark matter limits. The trigger efficiency of this detector was measured to be 100% down to an energy of 580 eV throughout the data used to extract the final dark matter limits. The stability of detector #8 during the dark matter run can be seen in Fig. 2 where the response to heater pulses is shown.

The reliability of the energy calibration method down to low energies was checked with a dedicated run, where a low activity ^{57}Co source was mounted inside the cryostat directly facing the crystals. Besides the 122 keV and 136 keV γ emission lines, this source gave a 14.4 keV line and a 6.4 keV Fe X-ray line. The source was chosen to be very weak to reduce the chance of contamination. Therefore a one week run gave only a small number of counts in the 14.4 keV and 6.4 keV lines. After applying the standard calibration method, which involves extrapolation from the 122 keV line to low energies, the measured energies for the 14.4 keV and 6.4 keV lines were found to be 15.16 ± 0.09 keV and 6.70 ± 0.07 keV, respectively (fit errors correspond to 90% CL). Hence our calibration procedure puts the 14.4 keV and 6.4 keV lines 5.3% and 5.4% too high. Since the lower energies most affect our dark matter limits, this tendency to shift events up in energy tends to put our limits on the conservative side.

The data used to set dark matter limit results come from a total run time of 138.8 h, of which 0.6 h is dead time following triggers. To avoid reliance on the detailed behaviour

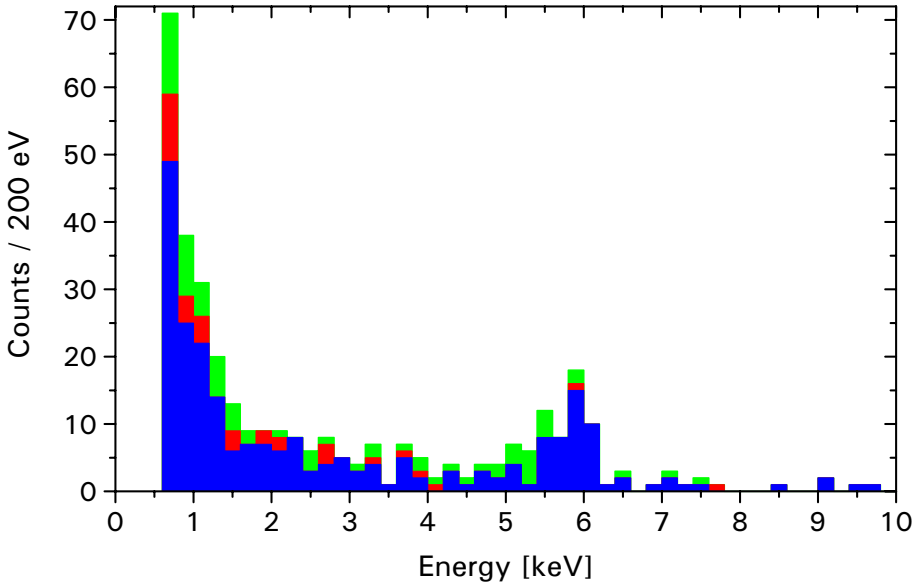

Figure 3: Energy spectrum of events in the dark matter run in 200 eV bins. The upper histogram shows the uncut data, the middle histogram the data after coincident events are rejected, and the lower histogram after the pulse-shape cut.

of the trigger efficiency at low-energies, a software threshold of 600 eV was used instead of the 580 eV 100% efficiency threshold measured. There were 374 events between threshold and 20 keV. Events in coincidence in two or more detectors cannot be due to WIMP interactions, and so can be discarded. This cut removed 73 events. Considering that only two detectors were active in this particular run, and that only one out of six sides faces the other crystal, the coincidence rate of almost 20% is surprisingly high. This suggests an immediate possibility to improve raw backgrounds by coincidence tagging with a more suitable arrangement of crystals. A final pulse shape examination of the remaining 301 events suggested another cut, namely removing spurious events with anomalous pulse shapes probably due to mechanical vibrations or electronic noise, and left 265 events. These are shown in Fig. 3. Finally, in the energy range from 15 keV to 25 keV the rate is (0.73 ± 0.22) counts/kg/day/keV and drops to about 0.3 counts/kg/day/keV at 100 keV.

As final results we present the WIMP limits obtained in Figs. 4,5. A detailed description of data taking and treatment as well as an extensive discussion of our method for obtaining WIMP limits has been published in [6].

2.3 Move from Hall B to Hall A

The move of CRESST from Hall B to Hall A proceeded as planned and was finished in December 2001. Obviously, no measurements were taken during the move. In order to finish in time, the experiment has been moved 'as is', i.e. no significant improvements or upgrades were attempted. Rather the effort has concentrated on reaching the same level of performance as before the move. All planned upgrades have thus been shifted to after a first test of the experiment after the move. The upgrade for the second phase of CRESST implies tests of its own. Therefore it appears more efficient to start these from

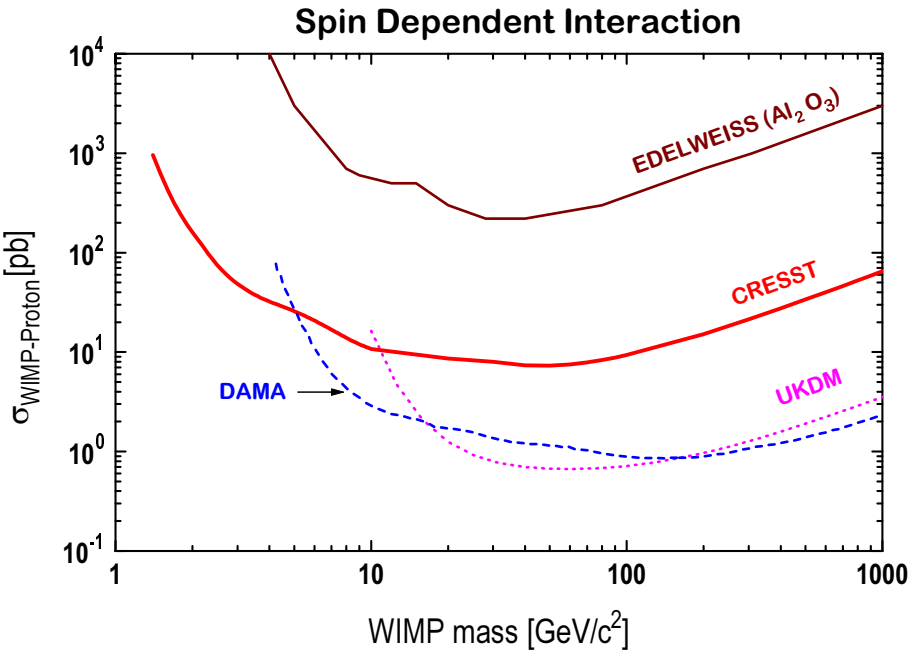

Figure 4: Equivalent WIMP-proton cross section limits (90% CL.) for spin–dependent interaction as a function of WIMP mass, from a 1.51 kg day exposure of a 262g sapphire detector. For comparison we show limits from the EDELWEISS dark matter search wit cryogenic sapphire detectors [7], from DAMA with NaI detectors using pulse-shape discrimination [8] and from the UK dark matter search with NaI detectors [9].

a known level of performance of CRESST I.

However, it is anticipated that establishing the former CRESST I performance will not take long, due to the great precautions taken during the move. In addition, the necessary developments for the upgrade have proceeded as far as possible in parallel: these include the extension to a seventy channel SQUID-readout system (Oxford), development of a $CaWO_4$ detector ensemble (holder, scintillating $CaWO_4$ crystal and light detector), infrastructure for detector production (Munich) and the additional neutron shield (Munich).

2.4 Summary

The status of CRESST at the end of 2001 therefore can be summarised as follows: the measurements for the first phase of CRESST have been finished and analysed. The move to Hall A is completed. The setup for first tests of performance after the move is prepared. Sapphire detectors from CRESST I are mounted in the coldbox for tests. As a starter for CRESST II, we have also mounted a first $CaWO_4$ detector assembly (common holder for the scintillating crystal and light detector). The first cool-down at the new location is expected to start early in 2002.

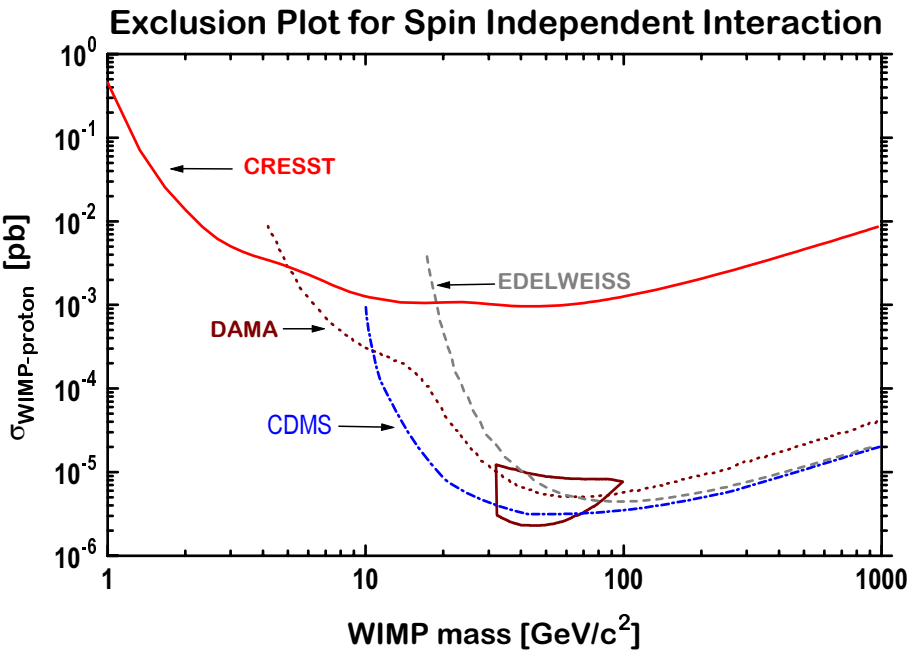

Figure 5: Equivalent WIMP–nucleon cross section limits (90% CL.) for spin–independent interaction as a function of the WIMP mass from a 1.51 kg day exposure of a 262g sapphire detector. For comparison DAMA NaI limits with pulse-shape discrimination [8], CDMS limits with statistical subtraction of the neutron background [10], limits from the UK coll. [9] and from the EDELWEISS coll. [11] are also shown together with the allowed 3σ CL. for a WIMP r.m.s. velocity of 270 km/s from the DAMA annual modulation data [12].

3 List of Publications

1. M. Altmann et al., Results and plans of the CRESST dark matter search, Proceedings X Int. Symp. on Lepton and Photon Interactions at High Energies, Rome, Italy, July 23-28 2001, Preprint astro–ph/0106314

2. G. Angloher et al., Limits on WIMP Dark Matter using Sapphire Cryogenic Detectors, submitted to Astropart. Phys.

3. Update of the Proposal to LNGS for a Second Phase of the CRESST Dark Matter Search, MPI-PhE/2001-02.

4. M. Loidl, S. Cooper, O. Meier, F. Proebst, G. Safran, W. Seidel, M. Sisti, L. Stodolsky, S. Uchaikin, Quasiparticle diffusion over several mm in cryogenic detectors, NIM A 465 (2001) 440

5. M. Sisti, O. Meier, M. Buehler, S. Cooper, V. Joergens, M. Loidl, U. Nagel, F. Proebst, W. Seidel, A. Stolovits, L. Stodolsky, S. Uchaikin, L. Zerle, Massive cryogenic particle detectors with low energy threshold, NIM A Vol. 466, No. 3

References

[1] N.J.C. Spooner, ed., Proc. Third Int. Workshop on *Identification of Dark Matter, IDM2000* (World Sci. Publ., 2000) York, UK

[2] A. Gabutti *et al.*, *Astropart. Phys.* **6**, 1 (1996); V.A. Bednyakov *et al.*, *Phys. Rev.* D **55**, 503 (1997)

[3] P. Colling *et al.*, *Nucl. Instrum. Methods* A **354**, 408 (1995)

[4] F. Pröbst *et al.*, *J. Low Temp. Phys.* **100**, 69 (1995)

[5] M. Bravin *et al.*, *Astropart. Phys.* **12**, 107 (1999)

[6] M. Altmann et al., Proceedings X Int. Symp. on Lepton and Photon Interactions at High Energies, Rome, Italy, July 23-28 2001, Preprint astro–ph/0106314; G. Angloher et al., submitted to Astropart. Phys.

[7] A. De Bellefon et al., *Astropart. Phys.* **6**, 35 (1996)

[8] R. Bernabei et al., *Phys. Lett.* B **389**, 757 (1996)

[9] N. Spooner et al., *Phys. Lett.* B **473**, 330 (2000)

[10] R. Abusaidi et al., *Phys. Rev. Lett.* **84**, 5699 (2000)

[11] A. Benoit et al., Preprint astro–ph/0106094

[12] R. Bernabei et al., *Phys. Lett.* B **480**, 23 (2000)

DAMA. Dark Matter Search

M. Amato[c], P. Belli[a], R. Bernabei[a,*], A. Bussolotti[a,@], F. Cappella[a,b], R. Cerulli[a], C.J. Dai[d], H. L. He[d], G. Ignesti[c], A. Incicchitti[c], H.H. Kuang[d], J.M. Ma[d] A. Mattei[c,@], F. Montecchia[a], F. Nozzoli[a,b], D. Prosperi[c],

in neutron measurements: M.Angelone[e], P.Batistoni[e], M.Pillon[e]

in recent measurements with $CaF_2(Eu)$ and CeF_3: F. Danevich[f], V.I. Tretyak[f], Yu.G. Zdesenko[f]

[a]Dip. di Fisica, Universita' di Roma "Tor Vergata" and INFN, sez. Roma2, Italy; [b]Laboratorio Nazionale del Gran Sasso, INFN, Assergi(Aq), Italy; [c]Dip. di Fisica, Universita' di Roma "La Sapienza" and INFN, sez. Roma, Italy; [d]IHEP, Chinese Academy, P.O. Box 918/3, Beijing 100039, China; [e]ENEA - C. R. Frascati, P.O. Box 65, I-00044 Frascati, Italy; [f]Institute for Nuclear Research, 252650 Kiev, Ukraine;

@ technical staff

Abstract

DAMA is searching for rare processes by developing and using several kinds of radiopure scintillators. The main running set-ups are: i) the $\simeq$ 100 kg NaI(Tl) set-up; ii) the $\simeq$ 6.5 kg ($\simeq$ 2 l volume) liquid Xenon (LXe) pure scintillator; iii) the R&D installation for tests and small scale experiments. Moreover, in the framework of devoted R&D for higher radiopure detectors and PMTs, sample measurements are regularly performed with the low background Ge detector of the DAMA experiment and at Ispra. Works to increase the exposed mass up to $\simeq$ 250 kg of NaI(Tl) (LIBRA set-up) are in progress.

1 Introduction

DAMA is devoted to the search for rare processes by developing and using low radioactivity scintillators. Its main aim is the search for relic particles (WIMPs: Weakly Interacting Massive Particles) embedded in the galactic halo, whose existence has been pointed out both by experimental observations and by theoretical considerations. Thus, our solar

*Spokesman of the DAMA collaboration

system, which is moving with respect to the galactic system, is continuously hit by a WIMP "wind". The quantitative study of this "wind" allows both to obtain information on the Universe evolution and to investigate Physics beyond the Standard Model.
The WIMPs are mainly searched for by elastic scattering on target nuclei, which constitute a scintillation detector; for this purpose, radiopure NaI(Tl), liquid Xenon and CaF_2(Eu) detectors are developed and used (main recent references are given in [1, 2, 3, 4, 5, 6, 7, 8, 9, 10, 11, 12, 13, 14] and in the 2001 publication list quoted in the following). In particular, the $\simeq$ 100 kg NaI(Tl) set-up has been realized to investigate the so-called WIMP "annual modulation signature". This experiment, in fact, can effectively exploit such a signature because of its well known technology, of its high intrinsic radiopurity, of its mass and of its suitable control of the operational parameters. The relevance of performing experiments with a proper clear model independent signature is evident.

An R&D activity to develop higher radiopure detectors is continuously carried out toward the creation of ultimate radiopure detectors as well as studies on their possible new applications (main references are given in [15] and in the 2001 publication list quoted in the following). As a result of one of these efforts, the exposed target-detector mass of the NaI(Tl) set-up is in progress to be enlarged up to $\simeq$ 250 kg. The installation of this set-up is planned at fall 2002.

Finally, profitting of the radiopurity achieved in the whole set-ups, several searches for other rare processes are also performed, such as for: i) $\beta\beta$ decay processes; ii) charge-non-conserving (CNC) processes; iii) Pauli exclusion principle (PEP) violating processes; iv) nucleon instability; v) exotics; etc. Also in these cases competitive results have been obtained so far (main recent references are given in [16] and in the 2001 publication list quoted in the following).

The main DAMA activities are summarized and briefly commented in the following.

2 The $\simeq$ 100 kg highly radiopure NaI(Tl) set-up

The main goal of the $\simeq$ 100 kg NaI(Tl) set-up is the search for WIMPs by the annual modulation signature (see [6, 7, 8, 10, 11, 12] and publication list in 2001); in addition, as mentioned above, it allows also to investigate other rare processes [16].
This set-up and its performances have been described in details in ref. [7]; since then several upgradings have been carried out. In particular, in summer 2000 the electronic chain and data acquisition system have been completely upgraded, while during August 2001 the new HV power supply system and the new preamplifiers prepared for the foregoing LIBRA set-up have been installed. Soon after, the data taking of a new annual cycle has been started.
Various kind of data analyses have been continued; some of them have been published during 2001.

2.1 On the WIMP annual modulation signature

The $\simeq$ 100 kg NaI(Tl) set-up has been realized to investigate the so-called WIMP "annual modulation signature". In fact, since the Earth rotates around the Sun, which is moving with respect to the galactic system, it would be crossed by a larger WIMP flux in June (when its rotational velocity is summed to the one of the solar system with respect to the Galaxy) and by a smaller one in December (when the two velocities are subtracted). The fractional difference between the maximum and the minimum of the rate is expected to be $\lesssim$ 7%. The annual modulation signature is very distinctive; in fact, a WIMP-induced seasonal effect must simultaneously satisfy many requirements: the rate must contain a component modulated according to a cosine function (1) with one year period (2) and a phase that peaks around $\simeq 2^{nd}$ June (3); this modulation must be found in a well-defined low energy range, where WIMP induced recoils can be present (4); it must apply to those events in which just one detector of many actually "fires", since the WIMP multi-scattering probability is negligible (5); the modulation amplitude in the region of maximal sensitivity must be $\lesssim$7% (6). Thus, only systematic effects also able to simultaneously satisfy these 6 requirements could mimic this signature; on the contrary of what is claimed by some parts [17], no one able to do it has been found or suggested by any one so far (for details see [12], where also absence of modulation in the background has been demonstrated). This can be easily understood considering the relevant number of peculiarities which have to be simultaneously satisfied.

In particular, we remind that the data collected in four annual cycles, DAMA/NaI-1 to DAMA/NaI-4 (total statistics 57986 kg·day) have been released up to now. They show a clear ($\simeq 4\ \sigma$ C.L.) presence of modulation with the proper distinctive features expected for a WIMP induced effect all simultaneously satisfied by the data over four independent experiments of one year each one. As mentioned above, a deep investigation has not offered any possible known systematics or side process able to mimic a WIMP induced seasonal effect and, thus, to account for the DAMA observed effect (see e.g. [11, 12] and references in 2001). In conclusion, the model independent approach, together with the absence of possible systematics or side processes able to mimic such a signature, suggests the presence of a WIMP contribution to the measured rate independently on the nature and coupling with ordinary matter of the involved WIMP particle [12].

To investigate the nature and coupling with ordinary matter of the possible WIMP candidate, an effective energy and time correlation analysis has to be performed within given model frameworks. We remind that a model framework is identified not only by general astrophysical, nuclear and particle physics assumptions, but also by the specific set of values used for all the parameters needed in the model itself and in related quantities (for example WIMP local velocity, v_0, form factor parameters, etc.) which are indeed affected by significant uncertainties. Obviously, varying the parameters values within their allowed intervals as well as varying any of the astrophysical, particle and nuclear physics assumptions, will consequently vary the allowed region (the same is for excluded limits). In the cumulative model dependent analyses of the data of the four annual cycles we have properly accounted also for the physical constraint arising from the upper limit on recoils we measured in ref. [5] (DAMA/NaI-0 running period) [1].

[1] It is worth to note that the simultaneous use of a discrimination technique and of the annual modu-

As regards possible model dependent cumulative analyses of the four annual cycles data, as first a particular model framework for a purely spin-independent (SI) coupled candidate, which equally couples to proton and neutron, has been considered in ref. [11]. There the existing uncertainties e.g. on the v_0 value have been included in the analysis. Obviously, in different model frameworks the expectations vary and, therefore, also the best fit values of the free parameters; for example, in the model framework of ref. [11] a WIMP mass $m_W = (72^{+18}_{-15})$ GeV and a SI cross section on nucleon (σ_{SI}) times the local density in 0.3 GeVcm^{-3} unit (ξ): $\xi\sigma_{SI} = (5.7 \pm 1.1) \cdot 10^{-6}$ pb correspond to the best fit position when $v_0 = 170$ km/s, while $m_W = (43^{+12}_{-9})$ GeV and $\xi\sigma_{SI} = (5.4 \pm 1.0) \cdot 10^{-6}$ pb are found when $v_0 = 220$ km/s. For simplicity the effect of the inclusion of known uncertainties on the parameters is expressed by giving as cumulative allowed region the superimposition of all the allowed ones and, thus, one cannot refer to a corresponding single set of best fit values (see e.g. [10, 11]).

Let us now comment that no other experiment can at present investigate the WIMP annual modulation signature with a sensitivity similar as the $\simeq 100$ kg highly radiopure DAMA NaI(Tl) set-up. Thus, only model dependent comparisons can be pursued with other experiments using different techniques and different target nuclei which should require a conservative actitude. For example, the claim for contradiction made by CDMS-I within a particular model framework for a purely SI coupled candidate was arbitrary both for experimental and theoretical reasons as we have pointed out e.g. in the Proc. of the XX Texas conf. (see reference list in 2001). Similar considerations can also be applied to the EDELWEISS experiment, while – at a larger extent – the results of indirect searches (as e.g. those from Superkamiokande) have large uncertainties due to the used assumptions in the evaluation of the signal, to the modellization of all the background processes, to their subtraction, to the model dependent comparison, etc. In addition, often the comparison is not pursued by considering the final allowed region quoted in ref. [11] for purely spin-independent coupled WIMPs.

In conclusion, the case of a purely spin-independent coupled WIMP candidate in the model framework of ref. [11] supports allowed WIMP masses up to 105 GeV (1 σ C.L.) and even up to 132 GeV (1 σ C.L.) if possible dark halo rotation is included. Further extension of the allowed region both in mass and cross section are obtained when including e.g. the uncertainties on some other parameters or different halo modelling. Theoretical implications of these results in terms of a neutralino with dominant SI interaction and mass above 30 GeV have been discussed in ref. [18, 19], while the case for an heavy neutrino of the fourth family has been considered in ref. [20].

lation signature cannot offer any reliable result since the real uncertainties, affecting the results obtained by the discrimination technique, applied over long data taking periods, are typically of the same order of magnitude or much larger than the effect searched for when investigating the annual modulation signature (which on the other hand acts itself as an effective background rejection). Moreover, the application of whatever technique of background discrimination cannot disentangle WIMP induced recoils from side processes (such as e.g. recoils induced by possible residual environmental neutrons, fission fragments, end-range alphas...) as well as from the tails of the various populations (e.m background, recoil, recoil-like, noise, possible not properly handled instrumental effects...); in addition, discrimination is in the practice always statistical. Thus, the real nature of discriminated events will be always based on a conjecture. Moreover, easily understandable systematic limitations will arise when discrimination procedures are applied over much longer data taking periods.

Since the ^{23}Na and ^{127}I nuclei are sensitive to both SI and SD couplings – on the contrary e.g. of ^{nat}Ge and ^{nat}Si which are sensitive mainly to WIMPs with SI coupling (only 7.8 % is non-zero spin isotope in ^{nat}Ge and only 4.7% of ^{29}Si in ^{nat}Si) – the analysis of the data has been extended considering the more general case of a WIMP having not only a spin-independent, but also a spin-dependent (SD) coupling different from zero, as it is also possible e.g. for the neutralino. In this case, an allowed volume in the four-dimensional space ($\xi\sigma_{SI}$, $\xi\sigma_{SD}$, m_W, θ) is obtained. Here, σ_{SD} is the point-like SD WIMP cross section on nucleon and $tg\theta$ is the ratio between the effective SD coupling constants on neutrons, a_n, and on proton, a_p; therefore, θ can assume values between 0 and π depending on the SD coupling. In this analysis the uncertainties on v_0 have been included; moreover, the uncertainties on the nuclear radius and the nuclear surface thickness parameter in the SI form factor, on the b parameter in the used SD form factor and on the measured quenching factors [5] have also been considered. This analysis (described in details in the paper quoted in the reference list of 2001 and already summarized in the LNGS report 2000) has shown that the DAMA data of the four annual cycles can also be compatible with a mixed scenario where both $\xi\sigma_{SI}$ and $\xi\sigma_{SD}$ are different from zero. Further investigations are possible to account for other known parameters uncertainties and for possible different model assumptions; as an example, we recall that for the SD form factor an universal formulation is not possible since the internal degrees of the WIMP particle model (e.g. supersymmetry in case of neutralino) cannot be completely separated from the nuclear ones. Thus, other formulations are possible for SD form factors and can be considered with evident implications on the obtained allowed volume and best fit values of the free parameters.

Further efforts carried out during 2001 on this subject regards several topics: i) further upgrading of the set-up (see above); ii) data taking of further annual cycles; iii) investigation of other possible model frameworks; iv) preparation of the new $\simeq$ 250 kg NaI(Tl) set-up, LIBRA.

In particular, in addition to the mixed SI/SD model framework, another model dependent scenario has been exploited. In fact, the model independent annual modulation effect observed by DAMA during four annual cycles has been analysed in terms of a particle Dark Matter candidate with preferred inelastic scattering [21]. As discussed in ref. [21], the inelastic Dark Matter could arise from a massive complex scalar split into two approximately degenerate real scalars or from a Dirac fermion split into two approximately degenerate Majorana fermions, namely χ_+ and χ_-, with a δ mass splitting. In particular, a specific model featuring a real component of the sneutrino, in which the mass splitting naturally arises, has been given in ref. [21]. It has been shown that for the χ_- inelastic scattering on target nuclei a kinematical constraint exists which favours heavy nuclei (such as ^{127}I) with respect to lighter ones (such as e.g. ^{nat}Ge) as target-detectors media. This kinematical constraint becomes increasingly severe as the nucleus mass, m_N, is decreased [21]. Moreover, this model scenario gives rise – with respect to the case of WIMP elastically scattering – to an enhanced modulated component, S_m, with respect to the unmodulated one, S_0, and to largely different behaviours with energy for both S_0 and S_m (both show a higher mean value) [21]. A dedicated cumulative energy and time correlation analysis of the DAMA experimental data has been carried out (see in the

reference list 2001) in a model framework, where aspects other than the interaction type have been handled as in the SI/SD mixed coupling case.

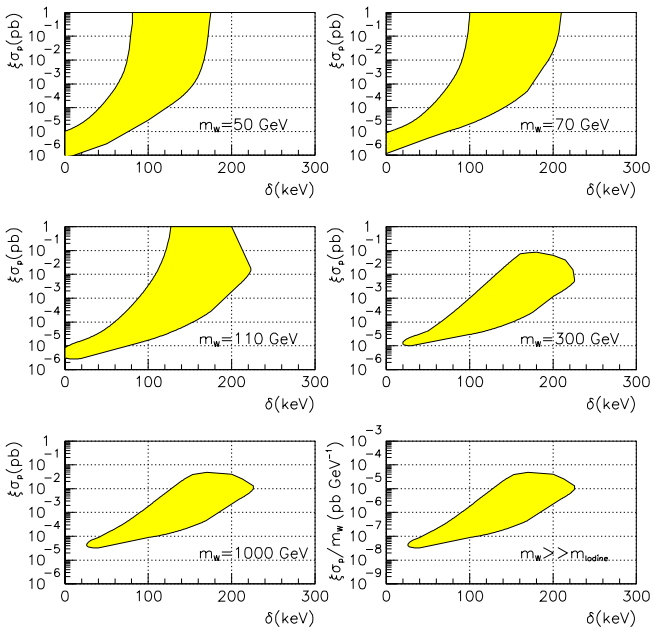

Figure 1: A "preferred" inelastic scattering model framework: examples of slices in the space ($\xi\sigma_p$, δ, m_W) for some m_W values (3 σ C.L.).

In this inelastic Dark Matter scenario an allowed volume in the space ($\xi\sigma_p$,m_W,δ) is obtained. For simplicity, Fig. 1 shows slices of such an allowed volume at some given WIMP masses (3 σ C.L.). It can be noted that when $m_W \gg m_N$, the expected differential energy spectrum is trivially dependent on m_W and in particular it is proportional to the ratio between $\xi\sigma_p$ and m_W; this particular case is summarized in the last plot of Fig. 1. The allowed regions reported there have been obtained by the superposition of those obtained when varying the values of the previously mentioned parameters according to their uncertainties. This also gives as a consequence that the cross section value at given δ can span there over several orders of magnitude. The upper border of each region is reached when the minimal velocity, which WIMP must have to scatter off inelastically, approaches the maximum WIMP velocity in the Earth frame for each considered model framework (in particular, for each v_0 value). Note that, as also mentioned above, each set of values (within those allowed by the associated uncertainties) for the previously mentioned parameters gives rise to a different expectation, thus to different best fit values. As an example we mention that when fixing the other parameters as in the above mentioned case, the best-fit values for a WIMP mass of 70 GeV are: i) $\xi\sigma_p = 2.5 \times 10^{-2}$ pb and $\delta = 115$ keV when $v_0 = 170$ km/s, ii) $\xi\sigma_p = 6.3 \times 10^{-4}$ pb and $\delta = 122$ keV when $v_0 = 220$ km/s.

Finally, we note that significant enlargement of the given allowed regions should be expected when including complete effects of model (and related experimental and theoretical parameters) uncertainties, varying consequently the best fit positions.

In conclusion the DAMA annual modulation data of four annual cycles have been analysed by energy and time correlation analysis in terms of purely SI, purely SD, mixed SI/SD, "preferred" inelastic WIMP scattering model frameworks. Moreover, possible different halo models can be also considered; a work on this subject has been carried out by some of us and will be discussed in the LNGS report 2002.

Finally, to effectively discriminate among the different possible model dependent scenarios further investigations are in progress. In particular, the data of the 5^{th} and 6^{th} annual cycles are at hand, while the set-up is running to collect the data of a 7^{th} annual cycle. Moreover, the LIBRA (Large sodium Iodine Bulk for RAre processes) set-up is under construction to increase the experimental sensitivity.

2.2 Search for solar axions

During 2001 the results of a search for possible signal due to Primakoff conversion of solar axions into photons in NaI(Tl) have been published. The used statistics, collected by the $\simeq$ 100 kg NaI(Tl) set-up, is 53437 $kg \cdot day$.

Various experimental and theoretical considerations have restricted at present the axion mass to the range $10^{-6}\text{eV} \lesssim m_a \lesssim 10^{-2}\text{eV}$ and $m_a \sim$ eV. It has also been noted that axions with a similar mass could be candidate as a possible component of the Dark Matter in the Universe.

In particular, axions can efficiently be produced in the interior of the Sun by Primakoff conversion of the blackbody photons in the fluctuating electric field of the plasma. The outgoing axion flux has an average energy, E_a, of about 4 keV since the temperature in the Sun core is $T \sim 10^7 K$. Assuming absence of direct coupling between the axion and the leptons (*hadronic axion*) and including helium and metal diffusion in the solar model, the flux of solar axions can be written as [22, 23]:

$$\frac{d\Phi}{dE_a} = \sqrt{\lambda}\frac{\Phi_0}{E_0}\frac{(E_a/E_0)^3}{e^{E_a/E_0}-1} \tag{1}$$

where $\lambda=(g_{a\gamma\gamma}\times 10^8/\text{GeV}^{-1})^4$ is a suitable dimensionless coupling, $\Phi_0=5.95\times 10^{14}$ cm^{-2}s^{-1} and $E_0=1.103$ keV.

Solar axions can produce detectable X–rays in crystal detectors via a coherent effect when the Bragg condition is fulfilled (depending on the direction of the incoming axion flux with respect to the planes of the crystal lattice) giving a strong enhancement of the possible signal. Following this approach, a distinctive signature for solar axion can be searched for by comparing the experimental counting rate with the rate expected by taking into account the position of the Sun in the sky during the data taking [24, 25, 26]. We note that positive results or bounds on $g_{a\gamma\gamma}$ obtained by this approach are independent on m_a and, therefore, overcome the limitations of some other techniques which are instead restricted to a limited mass range [27, 28].

The expected rate for solar axion in a crystalline detector is directly proportional to the adimensional constant λ. Two coordinates were introduced: θ_z, angle between the vector pointing to the Sun and one crystallographic axis (here the growth symmetry axis, gsa), and ϕ_{az}, angle between the horizontal plane and the plane containing both the Sun and gsa. To be the most conservative on the used crystals features (that is considering only

a symmetry around gsa), in the present analysis the expected counting rate has been calculated by averaging over the ϕ_{az} coordinate. This average reduces the amplitudes expected for the typical structures of the coherent solar axion conversion in the crystals, lowering at the same time the sensitivity achievable here with respect to the case when three crystalline axes orientations are available.
In Fig. 2a) the expected counting rate for solar axions in NaI(Tl) when $\lambda = 1$ – averaged over the whole solid angle – is shown as a function of the detected energy. Since the mean

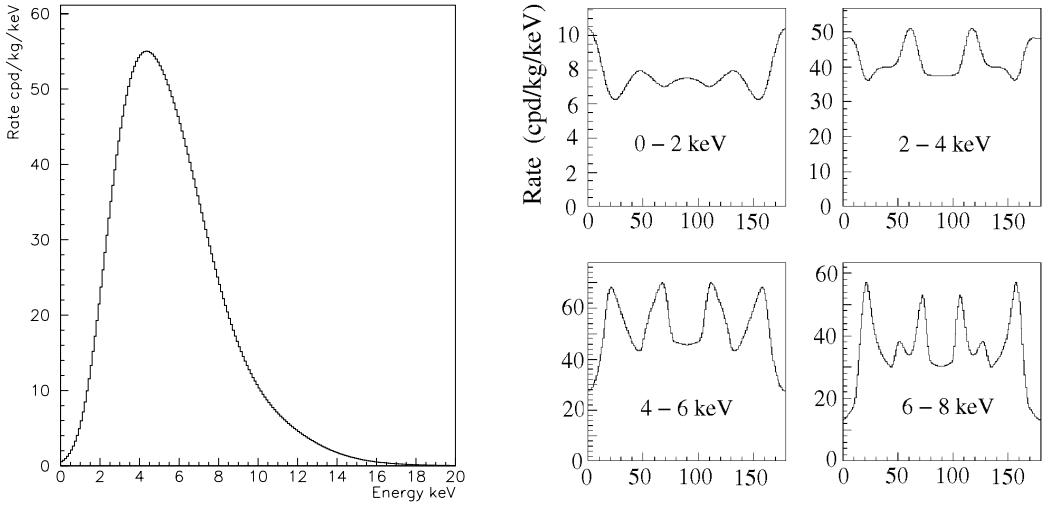

Figure 2: a) Expected counting rate for solar axions in NaI(Tl) for $\lambda = 1$ – averaged over the whole solid angle – as a function of the detected energy; b) Expected counting rate for solar axions in NaI(Tl) evaluated for $\lambda = 1$ as a function of θ_z in the energy intervals: 0-2 keV, 2-4 keV, 4-6 keV and 6-8 keV. The rate is averaged over ϕ_{az}.

value of the expected counting rate in energy intervals above 10 keV is significantly lower than at low energy, in the analysis the energy range 2 keV (software energy threshold of our experiment) to 10 keV has been considered. In Fig. 2b) the counting rate (averaged over ϕ_{az}) expected in the detectors is shown as a function of θ_z considering 2 keV energy bins. The data have been analysed as a function of θ_z instead of the time since the expected counting rate shows a clear periodicity as a function of θ_z and not of the time (the path of the Sun in the sky differs from day to day).
A preliminary simple approach – which does not exploit the time dependence of the possible solar axion signal – is based on the comparison of the expected rate averaged over the whole solid angle [Fig. 2a)] with the measured one. Notwithstanding its simplicity, this method can give the right scale of the sensitivity of the experiment. In the present case we obtain: $\lambda < 2 \times 10^{-2}$ (90% C.L.), and, consequently: $g_{a\gamma\gamma} < 4 \times 10^{-9} GeV^{-1}$ (90% C.L.).
To investigate with high sensitivity the possible presence of a solar axion signal or to achieve upper limit on λ (and, consequently, on $g_{a\gamma\gamma}$), we exploit the time dependence of the solar axion signal. Since - for manufacturing and/or assembling reasons - the gsa's of the nine crystals can be either parallel to one of the two small sides (2^9 possibilities)

or all parallel to the longest side (1 possibility), we have repeated the calculation of λ for all the possible configurations; all the determinations were compatible with the absence of signal. Considering the most conservative configuration, we quote for λ the value $(4.3 \pm 3.1) \times 10^{-4}$. According to standard procedure [29], this result gives an upper limit on the coupling of axions to photons: $\lambda \leq 8.4 \times 10^{-4}$ (90% C.L.), which corresponds to the limit: $g_{a\gamma\gamma} \leq 1.7 \times 10^{-9} GeV^{-1}$ (90% C.L.). In Fig. 3 the region in the plane $g_{a\gamma\gamma}$ versus m_a excluded at 90% C. L. by this experiment is shown. The obtained limit

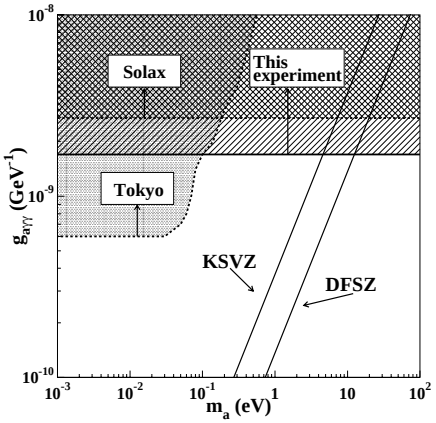

Figure 3: Exclusion plot for $g_{a\gamma\gamma}$ versus m_a. The limit achieved by the present experiment ($g_{a\gamma\gamma} \leq 1.7 \times 10^{-9} GeV^{-1}$ at 90% C.L.) is shown together with the expectations of the KSVZ and DFSZ models. The results of previous direct searches for solar axions by Solax [26] – exploiting the same technique as our experiment – and by the Tokyo helioscope [28] are also shown for comparison.

on λ is about one order of magnitude more stringent than the one set by the SOLAX and COSME collaborations [26, 25], while the limit on the coupling constant $g_{a\gamma\gamma}$ has been improved by a factor 1.6 with respect to these experiments. The obtained result is at present the best direct limit on solar axions conversion in crystals and for axion masses larger than $\simeq 0.1$ eV is better also than the limit set by the Tokyo helioscope. In conclusion, this experiment has explored the axion mass window $m_a \sim$ eV still open in the KSVZ model (where $g_{a\gamma\gamma} = 3.7 \times 10^{-10}\ GeV^{-1} \frac{m_a}{eV}$) and has allowed to exclude KSVZ axions for $m_a > 4.6$ eV at 90% C.L.

3 The LXe set-up

During the year 2001 some upgrading of the set-up has been performed. In particular: i) a general maintenance of the vacuum and cooling system has been carried out to improve its performances; ii) the monitoring system of the cryogenic and working parameters has been improved for on-line remote control and set of general alarms; iii) the electronic chain has been modified in order to collect both low energy signals and high energy signals on Transient Digitizers adding a passive power splitter before the preamplifiers.

During 2001, the $\simeq$ 6.5 kg liquid Xenon set-up of the DAMA experiment has taken data filled with Xenon enriched at 68.8% in ^{136}Xe. Thus, measurements to investigate $\beta\beta$ processes in ^{136}Xe and in ^{134}Xe have been performed. In addition at ENEA-Frascati further measurements on recoil over electron light response ratio for Xe in pure liquid Xenon scintillator have been realised and published.

Moreover, in this period a paper describing the DAMA LXe set-up in some details has also been published.

3.1 Further measurement of the recoil over electron light ratio for Xe in pure liquid Xenon scintillator

When the low energy data are analysed in terms of WIMP-nucleus scattering, it is necessary to evaluate the energy of the recoil nucleus in keV from its value known in keV electron equivalent (keV e.e.) as given by γ source calibrations. For this purpose it is necessary to determine the ratio (r) of the measured amount of light from a recoil nucleus to the amount of light from an electron of the same kinetic energy.

In 1992 our group considered the Lindhard theory [30] to evaluate a preliminary estimate of r [31], but it is unsuitable for this purpose since it does not account for all the processes which occur in pure LXe scintillation, such as for example the recombination effect. In particular, for comparison, we remind that the α/electron light ratio is very high in pure LXe scintillators: $\simeq$ 1.2 [32, 33], and that estimates by considering Xenon data [33, 34, 35] supports a recoil/electron light ratio not worse than $\simeq$ 0.5 [36] in the energy region of interest for WIMP search. Afterwards, our group has realized dedicated neutron calibrations [3]. These measurements were performed by a dedicated 40 cc detector, since the use of a neutron source is forbidden in a low background installation by the consequent activation of the irradiated materials. The measurements of r have been carried out both by the method of ref. [5, 37] with an Americium-Boron (Am-B) neutron source and by detecting scattered neutrons at two fixed angles using the $\simeq$ 14 MeV ENEA-Frascati neutron generator[38]. We obtained: i) in the first case, $r = 0.65\pm0.10$; ii) in the second case, $r = 0.49\pm0.04(\text{stat})\pm 0.06(\text{sys})$ and $r = 0.42\pm0.03(\text{stat})\pm 0.06(\text{sys})$ [3]. Since the determinations substantially agreed within the errors, the overall mean value and the half dispersion was calculated: 0.55 $\pm$ 0.11 and, then, the lower value 0.44 was cautiously considered in the evaluation of WIMP results from our experiment [3, 4]. For details see ref. [3]. The same neutron measurements also allowed a quantitative investigation of the possibility of a pulse shape discrimination between electromagnetic background and Xenon recoils, after preliminary studies on the different decay times between α and electron pulses. Results are reported in ref. [3].

To obtain the r value by detecting scattered neutrons at fixed angles also in the energy region previously investigated by means of the Am-B neutron source [3], data have been collected at the end of 2000 with the 40 cc LXe dedicated set-up at the ENEA-Frascati neutron generator by employing 2.5 MeV neutrons. In these measurements the ENEA-Frascati Neutron Generator [38] exploits the fusion reaction $^2H+^2H \rightarrow n+^3He$ to produce almost monoenergetic neutrons of about 2.5 MeV. The maximum intensity of neutrons during the data tacking was $\simeq 4.0 \cdot 10^8$ n/s over the whole solid angle. The reaction presents an anisotropy in the laboratory frame (about 18% forward). The LXe detector

is positioned at 90^0 with respect to the beam axis, about 3 m far. In this configuration the neutrons impinging on the detector have a mean energy of 2.52 MeV with an about 3% *r.m.s.* spread. The neutron yield is monitored by integral fission chambers, BF_3 counters, NE213 scintillator and primarily by a Silicon Surface Detector (SSD) to tag the ^{3}He particles produced by the fusion reaction.
The used set-up includes a 40 cc stainless steel vessel filled with natural Xe gas (99.998 % purity by Messer Griesheim). It has a MgF_2 optical window coupled to an EMI photomultiplier (PMT) with MgF_2 window too (quantum efficiency $\simeq$ 32%). No other material than the LXe is present inside the 40 cc stainless steel vessel. This vessel is insulated by an external stainless steel vacuum vessel (with an Aluminum window) and maintained at the working temperature by a cold finger in a LN_2 bath with heater/temperature controller. A $\simeq 10^{-6}$ mbar vacuum is required for the vacuum/filling/purification/recovery line and for inner vessel, while a $\simeq 10^{-3}$ mbar vacuum is instead sufficient for the external insulation vessel. As regards the purification system it is realized by a home-made getter – firstly activated at $\simeq 400\ ^0$C – which allows outlet impurities < 1 ppb for any component: O_2, N_2, CO, etc. [39]. It is followed by a cold Nitrogen trap, working at $\simeq 190$ K, to further purify the Xe from possible Rn, H_2O and other impurities that condense at this temperature and it is used during the full procedure of gas filling and liquefaction. The stainless steel bottle of Xenon is inserted in a stainless steel dewar. When the recovery procedure of the used Xenon starts, this dewar is filled with liquid Nitrogen and the Xenon is gradually stored back in the bottle while heating the liquid Xenon vessel. A low noise preamplifier is connected to the PMT as in the measurements performed by the set-up operating deep underground and the pulse shape of each event is recorded by a LeCroy Transient Digitizer over 1000 ns. The energy calibrations in keV electron equivalent are performed with a ^{109}Cd source (22 and 88 keV line) placed in the sensitive volume. Moreover, during the data taking, external ^{60}Co source is also used for calibrations. The scattered neutrons are tagged by using two 3" thick by 3" diameter NE213 detectors, surrounded by $\gtrsim$ 20 cm thick paraffin shield. To discriminate the scattered neutrons in NE213 against γ-rays the well known pulse shape identification of the neutrons has been used. In particular the known "head/tail" method [40] has been employed. The measurements have been performed at the four neutron scattering angles. See the reference quoted in the 2001 reference list for details.
As an example Fig. 4 shows the spectrum of the measured scintillation light for each event normalized to the expected kinetic recoil energy ($\simeq$ 2.5 MeV neutrons and scattering angle 145^0). As it can be easily inferred by this figure the recoil/electron light ratio is about 0.4. In particular, from the collected data, the following r values are obtained (0.41 ± 0.17), (0.46 ± 0.09), (0.37 ± 0.10) and (0.43 ± 0.08) at the mean recoil energy of 35 keV, 49 keV, 62 keV and 69 keV, respectively. The quoted errors include also the contribution from systematics due to calibration uncertainties in the given experimental situation, to geometry uncertainties and to neutron energy degrading in the thickness of the crossed vessels before entering the sensitive LXe volume.
In Fig. 5 the measured behaviour of r with the Xe nucleus recoil energy is shown; the r values measured in ref. [3] are also reported. As it can be seen, the present r determinations substantially agree with those of ref. [3]. The larger value found in the case of Am-B source data, which is averaged over a larger energy bin, could suggest a

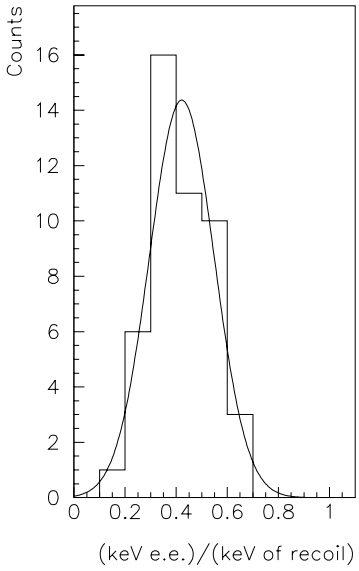

Figure 4: Scintillation light spectrum normalized to the expected kinetic energy of recoils measured by the pure LXe scintillator for neutron energy around 2.5 MeV.

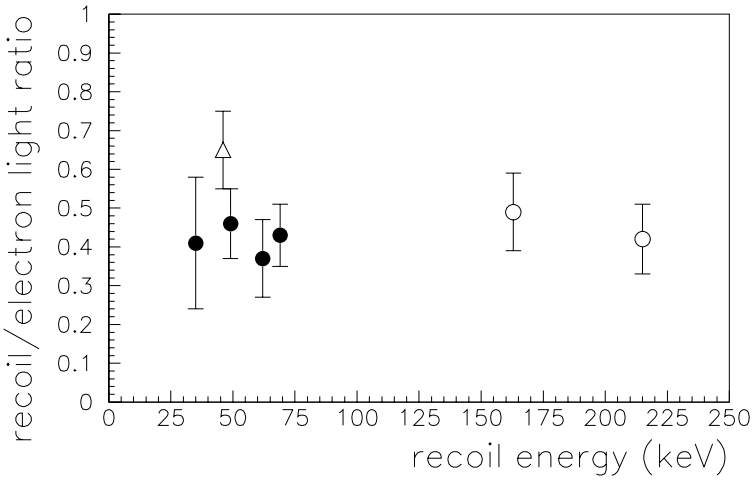

Figure 5: Measured behaviour of r with recoil energy: i) present experiment (filled circles); ii) values measured in ref. [3] (open circles: 14 MeV neutrons; open triangle: broadened Am-B neutrons). See text for comment.

behaviour with the recoil energy similar to those observed for other scintillators e.g. in ref. [41, 42, 43, 44]. The overall averaged value is: $r = 0.46 \pm 0.10$; this is in good agreement with the cautious value 0.44 used so far in our data analysis on WIMP search [3, 4].

For the sake of completeness, we mention that recoil/electron light ratios $\simeq 0.2$ are

quoted in ref. [45] [2]. However, we remark that: i) significant differences are often present in different experimental determinations of recoil/electron response for the same nuclei in detectors much more similar than those mentioned here; ii) in operating conditions, various specific experimental features (such as e.g. the initial purity of the used Xenon gas, the inner surface treatment, the reached vacuum before filling, the used purification line components and the degassing/release characteristics of all the materials of- and inside-the inner vessel, etc.) can give rise to the presence of different trace contaminants in different LXe set-ups which can differently affect the measured recoil/electron light ratio, similarly as different dopant concentrations in doped scintillators.

3.2 Search for $\beta\beta$ decay in ^{136}Xe

The $\simeq$ 6.5 kg liquid Xenon set-up of the DAMA experiment has been filled by Xenon enriched with 68.8% ^{136}Xe and data have been collected over a period of 6843.8 hours. The energy spectrum measured in the energy region 0.8 – 10 MeV is shown in Fig. 6. Since the experiment uses 6.5 kg of Xenon enriched at 68.8% [46] in ^{136}Xe, the collected useful statistics for the ^{136}Xe isotope is 3.49 kg $\times$ y.

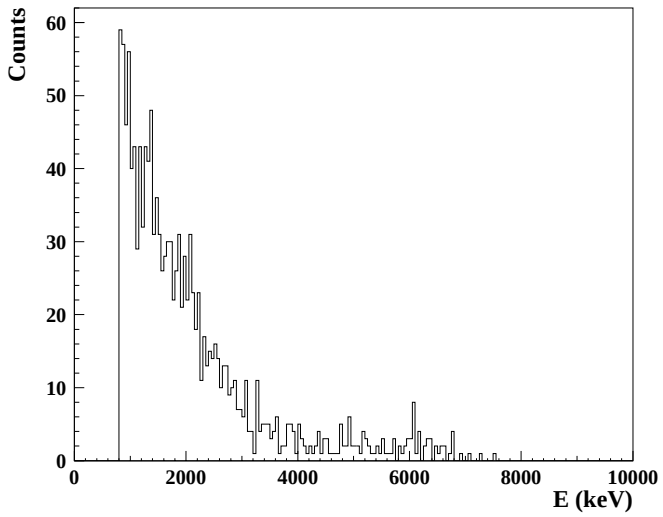

Figure 6: Experimental energy distribution (6843.8 hours). The energy bin is 50 keV.

The ^{136}Xe isotope is an excellent candidate to investigate $\beta\beta$ decay processes. In fact, the β decay to ^{136}Cs is kinematically forbidden; the natural abundance of the ^{136}Xe is appreciable (8.9 ± 0.1)% and enrichments are possible to obtain suitable sensitivity. Moreover, the mass difference between the ^{136}Xe and the daughter nucleus, ^{136}Ba, is large: (2.467 ± 0.007) MeV; this implies a large available phase space and, therefore, a large decay rate. This $\beta\beta$ decay can occur through the processes: i) $^{136}Xe \rightarrow^{136} Ba + 2e^-$; ii) $^{136}Xe \rightarrow^{136} Ba + 2e^- + 2\bar{\nu}_e$; iii) $^{136}Xe \rightarrow^{136} Ba + 2e^- + M$, where M indicates the

[2] Similar results were preliminary released by H. Wang in 1996 at IDM96 and this motivated an additional care also in our measurements 1998 [3].

Majoron. The response functions of the detector for the different $\beta\beta$ decay modes in ^{136}Xe were simulated by using EGS4 [47] and an event generator code [48]. Five possible processes have been simulated: i) $\beta\beta$ 2ν ($0^+ \rightarrow 0^+$); ii) $\beta\beta$ 2ν ($0^+ \rightarrow 2^+$); iii) $\beta\beta$ 0ν ($0^+ \rightarrow 0^+$); iv) $\beta\beta$ 0ν ($0^+ \rightarrow 2^+$); v) $\beta\beta$ $0\nu M$ ($0^+ \rightarrow 0^+$).

The $\beta\beta 0\nu$ decay modes have energy distributions almost completely contained in the considered energy window 0.8 – 3.25 MeV. The half-life limits for these channels have been obtained in two ways. Firstly, they have been evaluated by using the so-called "one σ approach": the excluded number of events for the considered decay channel is estimated as the square root of the number of background events in the given energy window, obtaining in this way: i) $T_{1/2} > 6.6 \cdot 10^{23}$ y (68% C.L.) for the $\beta\beta$ $0\nu(0^+ \rightarrow 0^+)$ decay mode; ii) $T_{1/2} > 4.1 \cdot 10^{23}$ y (68% C.L.) for the $\beta\beta$ $0\nu(0^+ \rightarrow 2^+)$ decay mode; iii) $T_{1/2} > 3.1 \cdot 10^{23}$ y (68% C.L.) for the $\beta\beta$ $0\nu M(0^+ \rightarrow 0^+)$ decay mode. Secondly, for each decay channel the number of events which could be ascribed to the considered decay mode has been determined by using the standard least squares method and by following the widely used procedure to fit the behaviour of the background in the considered energy interval with an empirical formula, obtaining for all the $\beta\beta$ 0ν channels results consistent with the absence of a signal. In this way we obtain: i) $T_{1/2} > 7.0 \cdot 10^{23}$ y (90% C.L.) for the $\beta\beta$ $0\nu(0^+ \rightarrow 0^+)$ decay mode; ii) $T_{1/2} > 4.2 \cdot 10^{23}$ y (90% C.L.) for the $\beta\beta$ $0\nu(0^+ \rightarrow 2^+)$ decay mode; iii) $T_{1/2} > 8.9 \cdot 10^{22}$ y (90% C.L.) for the $\beta\beta$ $0\nu M(0^+ \rightarrow 0^+)$ decay mode. For details see the reference given in the reference list of 2001. We note that the result for the decay channel $\beta\beta$ $0\nu(0^+ \rightarrow 0^+)$ has been obtained under the assumption that the right-handed currents can be neglected.

From these results upper limits on the effective neutrino mass, $\langle m_\nu \rangle$, and on the effective coupling constant Majoron-neutrino, $\langle g_M \rangle$ can be derived. Since these limits depend on the evaluation of the nuclear matrix elements, they have been calculated for various theoretical models [49, 50, 51, 52] as reported in Table 1. In addition, the result for the

Suhonen et al. [49]		Engel et al. [50]		Tomoda [51]		Muto et al. [52]	
$\langle m_\nu \rangle$ (eV)	$\langle g_M \rangle$ (10^{-5})	$\langle m_\nu \rangle$ (eV)	$\langle g_M \rangle$ (10^{-5})	$\langle m_\nu \rangle$ (eV)	$\langle g_M \rangle$ (10^{-5})	$\langle m_\nu \rangle$ (eV)	$\langle g_M \rangle$ (10^{-5})
< 1.8	< 5.9	< 2.2	< 7.1	< 1.5	< 4.8	< 1.8	< 5.7

Table 1: Upper limits on $\langle m_\nu \rangle$ and $\langle g_M \rangle$ achieved at 90% C.L. by the present experiment for the four different theoretical models of Ref. [49, 50, 51, 52].

decay mode $\beta\beta$ $0\nu(0^+ \rightarrow 0^+)$ can be extended to the more general case of the effective coupling constants $\langle \lambda \rangle$ (between right-handed leptonic and right-handed hadronic current) and $\langle \eta \rangle$ (between right-handed leptonic and left-handed hadronic current) different from zero. In Fig. 7 we plot the ellipsoid in the space ($\langle \lambda \rangle$, $\langle \eta \rangle$, $\langle m_\nu \rangle$) obtained from the present experimental data by considering the model by Muto et al. [52]. In this calculation the energy and angular distributions of the two outgoing electrons are (for simplicity) assumed to be the same as for the case $\langle \lambda \rangle = \langle \eta \rangle = 0$; this implies an uncertainty of about 5% in the ellipsoid evaluation.

We have also investigate the $\beta\beta$ 2ν decay mode in ^{136}Xe: $\beta\beta$ $2\nu(0^+ \rightarrow 0^+)$ and $\beta\beta$ $2\nu(0^+ \rightarrow 2^+)$. The efficiencies of these processes in the considered energy window are small; the energy distributions are smeared over a wider energy interval and the positions

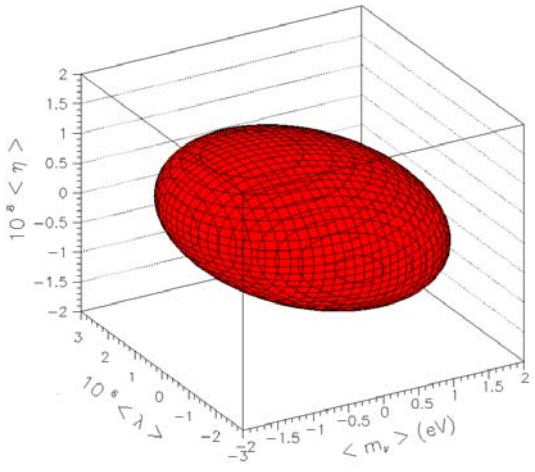

Figure 7: Ellipsoid obtained by considering the limit on the half-life for the decay channel $\beta\beta$ $0\nu(0^+ \rightarrow 0^+)$ obtained in this work. The values of $\langle m_\nu \rangle$, $\langle \lambda \rangle$ and $\langle \eta \rangle$ outside this ellipsoid are excluded at 90% C.L. by the present analysis.

of the maximum values are - contrary to the $\beta\beta 0\nu$ modes - practically outside or at the lowest energy limit in the considered energy window. Thus, to obtain the safest lower limits on the half-life of these $\beta\beta$ 2ν decay modes, they have been evaluated by setting the simple condition that a signal cannot exceed the measured differential counting rate. This gives rise to more modest but safer results; they have been obtained in two ways. Firstly, we consider the simple approach (which has been widely used e.g. also for the evaluation of exclusion limits in particle Dark Matter searches): the signal cannot exceed the experimental number of counts plus $n \times \sigma$ (where n gives the C.L.) in any energy interval, obtaining: i) $T_{1/2} > 1.0 \cdot 10^{22} y$ (90% C.L.) for the $\beta\beta$ $2\nu(0^+ \rightarrow 0^+)$ process; ii) $T_{1/2} > 0.9 \cdot 10^{22} y$ (90% C.L.) for the $\beta\beta$ $2\nu(0^+ \rightarrow 2^+)$ decay mode. Notwithstanding its simplicity, this method gives the right scale of the sensitivity of the experiment. Secondly, a more accurate and general standard procedure (widely used in literature to compare two distributions) has been considered by using the maximum likelihood function. In this way, we obtain: i) $T_{1/2} > 1.1 \cdot 10^{22} y$ (90% C.L.) for the $\beta\beta$ $2\nu(0^+ \rightarrow 0^+)$ process; ii) $T_{1/2} > 1.0 \cdot 10^{22} y$ (90% C.L.) for the $\beta\beta$ $2\nu(0^+ \rightarrow 2^+)$ decay mode.
In conclusion, new experimental limits have been obtained for the considered $\beta\beta$ decay processes in ^{136}Xe, improving the limits previously available by factors ranging between 1.5 and 65. Furthermore, upper bounds on the effective neutrino mass have been obtained by considering various theoretical models for the evaluation of the elements of the nuclear matrix; they vary between 1.5 eV and 2.2 eV (90% C.L.). Finally, in the framework of the same models we have also obtained upper limits on the effective coupling constant Majoron - neutrino; they range in the interval: $4.8 \cdot 10^{-5}$ and $7.1 \cdot 10^{-5}$ (90% C.L.).

Further data taking is in progress and various other data analyses on rare processes are under consideration.

4 R&D installation

The set-up named "R&D" is used for prototype tests and small scale experiments. During year 2001 new measurements with CaF_2(Eu) detectors have been performed in order to investigate the ordinary highly forbidden β decay, the $\beta\beta0\nu(0^+ \rightarrow 2^+)$ decay and the $\beta\beta2\nu(0^+ \rightarrow 2^+)$ in ^{48}Ca. In addition also a data taking with a CeF_3 scintillator has been carried out. Data analyses are in progress.

5 The low background DAMA Ge

Various R&D developments to improve low background set-ups and scintillators as well as new developments for higher radiopure PMTs are carried out. The related sample measurements are regularly carried out with the DAMA low background Ge detector running deep underground in the low background facility of the Gran Sasso Laboratory since many years.

6 Conclusions

The $\simeq$ 100 kg NaI(Tl) set-up is investigating for a 7^{th} annual cycle the WIMP annual modulation signature. The data of the 5^{th} and 6^{th} annual cycle are under analysis and further investigations on model dependent analyses are also in progress. In addition, works are in progress to build the $\simeq$ 250 kg NaI(Tl) LIBRA set-up.
The LXe set-up is running filled with Xenon enriched in ^{136}Xe.
The R&D set-up is running by using a BaF_2 scintillator.
The low background Ge is continuing the sample measurements.
Further data analyses to investigate various rare processes are continuing.

7 List of Publications during 2001

1. R. Bernabei, P. Belli, R. Cerulli, F. Montecchia, M. Amato, G. Ignesti, A. Incicchitti, D. Prosperi, C.J. Dai, H.L. He, H.H. Kuang, J.M. Ma, *Searching for signals from the dark Universe*, in the volume "Frontier objects in Astrophysics and Particle Physics", SIF Atti di Congressi vol. **73** (2001), 149.

2. R. Bernabei, P. Belli, R. Cerulli, F. Montecchia, M. Amato, G. Ignesti, A. Incicchitti, D. Prosperi, C.J. Dai, H.L. He, H.H. Kuang, J.M. Ma, *Results on the investigation of the WIMP annual modulation signature with the 100 kg NaI(Tl) set-up*, in the volume "The identification of Dark Matter", World sc. (2001), 331.

3. R. Bernabei, P. Belli, R. Cerulli, F. Montecchia, M. Amato, A. Incicchitti, D. Prosperi, C.J. Dai, *LXe DAMA experiment: results and perspectives*, in the volume "The identification of Dark Matter", World sc. (2001), 438.

4. R. Bernabei, M. Amato, P. Belli, R. Cerulli, C.J. Dai, H.L. He, G.Ignesti, A. Incicchitti, H.H. Kuang, J.M. Ma, F. Montecchia, D. Prosperi, *Recent results from the DAMA particle Dark Matter search*, in the volume "Cosmology and particle Physics, AIP conf. Proc. vol. **555** (2001), 189.

5. R. Bernabei, P. Belli, R. Cerulli, F. Montecchia, M. Amato, G. Ignesti, A. Incicchitti, D. Prosperi, C.J. Dai, H.L. He, H.H. Kuang, J.M. Ma, *Searching for signals from the dark Universe by DAMA at Gran Sasso*, Nucl. Phys. **B** (Proc. Supp.) **B91** (2001), 361.

6. R. Bernabei, M. Amato, P. Belli, R. Cerulli, C.J. Dai, H.L. He, A. Incicchitti, H.H. Kuang, J.M. Ma, F. Montecchia, D. Prosperi, *Investigating the DAMA annual modulation data in a mixed coupling framework*, Phys. Lett. **B 509** (2001), 197.

7. I. R. Barabanov, P. Belli, R. Bernabei, C.J. Dai, V. Gurentsov, A. Incicchitti, V. Kornukhov, E. Yanovich, *On the search for neutrino oscillation by artificial neutrino source*, New Journal of Physics **3** (2001), 5.1-5.7 (http://www.njp.org)

8. P. Belli, R. Bernabei, R. Cerulli, F. Montecchia, M. Amato, G. Ignesti, A. Incicchitti, D. Prosperi, C.J. Dai, H.H. He, H.H. Kuang, J.M. Ma, *Direct search for Dark Matter particles deep underground by DAMA experiment*, in the volume "Relativistic Astrophysics", 20th TEXAS SYMP., AIP (2001), 95.

9. R. Bernabei, P. Belli, A. Bussolotti, F. Cappella, R. Cerulli, C.J. Dai, A. Incicchitti, A. Mattei, F. Montecchia, D. Prosperi, *The liquid Xenon set-up of the DAMA experiment*, ROM2F/2001/09 and INFN/AE-01/02 on the on-line preprint at www.lngs.infn.it, to appear on **Nucl. Instr. & Meth**.

10. R. Bernabei, P. Belli, R. Cerulli, F. Montecchia, F. Nozzoli, A. Incicchitti, D. Prosperi, C.J. Dai, H.H. He, H.H. Kuang, J.M. Ma, S. Scopel, *Search for solar axions by Primakoff effect in NaI crystals*, Phys. Lett. **B 515** (2001), 6.

11. R. Bernabei, P. Belli, R. Cerulli, F. Montecchia, A. Incicchitti, D. Prosperi, C.J. Dai, M. Angelone, P. Batistoni, M.Pillon, *Light response of a pure Liquid Xenon scintillator irradiated by 2.5 MeV neutrons*, Eur. Phys. J.-direct **C11** (2001), 1.

12. P. Belli, R. Bernabei, M. Amato, F. Cappella, R. Cerulli, C.J. Dai, H.H. He, G. Ignesti, A. Incicchitti, H.H. Kuang, J.M. Ma, F. Montecchia, F. Nozzoli, D. Prosperi, *WIMP search by the DAMA experiment at Gran Sasso*, hep-ph/0112018 to appear in the Proc. of COSMO-01, Rovaniemi, Finland, August 2001.

13. R. Bernabei, M. Amato, P. Belli, F. Cappella, R. Cerulli, C.J. Dai, H.H. He, G. Ignesti, A. Incicchitti, H.H. Kuang, J.M. Ma, F. Montecchia, F. Nozzoli, D. Prosperi, *Results with the DAMA/NaI(Tl) experiment at LNGS*, to appear in the Proc. of TAUP-01, LNGS, September 2001

14. R. Bernabei, P. Belli, F. Cappella, R. Cerulli, C.J. Dai, A. Incicchitti, F. Montecchia, D. Prosperi, *Results with the DAMA/LXe experiment at LNGS*, to appear in the Proc. of TAUP-01, LNGS, September 2001

15. R. Bernabei, M. Amato, P. Belli, F. Cappella, R. Cerulli, C.J. Dai, H.H. He, G. Ignesti, A. Incicchitti, H.H. Kuang, J.M. Ma, F. Montecchia, F. Nozzoli, D. Prosperi, *Results with the DAMA experiment at LNGS*, to appear in the Proc. of "The LEP and SLC legacy", Siena, October 2001.

16. R. Bernabei, P. Belli, F. Cappella, R. Cerulli, F. Montecchia, A. Incicchitti, D. Prosperi, C.J. Dai, *Search for beta beta decay in ^{136}Xe at Gran Sasso*, INFN/AE-01/19 available as online preprint at www.lngs.infn.it, submitted for publication.

17. R. Bernabei, P. Belli, R. Cerulli, F. Montecchia, M. Amato, A. Incicchitti, D. Prosperi, C.J. Dai, H.L. He, H.H. Kuang, J.M. Ma, *Investigating the DAMA annual modulation data in the framework of inelastic Dark Matter*, Eur. Phys. J. **C** (2001) **DOI 10.1007/s100520100854**.

References

[1] P. Belli et al., Il N. Cim. C19 (1996), 537.

[2] R. Bernabei et al., Phys. Lett. B387 (1996), 222; Phys. Lett. B389 (1996), 783.

[3] R. Bernabei et al., Phys. Lett. B436 (1998), 379.

[4] R. Bernabei et al., New J. of Phys. 2 (2000), 15.1.

[5] R. Bernabei et al., Phys. Lett. B389, (1996), 757.

[6] R. Bernabei et al., Phys. Lett. B424, (1998), 195.

[7] R.Bernabei et al., Il N. Cim. A112 (1999), 545.

[8] R. Bernabei et al., Phys. Lett. B450 (1999), 448.

[9] R. Bernabei et al., Il N. Cim. A112 (1999), 1541.

[10] P. Belli et al., Phys. Rev. D61 (2000), 023512.

[11] R. Bernabei et al., Phys. Lett. B480 (2000), 23.

[12] R. Bernabei et al., Eur. Phys. J. C18 (2000), 283.

[13] R. Bernabei et al., Astrop. Phys. 7 (1997), 73.

[14] P. Belli et al., Nucl. Phys. B563 (1999), 97.

[15] R. Bernabei et al., Astrop. Phys. 4 (1995), 45; R. Bernabei,"Competitiveness of a very low radioactive ton scintillator for particle Dark Matter search", in the volume *The identification of Dark Matter*, World Sc. pub. (1997), 574; I. R. Barabanov et al., Astrop. Phys. 8 (1997), 67; I. R. Barabanov et al., Nucl. Phys. B546 (1999), 19.

[16] P. Belli et al., Astrop. Phys. 5 (1996), 217; R. Bernabei et al., Il N. Cim. A110 (1997), 189; R. Bernabei et al., Phys. Lett. B408 (1997), 439; R. Bernabei et al., Il N. Cim. A111, 347 (1998) & Il N. Cim. A, oct. 1998; P. Belli et al., Astrop. Phys. 10 (1999), 115; P. Belli et al., Phys. Rev. C60 (1999), 065501; P. Belli et al., Phys. Lett. B460 (1999), 236; P. Belli et al., Phys. Lett. B465 (1999), 315; R. Bernabei et al., Phys. Rev. Lett. 83 (1999), 4918; P. Belli et al., Phys. Rev. D61 (2000), 117301; R. Bernabei et al., Phys. Lett. B493 (2000), 12.

[17] D.E. Groom et al., Eur. Phys. J. C15 (2000), 1 revised version on september 2001 about Dark Matter, available on the web.

[18] A. Bottino et al., Phys. Lett. B402, 113 (1997); Phys. Lett. B423, 109 (1998); Phys. Rev. D59 (1999), 095004; Phys. Rev. D59 (1999), 095003; Astropart. Phys. 10 (1999), 203; Astropart. Phys. 13, 215 (2000); Phys. Rev. D62 (2000) 056006; Phys.Rev. D62 (2000) 056006; hep-ph/0010203; hep-ph/0012377.

[19] R.W. Arnowitt and P. Nath, Phys. Rev. D60 (1999), 044002; E. Gabrielli et al., hep-ph/0006266;

[20] D. Fargion et al., Pis'ma Zh. Eksp. Teor. Fiz. 68, (JETP Lett. 68, 685) (1998); Astropart. Phys. 12, 307 (2000).

[21] D. Smith and N. Weiner, Phys. Rev. D64 (2001) 043502.

[22] K. van Bibber, P.M. McIntyre, D.E. Morris and G.G. Raffelt, *Phys. Rev.* **D39** (1989) 2089.

[23] A.O. Gattone et al., *Nucl. Phys.* **B** (Proc. Suppl.) 70 (1999) 59.

[24] E.A. Pascos and K. Zioutas, *Phys. Lett.* **B323** (1994) 367.

[25] A. Morales et al., *hep-ex/0101037*.

[26] S. Cebrián et al., *Astropart. Phys.* **10** (1999) 397.

[27] C. Hagmann et al., *Phys. Rev. Lett.* **80** (1998) 2043; S. Matsuki, talk given at the II International Workshop on the Identification of Dark Matter (IDM98), Buxton, England, 7–11 September 1998.

[28] S. Moriyama et al., *Phys. Lett.* **B434** (1998) 147.

[29] Particle Data Group, R.M. Barnett et al., *Phys. Rev.* **D54** (1996) 1.

[30] J. Lindhard et al., Mat-Fys. Medd. **33** (1963) 10.

[31] P. Belli et al., Nucl. Instr. and Meth. A316 (1992) 55.

[32] P. Belli et al. Nucl. Instr. and Meth. A336 (1993) 336.

[33] M. Tanaka et al. Nucl. Instr. and Meth. A457 (2001) 454 and references therein.

[34] T.Doke et al., Nucl. Instr. and Meth. A291 (1990) 617.

[35] T. Doke et al. Nucl. Instr. and Meth. A327 (1993) 113.

[36] G. J. Davies et al., Phys. Lett. B320 (1994) 395.

[37] K. Fushimi et al., Phys. Rev. C47 (1993) R425.

[38] M. Martone et al., J. Nucl. Mat. 212-215 (1994) 1661; M. Pillon et al., Fus. Engin. and Design 28 (1995) 683; M. Angelone et al., Rev. Sci. Instr. 67 (1996) 2189.

[39] SAES Getters, Milano, Italy.

[40] R. Bernabei et al., Nucl. Instr. & Meth. A269 (1988), 167.

[41] T. Kishimoto et al., 2nd Resceu Int. Workshop Tokyo 1996.

[42] N.J.C. Spooner, paper available on
www.shef.ac.uk/ phys/research/pa/directional-0397.html.

[43] D. R. Tovey et al., Phys. Lett. B433 (1998) 150.

[44] S. Pecourt et al., Astrop. Phys. 11(1999) 457.

[45] F. Arneodo et al., Nucl. Instr. and Meth. A449 (2000) 147; D. Akimov et al., hep-ex/0106042.

[46] M. Balata, ISRIM measurements on 2000, private comm.

[47] W. R. Nelson et al., SLAC-265, UC-32 (E/I/A).

[48] F. Cappella, Thesis, Univ. Roma "Tor Vergata" A.A. 2000/2001.

[49] J. Suhonen et al., Nucl. Phys. A535 (1991) 91.

[50] J. Engel et al., Phys. Rev. C37 (1988) 731.

[51] T. Tomoda, Rep. Prog. Phys. 54 (1991) 53.

[52] K. Muto, E. Bender and H. V. Klapdor, Z. Phys. A334 (1989b) 187.

EAS-TOP. Cosmic Ray Experiment

M. Aglietta[a,b], B. Alessandro[b], P. Antonioli[c], F. Arneodo[d], L. Bergamasco[b,e], M. Bertaina[b,e], C. Castagnoli[a,b], A. Castellina[a,b], A. Chiavassa[b,e], G. Cini Castagnoli[b,e], B. D'Ettorre Piazzoli[f], G. Di Sciascio[f], W. Fulgione[a,b], P. Galeotti[b,e], P.L. Ghia[a,b], M. Iacovacci[f], G. Mannocchi[a,b], C. Morello[a,b], G. Navarra[b,e], O. Saavedra[b,e], G. C. Trinchero[a,b], , S. Valchierotti[b,e] P. Vallania[a,b], S. Vernetto[a,b], C. Vigorito[b,e]

[a] Istituto di Cosmo-Geofisica del CNR, Torino, Italy
[b] Istituto Nazionale di Fisica Nucleare, Sezione di Torino, Italy
[c] Istituto Nazionale di Fisica Nucleare, Sezione di Bologna, Italy
[d] Istituto Nazionale di Fisica Nucleare, LNGS, Assergi, L'Aquila, Italy
[e] Dipartimento di Fisica Generale dell'Università di Torino, Italy
[f] Dipartimento di Scienze Fisiche dell' Università and INFN, Sezione di Napoli, Italy

Abstract

The aim of the EAS-TOP experiment is the study of cosmic ray physics in the energy range between the direct measurements and the "giant" air shower arrays ($E_0 = 10^{13} \div 10^{16}$ eV). The array, located at Campo Imperatore, 2000 m a.s.l., 30^0 with respect to the vertical of the underground Gran Sasso Laboratories, has been in operation, in different configurations, between January 1989 and May 2000. Results have been reported on different items of cosmic ray physics: (i) the primary spectrum in the energy range overlapping the direct measurements, (ii) the characteristics of the *knee* in different EAS components, (iii) the spectrum and primary composition in the *knee* energy region ($E_0 = 10^{15} \div 10^{16}$ eV), (iv) EAS phenomenology, (v) anisotropies, (vi) gamma ray sources, (vii) the origin of penetrating showers, and (viii) some aspects of high energy interactions relevant for the interpretation of EAS data ($p - air$ cross section, large p_t events, reliability of high energy interaction models).

1 Introduction

The construction of the experimental knowledge of the physics of cosmic radiation requires the study of different aspects, such as the primary spectra and composition, the anisotropies, the primary gamma and neutrino radiations. Moreover, at energies beyond

10^{14} eV, measurements cannot be direct anymore: they have to be performed through the detection of the components of Extensive Air Showers (EAS), in a region in which the information on hadron interactions (*p-p, p-N*) from accelerator measurements is still not complete.

Figure 1: *Aerial view of part of the EAS-TOP array during winter time. The e.m. modules are visible out of the snow; the muon detector is located inside the shed on top of the picture.*

The EAS-TOP experiment has thus been planned for the study of the different aspects of cosmic ray physics in the energy range $E_0 = 10^{13} \div 10^{16}$ eV, between the direct measurements and the "giant" EAS arrays. This range includes the region of the "knee" of the primary spectrum ($E_0 = 10^{15} \div 10^{16}$ eV), whose understanding can provide a clue to the origin of galactic cosmic radiation. Such investigation requires the detection of different EAS components (e.m., hadron, Cherenkov light, GeV and TeV muons), which are essential to test the main features of hadronic interactions at ultra high energies, relevant for the extrapolation of the models elaborated from the accelerator data. On the other side, the lower energy range ($E_0 = 10^{13} \div 10^{14}$ eV) overlaps the direct measurements, and provides therefore a test of the methodologies used in EAS analysis, and new information in the region in which the balloon and satellite experiments lose statistics and the energy determination becomes non-calorimetric. In both energy ranges, the EAS-TOP location, above the underground Gran Sasso laboratories, with the unique possibility of surface and deep underground measurements, gives the possibility of exploiting the TeV muon number. This indeed represents a new important observable providing: a) the high energy secondary content produced above the central region in the analysis at the knee, and b) the selection of primaries based on their energy/nucleon and the reconstruction of the EAS geometry at the lower energies.

The surface-underground connection provides furthermore new data for the interpretation of the deep underground measurements, the understanding of the background and the calculation of event rates.

2 The detectors

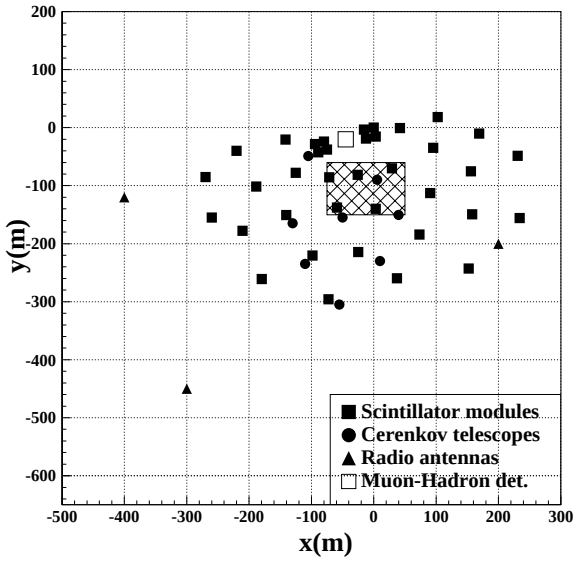

Figure 2: *The EAS-TOP array. The shaded area shows the core location region used for the N_e spectrum measurement.*

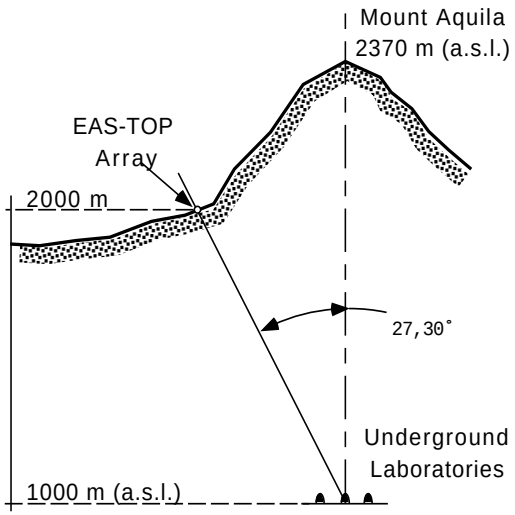

Figure 3: *The EAS-TOP array location with respect to the underground Gran Sasso laboratories.*

The basic detector configuration, shown in figs. 1-3, together with the array location with respect to the underground Gran Sasso Laboratories, consisted of:

- the e.m. detector: 35 modules of scintillators, 10 m^2 each, fully efficient for $N_e > 10^5$, for the measurement of the shower size (N_e), the core location and the arrival direction;

- the muon-hadron detector: 140 m^2 calorimeter with 9 layers of 13 cm iron absorbers and Iarocci tubes as active elements, operating in "quasi proportional" mode for hadron calorimetry at $E_h > 50$ GeV, and in streamer mode for muon counting at $E_\mu > 1$ GeV;

- the Cherenkov light detector: 8 telescopes with tracking capabilities loading 0.5 m^2 area light collectors equipped with imaging devices (96 pixels each with resolution 1.5 10^{-5} sr) and wide angle optics (7 photomultipliers for a total field of view of 0.16 sr);

- three radio antennas for EAS radio emission measurements;

- moreover, it operated in coincidence with the underground MACRO and LVD muon detectors ($E_\mu > 1.3$ TeV; full area $A_\mu^{\rm TeV} \approx 1000$ m^2).

The array has been implemented in the course of time: a) to improve the response to very inclined showers, with vertical scintillators in eight modules, and two vertical walls made of streamer tubes at the North and South sides of the calorimeter; b) for muon counting, with 130 m^2 scintillator detectors distributed in the field, shielded with 30 cm

iron absorber; c) for muon timing, with 40 m^2 RPC positioned below the bottom layer of the calorimeter [1]; d) for C.l. observation at high energies, with five QUASAR-370 photomultipliers, in cooperation with the TUNKA group of Institute for Nuclear Physics of Moscow State University [2].

The experiment results from a collaboration between INFN and CNR (Istituto di Cosmo-Geofisica, Torino).

To illustrate the characteristics of the detectors, some of their resolutions are shown in figs. 4-7 and described in the relative captions (figs. 4 and 5 for the e.m. detector, fig. 6 for the imaging Cherenkov, fig. 7 for the hadron calorimeter).

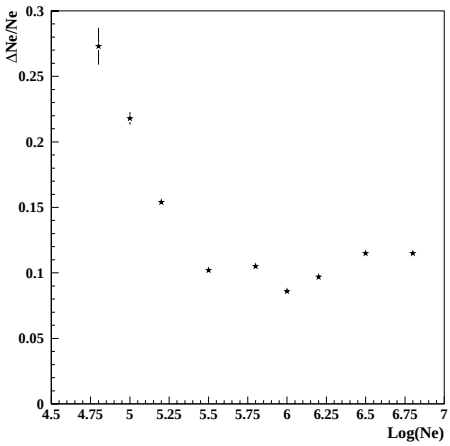

Figure 4: *Accuracy ($\Delta N_e/N_e$) in the determination of the shower size vs N_e. For zenith angles θ between 0° and 40° no dependence of the reconstruction accuracy on zenith angle is observed.*

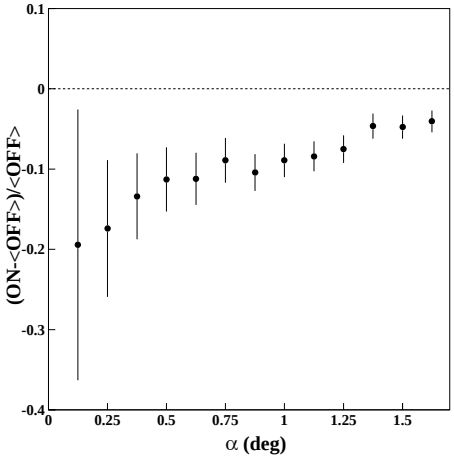

Figure 5: *The "moon shadow", represented as the fractional difference between the number of counts recorded inside a cone of aperture α around the center of the moon and those measured in two reference regions. The resulting angular resolution is 0.85º for all internal triggers, and 0.5º for $N_e > 10^5$.*

3 Results

The main results reported by EAS-TOP are summarized in the following.

[1] *Collaboration with: M. Ambrosio, C. Aramo, G. Battistoni, R. Fonte, A. Grillo.*

[2] *Collaboration with: E.E. Korosteleva, L.A. Kuzmichev, B.K. Lubsandorjev, V.V. Prosin.; work supported by INTAS under grant 96-0526 (coordinator A.M. Hillas).*

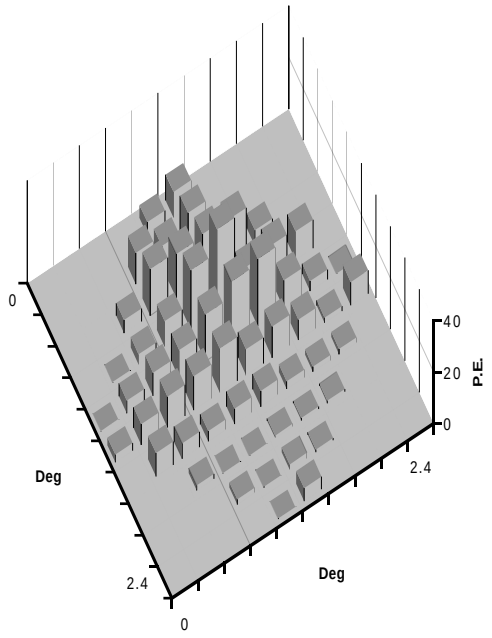

Figure 6: *Cherenkov light image as seen by an high resolution pmt.*

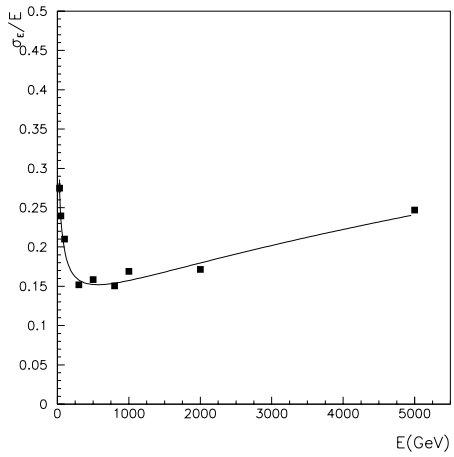

Figure 7: *Single hadron energy resolution of the calorimeter.*

3.1 The connection with the direct experiments

3.1.1 The hadron spectrum

The hadron spectrum in the atmosphere retains significant information on the primary energy/nucleon spectrum, which is dominated by the proton component. The explored primary energy range overlaps the direct measurements in a region in which their statistics becomes poor and whose knowledge is relevant for the interpretation of deep underground data. Hadron measurements are performed through the calorimeter by selecting large energy losses by means of a set of scintillators located below the second absorber layer; each of them is discriminated at the level of 30 particles, corresponding to an energy threshold $E_h^{th} \approx 30$ GeV. The total charge induced on the pads reading the proportional chambers of the 8 inner planes over an area of 1.3 m^2 is measured and converted to the equivalent number of vertical particles (N_{vp}) by means of calibration runs (periodically performed using single muon triggers). The conversion from N_{vp} to hadron energy is obtained through a simulation based on the Geant code, that includes the response of the chambers (see fig. 8). The chamber response itself has been calibrated in a beam test at CERN up to a particle density corresponding to 700 GeV hadron energy in the actual calorimeter configuration. The measured hadron flux at the atmospheric depth x=820 gcm^{-2}, between 30 GeV and 30 TeV, shown in fig. 9, is well represented by a single power law:

$S(E_h) = (2.25 \pm 0.21 \pm 0.34^{sys})\ 10^{-7}(\frac{E_h}{1000\ \mathrm{GeV}})^{(-2.79\pm0.05)}\ \mathrm{m^{-2}s^{-1}sr^{-1}GeV^{-1}}$.

The systematic uncertainties amount to 14% energy dependent (included in fig. 9 and in the fit), and 15% energy independent (i.e. resulting in a possible systematic shift). The code used to describe the cosmic ray interaction and propagation in the atmosphere (CORSIKA/QGSJET) has been tested by comparing its predictions to the measured ratio of hadron fluxes between sea level (KASCADE, 1000 gcm^{-2}) and mountain altitude (EAS-

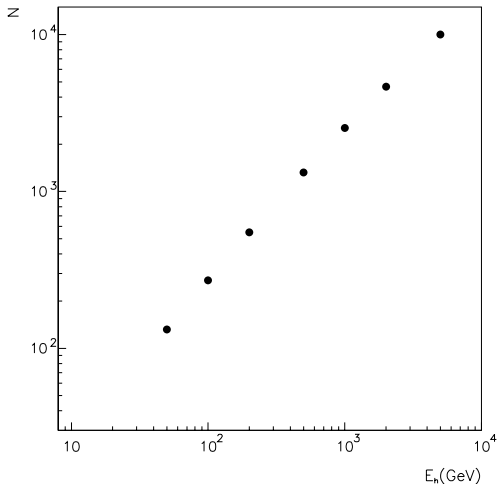

Figure 8: *Total number of induced equivalent particles in the calorimeter versus hadron energy.*

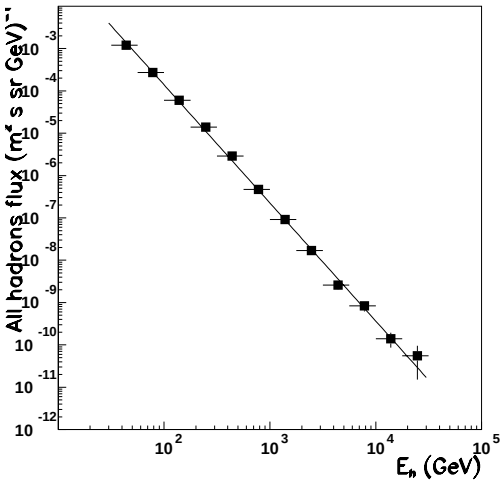

Figure 9: *The measured hadron flux at 820 gcm^{-2}.*

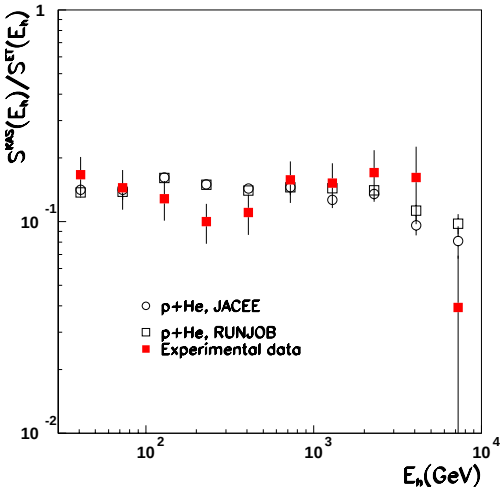

Figure 10: *Ratio of the experimentally measured hadron fluxes by KASCADE and EAS-TOP (full squares) compared to the expectation from the proton+helium primary spectra by JACEE (circles) and RUNJOB (squares).*

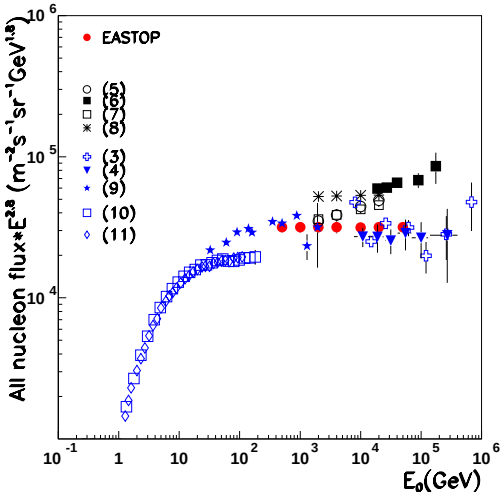

Figure 11: *The primary all nucleon spectrum (times $E^{2.8}$) as derived from hadron data. Results from other experiments are shown for comparison.*

TOP, 820 gcm^{-2}). Primary protons and helium nuclei were generated in quasi vertical direction ($\theta \leq 5^\circ$) with energy spectra according to JACEE and RUNJOB, calculating the expected hadron fluxes at each given observation level. The comparison between the calculated and measured ratios is shown in fig. 10: the experimental ratio is reproduced at better than 20 % by the simulation, independently on the used primary spectrum, in the considered energy range. The model can thus be reliably used to calculate the hadron propagation in the same energy range between the top of the atmosphere and the EAS-TOP observation level.

Assuming that all recorded hadrons are produced by primary protons, the primary "all nucleon" spectrum is obtained. It is in good agreement with the direct measurements (see fig. 11), and can be represented by a single power law:

$S(E_0) = (0.126 \pm 0.019 \pm 0.019^{sys})\ 10^{-3} (\frac{E_0}{1000})^{(-2.80^{+0.06}_{-0.08})}$ m^{-2}s^{-1}sr^{-1}GeV^{-1}.

By subtracting the helium contribution as measured from the direct experiments and taking into account its uncertainty, the primary proton spectrum has been obtained. It amounts to about 80% of the reported all nucleon flux and results also in good agreement with the JACEE and RUNJOB data.

3.1.2 The Cherenkov light and high energy muon data

The EAS-TOP and underground (MACRO, LVD) arrays offer a unique opportunity to study the energy range 10 $\div$ 100 TeV by selecting the primaries through their energy/nucleon by means of the TeV muon information (that further allows the reconstruction of the EAS core geometry), and by measuring the lateral distribution and spectrum of Cherenkov light (related to the total primary energy) with the surface telescopes. Due to the shower selection through the high energy muons ($E_\mu > 1.3$ TeV, i.e. primary energy $E_o > 1.3$ TeV/nucleon), in the energy range 10 TeV $< E_o <$ 40 TeV the selected primaries are mainly protons, while for 40 TeV $< E_o <$ 100 TeV they include both p and α particles.

We discuss here the combined EAS-TOP and MACRO analysis. The lateral distribution is constructed using the constant intensity cut technique: integral photon spectra corresponding to muon directions identifying shower cores falling inside 6 coronae around the Cherenkov telescopes (r $\in$ [0,20], [20,35], [35,50], [125,145], [145,165], [165,185] m) have been considered. The number of photons corresponding to the same rate in each corona are used to construct the lateral distribution. Frequencies are selected according to expression:

$$f\,(E > E_o) = \int_{E_o}^{\infty} \frac{dN_p}{dE} \cdot p_p^{\mu}(E) dE + \int_{E'_o}^{\infty} \frac{dN_{He}}{dE'} \cdot p_{He}^{\mu}(E') dE'$$

where E$_o$ and E'$_o$ represent respectively the proton and helium energies giving similar lateral distributions. $\frac{dN_p}{dE}$ and $\frac{dN_{He}}{dE}$ are the differential primary spectra: the JACEE and RUNJOB data have been used, with CORSIKA-QGSJET as interaction-propagation code in the atmosphere. As it can be seen from fig. 12, the experimental points match very well the simulated ones according to the JACEE proton and helium spectra, while the agreement is worse when frequencies are calculated using the RUNJOB data (fig. 13). This has to be ascribed to the lower contribution of the α component in the RUNJOB spectra, leading to a lower total intensity for the lightest components.

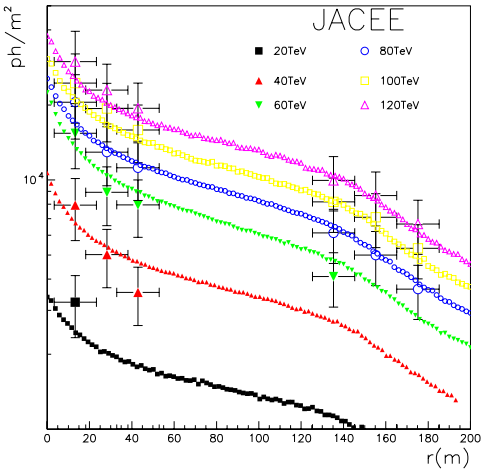

Figure 12: *Measured C.l. lateral distributions compared with simulated ones (290 $< \lambda <$ 630 nm) using the JACEE spectra.*

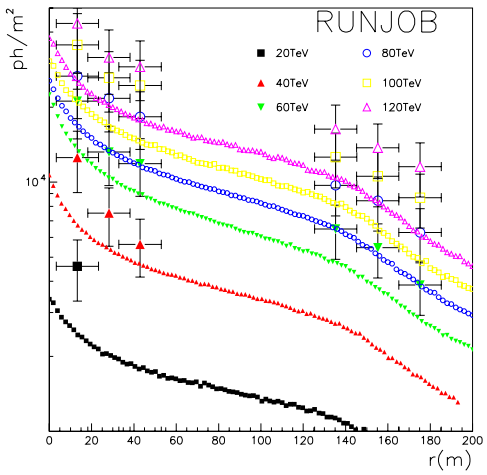

Figure 13: *Same as fig. 12 using the RUNJOB spectra.*

The errors on the x axis represent the widths of the coronae (uncertainties on the individual core locations), while, on the y axis, statistical and systematic errors are summed up in quadrature. The systematic error is of the order of 20% and its effect could result in a possible scaling of all curves without changing their shape. The shape of the l.d.f. reflects the rate of energy release in the atmosphere (i.e. the properties of the interaction, the primaries being dominated by the lightest components due to the TeV muon trigger requirement) while the absolute scale is mostly related to the event rate, i.e. the primary p and α spectra. The agreement of both of them (see fig. 12) shows both the adequacy of the CORSIKA-QGSJET code in describing the cascades in this energy range, and of the JACEE data in the 20 $\div$ 120 TeV region.

3.2 The knee region

3.2.1 The e.m. and muon size spectra

The discovery of the "knee" (about 40 years ago) was followed by a long debate, whether its origin should be ascribed to "astrophysical" or "hadron physics" reasons. Therefore the first goal of the present generation of experiments has been the best definition of the characteristics of the knee as observed in different EAS components also to verify their compatibility inside the known hadron interaction properties.

The measured shower size and muon size spectra around the knee are shown in figs. 14 and 15. The break in the N_e spectra results rather "sharp", the change in slope being limited in a region of $\Delta Log(N_e) \approx 0.1$, i.e. inside about 30% variation of N_e (the sharpness of the break of the N_μ spectrum is softened by the poissonian fluctuation of the number of detected muons). The best estimate of the knee energy is (2.7; 3.4; 4.1) PeV for proton,

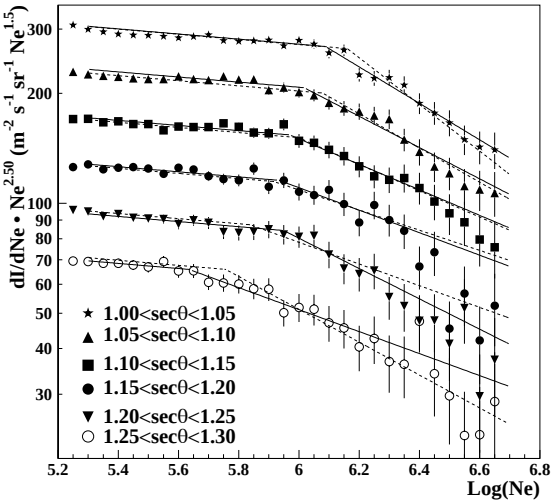

Figure 14: *Differential shower size spectra measured at different zenith angles (i.e. atmospheric depths), showing the knee position, and its shift with zenith angle.*

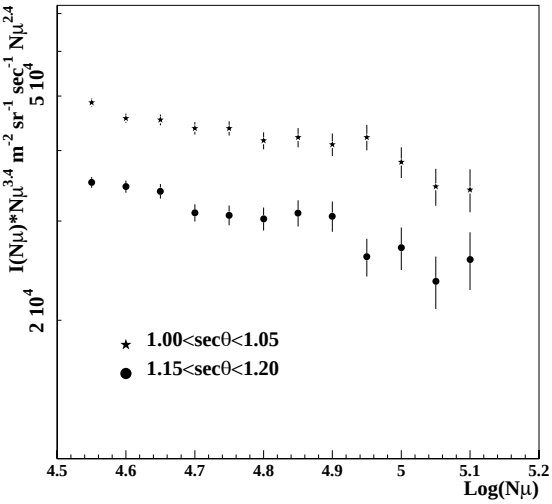

Figure 15: *Differential muon number spectra measured in two different intervals of zenith angles (i.e. atmospheric depths).*

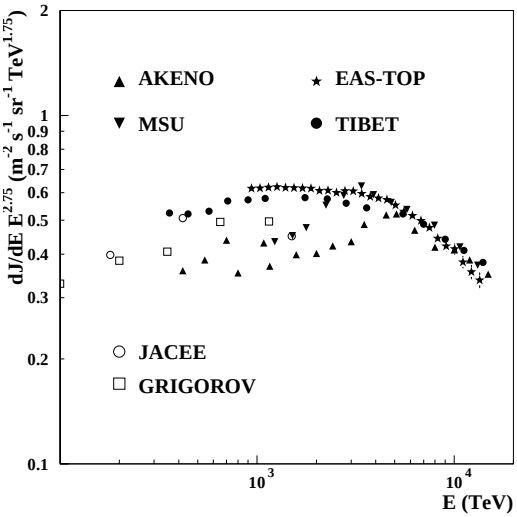

Figure 16: *The all particle energy spectrum obtained from the EAS-TOP shower size data, compared with the results of other experiments operating outside the atmosphere or at ground level.*

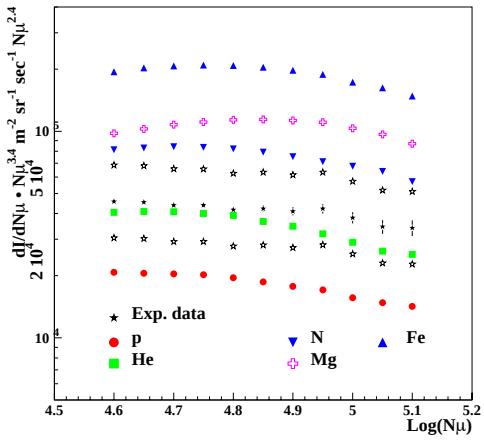

Figure 17: *Experimental muon number spectrum compared with the expectations from individual primaries, whose energy spectra reproduce the N_e one in the region of the knee. The upper and lower limits resulting from 10% systematic uncertainty in the muon number are also shown for the experimental data (empty stars).*

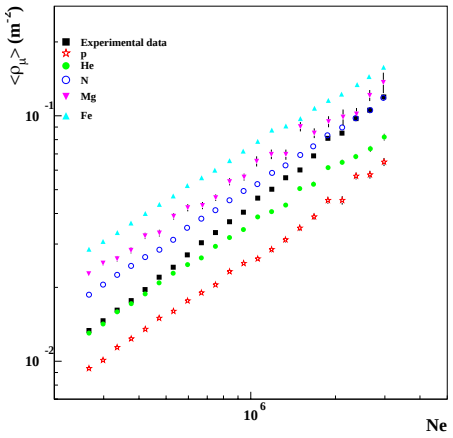

Figure 18: $< \rho_\mu^{200} >$ *vs* N_e *relation (measured and expected from individual elements for* $\gamma = 2.75$*) for all components.*

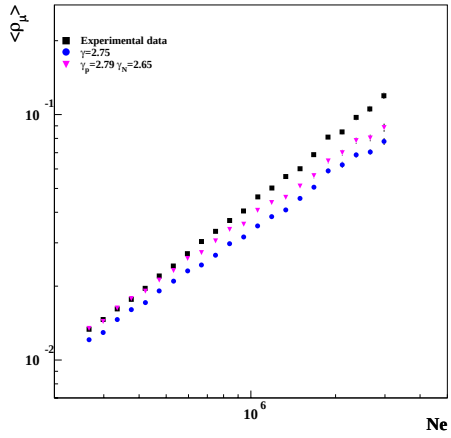

Figure 19: $< \rho_\mu >^{200}$ *vs* N_e *relation for mixed compositions obtained from the extrapolation of the direct data at 1 TeV with same spectral indexes and a steeper proton spectrum.*

helium and CNO primaries respectively; the all particle energy spectrum (obtained with the hypothesis of increasing primary mass, and HDPMJET hadron interaction code) is shown in fig. 16.

We remind here the observation (reported by EAS-TOP first) of the dependence of the shower size value at the knee (N_e^k) on the atmospheric depth (i.e. zenith angle), of the consistent relation between the N_e and N_μ spectra below and above the knee (see tabs. 1 and 2), of the knee in the muon number (N_μ^k), and of the constant intensities above the knee observed at different angles for both components, proving that the observed spectral break is a real effect characterized by given primary mass and energy, without the observation of any anomaly requiring changing properties of the hadron interaction.

From the comparison of the N_e and N_μ size spectra a first information on the bending component at the knee can be obtained. Indeed, due to the observations of the bending of both the N_e and N_μ spectra and their good consistency, the hypothesis that around the knee we observe the spectra of the same (unique) component is quite reasonable. Therefore, we can construct primary energy spectra for the different components reproducing the N_e spectrum, and from them obtain the associated N_μ size spectra. The results are shown in fig. 17: the experimental data coincide quite well with the expectations from helium primaries. CORSIKA/QGSJET is used for simulations: proton and nitrogen primaries are compatible with the data, if 10% systematic uncertainties are assumed.

3.2.2 The composition from the e.m. and GeV muon data

The composition analysis is performed for vertical showers ($1.00 < \sec\theta < 1.05$) in the range of size $5.4 < \mathrm{Log}(N_e) < 6.6$, i.e. just across the knee ($\mathrm{Log}(N_e) \simeq 6.13$). The parameters used in the analysis are the shower size N_e and the muon number observed in the muon detector at core distances $180 \div 210$ m ($N_{\mu_{200}}$) providing the muon den-

Table 1: *Parameters of the Ne spectra in different intervals of zenith angles.*

$\Delta \sec\theta$	γ_1	γ_2	$I(> Ne_k) \times 10^7$ m^{-2} s^{-1} sr^{-1}	$Log(Ne_k)$
$1.00 - 1.05$	2.56 ± 0.02	2.99 ± 0.09	0.99 ± 0.2	6.09 ± 0.05
$1.05 - 1.10$	2.55 ± 0.02	2.93 ± 0.11	1.01 ± 0.3	6.02 ± 0.07
$1.10 - 1.15$	2.55 ± 0.03	2.85 ± 0.12	0.93 ± 0.4	5.97 ± 0.08
$1.15 - 1.20$	2.56 ± 0.03	2.81 ± 0.16	0.80 ± 0.4	5.93 ± 0.14
$1.20 - 1.25$	2.59 ± 0.03	2.91 ± 0.26	0.52 ± 0.3	5.95 ± 0.11
$1.25 - 1.30$	2.55 ± 0.07	2.80 ± 0.11	1.30 ± 0.6	5.63 ± 0.12

Table 2: *Parameters of the $N\mu$ spectra in different intervals of zenith angles (the analysis is performed in terms of $\rho_\mu^{r=150\mathrm{m}}$; here N_μ is given for easier comparison, by using the average l.d.f.).*

$\Delta \sec\theta$	γ_1	γ_2	$I(> N\mu_k) \times 10^7$ m^{-2} s^{-1} sr^{-1}	$Log(N\mu_k)$
$1.00 - 1.05$	3.18 ± 0.07	3.44 ± 0.10	1.32 ± 0.3	4.66 ± 0.10
$1.05 - 1.10$	3.23 ± 0.15	3.40 ± 0.12	1.03 ± 0.3	4.62 ± 0.10
$1.10 - 1.15$	3.20 ± 0.07	3.34 ± 0.12	1.09 ± 0.3	4.65 ± 0.12
$1.15 - 1.20$	3.12 ± 0.10	3.45 ± 0.15	1.28 ± 0.3	4.60 ± 0.10

sity $\rho_\mu = \rho_{\mu_{200}}$. The observed average $< \rho_\mu >$ vs N_e relation is compared in fig. 18 with the expectations from individual components obtained with simulations based on CORSIKA/QGSJET. The experimental data drift, with increasing shower size, from the average primary mass of helium to the nitrogen one in the simulated data. Different interaction models (always in the CORSIKA frame) lead to similar results. In fig. 19 the experimental data are compared with the expectations from the extrapolation of the direct measured fluxes at 1 TeV with: a) same spectral indexes ($\gamma = 2.75$), and b) a steeper proton spectrum ($\gamma_p = 2.79$), against $\gamma_n = 2.65$ for all heavier nuclei. This shows both the good agreement at the lower energies with the direct data, and the insufficiency of such extrapolation to explain the increasing slope of the $N_\mu - N_e$ relation.

The evolution of the abundances of the individual components has been studied by fitting the experimental $N_{\mu_{200}}$ distributions, measured in different ranges of shower sizes ($\Delta Log(N_e) = 0.2$), with simulated distributions. A satisfactory description of the experimental data has been obtained with a three component composition: light, intermediate and heavy. The light component is constructed with a mixture of 50% proton and 50% helium, the intermediate is represented by N and the heavy by Fe. The relative abundances of the three elements in each range of N_e are obtained directly from the fits to the $N_{\mu_{200}}$ distribution (see e.g. fig. 20).

The relative abundances in the six ranges of shower sizes are given in fig. 21, in which the decreasing weight of the light component is observed. From these abundances, using the experimental size spectrum, and converting to energy with the same simulation, the energy spectrum of each component is derived (see fig. 22). The evolution of $< logA >$ vs energy obtained from these spectra is plotted in fig. 23. The three analysis (comparison of

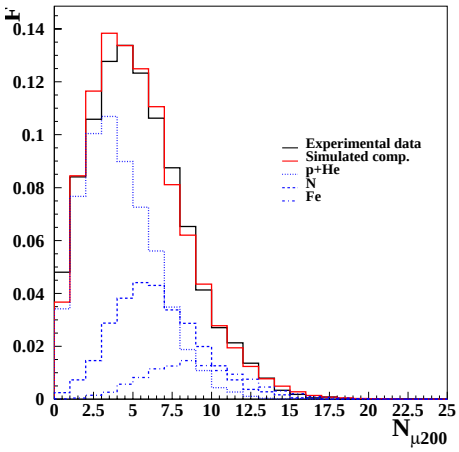

Figure 20: *$N_{\mu 200}$ distributions: data and three components fit in the range $5.8 < Log(N_e) < 6.0$. The contribution of each element is also plotted (e.m. and GeV muon data).*

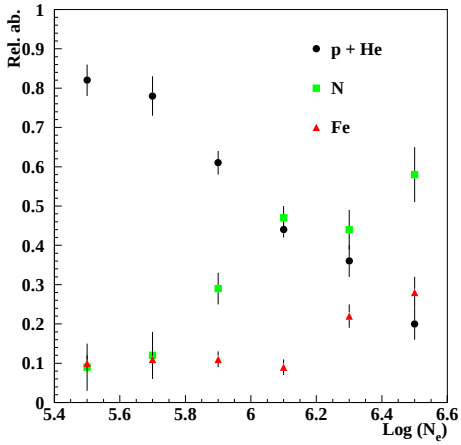

Figure 21: *Relative abundances of the three components in different intervals of shower sizes from the e.m. and GeV muon data.*

the spectra of the e.m. and muon size numbers, evolution of the average $N_\mu - N_e$ relation, slopes of the light, medium and heavy contributions) lead to a composition becoming heavier at the knee due to a break in the spectrum of a light component.

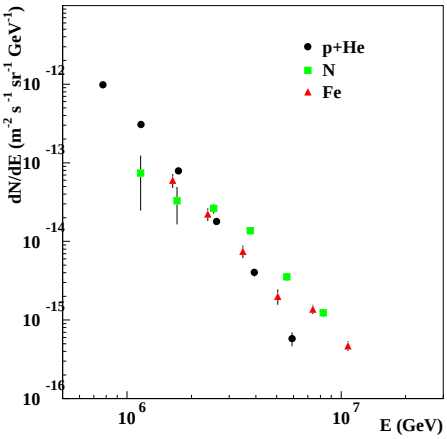

Figure 22: *Energy spectra of the p+He , N and Fe with the three components model.*

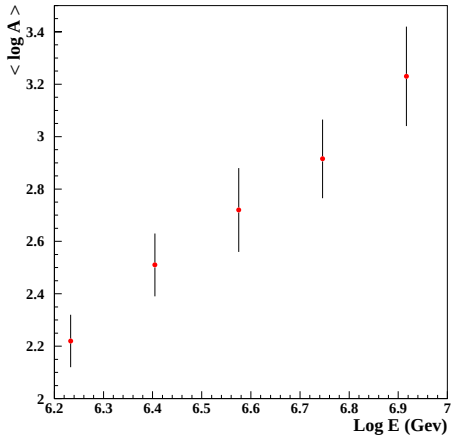

Figure 23: *$< logA >$ as a function of primary energy in the region of the knee.*

3.2.3 The composition from the e.m. and TeV muon data

A similar analysis has been performed by fitting, in different intervals of shower sizes, the muon size distribution observed deep underground by MACRO. The results concerning the

spectra of the light and heavy components, and the evolution of the average logarithmic mass are shown in figs. 24 and 25. They are in good agreement with the ones obtained with GeV muons concerning the origin of the knee as a break in the light component and the related increase of the average mass of the primaries. The difference in rapidity region of production of the secondaries is $\Delta y \approx 4$, the TeV muons being produced about one rapidity unit beyond the central region. This demonstrates the good consistency of the CORSIKA-QGSJET model in describing the data in these energy and kinematic regions.

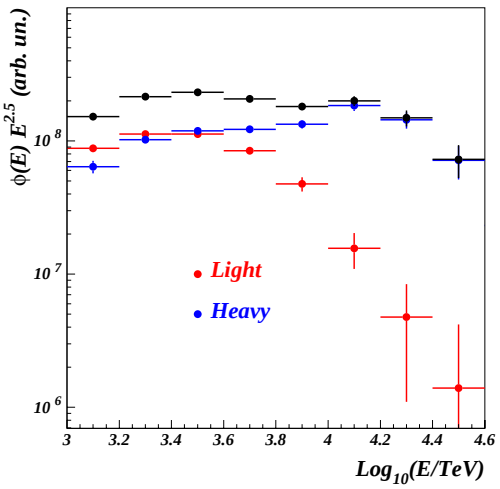

Figure 24: *Energy spectra of the p+He and Mg+Fe with the two components model (EAS-TOP and MACRO data).*

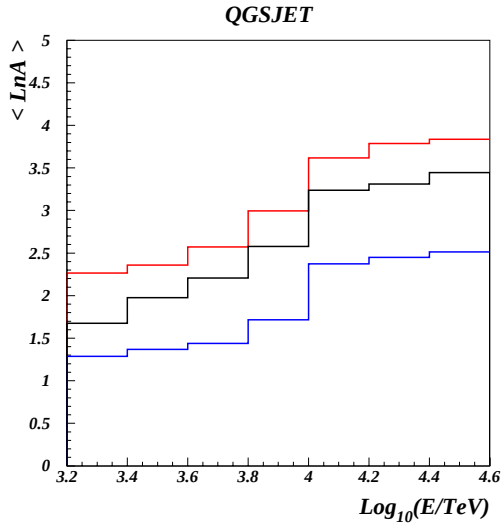

Figure 25: $< logA >$ *as a function of primary energy in the region of the knee (the upper and lower lines show the 1 s.d. uncertainties).*

The consistency of the identification of different primaries through the GeV and TeV muons has been checked by selecting, among events observed in coincidence with LVD, "very heavy" and "light" enriched primary beams respectively through: (a) large $N_\mu{}^{TeV}$ muon numbers for $N_e > 2 \cdot 10^5$ (which have low probability of being due to fluctuations of light primaries), and (b) large muon energy losses: $\Delta E_\mu/\Delta L > 4$ MeV/cm in the LVD counters crossed by the track (i.e. high energy/nucleon) for $N_e < 2.10^5$. The $N_e - N_\mu{}^{\rm GeV}$ relations at the surface are shown for all events, and for the selected ones in figs. 26 and 27, respectively. The selected events fall on clearly identified and distinct regions of the chosen parameters, as expected from the simulation code.

3.2.4 Cherenkov light measurements in the knee region

A wide angle Cherenkov light detector, based on five QUASAR-370 photomultipliers installed on five telescopes, has been operating for 154 hours in good atmospheric conditions at energy threshold $E_{th}^C \approx 300$ TeV. The surface of each photomultiplier is 0.1 m^2, and the full opening angle 45°.

The e.m. detector data are used to localize the core position also for the Cherenkov light (C.l.) reconstruction. The common analysis is performed on the basis of shower size

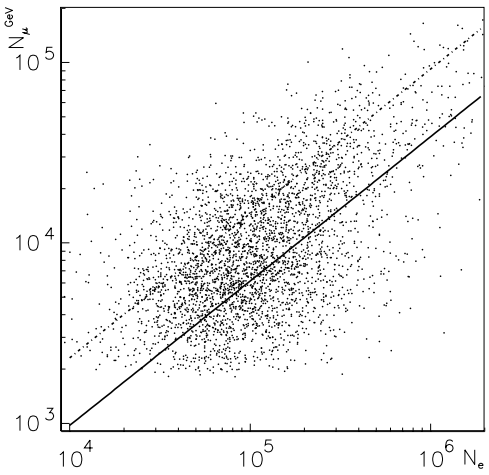

Figure 26: *Experimental N_μ^{GeV} vs. N_e data. The average predictions of the simulation for Fe (dashed) and proton primaries (solid line) are also shown.*

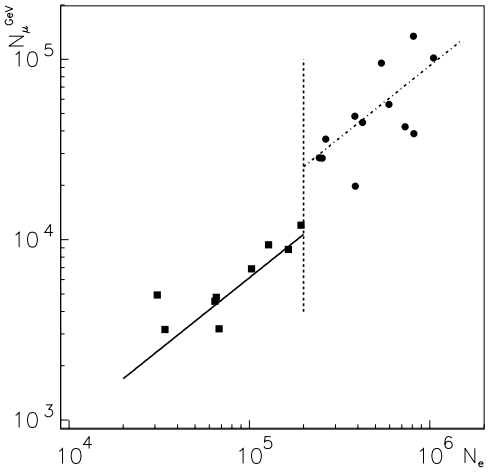

Figure 27: *N_μ^{GeV} vs. N_e for selected 'very heavy' and 'light' primaries obtained by applying cuts (a) (circles) and (b) (squares) (see text). For simulated data see fig. 26 (EAS-TOP and LVD data).*

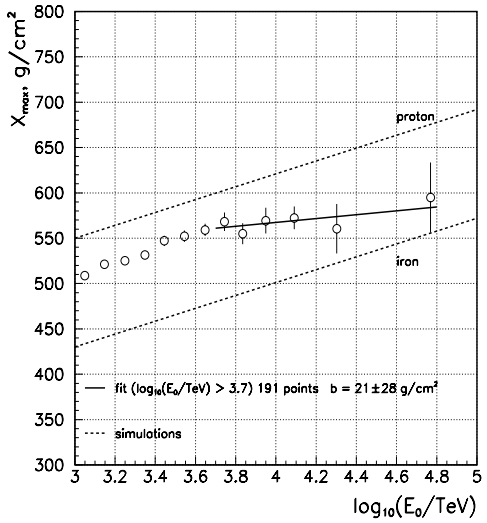

Figure 28: *Dependence of the average value of X_{max} on primary energy compared with the expectations from CORSIKA/QGSJET.*

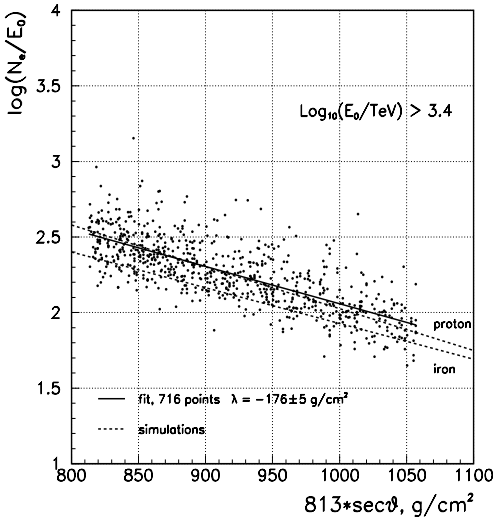

Figure 29: *EAS absorption curve (individual points and average) obtained from the combined Cherenkov and e.m. data, compared with the expectations from CORSIKA/QGSJET.*

(N_e), arrival zenith angle (θ), C.l. photon density at 100 m from the core (Q_{100}), and slope of the C.l. lateral distribution (R_0). As interesting examples of the data obtained from the correlated analysis, the average depth of shower maximum X_{max} as a function of primary energy, and the absorption curve of the shower size of showers of energies $E_0 > 10^{3.4}$ TeV are shown in figs. 28 and 29, respectively.
Primary energy is obtained from Q_{100}:
$log_{10}E_0 = 0.9 \cdot log_{10}Q_{100} + 2.13 + (\sec\theta - 0.8)^2$
with E_0 measured in TeV, and Q_{100} in $[\mathrm{ph} \cdot \mathrm{cm}^{-2} \cdot \mathrm{eV}^{-1}]$.
Q_{100} and R_0 are obtained through the fit to the C.l. lateral distribution:
$Q(R) = Q_{100} \cdot \exp((100 - R)/R_0)$.
The depth of shower maximum $X_{max}[\mathrm{g/cm}^2]$ is obtained from the distance to the EAS maximum $\Delta X[\mathrm{g/cm}^2]$ measured through R_0[m]:
$\Delta X = 672 - 400 \cdot (\log R_0 - 2.74)^2$
$X_{max} = X_0 \cdot \sec\theta - \Delta X$
The experimental data are compared with events simulated with the CORSIKA-QGSJET code. From such comparison it results that the model provides a good description of the experimental data, concerning also the longitudinal development which was not tested through other data. The changing elongation rate (i.e. slope of X_{max} vs. E_0) above the knee is in agreement with the expectations from a primary composition becoming heavier, although the statistics is not sufficient for an independent conclusion from this measurement.

3.3 The anisotropies

The anisotropy data (and their evolution with energy) carry information on the propagation properties of the primary particles in the interstellar medium; in particular they can validate the astrophysical explanation of the knee. The measurement has been performed with 4-fold coincidences, at average primary energy $E_0 \approx 2.10^{14}$ eV, with a total of 1.3 10^9 events. For the vertical sample ($\theta < 20^0$) the counting rate vs. the local sidereal time in 20' time intervals is shown in fig. 30, where the first harmonic (significance 5.9 s.d.) over the fluctuations in the individual channels is clearly seen.

The best fit of the vertical and inclined data gives, as first harmonic of the sidereal anisotropy (at the equatorial plane):

$A_{sid,\delta=0^0} = (3.73 \pm 0.57) \cdot 10^{-4}$, $\varphi_{sid} = 1.82 \pm 0.49$ h lst, with significance 6.5 s.d..

The consistency of the data is proved by:

i) the absence of significant anisotropies in antisidereal time (maximum amplitude 2.2 s.d., i.e. much lower than the observed solar and sidereal amplitudes);

ii) the consistency of the phases of the solar and sidereal anisotropies observed in the East and West directions;

iii) the observation of the expected dependence of the amplitude of the anisotropy over the declination (δ): $A \propto cos(\delta)$;

iv) the correct rotation of the solar vector during the year, as expected from the combination of the measured solar and sidereal anisotropies;

v) the observation of the expected solar anisotropy due to the motion of revolution of the Earth around the Sun, with significance 7.4 s.d.: $A_{sol,\delta=0^0} = (4.06 \pm 0.55) \cdot 10^{-4}$, and

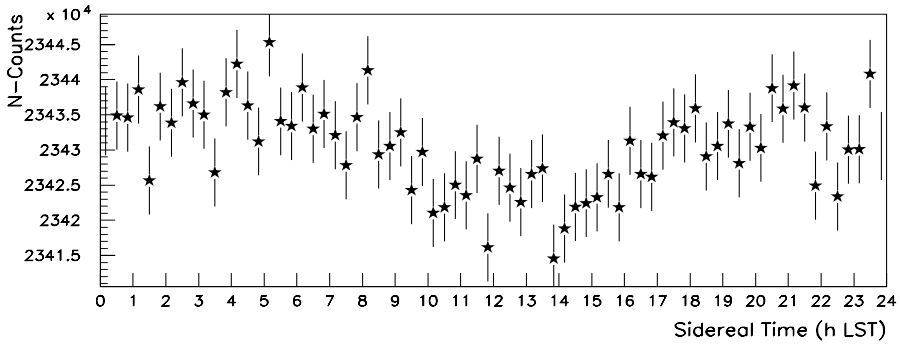

Figure 30: *Vertical events counting rate vs. the local sidereal time.*

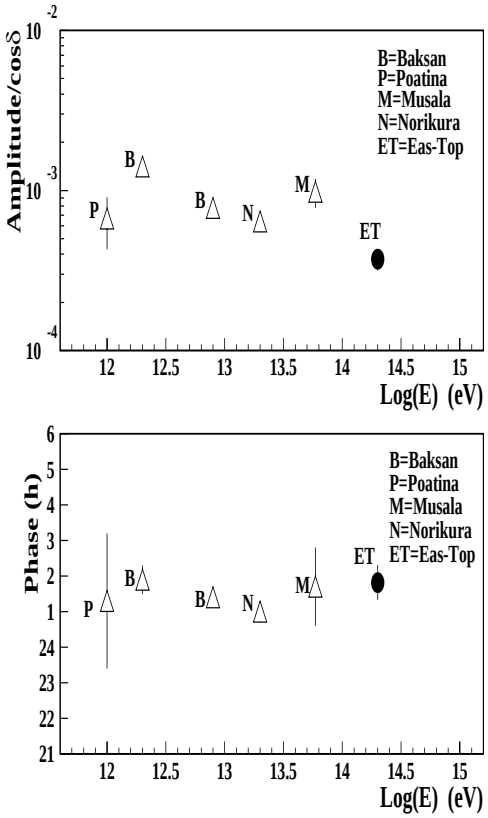

Figure 31: *Amplitudes and phases (h, l.s.t.) of the c. r. anisotropy reported in the energy range* $10^{12} - 2.10^{14}$ *eV.*

Figure 32: *Location in galactic coordinates of the average pointing of the telescope for different cosmic ray intensities (increasing with increasing darkness).*

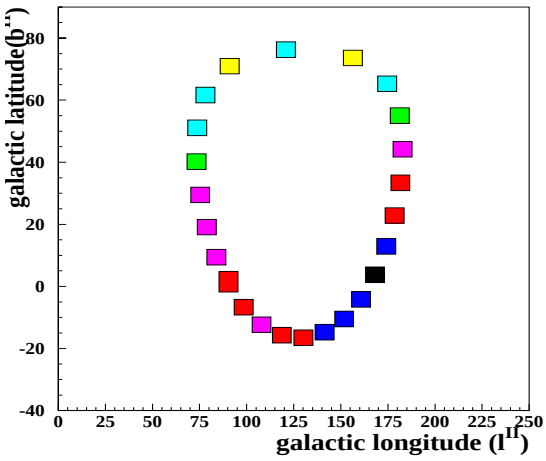

$\varphi_{sol} = 4.92 \pm 0.5$ h; the expected values, due to the Compton-Getting effect, being 4.7 $\cdot 10^{-4}$ and 6.0 h.

The EAS-TOP measurement is shown in fig. 31 together with the lower energy data, showing that the amplitude and phase of the anisotropy are quite constant over the whole energy range ($A_{sid} \approx (5 \div 10) \times 10^{-4}$, and $\varphi_{sid} \approx 1$ h lst).

From the "astronomical" point of view such direction has no evident interpretation:

the main indication with this respect can be inferred from fig. 32, where the variations of the counting rate are shown vs. the average pointing of the telescope in galactic coordinates, resulting in a lack of events from the direction of the higher galactic latitudes. On other side, the constancy and phase of the first harmonic versus primary energy would lead, as most likely interpretation, either to a convective mechanism or to a Compton Getting effect due to the motion of the Solar System with speed $v > 25$ km/s with respect to the cosmic ray rest system. A possible interpretation of the knee (in agreement with the increasing of the average mass number of the primaries in this energy range) was proposed long time ago by Peters and Zatsepin, and is based on the diffusion of higher rapidity primaries out of the Galaxy. A diffusion model has been developed at lower energies to explain the $\bar{p}$ flux, the e^+ to e^- and the secondary to primary ratios and their energy dependence. The general parameters of the model (diffusion coefficient $D(R) \approx 10^{28} \cdot R^{0.3}$ cm^2 s^{-1}, R in GV) predict an anisotropy dependence on primary energy $A \propto E_0^{0.3}$, which is not observed up to 2.10^{14} eV.

3.4 Gamma-ray astronomy

3.4.1 Candidate sources and diffuse emission

The search for γ-ray emission at the highest energies, whose propagation is not strongly affected by the infrared or cosmic background cutoff (i.e. $E_\gamma \leq 10^{14}$ eV), is still the main tool for the identification of cosmic ray sources in the Galaxy or in the nearby Universe. A systematic search for γ-ray sources has therefore been undertaken, looking for different candidates: Pulsars, SNRs, X-ray binaries, the BL Lac objects (Mrk421, Mrk501, recently detected at TeV energies), for steady and transient emissions, and over a whole survey of the visible sky. No D.C. emission has been detected; the exact values of the energy thresholds and the obtained upper limits depend on the source declination. As examples the 90% c.l. limits obtained from the Crab Nebula are $\Phi(> 20\text{TeV}) < 2.6 \cdot 10^{-13}\text{cm}^{-2}\text{s}^{-1}$, and $\Phi(> 100\text{TeV}) < 3.9 \cdot 10^{-14}\text{cm}^{-2}\text{s}^{-1}$. The Crab Nebula remains the only object from which a significant transient effect has been observed on February 23, 1989, in coincidence with the Baksan and Kolar Gold Field arrays. No transient effect has been observed from any direction of the sky (also in coincidence with other arrays as Baksan[3]), and the experimental distributions over 10 years of data taking reproduce the statistical expectations up to the largest fluctuation level (5 s.d.), thus showing the stability of the detector.

The obtained upper limits from SNRs, as γ Cyg, IC443, Monoceros, together with the EGRET data, indicate a spectral index $\gamma > 2.2$, thus not supporting a π^0 decay (produced by cosmic ray proton interactions) origin of the gamma radiation, and therefore still not providing a direct proof of c.r. acceleration in SNRs.

We report here the application of the technique to the study of EHE cosmic rays. 47 EHE events above $4 \cdot 10^{19}$ eV (i.e. GKZ cutoff) have been observed by the AGASA experiment. A clustering effect has been probably detected, into one triplet and three doublets. The corresponding directions have been searched for UHE γ-ray emission in

[3] *Collaboration with: V.V. Alekseenko and the Baksan Collaboration; work supported by INTAS under grant 93-303 (coordinator J. Osborne).*

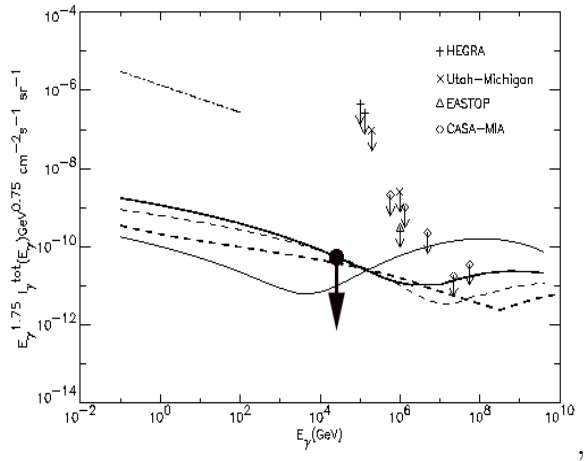

Figure 33: *Expected intensity of γ-rays from Blasi, 1999, for m_X =10^{14} GeV (thick lines) and m_X =10^{13} GeV (thin lines). The solid lines refer to SUSY-QCD fragmentation function and the dashed lines to ordinary QCD one. Crosses, triangles and diamonds indicate experimental upper limits to diffuse emission. Full dot and arrow represent the result of the present analysis.*

two data sets (fourfold: L.E. triggers, and sevenfold internal events: H.E. triggers). From none of them a significant excess is observed: 90% c.l. upper limits to the flux for each observed position are $\Phi_{\gamma,1}(> 25 \text{ TeV}) < (1.1 - 2.4) \cdot 10^{-13}$ cm^{-2} s^{-1}, and, for the sum of all of them, $\Phi_{\gamma,\Sigma}(> 25\text{TeV}) < 8.5 \cdot 10^{-14}$ cm^{-2} s^{-1}. The lack of a γ-ray signal provides constraints to the mechanisms of acceleration of EHE cosmic rays, both in the frame of "bottom-up" models and of "top-down" ones.

Concerning the latter, we consider the model of Blasi, 1999, in which the flux of UHE γ-rays is calculated from the decay of super-heavy relic particles clustered in the galactic halo. If these particles cluster at the positions corresponding to the arrival directions of cosmic rays with energy $E_0 > 4 \cdot 10^{19}$ eV, the diffuse intensity I_γ would be concentrated in point-like γ-ray sources. We convert the upper limit Φ_Σ to I_γ through expression: $I_\gamma = \Phi_\Sigma \cdot \frac{1}{4\pi} \cdot \frac{9}{47}$ cm^{-2} s^{-1} sr^{-1}. The limit obtained through L.E. triggers (not affected by absorption on low energy photons in space) is shown in fig. 33, compared with Blasi calculations. In this frame, X-masses m_X >10^{14} GeV are excluded for ordinary QCD fragmentation function in hadron production.

Concerning conventional EHE cosmic ray acceleration, the clustering effect suggests the possibility of " nearby" sources (D <30 Mpc). Cosmic ray interactions in the source produce a γ-ray flux (at E$_0 \approx$ 100 TeV: $\frac{I_\gamma}{I_p} \approx 6{\cdot}10^{-4} \times x$, where x in g cm^{-2} is the target thickness). For our case, using as I_p the extrapolation back to the 100 TeV region of the suggested and measured power law spectrum (γ=3), for the 3 events (over 47) of the AGASA triplet, we obtain $\frac{I_\gamma}{I_p}$ <3.3·10^{-7}, i.e. x^{source}_{matter} <5·10^{-4} g cm^{-2}. Concerning photons, from π_0 photoproduction we obtain: $x^{source}_{photon} < 1.5 \cdot 10^{23}$ ph cm^{-2} for E$_{ph} \approx$ KeV. The upper limit on matter column density sets a constraint to the dimension (d) of the proposed sources: $d < 1$ Mpc also for intergalactic matter density (excluding e.g. acceleration in sites as the core of Virgo cluster).

An upper limit to the flux of Ultra High Energy (UHE) γ-rays in the primary cosmic radiation has been obtained by selecting Extensive Air Showers with low muon content. For EAS electron sizes $N_e > 6.3 \cdot 10^5$, no showers are observed with core located inside the fiducial area and no muons recorded in the 140 m^2 muon detector, during a live time of 8440 h. The 90% c.l. upper limit to the relative intensity of γ-ray with respect to cosmic ray (c.r.) primaries is $I_\gamma / I_{c.r.} < 7.3 \cdot 10^{-5}$ at primary energy $E_0 \geq 1 \cdot 10^{15}$ eV (i.e. $I_\gamma (> 1 \cdot 10^{15}$ eV $) < 1 \cdot 10^{-14}$ cm^{-2} s^{-1} sr^{-1}), a limit which is much lower than reported in previous measurements.

3.4.2 Transients and Gamma Ray Bursts

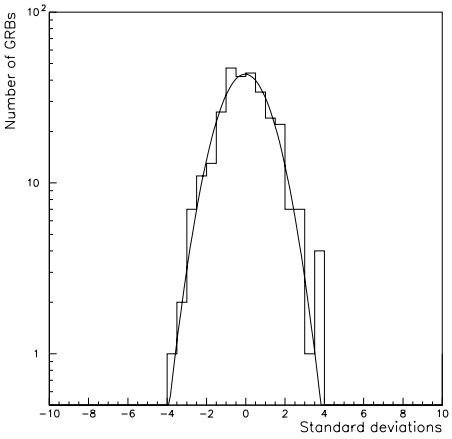

Figure 34: *Distribution of the excesses, in unit of standard deviations, observed in coincidence with 292 BATSE GRBs.*

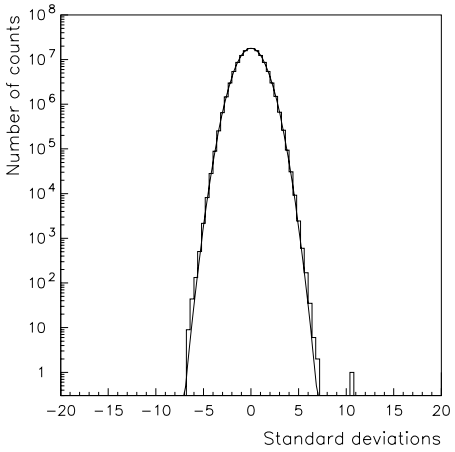

Figure 35: *Distribution of the excesses of duration Δt = 1 s in units of standard deviations, obtained in the "all sky" survey.*

Systematic searches for gamma-ray bursts, both correlated and uncorrelated with satellite observations, have been performed at different energy thresholds and with different techniques.
At energy E > 10 GeV from the study of the single particle counting rate in the e.m. detector, no candidate has been observed in coincidence with 292 BATSE GRBs and the typical upper limits obtained on the energy fluence are F(10 GeV$\div$1 TeV)$\sim$($10^{-4} \div 10^{-3}$) erg cm^{-2} for the events with zenith angle $\theta < 30°$ (fig. 34). A single statistical significant excess (10.6 standard deviation, see fig. 35) has been observed on 1992 July 15 at 13:22:26 UT. Assuming this excess as due to a gamma-ray burst with zenith angle θ=30°, the corresponding 10 GeV$\div$1 TeV energy fluence is 1.5 10^{-3} erg cm^{-2} (satellite detector data being not available for a coincidence analysis).

A method for searching for γ-ray bursts at VHE has been developed by looking for short duration time variations in the counting rate of corresponding wide angle C.l. detectors, at trigger threshold $N_{phe}^{th} = 200$ photoelectrons/PM corresponding to $E_0^{th} \approx 10$ TeV. No significant excess has been observed too (the largest one having a probability $p \approx 20\%$ of being produced by statistical fluctuations).

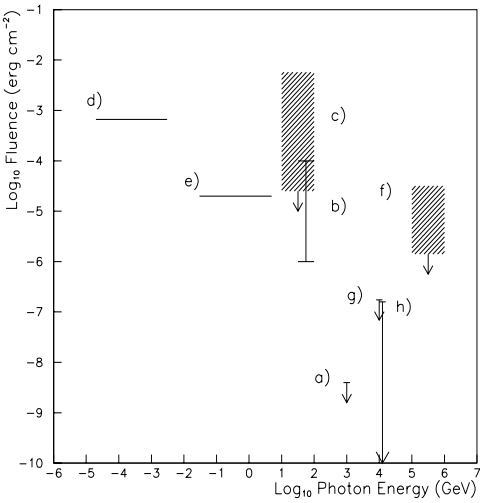

Figure 36: *GRBs: detections and upper limits to the energy fluences reported by different experiments: (a) WHIPPLE; (b) MILAGRITO during GRB 970417a; (c) EAS-TOP scintillator array (single particles) during 45 BATSE bursts; (d,e) BATSE and EGRET, respectively, during GRB 940217; (f) EAS-TOP (EAS) during 56 BATSE bursts; (g) EAS-TOP Cherenkov; (h) HEGRA.*

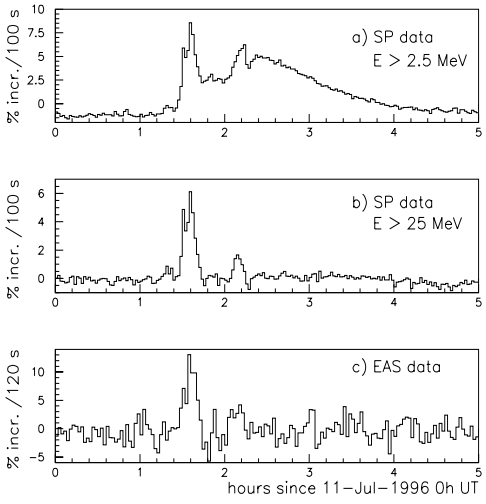

Figure 37: *The July 11 event: a) increase of the single particle counting rate of a low threshold detector; b) the same for an higher threshold detector; c) the EAS counting rate.*

The obtained upper limits are reported in fig. 36, including also the results from other experiments.

3.5 Atmospheric effects

Some episodes in which perturbed atmospheric conditions affect the cosmic ray counting rate at ground level have been observed. The effect appears as an increase in the single particle counting rate of about (5 - 15 %) correlated with rainfalls, and is larger for detectors with lower energy thresholds ($E_{th} \approx 3$ MeV). This is interpreted as due to the decay of Radon daughters contained in radioactive aerosol transported to the ground by the rain. Moreover, during some of such episodes, characterized by the presence of thunderstorms and lightning activity, significant excesses in the air shower counting rate have been observed. Such effect implies the acceleration of air shower particles by the electric field associated with charged thunderclouds above the detector site. The time evolution of one of such events, in EAS and in detectors with different energy thresholds,

is shown in fig. 37 [4].

3.6 High energy interactions

Cosmic rays represent still the source of the highest energy particles available for the study of hadron interactions. In our energy region most significant information can be obtained for the case of proton-nucleus ("p-air") interactions. We will discuss here two of such measurements.

3.6.1 The $p-air$ total cross-section

The method is based on the selection of showers with given primary energy ($E_1 < E_0 < E_2$) according to the detected muon number $N_\mu(E_0, r, E_\mu > 1\,\mathrm{GeV})$. Primary proton showers near maximum development are selected according to their location in the upper bound of the (N_e) distribution ($N_e > N_e^i$). The attenuation length of p-primaries in atmosphere ($\Lambda_{\rm obs}$) is measured from the frequency attenuation rate of such showers vs. zenith angle:

$$f(\theta) = \Gamma(\theta) f(0) \exp[-x_0(\sec\theta - 1)/\Lambda_{\rm obs}], \qquad (1)$$

where $\Gamma(\theta)$ is the calculated acceptance. The obtained values of $\Lambda_{\rm obs}$ ($\Lambda_{\rm obs} = 75 \pm 7\,\mathrm{g/cm^2}$, possibly underestimated of about 10% in case of heavier nuclei contamination) is in better agreement with models predicting longer absorption lengths such as HDPM and VENUS.

Table 3: Values of $\sigma_{\rm in}^{p-\rm air}$(mb) inferred from experimental data using k factors derived from different interaction models and different N_e^i cuts.

$\log N_e^i$	6.0	6.1	6.2
HDPM	419 ± 50	381 ± 52	375 ± 61
VENUS	380 ± 42	343 ± 44	369 ± 60
DPMJET	380 ± 40	350 ± 42	358 ± 52
QGSJET	407 ± 44	373 ± 46	358 ± 52
SIBYLL	524 ± 69	440 ± 60	358 ± 53

From the simulation, the obtained attenuation length $\Lambda_{\rm obs}^{\rm sim}$, compared to the interaction mean free path $\lambda_{p-\rm air}^{\rm sim}$, provides the factor $k = \Lambda_{\rm obs}^{\rm sim}/\lambda_{p-\rm air}^{\rm sim}$. This factor includes shower fluctuations, detectors response and some features of the interaction model. The values of k are similar and stable for all considered models: $k^{typ} \approx 1.1$ for N_e^i cut high enough to select p-showers near maximum development (i.e. $N_e = 10^{6.1} - 10^{6.2}$, see tab. 3).

From $\lambda_{p-\rm air} = \Lambda_{\rm obs}/k$ the measurement of $\lambda_{p-\rm air}$ and consequently of $\sigma_{\rm in}^{p-\rm air}$(mb) $= 2.41 \times 10^4/\lambda_{p-\rm air}$ is obtained. Results are reported in tab. 3, where the $\log N_e^i = 6.2$ cut should be considered, due to the convergence of k values and smaller contamination of heavier nuclei. Differences between $\sigma_{\rm in}^{p-\rm air}$ values derived from each interaction model are well inside the statistical uncertainties. A helium contamination (considering equal p and He fluxes at $E_0 \approx 10^{15}$ eV) would result in the reduction of the $\sigma_{\rm in}^{p-\rm air}$ values of about

[4] *The data have been analyzed in conjunction with a parallel measurement performed with a NaI detector, lead by M. Brunetti, D. Cattani, S. Cecchini, M. Galli, G. Giovannini, A. Pagliarin.*

10%. The obtained range for $\sigma_{\rm in}^{p-{\rm air}} = (300 \div 400)$ mb is lower than previously reported in air shower measurements, that have to be treated as upper limits.

3.6.2 Large-pt physics

Multicore Extensive Air Showers have been recorded in the upper layer of the EAS-TOP calorimeter (unshielded; examples of a single core and a multicore event are shown in figs. 38 and 39).

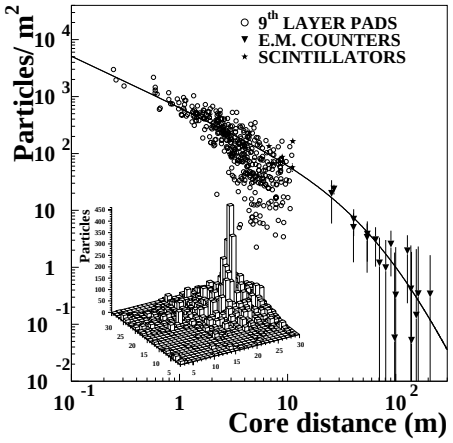

Figure 38: *A single core EAS: the reconstructed lateral distribution function and the core region as observed by the upper unshielded layer of the calorimeter.*

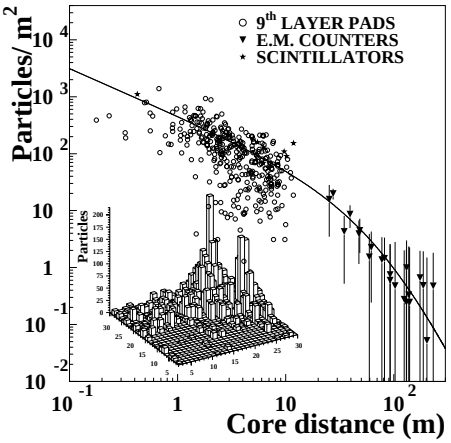

Figure 39: *A multicore EAS: the reconstructed lateral distribution function of the main shower and the central region are shown.*

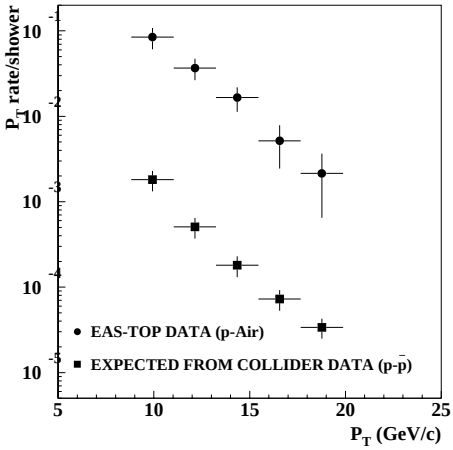

Figure 40: *Measured p_t rate in multicore EAS compared with the expected one from the $p - \bar{p}$ collider cross section data.*

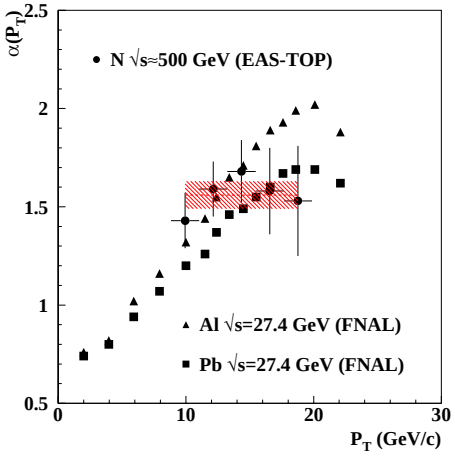

Figure 41: *The EAS-TOP measurement of the α parameter compared with existing data at fixed target experiments. The dashed box indicates, in the range $10 \leq p_t \leq 20$ GeV/c, the mean value of α with its uncertainty.*

From such data, the cross section for large p_t jet production for transverse momentum $10 \leq p_t \leq 20$ GeV/c and rapidity $1.6 \leq \eta \leq 2.6$ in p-N ($p - air$) interactions is studied. The projectiles are the leading particles interacting at atmospheric depths between 250 and 480 g cm^{-2}, the CMS energy of interaction being $\sqrt{s} \approx 500$ GeV. The slope of the p_t distribution agrees with the expected one from the $p - \bar{p}$ collider data at the same CMS energy (fig. 40). The measured jet production cross section in $p - N$ interactions with respect to $p - \bar{p}$ interactions is $(d\sigma/dp_t)^{jet}_{pN} = (d\sigma/dp_t)^{jet}_{p\bar{p}} \cdot A^{\alpha}$, the measured value of α being $\alpha = 1.56 \pm 0.07$ for $A = 14.7$ (average mass number of *air* nuclei). Such value agrees with the one obtained in $p - nucleus$ accelerator measurements at $\sqrt{s} \simeq 30$ GeV in the same range of transverse momentum and rapidity (see fig. 41). No indication of increasing value of α with energy (i.e. of the entity of the "Cronin effect") is found.

3.6.3 Penetrating showers

The detection of EAS at very large zenith angles (HAS) can be a tool for the search of UHE penetrating particles and neutrinos from cosmic ray sources. Indeed, events at large zenith angles have been observed, but never fully explained.

In the EAS-TOP data, at zenith angles $\theta > 65°$, an excess of events (HAS) is observed above the rate of EAS as expected from their attenuation length in the atmosphere (see fig. 42).

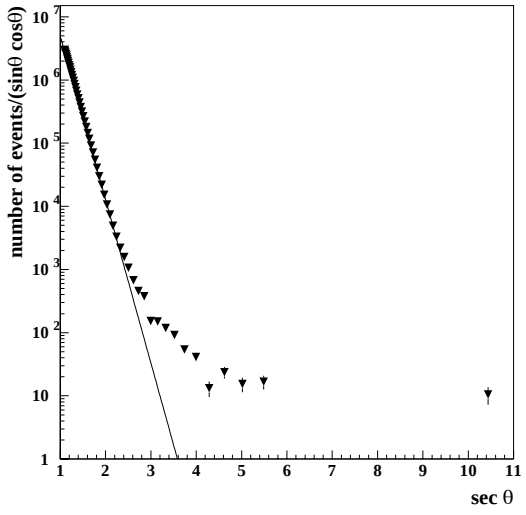

Figure 42: *The zenith angle distribution of a sample of EAS as measured by the EAS-TOP e.m. array.*

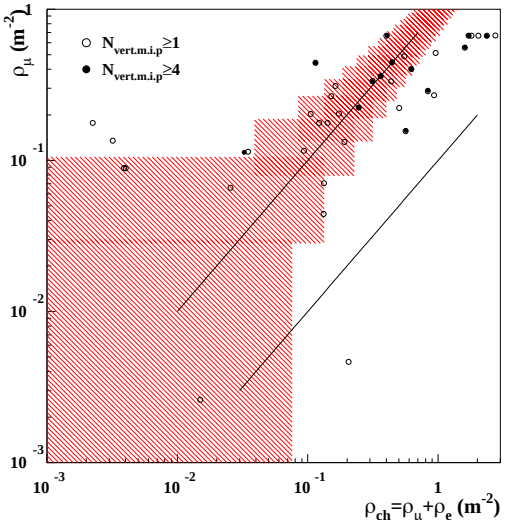

Figure 43: *Particle density as measured by the scintillator and tracking detectors. 1 s.d. error boxes are shown. ρ_μ is "saturated" at 0.7 m^{-2}. Empty (full) symbols represent events at 1 (4) vertical m.i.p. level. The $\rho_\mu = 0.1\rho_{ch}$ line is also shown: hadron and neutrino initiated showers are expected to populate the region at the right of such line.*

The physical nature of the anomalous arrival directions of HAS is confirmed by the absence of events from the direction of the sky shaded by the top of the mountain on which the array is located, and by the dependence of the barometric effect on zenith angle: such an effect indicates the presence of a "non-attenuated" EAS component amounting to about 30% of the total EAS flux at 70°, and dominating at larger zenith angles.

A clue to the understanding of such events is provided by their muon content: in 575 common observation days of the e.m. and muon detectors, 37 events have been recorded with $\theta \geq 75°$. Very few of such showers have a negligible content of muons i.e. could be μ-poor as expected for μ induced showers in the atmosphere. The 2 over 37 events with no muon in the μ-detector correspond to events with rather small energy losses in the scintillators, compatible with the absence of muons in the tracking module respectively at 1. and 3.5 s.d.. For all other events, the muon density ($\rho_\mu \approx \bar{n}_\mu / A_\mu \approx 0.3$ muons m^{-2}) is comparable with the total density of charged particles measured by the scintillator modules (the comparison is done by using the data of scintillators located at the same distance as the muon detector from the module with the highest recorded number of particles, assumed as approximate shower core location). The charged particle density, as measured by the scintillator detector ($\Delta E / \Delta E_{m.i.p.}$), and the muon density measured by the tracking detector at the same core distances are compared in fig. 43: all experimental points lay inside a ± 2 s.d. interval around the 1 to 1 correlation line. This is expected from "pure" muon showers, indicating a marginal content of electrons.

In parallel, an experiment has been performed to detect "Horizontal muon bundles" (HMB) ($N_\mu \geq 3$ and $\theta \geq 75°$ events, selected through the trigger provided by the "vertical walls" on the South and North sides of the muon-hadron detector), that have been recorded at a rate of 8.4 events day^{-1}. These events can be easily interpreted as EAS originated at large distances in the atmosphere, in which the e.m. component has been completely absorbed and the remnant muons are observed. It has been shown that, as the muon multiplicity increases, the two classes of events (HAS and HMB) coincide: the muon content of scintillator triggered events (showing that the muon density includes the total density of the ionizing components), and the rate of muon bundle triggers (corresponding to the scintillator ones for large enough muon densities) lead to the conclusion that HAS are largely dominated by muon showers. The e.m. component in such case is essentially due to local muon interactions with small energy losses (delta rays, direct pairs). The expected rate of such events has been calculated by using a simulation code to propagate very inclined Extensive Air Showers in the atmosphere (CORSIKA-QGSJET). Inside the uncertainties on the primary spectrum and composition, the experimental event rate and multiplicity distribution can thus be fairly well explained. It appears that events with detected muon multiplicities $N_\mu \geq 10$ are due to primaries with typical energy $E_0 \approx 10^{17}$ eV, detected at core distances $r \approx 500$ m, the total muon number for such events being $N_\mu \geq 10^4$.

UHE cosmic neutrinos produce showers with muon content "lower" or "similar" to ordinary cosmic ray showers. In fig. 43 a $\rho_\mu = 0.1 \rho_{\mu+e}$ line is drawn, as an upper limit to the muon content of neutrino induced showers. Also in fig. 43 the muon density vs. (muon+electron) density is shown for events with energy losses triggering the scintillators above the 1 effective particle level at $\theta \geq 75^0$. For none of such events the quoted limit is exceeded, i.e. the e.m. component is never 10 times larger than the muon one, as would be

expected for neutrino induced events. From such upper limit in the 575 days of common operation of the muon and e.m. detectors, an upper limit to the diffuse neutrino intensity (at 90 % c.l.) is derived for $E_\nu \approx 10^5$ GeV: $\frac{dI_\nu}{dE_\nu} < 8.5 \times 10^{-14} (\frac{10^5}{E_\nu})^2 \mathrm{cm}^{-2}\mathrm{s}^{-1}\mathrm{sr}^{-1}\mathrm{GeV}^{-1}$ and for resonant events (for $E_{\bar{\nu}_e} = 6.4 \cdot 10^6$ GeV): $\frac{dI_{\bar{\nu}_e}}{dE_{\bar{\nu}_e}} < 4.3 \times 10^{-18} \mathrm{cm}^{-2}\mathrm{s}^{-1}\mathrm{sr}^{-1}\mathrm{GeV}^{-1}$.

4 Conclusions

The general conclusions can be summarized as follows:

- the transition from the direct measurements to the EAS experiments is well understood; the proton spectrum obtained from the hadron measurements agrees with both the JACEE and RUNJOB ones, while the total light component (p + He) flux (from TeV muons and C.l. data) is in better agreement with the higher values reported by JACEE (that we remind imply a primary flux dominated by helium above 10^{14} eV);

- a consistent picture of the knee is obtained in e.m. and muon (GeV and TeV) components: the break in the spectrum is rather sharp, in better agreement with a source effect rather than a propagation one; the break is observed in the spectrum of a light component with no break in the heaviest one (Fe), whose detection requires a measurement extending up to above 10^{17} eV (under the hypothesis, compatible with the data, of a rigidity dependent break for the different components);

- data from different observables (e.m. measurements, hadrons, GeV and TeV muons, Cherenkov light) show good agreement and prove the adequacy of the hadron interaction model used (CORSIKA/QGSJET) up to the knee energies;

- the sidereal anisotropy has been measured at mean primary energy $E_0 = 2.10^{14}$ eV: up to such energy no energy dependent effect, as would be expected from diffusion processes, is observed;

- γ-ray astronomy data do not reveal any signal at energies above the "e.m. origin" range: there is therefore still no direct evidence of acceleration in SNRs, as well as from the UHE clusters directions;

- the search for γ-ray transients proves the excellent stability of the detector: two candidate episodes have been observed in 10 years of data taking, from the Crab Nebula at $E_0 \approx 100$ TeV in coincidence with the Baksan and KGF arrays on February 23, 1989, and in the single particle counting rate on July 15, 1992;

- increases in the EAS counting rates have been detected during thunderstorms (associated with high values of the atmospheric electric field); the effect is quite significant and needs to be investigated in connection with the next generation of experiments looking for rare extremely high energy events;

- measurements of high energy hadron physics have been performed, such as of the $p-air$ cross section and the cross section for large p_t jet production in $p-air$ interactions; this, together with the explanation of the nature of penetrating showers, has solved two old puzzles in Extensive Air Shower physics, i.e. the "multicore" and the "horizontal" air shower phenomena.

5 Collaborators and Institutions

M. Aglietta, B. Alessandro, V.V. Alexeenko, P. Antonioli, F. Arneodo, V.S. Berezinsky, L. Bergamasco, M. Bertaina, A. Campos Fauth, A. Castellina, C. Castagnoli, C. Cattadori, A. Chiavassa, G. Cini Castagnoli, B. D'Ettorre Piazzoli, G. Di Sciascio, W. Fulgione, P. Galeotti, A. Gazizov, P. L. Ghia, R. Granella, M. Iacovacci, E.E. Korosteleva, L.B. Konstantinovich, L.A. Kuzmichev, A.S. Lidvansky, A. Lima de Godoi, B.K. Lubsandorzhiev, G. Mannocchi, C. Melagrana, N. Mengotti Silva, C. Morello, G. Navarra [5], H. Nogima, L. Periale, P. Picchi, V.V. Prosin, L. Riccati, O. Saavedra, M. Serio, A. Stamerra, G. C. Trinchero, A. Turtelli, P. Vallania, S. Valchierotti, S. Vernetto, C.Vigorito
Technical staff: C. Barattia, M. Canonico, G. Giuliani, A. Giuliano, F. Gomez, G. Pirali
Istituto Nazionale di Fisica Nucleare, Sezione di Torino, Torino, Italy
Istituto di Cosmo-Geofisica del CNR, Torino, Italy
Dipartimento di Fisica Generale dell' Università di Torino, Torino, Italy
INFN, Laboratori Nazionali del Gran Sasso, Assergi (AQ), Italy
Dipartimento di Scienze Fisiche dell' Università and INFN, Napoli, Italy
Istituto Nazionale di Fisica Nucleare, Sezione di Bologna, Bologna, Italy
Instituto di Fisica, Universidade Estadual, de Campinas, Campinas (SP), Brazil
Institute of Physics, National Academy of Sciences of Belarus, Minsk, Belarus
Institute for Nuclear Research, Russian Academy of Sciences, Moscow, Russia
Institute for Nuclear Physics, Moscow State University, Moscow, Russia
Universidade de Sao Paulo, Sao Paulo (SP), Brazil

6 List of publications in 2001

1. "The primary proton spectrum in the range $0.5 \div 50$ TeV from the observation of hadrons at EAS-TOP"
   Proc 27th International Cosmic Ray Conference, **1**, 3 (Hamburg, 2001)

2. "The lateral distribution of Cherenkov light in $10-100$ TeV primary proton showers"
   Proc 27th International Cosmic Ray Conference, **1**, 14 (Hamburg, 2001)
   (EAS-TOP and MACRO Coll.)

3. "Cosmic Ray composition around the knee from EAS electromagnetic and muon data"
   Proc 27th International Cosmic Ray Conference, **1**, 120 (Hamburg, 2001)
   (EAS-TOP and MACRO Coll.)

4. "Study of the composition around the knee through the electromagnetic and muon detectors data at EAS-TOP"
   Proc 27th International Cosmic Ray Conference, **1**, 124 (Hamburg, 2001)

5. "A search for $20 \div 100$ TeV γ-rays from the Crab Nebula with 10 years of EAS-TOP data"
   Proc 27th International Cosmic Ray Conference, **6**, 2411 (Hamburg, 2001)

[5] *spokesperson*

6. "The EAS counting rate during thunderstorm"
   Proc 27th International Cosmic Ray Conference, **10**, 4165 (Hamburg, 2001)

7. "QUEST: wide angle Cherenkov light measurements at EAS-TOP"
   Proc 27th International Cosmic Ray Conference, **1**, 226 (Hamburg, 2001)

8. "Study of CR primaries and their cascades at $E_o = 10 \div 100$ TeV through EAS-TOP and MACRO"
   Nuclear Physics B (Proc. Suppl.), in press
   (EAS-TOP and MACRO Coll.)

9. "The primary all-nucleon spectrum in the range $0.5 \div 50$ TeV from the observation of hadrons at EAS-TOP"
   Nuclear Physics B (Proc. Suppl.), in press

10. "Study of the bending component at the knee of the cosmic ray primary spectrum"
    Nuclear Physics B (Proc. Suppl.), in press

11. "Cosmic Ray composition around the knee from EAS electromagnetic and muon data"
    Nuclear Physics B (Proc. Suppl.), in press
    (EAS-TOP and MACRO Coll.)

7 Main publications (1990-2000)

- "Simultaneous observation of extensive air showers and deep underground muons at the Gran Sasso Laboratory" *Physical Review D,* **42***, 1396 (1990)*

- "Detection of the UHE burst from the Crab Nebula on February 23, 1989 from the EAS-TOP array" *Europhysics Letters, 1,* **15***, 81 (1991)*

- "EAS-TOP: Lateral and Temporal Characteristics of Extensive Air Showers" *Il Nuovo Cimento,* **15C***, 5, 713 (1992)*

- "EAS-TOP: Results of Gamma-Ray Astronomy at 10^{14} eV" *Il Nuovo Cimento,* **15C***, 5, 723 (1992)*

- "Search for 100 TeV γ-ray emission from the galactic disk" *The Astrophysical Journal,* **397***, 148 (1992)*

- "Fractal Behavior of Cosmic Ray Time Series: Chaos or Stochasticity?" *Journal of Geophysical Research,* **98***, A9, 15,241 (1993)*

- "UHE cosmic ray event reconstruction by the electromagnetic detector of EAS-TOP" *Nucl. Instr. and Methods in Physics Research* **A336***, 310 (1993)*

- "Results on candidate UHE Gamma-Ray Sources by the EAS-TOP array (1989-1993)" *Astroparticle Physics,* **3***, 1 (1994)*

- "The limit to the UHE extraterrestrial neutrino flux from the observations of Horizontal Air Showers at EAS-TOP" *Physics Letters B* **333**, *555 (1994)*
- "Study of the primary cosmic ray composition around the knee of the energy spectrum" *Physics Letters B,* **337**, *376 (1994)*
- "Search for Gamma Ray Bursts at photon energies $E \geq 10$ GeV and $E \geq 80$ TeV" *The Astrophysical Journal,* **469**, *305 (1996)*
- "A measurement of the solar and sidereal cosmic ray anisotropy at $E_0 \sim 10^{14}$ eV" *The Astrophysical Journal,* **470**, *501 (1996)*
- "A limit to the rate of Ultra High Energy γ-rays in the primary cosmic radiation" *Astroparticle Physics,* **6**, *71 (1996)*
- "The shapes of the atmospheric Cherenkov light images from extensive air showers" *Astroparticle Physics,* **6**, *143 (1997)*
- "Comparison of the electron and muon data in Extensive Air Showers with the expectations from a cosmic ray composition and hadron interaction model" *Il Nuovo Cimento,* **112B**, *2-3, 139 (1997)*
- "The High Energy Muon Spectrum in Extensive Air Showers: First Data from LVD and EAS-TOP at Gran Sasso" *Astroparticle Physics,* **9**, *185 (1998)*
- "The hadron calorimeter of EAS-TOP: operation, calibration and resolution" *Nuclear Instruments and Methods in Physics Research A,* **420**, *117 (1999)*
- "Study of Markarian 421 in the γ-ray energy range 30-100 TeV" *Nuclear Physics B,* **70**, *506 (1999)*
- "Identification of light and very heavy cosmic ray primaries at $E_0 \approx 10^{15}$ eV from surface and deep underground measurements at th Gran Sasso Laboratories" *Nuclear Physics B,* **70**, *512 (1999)*
- "The EAS Size Spectrum and the Cosmic Ray Energy Spectrum in the Region $10^{15} - 10^{16}$ eV" *Astroparticle Physics,* **10**, *1 (1999)*
- "Study of jet production in p-N interactions at $\sqrt{s} \approx 500$ GeV in EAS multicore events" *Physics Letters B,* **460**, *474 (1999)*
- "Search for high energy GRBs with EASTOP" *Astronomy and Astrophysics Suppl. Ser.,* **138**, *595 (1999)*
- "The cosmic ray anisotropy at $E_0 > 100$ TeV" *Adv. Space Res.,* **23**, *603 (1999)*
- "Search for $E_\gamma \approx 10^{14}$ eV γ-ray sources from a full sky survey at EAS-TOP" *Proc 26th International Cosmic Ray Conference,* **4**, *68 (Salt Lake City, 1999)*
- "Study of Horizontal Air Showers at EAS-TOP" *Proc 26th International Cosmic Ray Conference,* **2**, *24 (Salt Lake City, 1999)*

- "The proton attenuation length and the p-air inelastic cross section at $\sqrt{s} \approx 2$ TeV from EAS-TOP" *Nuclear Physics B,* **75A**, *220 (1999)*
- "Study of the cosmic ray primary spectrum at $10^{15} < E_0 < 10^{16}$ eV with the EAS-TOP array" *Nuclear Physics B,* **85**, *318 (2000)*
- "High Energy muons and atmospheric Cerenkov light in EAS" *Nuclear Physics B*, **75A**, 259 (1999)
- "Search for Gamma Ray Bursts at $E_0 \approx 10^{13}$ eV" *SIF Conference Proceedings,* **68**, *7 (2000)*
- "Search for $E_\gamma > 5.10^{13}$ eV γ-ray transients through the BAKSAN and EAS-TOP correlated data" *Astroparticle Physics,* **14**, *189 (2000)*

GENIUS-TF and GENIUS. Prospects for Cold Dark Matter and Solar Neutrino Search

H.V. Klapdor-Kleingrothaus*[a], A. Dietz[a], C. Dörr[a], G. Heusser [a], T. Kihm[a], I.V. Krivosheina[a,b], A. Mazza[a], H. Strecker[a], C. Tomei[a,c]

[a] Max-Planck Institut, Heidelberg, Germany
[b] Institute of Radiophysical Research, Nishnij Novgorod, Russia
[c] University of L'Aquila, Italy
* Spokesman of the GENIUS and GENIUS-TF Collaboration

Abstract

The new project GENIUS will cover a wide range of the parameter space of predictions of SUSY for neutralinos as cold dark matter. Further it has the potential to be a real-time detector for low-energy (*pp* and ^{7}Be) solar neutrinos. A GENIUS Test Facility has just been funded and will come into operation in Gran Sasso by end of 2002.

1 GENIUS and Low-Energy Solar Neutrinos

Concerning solar neutrino physics, the total *pp* neutrino flux has not been measured and also no real-time information is available for the latter.

GENIUS which has been proposed for solar ν detection in 1999 [3, 6], could measure the *full pp* (and ^{7}Be) neutrino flux in real time (Fig. 1).

The main idea of GENIUS, originally proposed for double beta and dark matter search [6] is to achieve an extremely low radioactive background (factor of > 1000 smaller than in the HEIDELBERG-MOSCOW experiment) by using 'naked' detectors in liquid nitrogen.

While for cold dark matter search 100 kg of *natural* Ge detectors are sufficient, GENIUS as a solar neutrino detector would contain 1-10 tons of enriched ^{70}Ge or ^{73}Ge.

That Ge detectors in liquid nitrogen operate excellently, has been demonstrated in the Heidelberg low-level laboratory [9, 2] and the overall feasibility of the project has been shown in [6, 9, 7, 8].

The potential of GENIUS to measure the spectrum of low-energy solar neutrinos in real time has been studied by [3, 6, 8]. The detection reaction is elastic neutrino-electon scattering $\nu + e^- \longrightarrow \nu + e^-$.

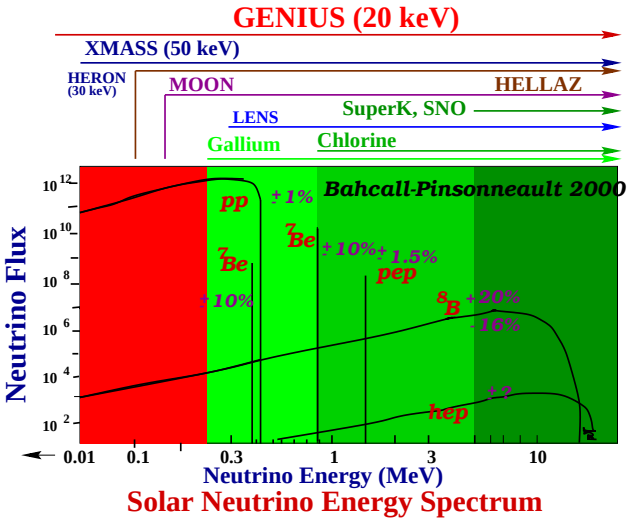

Figure 1: The sensitivity (thresholds) of different running and projected solar neutrino detectors (see [15] and our home-page: $http://www.mpi-hd.mpg.de/non\_acc/$).

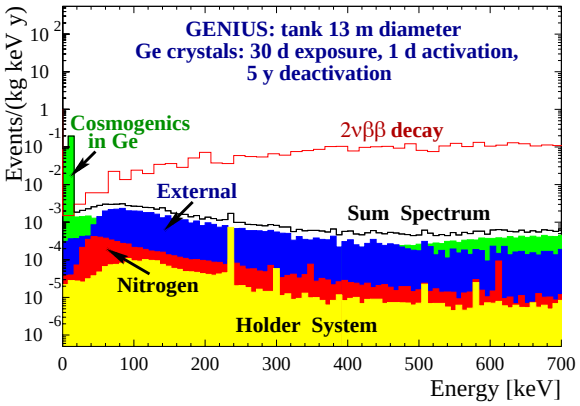

Figure 2: Total background in a 13 m liquid nitrogen tank for detectors produced under the special given conditions (tritium neglected) (see [8]).

The maximum electron recoil energy is 261 keV for the pp neutrinos and 665 keV for the ^7Be neutrinos. The recoil electrons can be detected through their ionization in a HP Ge detector with an energy resolution of 0.3%. GENIUS can measure only (like BOREXINO, and others) but with much better energy resolution) the energy distribution of the recoiling electrons, and not directly determine the energy of the incoming neutrinos. The dominant part of the signal in GENIUS is produced by pp neutrinos (66%) and ^7Be neutrinos (33%). The detection rates for the pp and ^7Be fluxes are according to the Standard Solar Model [17] $R_{pp} = 35$ SNU $= 1.8$ events/day ton (18 events/day 10 tons) and $R_{^7Be} = 13$ SNU $= 0.6$ events/day ton (6 events/day 10 tons) (1 SNU $= 10^{-36}$/s target atom).

To measure the low-energy solar ν flux with a signal to background ratio of 3:1, the required background rate is about 1×10^{-3} events/kg y keV in this energy range. This is about a factor of 10 smaller than what is required for the application of GENIUS for cold dark matter search. This can be achieved if the liquid nitrogen shielding is increased to

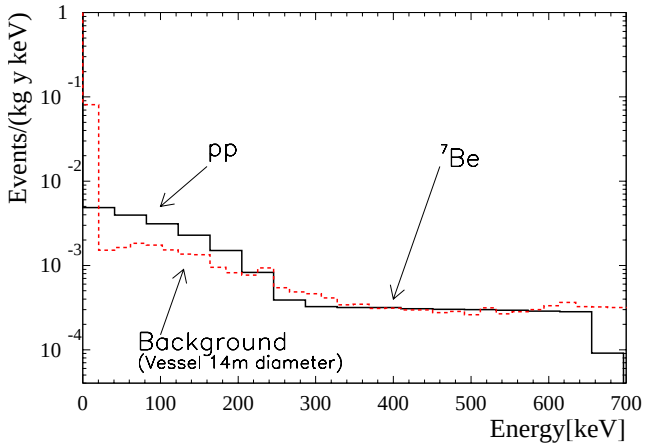

Figure 3: Simulated spectrum of low-energy solar neutrinos (according to SSM) for the GENIUS detector (1 tonne of Ge) (from [4], and estimated background).

at least 13 m in diameter and production of the Ge detectors is performed underground (see [3, 8], and Fig. 2).

Another source of background is coming from $2\nu\beta\beta$ decay of ^{76}Ge, which is contained in *natural* Ge with 7.8%. Using enriched ^{70}Ge or ^{73}Ge (>85%) as detector material, the abundance of the $\beta\beta$ emitter can be reduced up to a factor of 1500. In this case the *pp*-signal will not be disturbed by $2\nu\beta\beta$ decay (see [8] and Fig. 2).

The expected spectrum of the low-energy signal in the SSM is shown in Fig.3.

After the unfavouring of the SMA solution by Superkamiokande, it is important to differentiate between the LMA and the LOW solution. Here due to its relatively high counting rate, GENIUS will be able to test in particular the LOW solution of the solar ν problem by the expected day/night variation of the flux (see [7, 8]).

2 GENIUS and Cold Dark Matter Search

GENIUS would already in a first step, with 100 kg of *natural* Ge detectors, cover a significant part of the MSSM parameter space for prediction of neutralinos as cold dark matter (Fig. 4) (see, e.g. [10, 11, 12, 1]). For this purpose the background in the energy range < 100 keV has to be reduced to 10^{-2} (events/kg y keV). At this level solar neutrinos as source of background are still negligible (see Fig. 2). Fig. 4 shows together with the expected sensitivity of GENIUS, for this background, predictions for neutralinos as dark matter by two models, one basing on supergravity [12], another basing on the MSSM with more relaxed unification conditions [10, 11].

The sensitivity of GENIUS for Dark Matter corresponds to that obtainable with a 1 km^3 AMANDA detector for *indirect* detection (neutrinos from annihilation of neutralinos captured at the Sun) (see [13]). Interestingly both experiments would probe different neutralino compositions: GENIUS mainly gaugino-dominated neutralinos, AMANDA mainly neutralinos with comparable gaugino and Higgsino components (see Fig. 38 in [13]). It should be stressed that, together with DAMA, GENIUS will be for the foreseeable future

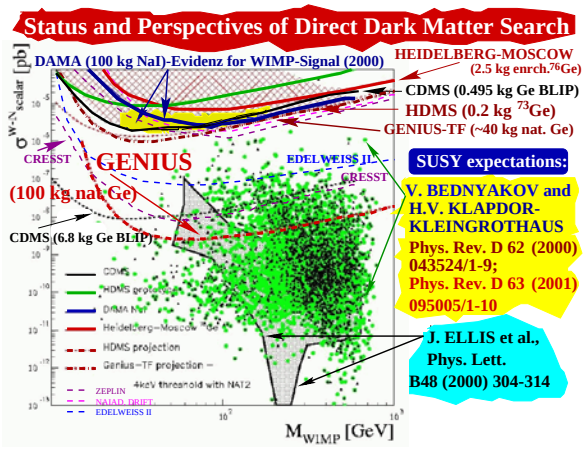

Figure 4: WIMP-nucleon cross section limits in pb for scalar interactions as function of the WIMP mass in GeV. Shown are contour lines of present experimental limits (solid lines) and of projected experiments (dashed lines). Also shown is the region of evidence published by DAMA. The theoretical expectations are shown by two scatter plots, - for accelerating and for non-accelerating Universe (from [10, 11]) and by the grey region (from [12]). *Only* GENIUS will be able to probe the shown range also by the signature from seasonal modulations.

the only future Dark Matter experiment, which would be able to positively identify a dark matter signal by the seasonal modulation signature.

3 GENIUS-TF

As a first step of GENIUS, a small test facility, GENIUS-TF, is at present under installation in the Gran Sasso Underground Laboratory [14]. With about 40 kg of natural Ge detectors operated in liquid nitrogen, GENIUS-TF (see Fig. 5) could test the DAMA seasonal modulation signature for dark matter. No other experiment running, or projected at present, will have this potential [5]. Up to summer 2001, already six 2.5 kg Germanium detectors with an extreme low-level threshold of ∼500 eV have been produced.

4 List of Proceedings (2001)

1. H.V. Klapdor-Kleingrothaus (ed.), Dark Matter in astro- and Particle Physics., Proc. of DARK2000, Heidelberg, GERMANY, July 10-14, 2000, Berlin, Germany: Springer (2001) 740 p.

5 List of Publications (2001)

1. V.A. Bednyakov, H.V. Klapdor-Kleingrothaus, Phys. Rev. D 63 (2001) 095005 and hep-ph/0011233.

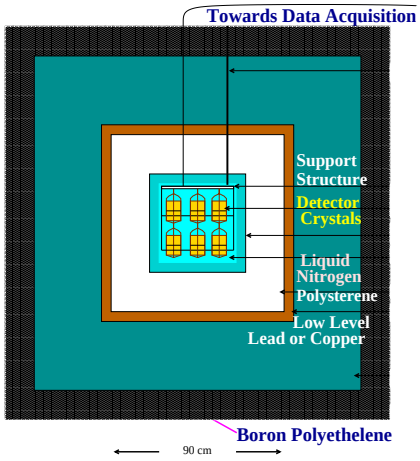

Figure 5: Conceptual design of the Genius TF. Up to 14 detectors will be housed in the inner detector chamber, filled with liquid nitrogen. As a first shield 5 cm of zone refined Germanium, or extremely low-level copper will be used. Behind the 20 cm of polystyrene isolation another 35 cm of low level lead and a 15 cm borated polyethylene shield will complete the setup.

2. S. Kolb, M. Hirsch, H.V. Klapdor-Kleingrothaus, O. Panella, Phys. Rev. D 64 (2001) 115006 and hep-ph/0102175.

3. V.A. Bednyakov, H.V. Klapdor-Kleingrothaus and H. Tu, Phys. Rev. D 63 (2001) 095005 (1-10) and in Proc. of DARK2000, Springer, Heidelberg (2001) Springer, Heidelberg (2001) 667 - 676.

6 List of Conference Contributions (2001)

1. H.V. Klapdor-Kleingrothaus, in Proc. of LowNu2, December 4 and 5, 2000, Tokyo, Japan, to be published in World Scientific (2001) (eds) Y. Suzuki et al., and Preprint: hep-ph/0104028.

2. H.V. Klapdor-Kleingrothaus, in Proc. of NOW2000, Conca Specchiulla (Otranto, Italy), September 9-16, 2000, Nucl. Phys. Proc. Suppl. 100, : (2001) 350 - 355, and Preprint: hep-ph/0104074.

3. H.V. Klapdor-Kleingrothaus, B. Majorovits, L. Baudis, A. Dietz, G. Heusser, I. Krivosheina, H. Strecker, in Proc. of DARK2000, Springer, Heidelberg (2001) 553-568 and Preprint: hep-ph/0103082.

4. S. Kolb (Heidelberg, H.V. Klapdor-Kleingrothaus, M. Hirsch, O. Panella, in Proc. of DARK2000, Springer, Heidelberg (2001) Springer, Heidelberg (2001) 276-282.

5. H.V. Klapdor-Kleingrothaus, in Proc. of NANPino, Dubna, Russia, July 19-22, 2000, Particles and Nuclei, Letters, issues 1/2 (2001) 20-39 and and Preprint: hep-ph/0103319.

6. H.V. Klapdor-Kleingrothaus, B. Majorovits in Proc. of IDM2000, England, September 18-22, 2000, World Scientific (2001) 593-602 and Preprint:hep-ph/0103079.

7. H.V. Klapdor-Kleingrothaus and B. Majorovits , in Proc. of IDM2000, England, September 18-22, 2000, World Scientific (2001) 354 and Preprint:hep-ph/0103079.

8. H.V. Klapdor-Kleingrothaus et al. in Proc. of DM 2000, Marina del Rey, California, 23-25 Feb 2000, Springer 2001, edited by D. Cline, (2001) 493-504 and astro-ph/0005568

9. L. Baudis, A. Dietz, G. Heusser, B. Majorovits, H. Strecker, H.V. Klapdor-Kleingrothaus, hep-ex/0012022.

References

[1] H.V. Klapdor-Kleingrothaus, "60 Years of Double Beta Decay", *World Scientific, Singapore* (2001) 1253 p.

[2] L. Baudis, G. Heusser, B. Majorovits, Y. Ramachers, H. Strecker and H.V. Klapdor–Kleingrothaus *Nucl. Instr. Meth.* **A 426** (1999) 425.

[3] L. Baudis and H.V. Klapdor-Kleingrothaus, *Eur. Phys. J.* **A 5** (1999) 441-443 and in Proc. BEYOND'99 Castle Ringberg, Germany, 6-12 June 1999, ed. by H.V. Klapdor-Kleingrothaus and I.V. Krivosheina, *IOP Bristol* (2000) 1023 - 1036.

[4] H.V. Klapdor-Kleingrothaus et al. to be publ., and *http* : *//www.mpi − hd.mpg.de/non_acc/*

[5] H.V. Klapdor-Kleingrothaus, in Proc. of LP01, July 23 - 28, 2001, Rome, Italy, *World Scientific, Singapore* (2002)

[6] H.V. Klapdor-Kleingrothaus et al. *MPI-Report* **MPI-H-V26-1999** and *Preprint: hep-ph/***9910205** and in Proc. of BEYOND'99 Castle Ringberg, Germany, 6-12 June 1999, ed. by H.V. Klapdor-Kleingrothaus and I.V. Krivosheina, *IOP Bristol* (2000) 915 - 1014.

[7] H.V. Klapdor-Kleingrothaus, in Proc. of NOW2000 *Nucl. Phys.* **B 100** (2001) 350-355 and 309-313, ed. G. Fogli and *Preprint: hep-ph/***0102277**, *Preprint: hep-ph/***0102276**.

[8] H.V. Klapdor-Kleingrothaus, in Proc. of LowNu2 December 4 and 5 (2000) Tokyo, Japan, ed: Y. Suzuki, World Scientific, Singapore (2001), home page: *http://www-sk.icrr.u-tokyo.ac.jp/neutlowe/2/transparency/ index.html*

[9] H.V. Klapdor-Kleingrothaus, J. Hellmig and M. Hirsch, *J. Phys.* **G 24**, 483 (1998).

[10] V.A. Bednyakov and H.V. Klapdor-Kleingrothaus, *Phys. Rev.* **D 62** (2000) 043524.

[11] V.A. Bednyakov and H.V. Klapdor-Kleingrothaus, *Preprint: hep-ph/***0011233** (2000) and *Phys. Rev.* **D 63** (2001) 095005.

[12] J. Ellis, A. Ferstl and K.A. Olive, *Phys. Lett.* **B 481**, 304–314 (2000) and *Preprint: hep-ph/***0001005** and *Preprint: hep-ph/***0007113**.

[13] J. Edsjö, *http://www.physto.se/edsjo/*

[14] H.V. Klapdor-Kleingrothaus, L. Baudis, A. Dietz, G. Heusser, I.V. Krivosheina, B. Majorovits and H. Strecker, hep-ex/0012022, Subm. for Publ. (2001).

[15] see: *http://www.sns.ias.edu.jnb/*

[16] J.N. Bahcall, *Neutrino Astrophysics*, Cambridge Univ. Press (1989).

[17] J.N. Bahcall, S. Basu and M. Pinsonneault, *Phys. Lett.* **B 433**, 1 (1998).

GNO. Gallium Neutrino Observatory

M. Altmann[a], M. Balata[b], P. Belli[c], E. Bellotti[d],
R. Bernabei[c], E. Burkert[e], C. Cattadori[d], G. Cerichelli[f],
R. Cerulli[c], M. Chiarini[f], M. Cribier[g], S. d'Angelo[c],
G. Del Re[f], K. Ebert[h], F. von Feilitzsch[a], N. Ferrari[b],
W. Hampel[e], F. X. Hartmann[e] E. Henrich[h], G. Heusser[e],
J. Kiko[e], T. Kirsten[e], L. Ioannucci[b], D. Motta[e], T. Lachenmaier[a],
J. Lanfranchi[a], M. Laubenstein[b], L. Pandola[b], S. Nisi[b] ,
F. Petricca[d], H. Richter[e], M. Weneser[a], L. Zanotti[d]

[a] Physik Department E15, Technische Universität München (TUM),
James-Franck Straße, D-85748 Garching b. München, Germany
[b] INFN, Laboratori Nazionali del Gran Sasso (LNGS),
S.S. 17/bis Km 18+910, I-67010 L'Aquila - Italy
[c] Dip. di Fisica, Università di Roma Tor Vergata and INFN, Sez. Roma II,
Via della Ricerca Scientifica, I-00133 Roma - Italy
[d] Dip. di Fisica, Università di Milano Bicocca, and INFN Sez. Milano,
Piazz.le delle Scienze 3, I-20126 Milano - Italy
[e] Max-Plank-Institut für Kernphysik (MPIK), P.O.B. 103980,
D-69029 Heidelberg - Germany
[f] Dip. di Ingegneria Chimica e Materiali, Università dell'Aquila,
Località Monteluco di Roio, 67100 L'Aquila - Italy
[g] DAPNIA/Service de Physique de Particules, CE Saclay,
F-91191 Gif-sur-Yvette Cedex - France
[h] Institut für Technische Chemie, Forschungszentrum Karlsruhe (FZK),
Postfach 3640, D-76021 Karlsruhe, Germany

Abstract

GNO (Gallium Neutrino Observatory) is monitoring the low energy solar neutrino flux with a 30 tons gallium detector at LNGS. During the year 2001, 13 solar runs and 4 blank runs have been successfully done; in total 43 solar runs (corresponding to $\approx$ 1230 days of live time) have been accumulated since spring 1998 when GNO started the data taking. Data from the first 35 solar runs (1015 days of live time) have been evaluated and results were released at the TAUP2001 conference; the neutrino interaction rate measured by GNO as from solar runs SR1-SR35 is : 67.7 $\pm$7.2 (stat.)$\pm$3.2 (sys.) SNU. The combined result from both GNO and GALLEX together is 73.3 $\pm$4.7 (stat.)$\pm$4.0 (sys.) SNU. In this report we describe the various activities carried on during 2001, and the R&D in progress.

1 Introduction

The gallium solar neutrino experiment at Laboratori Nazionali del Gran Sasso detects solar neutrinos via the reaction $^{71}Ga\,(\nu_e, e\,)^{71}Ge$, which has a threshold of 233 keV. The detector is sensitive mainly to pp-neutrinos (53% of the interaction rate according to the standard solar model [1]), with smaller contributions from ^{7}Be ν (27%), ^{8}B ν (12%), and CNO ν (8%).

The target consists of 101 tons of a $GaCl_3$ solution in water and HCl, containing 30.3 tons of natural gallium; this amount corresponds to $\sim 10^{29}$ ^{71}Ga nuclei.

The ^{71}Ge atoms produced by solar neutrinos (at a rate of about 0.6 per day, one half of the amount predicted by solar models) are extracted from the gallium tank every 4 weeks [2] and introduced in low-background gas proportional counters [3] as germane gas (GeH_4). The decay of ^{71}Ge (e.c., τ=16.5 days) produces a signal in the counters consisting of a point-like ionization at 10.4 keV, or 1.1 keV. The signal is recorded by fast digitizers in order to allow background reduction by pulse shape analysis. The solar neutrino interaction rate on ^{71}Ga is deduced from the number of ^{71}Ge atoms observed. For a complete description of the experimental procedure see [4].

The gallium detector was operated between 1991 and 1997 by the GALLEX collaboration: 65 'solar runs' were performed. The solar neutrino capture rate on ^{71}Ga was measured with a global uncertainty of 10% as: 77.5 $\pm$ 6.2 (stat.) $^{+4.3}_{-4.7}$ (sys.) SNU[1] (1σ) [4]. This result has important physical implications both for astrophysics and for particle physics (for discussion see for example [5]).

After maintenance of the chemical plants and renovation of the DAQ and electronics, a new series of measurements was started in April 1998, within the GNO (Gallium Neutrino Observatory) project [6]. The experiment is presently running with 30 tons of gallium (GNO30). The goals of GNO are:
- measurement of the interaction rate of low energy solar neutrinos on gallium, with an accuracy of 4-5% (half of the error achieved in GALLEX);
- monitoring of the neutrino flux over a complete solar cycle.

The result from the first three years of running of GNO, although compatible with the GALLEX result, is even lower: $67.7 \pm 7.2(stat) \pm 3.2(syst)$ The central value is lower

[1] 1 SNU (Solar Neutrino Unit) = 10^{-36} captures per second and per absorber nucleus.

than the rate expected from pp neutrinos only which, for a large class of solar models, is independent from the details of the models themselves. Therefore the gallium results strongly support and confirm that the solution of the solar neutrino problem must be found in the ν physics domain, i.e. in the flavor mixing. After the SNO results [7], which demonstrate (at present at level of 3.1 σ) that active neutrinos other than ν_e reach the Earth, the knowledge of the interaction rate with a low energy threshold is essential to define the mixing mechanism and the oscillation parameters. When the ^{7}Be interaction rate will be measured by Borexino, the entire set of data on rates and on other effects (day-night, seasonal, energy spectrum distortion) will be available, together with data from accelerators and reactors, it will be possible to define with good accuracy the pattern of ν mixing.
Finally let us remark that next generation real-time experiments able to lower the threshold to cover the pp energy region are still in a R&D phase and are not expected to start observations at least in the next 5 years (for a review see for example [23]).

In section 2 we describe the GNO solar neutrino observations performed until now (1015 days of live time). In section 3 we report the experimental activity carried on during 2001. In section 4 we describe several items of the R&D activity in progress.

2 Solar neutrino observations

2.1 Run schedule

GNO started solar neutrino observations in May 1998. 13 solar runs and 4 blank runs were successfully performed in the year 2001, as listed in Table 1. A similar list of previous extractions can be found in the LNGS annual report for 2000 [13]. At the beginning of January 2002, counting was completed for 38 solar runs and 7 blanks; other 5 solar runs and 2 blanks are still counting.

2.2 Data analysis

As mentioned in sect.1, the extracted Ge is inserted, as GeH_4, in proportional counters; genuine ^{71}Ge decays give a characteristic signal on the fast digitizer with a fast rise time, because they produce a point-like ionization in the counting gas: the recorded pulses are fast compared to most background events. Pulses with amplitudes compatible with L and K captures (corresponding respectively to 1.1 and 10.4 keV) are selected according to their shape; for the pulse shape discrimination we used untill now a one parameter cut. We consider the rise-time (RT) from 8% to 60% of the pulse amplitude; RT is required to be less than 40-45 ns, depending on the specific counter and gas mixture. The cut has a high efficiency for ^{71}Ge signals ($\geq$ 95%) and rejects most background. The time momenta distribution of the pulses is then analyzed via maximum likelihood analysis.

2.3 Results

Data from the first 35 GNO solar runs (extractions performed from May 1998 until May 2001) have been evaluated and results have been presented at the TAUP 2001 conference

Table 1: Summary of GNO runs performed between January 2001 and December 2001. For each extraction the following data are reported: extraction label; DAQ lable (SR=Solar Run, BL=BLank); extraction date, referred to the end of the extraction; exposure time in days; counter type and number used for ^{71}Ge counting (Fe=Iron cathode, Si=Silicon cathode, FC=Iron shaped cathode, SC=Silicon shaped cathode); counting time (status at 10-Jan-2002); chemical yield (tank to counter), measured by non-radioactive Ge carrier.

Extraction label	Type	Date	Exposure (days)	Counter	Counting time (days) (10-Jan-2002)	Chemical yield (%)
EX40	SR31	10-jan-01	27	FC-126	163.3	96.2
EX41	SR32	07-feb-01	28	SC-139	165.6	95.0
EX42	SR33	07-mar-01	28	Si-106	166.7	97.8
EX43	BL6	08-mar-01	1	Si-108	165.8	95.1
EX44	SR34	04-apr-01	27	FC-093	167.8	92.3
EX45	SR35	03-may-01	28	SC-138	166.8	95.1
EX46	SR36	30-may-01	28	Fe-039	160.9	96.5
EX47	BL7	31-may-01	1	SC-156	160.9	94.3
EX48	SR37	27-jun-01	27	FC-126	166.7	95.3
EX49	SR38	25-jul-01	28	SC-151	166.8	95.3
EX50	SR39	22-aug-01	28	SC-150	140(*)	98.7
EX51	SR40	19-sep-01	28	Fe-112	112(*)	96.2
EX52	BL8	20-sep-01	1	Si-119	111(*)	94.4
EX53	SR41	17-oct-01	27	SC-139	85(*)	94.1
EX54	SR42	14-nov-01	28	Si-108	57(*)	97.2
EX55	SR43	12-dec-01	28	SC-138	28(*)	95.9
EX56	BL9	13-dec-01	1	Fe-039	27(*)	93.8

(*) counters still counting (at 10-jan-2002)

[8]. A total of 172 decaying ^{71}Ge atoms were identified from the 1015 days of exposure in solar runs SR1-SR35. The corresponding ν interaction rate is 67.7 $\pm$7.2 (stat.)$\pm$3.2 (sys.) SNU [8]. The combined result for GALLEX and GNO (65+35=100 solar runs, corresponding to 1594+1015=2609 days of live time) is 73.3 $\pm$4.7 (stat.)$\pm$4.0 (sys.) SNU [8]. Results from the single GNO solar runs are reported in Table 2. For further information on the GNO results, their interpretation, data analysis, and for a discussion of the systematics of the experiment see references [8] and [10].

3 Experimental activity during 2001

3.1 Extraction system and synthesis line

During 2001 the following activities were performed at the extraction and synthesis plants:
- 17 extractions (13 solar runs and 4 blanks) were successfully performed (see Table 1);

Table 2: Measured solar neutrino capture rate (SNU) in the GNO solar runs SR1-SR35. For details on the distribution of single run results and their interpretations, and time-dependent analyses of the signal we refer to ref. [8].

Extraction lable	DAQ lable	Counter	Counting time (d)	Excess counts	Backgr. (cpd)	SNU
GNO-I solar runs						
EX003	SR01	sc138	179.6	5.6	0.023	$\mathbf{73}^{+45}_{-36}$
EX004	SR02	fe118	173.5	3.2	0.044	$\mathbf{49}^{+46}_{-34}$
EX005	SR03(*)	si114	162.3	6.2	0.185	$\mathbf{91}^{+62}_{-50}$
EX006	SR04	si113	138.8	4.6	0.083	$\mathbf{66}^{+50}_{-39}$
EX007	SR05(*)	fe093	137.7	0.0	0.204	$\mathbf{0}^{+40}_{-34}$
EX008	SR06	si108	166.5	3.0	0.058	$\mathbf{36}^{+49}_{-37}$
EX009	SR07	sc136	180.6	9.1	0.064	$\mathbf{122}^{+56}_{-46}$
EX010	SR08	fc102	179.4	0.0	0.106	$\mathbf{0}^{+45}_{-36}$
EX011	SR09	sc135	194.7	7.3	0.024	$\mathbf{96}^{+52}_{-42}$
EX013	SR10	sc139	187.4	8.6	0.016	$\mathbf{129}^{+54}_{-43}$
EX014	SR11	fe039	180.4	3.5	0.024	$\mathbf{55}^{+41}_{-30}$
EX015	SR12	fe043	179.4	1.2	0.207	$\mathbf{17}^{+67}_{-45}$
EX016	SR13	sc136	165.8	7.0	0.053	$\mathbf{87}^{+51}_{-41}$
EX017	SR14	fe093	167.7	7.0	0.086	$\mathbf{117}^{+70}_{-56}$
EX018	SR15	fc102	165.6	3.8	0.064	$\mathbf{51}^{+40}_{-30}$
EX019	SR16	si113	165.4	3.6	0.086	$\mathbf{47}^{+47}_{-37}$
EX020	SR17	sc139	166.5	3.1	0.031	$\mathbf{37}^{+33}_{-24}$
EX021	SR18	fe039	166.6	4.0	0.019	$\mathbf{55}^{+45}_{-35}$
EX022	SR19	si106	165.5	4.6	0.047	$\mathbf{69}^{+51}_{-39}$
GNO-II solar runs						
EX024	SR20	si108	164.6	4.9	0.038	$\mathbf{77}^{+51}_{-39}$
EX025	SR21	fc093	167.8	2.0	0.089	$\mathbf{29}^{+51}_{-33}$
EX026	SR22	fc174	166.6	0.5	0.061	$\mathbf{3}^{+36}_{-24}$
EX028	SR23	sc136	167.8	10.6	0.027	$\mathbf{143}^{+57}_{-47}$
EX029	SR24	fe039	165.8	5.3	0.049	$\mathbf{81}^{+51}_{-39}$
EX032	SR25	si106	167.7	4.8	0.058	$\mathbf{69}^{+58}_{-46}$
EX033	SR26	sc138	167.8	7.1	0.056	$\mathbf{89}^{+48}_{-38}$
EX034	SR27	si108	166.6	3.8	0.058	$\mathbf{47}^{+52}_{-40}$
EX036	SR28	fc174	166.6	4.1	0.050	$\mathbf{60}^{+41}_{-29}$
EX037	SR29	fc102	167.5	0.0	0.132	$\mathbf{0}^{+36}_{-24}$
EX038	SR30	sc136	166.5	8.6	0.034	$\mathbf{119}^{+54}_{-44}$
EX040	SR31	fc126	163.3	6.4	0.093	$\mathbf{103}^{+60}_{-49}$
EX041	SR32	sc139	165.6	6.9	0.020	$\mathbf{88}^{+44}_{-34}$
EX042	SR33	si106	166.7	3.8	0.067	$\mathbf{51}^{+47}_{-36}$
EX044	SR34	fc093	167.8	8.2	0.095	$\mathbf{121}^{+63}_{-52}$
EX045	SR35	sc138	166.7	3.4	0.030	$\mathbf{45}^{+36}_{-25}$

(*) No RT cuts applied

Table 3: Carrier solutions concentration.

Carrier	Date of preparation	N. pair meas.	Conc.$_{new}$	$\pm$ [nmol/g]	Conc.$_{old}$	Δ [%]
Ge 70	31-08-95	19	0.99191	0.0084	0.984	0.80
Ge 72	18-10-97	20	0.9918	0.0100	1.0141	-2.20
Ge 74	19-10-97	20	0.99034	0.0067	1.0037	-1.33
Ge 76	29-02-93	21	0.96143	0.0075	0.976	-1.49

- a new precise characterization of the extraction plant and of the kinetics of Ge desorption was performed [9] in order to further optimize the desorption and concentration times. Results on desorption time profile confirm old measurement done at the beginning of GALLEX, and moreover indicates that a speed up of 1 h (over 2 h) in the concentration phase of is feasible keeping the same yield.
- maintenance of the building safety equipment: building ventilation system, tank leak sensor, HCl leak detector;
- maintenance of gallium tank, absorber plant, auxiliary plants;
- maintenance of the main building, containing the gallium tank: care of the structure, of the electrical plant, water distribution piping, etc.

3.2 Atomic absorption analysis

In year 2001 we performed 2 extensive campaigns of atomic absorption spectroscopy (AAS) measurements (march and september) to redetermine carrier solution concentration. Table 3 reports the newly determined values as well as the old ones adopted up to now. As the accuracy has improved compared to old measuraments, the newly determined concentration values will be adopted in the determination of extraction yields after a third series of measurements planned for february 2002.
Moreover AAS has been carried on at LNGS to control the extraction yield; Table 4 lists the yields as directly determined by calibrated volumes at the Baratron pump after the synthesis, and the AAS yield determination. We can notice that the two results are in very good agreement better then axpected from the evaluated accuracy of the two methods ($\approx$ 1.5 % for the volume determination, and $\approx$ 2.0 % for the AAS).

3.3 Electronics and DAQ system

The improvement on the electronics set-up as compared with the GALLEX one was described in the previous LNGS annual reports [11] and [12]. During 2001 the counting system was upgraded with a new digitizer (TDS2). Each event from proportional counters is now digitized on three different time scales: TDF (time window: 409.6 ns); TDS1 (time window: 819.2 μs); TDS2 (time window: 8.192 μs). Fast decays from point-like ionization are selected using the TDF pulse (figure 2 (a) and (b), as described in sections 2 and 3.6);

Table 4: Tank to counter yields measured by volume standards and by Atomic Absorption Spectroscopy (AAS) in the first 52 GNO extractions

Extr	AAS	Bar	Extr	AAS	Bar	Extr	AAS	Bar	Extr	AAS	Bar
ex01	96.7	94.5	ex14	95.9	97.7	ex27	95.6	95.2	ex40	97.8	95.3
ex02	95.7	96.7	ex15	94.4	95.4	ex28	95.9	95.5	ex41	96.7	95.4
ex03	98.6	96.2	ex16	95.8	94.7	ex29	95.2	94.0	ex42	97.2	98.3
ex04	95.6	93.7	ex17	96.1	95.1	ex30	97.7	98.7	ex43	93.7	95.7
ex05	95.7	94.6	ex18	97.6	97.6	ex31	95.2	95.7	ex44	93.7	93.0
ex06	94.0	97.9	ex19	95.8	95.3	ex32	94.4	94.7	ex45	97.1	95.2
ex07	94.6	95.7	ex20	95.1	95.2	ex33	95.1	95.0	ex46	98.7	97.7
ex08	97.8	94.7	ex21	96.1	94.6	ex34	97.9	99.3	ex47	95.8	95.2
ex09	99.1	94.5	ex22	97.1	90.4	ex35	95.4	96.5	ex48	96.3	94.5
ex10	97.8	97.9	ex23	94.2	95.7	ex36	93.5	94.9	ex49	99.0	95.3
ex11	95.3	95.5	ex24	94.5	94.7	ex37	96.6	94.5	ex50	99.4	98.7
ex12	92.5	93.7	ex25	95.4	94.7	ex38	97.4	98.3	ex51	96.3	96.1
ex13	94.4	94.4	ex26	97.7	97.9	ex39	94.5	94.9	ex52	95.9	94.9

TDS1 is used to flag Bi-Po events within a Rn chain (figure 2 (e)), see section 3.5; TDS2 was introduced to reject with high efficiency electronic noise with a simple pulse shape analysis. This is evident when one compares the TDS2 pulses in figure 2 (a) and (b) (from ionization events) with the pulses (c) and (d) (produced by electronic noise).

3.4 ^{69}Ge and ^{71}Ge calibrations

One of the most important goals for GNO is to substantially reduce the systematic error that affected the final GALLEX result; we faced in 2001 this problem starting an intense activity for the determination of the counting efficiencymof individual counters at 1% level. In fact, the major component ($\approx 4\%$) of the systematic error comes from the actual knowledge of this parameter. For the absolute calibration we fill the counter with ^{69}Ge activity (≈ 50 Hz); ^{69}Ge decays ($t_{1/2} = 39$ h) through E.C. to ^{69}Ga emitting a 1.106 MeV γ ray with a B.R of 27% which escapes from the counter, given its small volume; the x-rays and Auger electrons from the prompt rearrangement of ^{69}Ga atom is of course the same as for ^{71}Ga produced in ^{71}Ge E.C. Then the counter is inserted in a well shaped NaI detector having 4π geometry; the ratio between the number of events detected in coincidence by (NaI AND counter) and the number of events detected by NaI gives directly the efficiency of the counter. Table 5 lists the counting efficiency for the calibrated counters; the 5 counters calibrated in 2001 (june and december) are distinguished by a $^{+}$. In former time (GALLEX) the counting efficiency ϵ was determined for a few counters filled with a calibrated ^{71}Ge activity and extrapolating on other counters of the same type using individual total volume and longitudinal moltiplication curves. At present we have 8 absolute calibrated counters that counted 21 GNO runs and 41 GALLEX runs.
^{69}Ge measurements are performed at MPI in Heidelberg, as we always adopted a safe

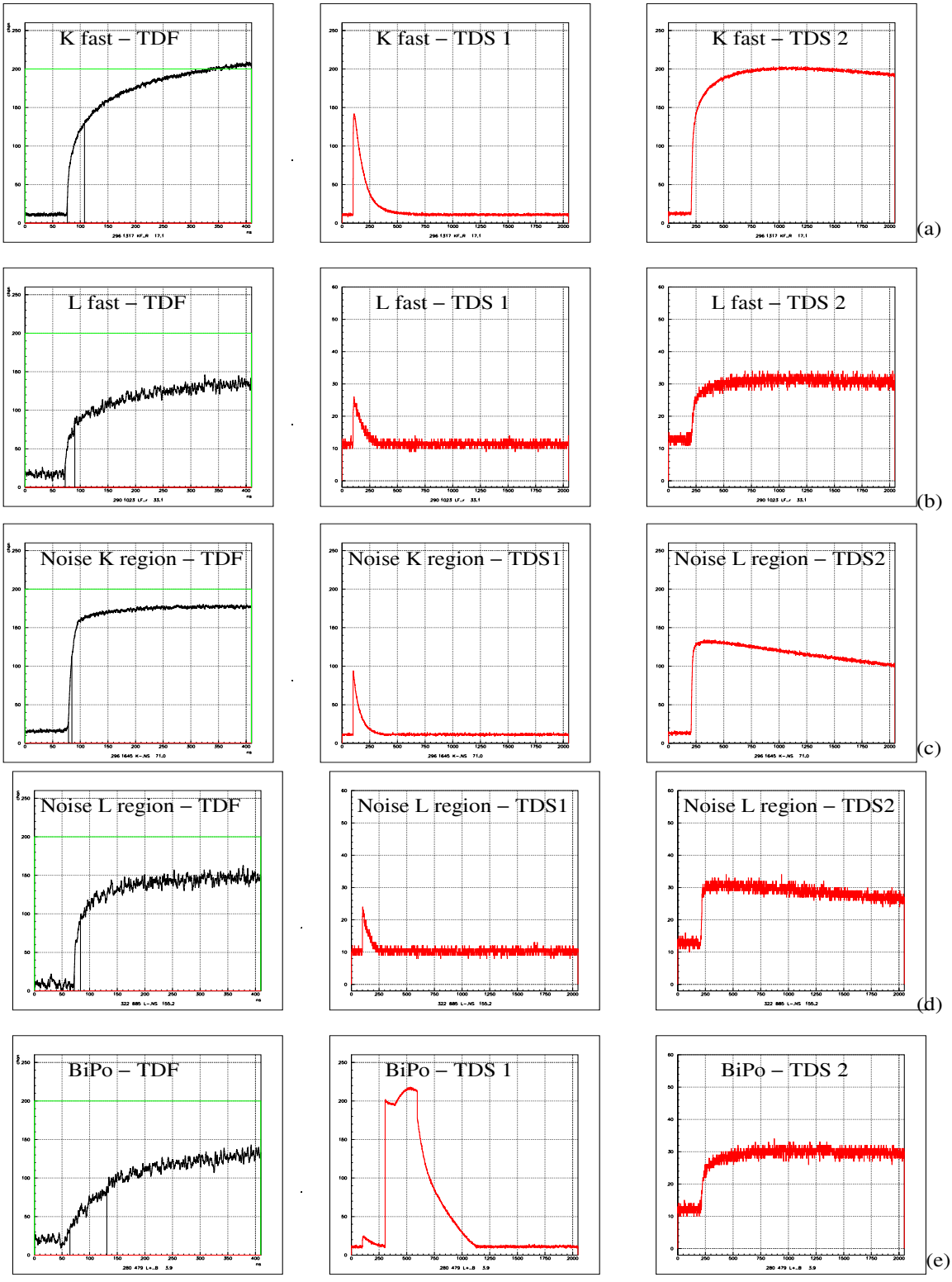

Figure 1: Examples of pulses digitized by the GNO DAQ system. (a) Fast ionization pulse inside the K energy window; (b) Fast ionization pulse inside the L energy window; (c) Noise pulse in the K energy region; (d) Noise pulse in the L energy region; (e) Bi-Po event. For comments see text.).

Table 5: Counting efficiencies for absolutely calibrated counters.

Counter	Counting efficiency (%)		GNO		GALLEX		
	^{69}Ge cal.	old determ.	Solar r.	Blank r.	Solar r.	Blank r.	Source/As r.
Fe43*		76.7±2.1	1	0	4	1	0
FC93^{+}	79.9±0.7	80.0±4.0	4	1	1	0	1
Fe39*		76.4±2.1	4	2	5	1	3
FC102^{+}	78.9±0.9	81.4±4.0	3	1	0	0	1
Si106^{+}	74.8±1.0	77.1±4.0	3	0	3	3	2
FC174^{+}	78.8±0.6	81.7±4.0	2	0	0	0	1
Si119*		77.2±2.1	0	1	4	3	3
SC136^{+}	80.9±0.7	82.3±4.0	4	0	2	2	1
Fe103			0	0	3	3	4
Total			21	5	22	14	16

$^{+}$ Counters calibrated in 2001 with ^{69}Ge; * Counters calibrated in former time with ^{71}Ge.

policy of never manipulate any significant Ge activity at LNGS. When the ^{71}Ge activity, produced together with the ^{69}Ge, is at a level of 1 Hz, the counter is brought to LNGS and ^{71}Ge spectra are collected to be used as reference pulses for the neural network analysis. Then the counter goes back to Heidelberg where it is emptied and then back again to LNGS to measure the background for a couple of months. Each counter filled with Ge activity is removed from the pool of counters to be used for solar runs for about 5-6 months and it is reintroduced only when the background is compatible with the required standard. Ge activity is produced at the CN accelerator at INFN Laboratori Nazionali di Legnaro; ≈ 0.4 g of $^{nat}GaO_2$ are irradiated with 7 MeV protons, to produce the reaction $^{69,71}Ga(p,n)^{69,71}Ge$. After 20 minutes of irradiation at 20nA proton current we obtain enough activity to transport the irradiated GaO_2 to Heidelberg and then perform the absolute calibration of 2-3 counters with the same batch.

3.5 Radon test

The experience with GALLEX has shown that a few Rn atoms are sometimes introduced in the counters during the synthesis and counter filling operations. The decays of Rn and its daughters can produce events which simulate real ^{71}Ge events, and are concentrated in the first days of counting (the half-life of ^{222}Rn is 3.83 days). A 'Rn cut' is introduced in the data analysis, by defining a dead time for each detected Rn decay chain (see [25] for details). The efficiency of this cut was evaluated in GALLEX to be (91±5)% [15], and the uncertainty on that number represents a relevant component of the systematic error in the experiment ($\approx 1.5\%$, see [10]). We started a Rn test to further improve the characterization and understanding of Rn events, and to decrease the systematic uncertainty due to the Rn cut. Rn atoms are emanated by a Ra source and diffuse through a capillar and a valve into the active volume of a proportional counter. The

optimal Rn decay rate for a good measurement is of the order of 4-5 Rn chains per day, as one has the need to have a low activity (in order not to overlap different chains) and the requirement to collect a sufficiently large statistic. This rate was reached after a careful fine tuning of source strenght and opening of the valve. The measurement was carried-on from 20-May-99 to 8-Mar-01 (1.8 years counting time). The decay of the Rn atoms and its daughters was recorded with the same counter filling, electronics and DAQ used for standard runs. The analysis of the data acquired allows a good understanding of the Rn chain events (see [13]). After this long measurement we closed the emanation valve and started to measure the intrinsic background of the counter; this is presently ongoing (220 days counting time). With the presently available data the estimate of the Rn cut inefficiency is (1.7±4.7)%, and agrees well with the previous GALLEX estimates (9±5)%. We plan to continue the background measurement in order to accumulate 1.5 yars of counting time, which will allow a determination of the inefficiency with an accuracy $\leq$4%.

3.6 Pulse shape analysis

Data analysis is carried on with the energy-rise-time method described in section 2; a more sophisticated pulse-shape (PS) analysis based on fitting the whole pulse rather than the rise-time (RT) only is now developed. Each pulse is fitted with the typical point-like ionization pulse (reconstructed from the X-ray counter calibration, see [12]) convoluted with a charge collection function and with the electronic response function. The width of the collection function is proportional to the spreading of the primary charge inside the counter gas. Cuts can be defined on several parameters of the charge collection function, which are evaluated from the fit of the pulses themselves.
In this PS analysis, the same energy cut as E-RT analysis is maintained. Once the PS parameters have been evaluated, the acceptance or rejection of an event is made by a neural network (NN). The NN algorithm, which has been implemented as a software code, uses the PS parameters as inputs and gives a unique (continuum) value $R \in [0, 1]$ as output. A cut R_{cut} on this output can be fixed (i.e. $R_{cut} = 0.5$), so that a pulse is accepted as a ^{71}Ge decay if its PS fitted parameters give a NN output R greater than R_{cut}. The NN-based analysis provides several advantages when compared to standard RT analysis:

- in the calculation of the output R, the input parameters receive different weights, according to their actual discrimination powers. This means that the less significant parameters do not affect very much the final results.

- the NN learns to compute the function R(inputs) through representative examples (both from ^{71}Ge and background calibrations). It is not necessary to provide general selection criteria (as usually happens) but only a suitable sample of training examples. It has been assumed, as a conventional choice, that ^{71}Ge decay pulses have the output $R = 1$ and background events have $R = 0$.

- the part of the parameters-space which characterizes the selected pulses has not necessarily box-shaped, as would happen if constant cuts for each parameter were fixed.

Table 6: Selection and noise rejection efficiencies for RT and NN analyses methods. The background rejection efficiency was evaluated from a calibration with a ^{137}Cs γ source.

Window	Selection eff. [%]		Background rejection eff. [%]	
	RT analysis	NN analysis	RT analysis	NN analysis
L	96.6	95.3	65.7	87.8
K	96.3	94.0	73.5	77.1

As L and K captures originate different classes of pulses, they are treated with a different NNs with different inputs. After a preliminary training stage, the network can be used to analyse data.

Figure 2 shows the application of the NN analysis on a "virtual" run (constructed by mixing several calibration runs) containing both ^{71}Ge and background events. The distribution of the network outputs has two sharp peaks located at the positions $R = 0$ (background events) and $R = 1$ (^{71}Ge events), so a clear characterization of the pulses in two different classes is obtained. As the valley between the two peaks is not populated, the analysis results is robust.

The NN analysis provides a selection efficiency which is a bit lower than RT analysis (see table 6) but background rejection efficiency is much better, mainly in the L window. This allow to get an improved signal-to-noise ratio and a more clean signal: consequently, a lower statistical error is obtained after the maximum likelihood (ML) analysis.

Table 7 compares the results from the NN analysis of the GNO solar runs[2] with the E-RT method. The two results are statistically compatible at the level of 0.8 σ (the 1 σ level is $\sigma \approx 3.5$ SNU). The compatibility has been evaluated by a MC simulation (for details on the method see [19]), taking into account that the event sets selected by the two analyses are not independent.

The NN analysis provides a 15% improvement of the signal-to-noise ratio and a 0.3 SNU reduction of the absolute statistical error. As the NN must be trained with real ^{71}Ge pulses and as the pulse shape may vary from a counter to an other, the method will be excellently used only when all the available counters have a their own absolute ^{71}Ge or ^{69}Ge calibration (see par. 3.4). When a run with a not calibrated counter is analysed with NN, an additional contribution to systematic error arises (about 2%) because it is necessary to extrapolate the ^{71}Ge training examples from one of the calibrated counters to the not calibrated one; this trouble is not found in the RT method because cerium calibrations can be used instead of ^{71}Ge. The only contribution to the systematic error from the calibrated counters for the NN analysis is due to the choice of the actual training examples among the whole set: we evaluated that this component is $\approx 1.0\%$ (preliminary result) for the L window and $\approx 1.5\%$ for the K window. This is of the same order as the systematic error estimated for the RT selection.
For further information on the NN-based PS analysis, see reference [24].

[2]The method could not be applied to the very first 3 runs, because the electronics had not yet its optimal settings.

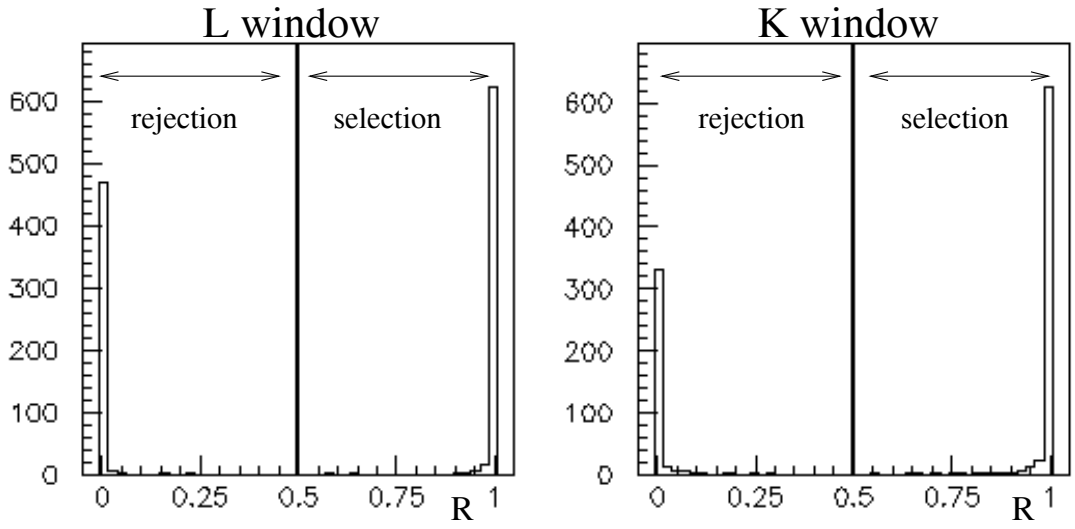

Figure 2: Distribution for the output values R of the NN analysis.

4 Plans for the future and R&D activities

4.1 Solar neutrino observations

We plan to go on with 4-week exposure solar runs over the next years. The only planned interruptions are foreseen for the ν calibration (see sect. 4.3) and for 1-day exposure blanks every three months.

4.2 Counter calibrations and tests

The Rn test (see par. 3.5) will be completed next year with the presently ongoing long background measurement. We will also complete the absolute determination of counting efficiency of all available proportional counters. In year 2002 a new production of counters will start at Max Planck Institute (Heidelberg) as we need to increase the number and renew the pool of available counters; they will be calibrated with ^{69}Ge before they are used for solar runs. [3].

4.3 Neutrino source

The gallium detector was calibrated two times (in 1994 and in 1995) with a man-made electron-neutrino source with known activity [17]. A very intense ($\approx$ 2 MCi) ^{51}Cr ν source was prepared for the calibrations at the Siloe reactor in Grenoble (France) and transported to LNGS after irradiation. ^{51}Cr is an isotope ideal for the calibration of the gallium detector: it has a meanlife of 40 days, and it emits two monochromatic neutrino lines at 750 keV (90%) and 430 keV (10%). The ratio R between the measured ^{71}Ge production rate and the expected production rate as deduced from the known source

[3] In the present status we have 18 counters available; 9 of them were absolutely calibrated.

Table 7: For each selection method (neural network and rise time) are shown: the $\nu_e - {}^{71}$Ga interaction rate (all corrections included), the number of events that are attributed to ^{71}Ge decays from ML analysis and the number of those attributed to background events. The quoted errors are only statistical. The data taking periods named GNO I and GNO II correspond to the two data release respectively from ref. [10] and ref. [8].

	Run	Energy	NN selection			RT selection		
		window	Rate (SNU)	^{71}Ge	bck	Rate (SNU)	^{71}Ge	bck
GNO I	1 - 19	L	$60.7^{+15.1}_{-13.7}$	37	115	$71.1^{+16.5}_{-15.1}$	44	134
		K	$57.9^{+12.7}_{-11.7}$	42	78	$59.5^{+12.9}_{-11.9}$	43	81
		L+K	$59.0^{+9.6}_{-9.0}$	79	185	$64.2^{+10.1}_{-9.5}$	87	205
GNO II	20 - 35	L	$66.25^{+16.8}_{-15.2}$	35	56	$77.4^{+18.4}_{-17.0}$	42	87
		K	$72.3^{+14.6}_{-13.3}$	43	59	$69.1^{+14.3}_{-13.0}$	42	60
		L+K	$70.0^{+10.8}_{-10.1}$	78	111	$72.5^{+11.2}_{-10.6}$	84	141
GNO I+II	1 - 35	L	$63.3^{+11.1}_{-10.4}$	72	171	$74.0^{12.1}_{-11.5}$	86	219
		K	$64.7^{+9.5}_{-8.9}$	85	137	$64.1^{+9.5}_{-8.9}$	85	139
		L+K	64.2±6.9	157	308	67.7±7.2	172	344

activity was found to be R = 0.93 ± 0.08 [18]. This proofs the absence of any unknown systematic errors at a level of less than 10%. Together with the results of the so called 'Arsenic test' (see ref. [4]), the source calibrations provide a measurement of the neutrino cross section on ^{71}Ga. Presently the collaboration is evaluating the feasibility of a new source experiment, with the aim of measuring as accurately as possible the ν ^{71}Ga cross section at energies close to those of the ^{7}Be solar ν.

Contacts are under way with the Research Institute of Atomic Reactors (RIAR) at Dimitrovgrad (Russia), for the irradiation of the enriched Cr samples previously used in GALLEX. A detailed design of the irradiation procedure and of the source handling and transportation is under discussion.

4.4 Cryogenic detectors

The E.C. of ^{71}Ge occurs mainly (84%) on the K shell; the excited ^{71}Ga atom subsequently emits Auger electrons of 10 KeV or X rays. Not all the emitted X-rays convert into the gas of the proportional counter, and events appear as "L events". To improve the efficiency at 10 KeV, it has been proposed to use cryogenic detectors which guarantee a practically 100% efficiency and a fine energy resolution. An R&D program started a few years ago and achieved significant technical results; the structure of the detector and the deposition of ^{71}Ge on it have been defined and positively tested [16]. At present, the problem of background is under investigation; a dedicated set-up is under construction at Garching. After these tests, the future program to complete the R&D phase will be planned and, finally, the merits of these detectors with respect to the proportional counters will be evaluated for further decision on their use in the experiment.

5 Conclusions

The gallium detector at LNGS is monitoring low energy solar neutrinos since May 1991 with 30 tons of natural gallium. From the 65 GALLEX solar runs plus the 35 GNO solar runs, the solar neutrino interaction rate on gallium has been measured with an overall accuracy of $\sim 8.4\%$. Data taking is going on regularely with four-week-exposure runs, with the aim to reach an accuracy of the order of 5%, and to study possible time dependences of the signal at 10-15% level. During year 2001 an intense experimental activity started to refine the determination of all experimental parameters relevant for the reduction of systematics, namely the counter efficiencies and the extraction yield. A completely new and independent pulse shape analysis has been developed (see par. 3.6) and the connected systematics evaluated. The ratio of experimental to theoretical solar neutrino (Standard Solar Model) interaction rate is

$$\begin{aligned} GNO^{RT}/SSM &= 0.525 \pm 0.061 \ (stat \ \& \ syst) \\ GNO^{NN}/SSM &= 0.503 \pm 0.053 \ (stat \ only) \\ GALLEX/SSM &= 0.600 \pm 0.059 \ (stat \ \& \ syst) \end{aligned}$$

The experimental rates come from GNO (35 solar runs, i.e. from July 1998 till May 2001), both for rise time (RT) and neural network (NN) analysis, and from GALLEX.

6 Acknowledgemnts

We want to thank Dr. Paolo Colautti, Dr. Ing. Federico Cervellera and the staff of CN Van der Graaf accelerator in Legnaro, and specially the CN operator Stefano Contran, for their precious and friendly help in the ^{69}Ge production. We aknowldge also the help of Dr. Keith Rowley in the synthesis work and the LNGS and other collaborating institute staffs for the support continuously given to GNO.

7 List of Publications (2001)

1. GNO collaboration, "GNO progress report for 2000", LNGS annual Report 2000, 57-68, GNO report n.15

2. E. Bellotti,"Solar neutrino observations; GNO" Nucl. Phys. (Proc.Suppl.) 91(2001) 44-49, GNO report n.16

3. N. Ferrari, "GNO and its performances", Nucl. Phys. (Proc.Suppl.) 100(2001) 48-50, GNO report n.17

8 List of Conference Presentations (2001)

1. C. Cattadori, "Update of solar neutrino interaction rate measurement from GNO at LNGS", TAUP 2001, LNGS, September 2001.

2. F. Petricca, "L'esperimento GNO", SIF 2001, Milano, September 2001

3. L. Pandola, "Analisi dei segnali nell'esperimento GNO", SIF 2001, Milano, September 2001

4. J.-C. Lanfranchi et al.: 'Entwicklung von Kryodetektoren für GNO', Spring meeting of the German Physical Society, 26.-30.3.2001, Hamburg, Germany.

5. T. Lachenmaier et al.: 'Development of Cryogenic Detectors for GNO', XIth Int. School on Particles and Cosmology, 18.-24.4.2001, Baksan, Russia.

6. T. Lachenmaier et al.: 'Development of Cryogenic Detectors for GNO', 9th Int. Workshop on Low Temperature Detectors (LTD-9), 23.-27.7.2001, Madison, USA.

References

[1] J.N.Bahcall, Astrop. J. 555 (2001) 990; S. Turck-Chiéze et al, Nucl. Phys. (Proc. Suppl.) 87 (2000) 162-171; V.Castellani et al., Nucl. Phys. (Proc. Suppl.) 70 (1999) 301-314.

[2] E.Henrich et al., 'GALLEX, a challenge for chemistry', Proc. IV Int'l. Solar Neutrino Conf., ed. W.Hampel, MPI Kernph., Heidelberg (1997) 151-162.

[3] R.Wink et al. Nucl. Inst. and Meth. A329 (1993) 541.

[4] GALLEX collaboration, Phys.Lett. B285 (1992) 376; Phys.Lett. B314 (1993) 445; Phys.Lett. B327 (1994) 377; Phys.Lett. B342 (1995) 440; Phys.Lett. B357 (1995) 237; Phys.Lett. B388 (1996) 384; Phys.Lett B436 (1998) 158; Phys.Lett. B447 (1999) 127.

[5] T.Kirsten, Rev.Mod.Phys. 71 (1999) 1213-1232.

[6] E.Bellotti et al., GNO collaboration, LNGS report INFN/AE-96-27.

[7] SNO collab., Phys. Rev. Lett. 87(2001)071301

[8] C.Cattadori, 'Update of solar neutrino interaction rate measurements from GNO at LNGS', TAUP2001, LNGS, September 2001.

[9] L.Cremonese, Tesi di Laurea, Università degli Studi dell'Aquila

[10] GNO collaboration, Phys Lett. B 490 (2000) 16-26.

[11] GNO collaboration, LNGS annual report 1998, pag. 55-69.

[12] GNO collaboration, LNGS annual report 1999, pag. 57-68.

[13] GNO collaboration, LNGS annual report 2000, pag. 57-68.

[14] G.Heusser, 'Characteristics of the GALLEX Spectrometer','Trends in Astroparticle Physics', ed. P. Ch. Bosetti, (1994) p.33, Teubner, Leipzig.

[15] H.Lalla, 'Zeitabhängiger Untergrund im GALLEX- Sonnenneutrino-Experiment', thesis, Ruprecht-Karls-Universität Heidelberg (1993).

[16] M.Altmann et al., Nucl.Inst.Meth. A444 (2000) 96-99.

[17] M. Cribier et al., Nucl. Inst. and Meth. A 378 (1996) 233-250.

[18] GALLEX collaboration, Phys Lett. B 436 (1998) 158.

[19] M.Altmann, Gallex internal note GX-124 (1998).

[20] SuperKamiokande Collaboration, Phys.Rev.Lett. 86 (2001) 4651.

[21] SNO collaboration, Phys.Rev.Lett. 87 (2001) 071301.

[22] Borexino collaboration, this report.

[23] S.Schoenert, 'Future solar and reactor experiments', TAUP2001, LNGS, September 2001.

[24] L.Pandola, Tesi di Laurea, Università degli Studi dell'Aquila, October 2001.

[25] F. Petricca, Tesi di Laurea, Università degli Studi di Milano, October 2001.

HDMS. Dark Matter Search

H.V. Klapdor-Kleingrothaus*[a], A. Dietz[a], G. Heusser[a],
I.V. Krivosheina[a,b], D. Mazza[a], H. Strecker[a], C. Tomei[a,c]

[a] Max-Planck Institut, Heidelberg, Germany
[b] Institute of Radiophysical Research, Nishnij Novgorod, Russia
[c] University of L'Aquila, Italy
* Spokesman of the Collaboration

Abstract

The Heidelberg Dark Matter Search (HDMS) is an experiment designed for the search for WIMP dark matter. It is using a special configuration of Ge detectors, to efficiently reduce the background in the low-energy region below 100 keV. After one year of running the HDMS detector prototype in the Gran Sasso Underground Laboratory, the inner crystal of the detector has been replaced with a HPGe crystal of enriched ^{73}Ge. The final setup started data taking in Gran Sasso in August 2000. The performance and the first results of the measurement with the final setup are discussed.

1 Introduction

Weakly Interacting Massive Particles (WIMPs) are leading candidates for the dominant form of matter in our Galaxy. These relic particles from an early phase of the Universe arise independently from cosmological considerations in supersymmetric particle physics theories as neutralinos - the lightest supersymmetric particles.

Direct WIMP detection experiments exploit the elastic WIMP scattering off nuclei in a terrestrial detector [1]. However, detecting WIMPs is not a simple task. Their interaction with matter is very feeble ($\sigma \leq \sigma_{weak}$) and predicted rates in supersymmetric models range from 10 to 10^{-5} events per kilogram detector material and day [2, 3, 4, 5, 6]. Moreover, for WIMP masses between a few GeV and 1 TeV, the energy deposited by the recoil nucleus is less then 100 keV. Thus, in order to be able to detect a WIMP, an experiment with a low-energy threshold and an extremely low radioactive background is required. Since the reward would be no less than discovering the dark matter in the Universe, a huge effort is put into direct detection experiments. More than 20 experiments are running at present and even more are planned for the future (for recent reviews see [7, 8, 9]).

2 Description of the experiment

HDMS operates two ionization HPGe detectors in a unique configuration [10]. A small, p-type Ge crystal is surrounded by a well-type Ge crystal, both being mounted into a common cryostat system (see Figure 1 for a schematic view). Two effects are expected to reduce the background of the inner target detector with respect to our best measurements with the Heidelberg-Moscow experiment [11]. First, the anticoincidence between the two detectors acts as an effective suppression of multiple scattered photons. Second, we know that the main radioactive background of Ge detectors comes from materials situated in the immediate vicinity of the crystals. In the case of HDMS the inner detector is surrounded (apart from the thin isolation) by a second Ge crystal - one of the radio-purest known materials. In order to reduce the background with respect to the prototype detector, the following changes has been made:

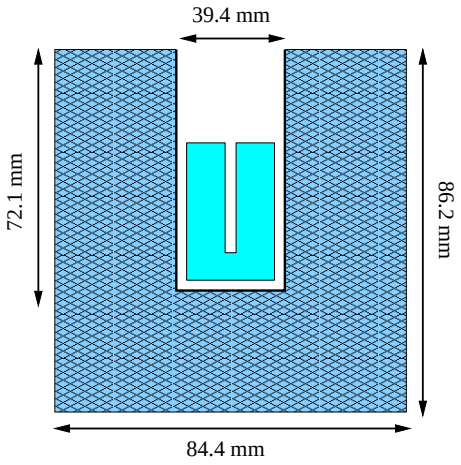

Figure 1: Schematic view of the HDMS detector configuration. All events which are seen in both the inner and the outer Ge-detector can be considered as background events, not resulting from a WIMP-nucleon recoil.

- The inner detector has been replaced by a crystal grown out of HPGe material enriched in ^{73}Ge. This has the effect that the mother isotope of cosmogenic ^{68}Ge production, ^{70}Ge (^{70}Ge(n,t)^{68}Ge), is deenriched by up to a factor of 50. Thus the decay of ^{68}Ge will be suppressed by this factor with respect to a natural HPGe crystal.
- The contacts of the HPGe crystals were pinched in order to avoid the use of soldering tin inside the detector cap.
- The crystal holder system has been replaced. The new material is from the same sample as the material used in the Heidelberg–Moscow $\beta\beta$ experiment, which is known to be very clean.

Some technical details are listed in Table 1, for more details see [12].

Table 1:
Technical data of the detector in the final setup.

Property	Inner Detector	Outer Detector
Crystal Type	p–type	n–type
Mass [g]	202	2111
Active Volume [cm^3]	37	383
Crystal diameter [mm]	35.2	84.4
Crystal length [mm]	40.3	86.2
Operation Bias [V]	+2500	-1500
Energy resolution FWHM (1332 keV) [keV]	1.87	4.45
Energy threshold [keV]	4.0	7.5

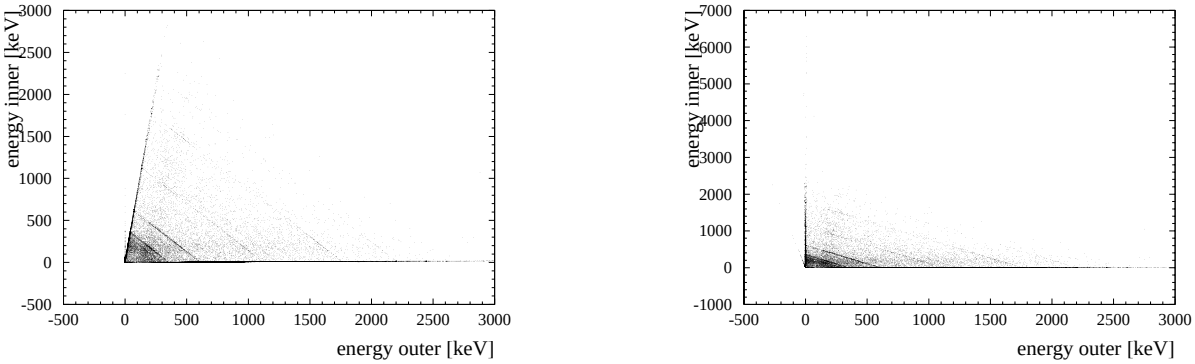

Figure 2: Scatter plot of the measured data. Each dot corresponds to one event. The y- and x-axis display the energy deposited in the inner- and outer detector, respectively. Left: Before the correction for pick-up signals the zero energy axes have a non-zero slope. Right: After the correction the zero energy axes correspond to the y- and x- axes.

2.1 The anti-coincidence and the crosstalk

Due to the special concentric design, the spatial separation between the two detectors is very small. This gives rise to pick-up signals. If one of the detectors sees an event, a cross talk signal is induced in the other one.

Recording spectra of calibration sources with the list mode allows to visualize this pick-up signal (see Fig. 2). The anti-coincidence cut between the two detectors to recognize multiple scattered background events can only be applied, if the cross talk is eliminated. This cut is made by defining all events as background events, in which an energy deposition is seen in both detectors above the energy threshold of the proper detector.

It was shown that the cross talk is linear with energy and stable over time and can be corrected for off-line [13]. Once the correction is made, the anti-coincidence can be applied.

Property	Inner Detector	Outer Detector
	final setup	
Threshold	(4.0±0.2)keV	(7.5±0.2)keV
Energy res. at zero keV extrapolated	(0.76±0.05) keV	(2.82±0.06) keV
at zero keV after correction	(0.83±0.01)keV	(2.91±0.04) keV
at 81 keV	(0.95±0.03) keV	
at 344 keV		(3.03±0.03)keV
at 1408 keV		(4.46±0.02)keV

Table 2: Energy resolutions for different energies and thresholds of the current final detector configuration.

2.2 Measurements at the Gran Sasso underground laboratory

The final setup of the HDMS was installed at the LNGS in August 2000, the data used for the analysis are taken from February 2001 to September 2001 in order to let the cosmogenic isotopes decay. The time stability of the energy resolution, threshold and calibration parameters (slope and intercept of energy calibration) have been checked elsewhere [12, 14]. The measured energy resolutions and thresholds of the detectors are listed in Tab. 2. They correspond to standard values for detectors of this size.

The individual typical duration of a run was about 23 hours. The experiment was stopped daily and the most important detector parameters like leakage current and mean count rates were checked. No substantial fluctuations were recorded.

After the individual runs were calibrated and corrected for the crosstalk, they were added to provide the sum spectra. From the sum spectrum of the inner detector (after the anti-coincidence cut) the limits on WIMP dark matter can be extracted.

Although the statistics of the inner detector is low, the sum-spectrum (see Fig. 3) shows some lines of isotopes from the U/Th natural decay chains as well as some X-ray lines which are dominating the region below 10 keV(see Fig. 4). The most obvious structure in the low energy region is a peak at 10.37 keV resulting from the decay of ^{68}Ge and a peak around 9 keV, which could arise from ^{65}Zn. Note that for the low energy region (Fig. 4) there are no more indications for a contamination with ^{210}Pb in comparison with the results from the prototype-detector [12]. Also the structure at 32.5 keV, which is meanwhile understood (see [15]), vanished completely.

If the anti-coincidence is evaluated in the energy region between 50 keV and 100 keV, the background reduction factor is 4.5. The counting rate after the anti-coincidence in this energy region is 0.27 events/(kg d keV), thus comparable to the value measured in the Heidelberg-Moscow experiment with the enriched detector ANG2 [11]. In the energy region between 11 keV and 40 keV the background index is 0.43 events/(kg d keV.).

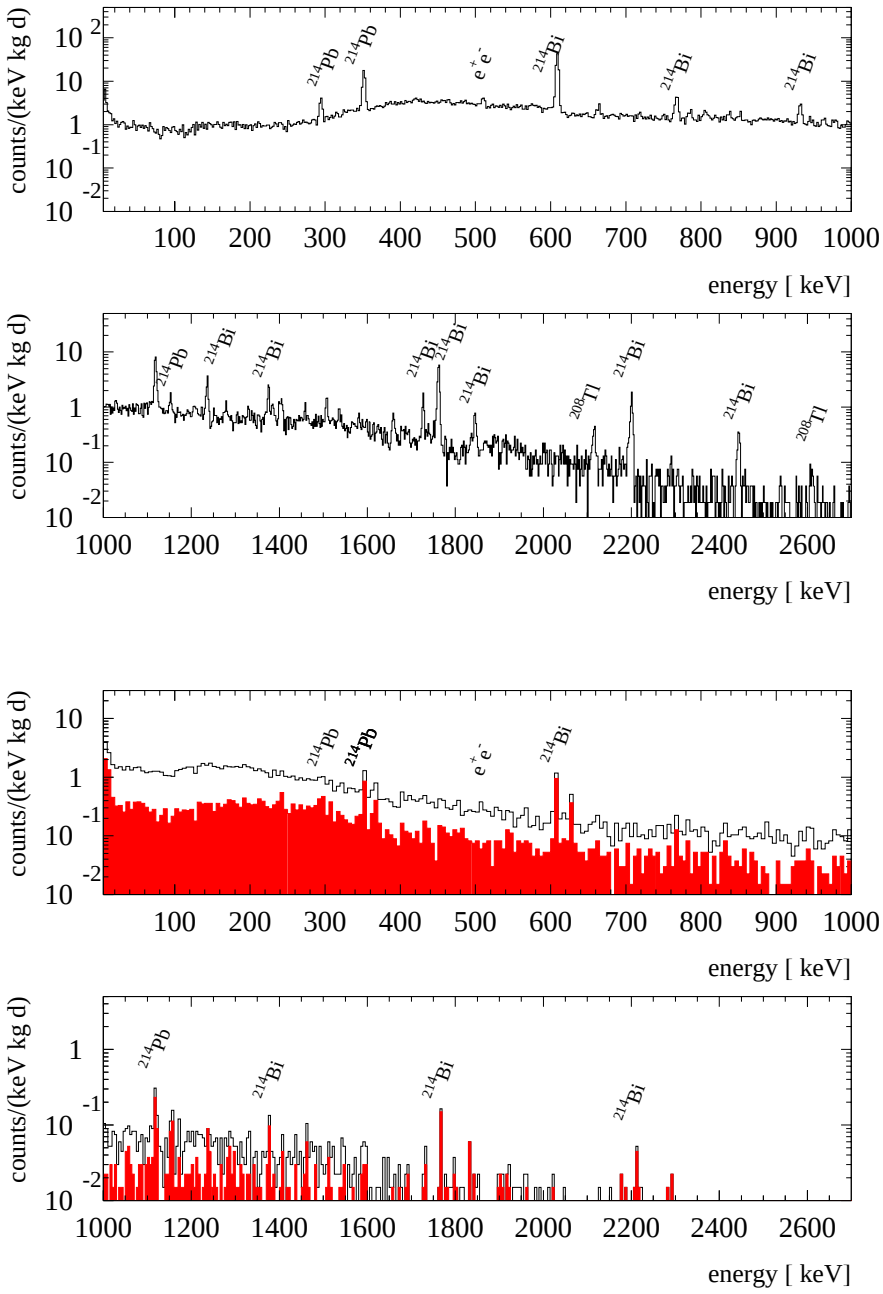

Figure 3: Spectra of the HDMS detectors of the final setup after a total measuring time of 132.4 days. Upper figure: outer detector; lower figure: inner detector - the open histogram denotes the overall spectrum, the filled histogram corresponds to the spectrum after the anti-coincidence cut with the outer detector. The most prominent lines are labeled.

2.3 Dark matter limits

Since many cosmogenic isotopes have half-lifes below 300 days, typically the count rate in low-level detectors decreases considerably after one year of storage underground.

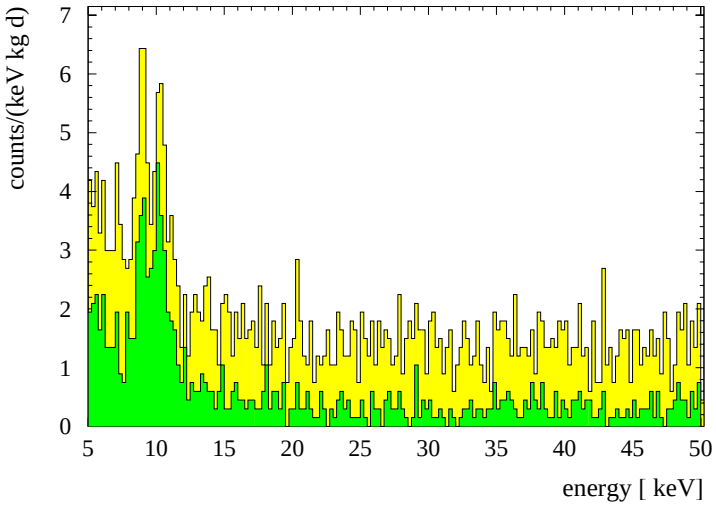

Figure 4: Low-energy spectrum of the inner, natural Ge detector before and after (open and solid histograms, respectively) the anti coincidence is applied with the outer Ge detector. The internal, low-energy x rays are not removed by the anti-coincidence.

For this reason only the last 132.4 days, corresponding to 26.74 kg d of measurement for the inner detector were used for the evaluation of the final HDMS setup data. The procedure of extracting limits on WIMP dark matter from the obtained spectrum follows the method described in [11].

The resulting upper limit is shown in the exclusion plot in figure 5. Already now the limit given by the HDMS experiment is slightly better than the limit given by the Heidelberg–Moscow $\beta\beta$ experiment for low WIMP masses. This due to the fact that the energy threshold of 5 keV has been obtained for this measurement (compare to 9 keV threshold of the Heidelberg–Moscow $\beta\beta$ experiment [11]).

3 Conclusion

The detectors for the final HDMS setup, constructed with some improvements to reduce the background, were installed in the LNGS in August 2000. It took data for 132.4 days corresponding to 26.74 kg days. The offline correction for the crosstalk has been applied to the data and a sum spectrum was created, where most of the background sources were identified. The background reduction factor in the inner detector through anti-coincidence is about 4.5. The background in the low-energy region of the inner detector (with exception of the region still dominated by cosmogenic activities) is already comparable to the most sensitive dark matter search experiments.

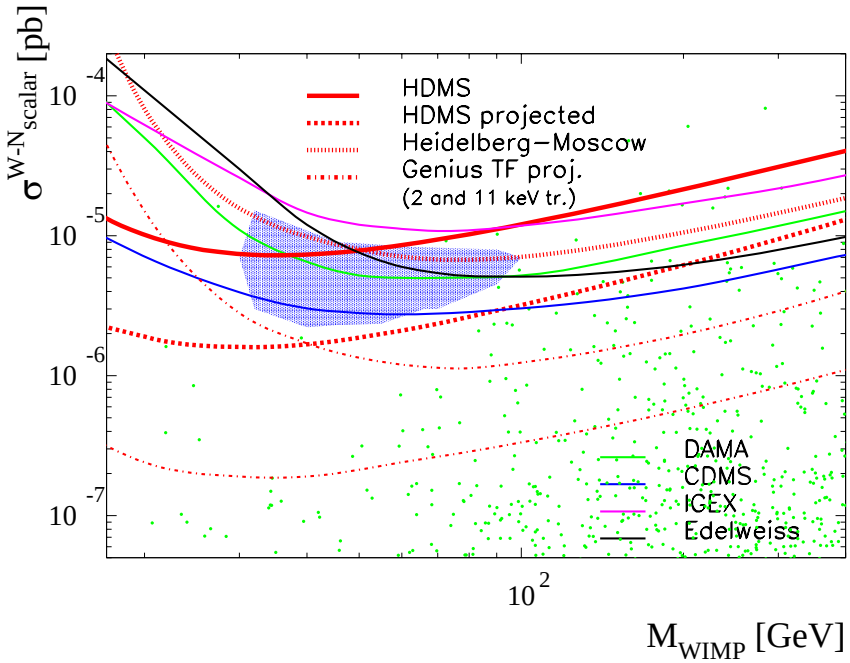

Figure 5: Exclusion plot for the presently most sensitive WIMP dark matter direct search experiments. The shaded area represents the 3σ region allowed by the DAMA experiment [16]. Even now, some parts of this region can be tested by the HDMS experiment. Also shown are the present limits from the DAMA experiment [17], the CDMS experiment [18], the IGEX experiment [19], and the Edelweiss experiment [20]. The scatter plot represents neutrino cross-sections within the framework of the general low-energy effective MSSM with cosmologically viable relic density in a flat accelerating universe [21]

4 List of Proceedings (2001)

1. H.V. Klapdor-Kleingrothaus (ed.), Dark Matter in astro- and Particle Physics., Proc. of DARK2000, Heidelberg, GERMANY, July 10-14, 2000, Berlin, Germany: Springer (2001) 740 p.

5 List of Publications (2001)

1. L. Baudis, A. Dietz, B. Majorovits, F. Schwamm, H. Strecker, H.V. Klapdor-Kleingrothaus Phys. Rev. D 63 (2001) 022001 and astro-ph/0008339.

6 List of Conference Contributions (2001)

1. H.V. Klapdor-Kleingrothaus et al. in Proc. of IDM2000, York, England, 18-22 Sep. 2000, World Scientific (2001) 415-420 and hep-ph/0103077.

2. H.V. Klapdor-Kleingrothaus et al., in Proc. of DARK2000, Springer, Heidelberg

(2001) Springer, Heidelberg (2001) 553-568 and hep-ph/0103082.

References

[1] M.W. Goodman and E. Witten, Phys. Rev. D **31** (1985) 3059.

[2] G. Jungmann and M. Kamionkowski, K. Griest, Phys. Rep. **267** (1996) 195

[3] V. Bednyakov, H.V. Klapdor–Kleingrothaus, S.G. Kovalenko and Y. Ramachers, Z. Phys. A **357** (1997) 339

[4] Bottino et al., hep-ph/0001309.

[5] V. Bednyakov and H.V. Klapdor-Kleingrothaus, Phys. Rev. D **62** (2000) 043524 and hep-ph/9908427

[6] V. Bednyakov, H.V. Klapdor-Kleingrothaus, hep-ph/0011233

[7] H.V. Klapdor-Kleingrothaus and Y. Ramachers, Euro. Phys. J. A **3** (1998) 85

[8] L. Baudis and H.V. Klapdor-Kleingrothaus in *Proc. of Beyond the Desert 1999*, ed. by H.V. Klapdor–Kleingrothaus, I.V. Krivosheina (IOP Bristol 2000), p.881

[9] Y. Ramachers, astro-ph/9911260 and in Proc. XI Rencontres de Blois, Frontiers of Matter, France, June 27 - July 3, 1999

[10] L. Baudis, J. Hellmig, H.V. Klapdor-Kleingrothaus, B. Majorovits, Y. Ramachers and H. Strecker, Internal Report, Proposal MPI H-V2-1998 and Nucl. Inst. Meth. **A 385** (1997) 265

[11] HEIDELBERG MOSCOW COLLABORATION, Phys. Rev. D **59** (1999) 022001 and Preprint hep-ex/9811045

[12] L. Baudis, A. Dietz, B. Majorovits, F. Schwamm and H. Strecker, H.V. Klapdor-Kleingrothaus, Phys. Rev. D **63** (2000) 022001, astro-ph/0008339

[13] Y.A. Ramachers, PhD thesis, University of Heidelberg, 1998

[14] L. Baudis, PhD thesis, University of Heidelberg, 1999

[15] H.V. Klapdor-Kleingrothaus et al. in Proc. of DARK 2000, Heidelberg, Germany, 10-14 July 2000, edited by H.V. Klapdor-Kleingrothaus, Springer, Heidelberg (2001) 553-568.

[16] R. Bernabei *et. al.*, Phys. Lett. **B 480** (2000) 23

[17] R. Bernabei *et. al.*, Phys. Lett. **B 389** (1996) 757

[18] R. Abusaidi *et. al*, Phys. Rev. Lett. **84** (2000) 5699

[19] F.T. Avignone III, presented at the Dark Matter 2000, Marina Del Rey, CA, USA, February 23-25, 2000

[20] A. Benoit *et. al*, astro-ph/0106094

[21] H.V. Klapdor-Kleingrothaus, V.Bednyakov and E. Zaiti, to be publ. (2002).

Heidelberg-Moscow Experiment on $\beta\beta$ decay

H.V. Klapdor-Kleingrothaus*[a], A. Dietz[a], H.L. Harney[a], I.V. Krivosheina[a,b]

[a] Max-Planck Institut, Heidelberg, Germany
[b] Institute of Radiophysical Research, Nishnij Novgorod, Russia
* Spokesman of the Heidelberg-Moscow Collaboration

Abstract

The data of the HEIDELBERG-MOSCOW double beta decay experiment for the measuring period August 1990 - May 2000 (54.9813 kg y or 723.44 molyears), published recently, are analyzed using the potential of the Bayesian method for low counting rates. First indication for neutrinoless double beta decay is observed giving first evidence for lepton number violation [1].

The HEIDELBERG-MOSCOW double beta decay experiment in the Gran Sasso Underground Laboratory searches for double beta decay of $^{76}Ge \longrightarrow ^{76}\ Se + 2\ e^- + (2\nu)$ since 1990. It is the most sensitive double beta experiment since eight years now. The experiment operates five enriched (to 86%) high-purity ^{76}Ge detectors, with a total mass of 11.5 kg, the active mass of 10.96 kg being equivalent to a source strength of 125.5 mol ^{76}Ge nuclei. This is the largest source strength in use.

The high energy resolution of the Ge detectors assures that there is no background for a $0\nu\beta\beta$ line from the two-neutrino double beta decay in this experiment.

The unique feature of neutrinoless double beta decay is that a measured half-life allows to deduce information on the effective Majorana neutrino mass $\langle m\rangle$, which is a superposition of neutrino mass eigenstates. The half-life is given, when ignoring contributions from right-handed weak currents, by

$$[T^{0\nu}_{1/2}(0^+_i \rightarrow 0^+_f)]^{-1} = C_{mm}\frac{\langle m\rangle^2}{m_e^2} \tag{1}$$

$$\langle m\rangle = |m^{(1)}_{ee}| + e^{i\phi_2}|m^{(2)}_{ee}| + e^{i\phi_3}|m^{(3)}_{ee}|\ , \tag{2}$$

Here $|m^{(i)}_{ee}|\exp(i\phi_i)$ $(i = 1, 2, 3)$ are the contributions to $\langle m\rangle$ from individual mass eigenstates, with ϕ_i denoting relative Majorana phases connected with CP violation and, C_{mm} denotes a nuclear matrix element, which can be calculated.

The Q value of $0\nu\beta\beta$ decay has been determined to be $Q_{\beta\beta} = 2039.006(50)$ keV in a recent precision experiment [8].

We have performed a new, refined analysis of the data obtained in the HEIDELBERG-MOSCOW experiment during the period August 1990 - May 2000 [5]. The analysis concentrates on the neutrinoless decay mode which is the one relevant for particle physics (see, e.g. [3, 6]).

We have analyzed the combined spectrum of the five enriched detectors obtained over the period August 1990 - May 2000, with a statistical significance of 54.981 kg y (723.44 molyears), the spectrum obtained with detectors Nr. 1,2,3,5 over the period August 1990 - May 2000, with a significance of 46.502 kg y and the spectrum of single site events (SSE) obtained for detectors 2,3,5 in the period November 1995 - May 2000, under the restriction that the signal simultanously fulfills the criteria of *all three* methods of pulse shape analysis we have recently developed [9, 10] and with which we operate all detectors except detector 1 (significance 28.053 kg y). Double beta events are single site events confined to a few mm region in the detector, corresponding to the track length of the emitted electrons, in contrast to e.g. multiple scattering γ - events. From simulation we expect that about 5% of the double beta single site events should be seen also as MSE. This is caused by bremsstrahlung of the emitted electrons [11].

All the spectra are obtained after rejecting coincidence events between different Ge detectors and events coincident with activation of the muon shield. The spectra are taken in bins of 0.36 keV. We do the analysis of the measured spectra with and without the data of detector 4 since the latter does not have a muon shield and has the weakest energy resolution. We ignore for each detector the first 200 days of operation, corresponding to about three half-lives of ^{56}Co ($T_{1/2} = 77.27$ days), to allow for some decay of short-lived radioactive impurities.

The total rate averaged over the energy range 2000 - 2080 keV is found to be (0.17 ± 0.01) events/ kg y keV (*without* pulse shape analysis). Considering *all* data as background, this is the lowest value obtained in such type of experiments. The energy resolution at the $Q_{\beta\beta}$ value in the sum spectra is extrapolated from the strong lines in the spectrum to be (4.00 ± 0.39) keV for the spectra with detector 4, and (3.74 ± 0.42) keV (FWHM) for those without detector 4. The energy calibration of the experiment has an uncertainty of 0.20 keV. For more experimental details see [5, 7].

We analysed the spectra with the Bayesian method, which is used widely at present (see, e.g. [12]). This method is particularly suited for low counting rates, where the data follow a Poisson distribution, that cannot be approximated by a Gaussian (see, also [13]).

The Bayesian peak detection procedure yields lines at the positions of known weak γ-lines from the decay of ^{214}Bi at 2010.7, 2016.7, 2021.8 and 2052.9 keV [14]. In addition, a line centered at 2039 keV shows up. This is compatible with the Q-value [8, 15] of the double beta decay process. We emphasize, that at this energy no γ-line is expected according to Monte Carlo simulations of our setup, and to the compilations in [14].

We find a probability of K = 97% that there is a line at 2039.0 keV in the measured spectra [1]. This is a confidence level of 2.2 σ in the usual language.

Under the assumption that the signal at $Q_{\beta\beta}$ is not produced by a background line of presently unknown origin, we can translate the observed number of events into half-lives. We give in Table 1 conservatively the values obtained with the Bayesian method and not those obtained with the PDG method. Also given in Table 1 are the effective neutrino masses $\langle m \rangle$ deduced using the matrix elements of [2].

Significance $[kg\,y]$	Detectors	$T^{0\nu}_{1/2}$ y	$\langle m \rangle$ eV	Conf. level
54.9813	1,2,3,4,5	$(0.80 - 35.07) \times 10^{25}$	(0.08 - 0.54)	95% *c.l.*
54.9813	1,2,3,4,5	$(1.04 - 3.46) \times 10^{25}$	(0.26 - 0.47)	68% *c.l.*
54.9813	1,2,3,4,5	1.61×10^{25}	0.38	Best Value
46.502	1,2,3,5	$(0.75 - 18.33) \times 10^{25}$	(0.11 - 0.56)	95% *c.l.*
46.502	1,2,3,5	$(0.98 - 3.05) \times 10^{25}$	(0.28 - 0.49)	68% *c.l.*
46.502	1,2,3,5	1.50×10^{25}	0.39	Best Value
28.053	2,3,5 SSE	$(0.88 - 22.38) \times 10^{25}$	(0.10 - 0.51)	90% *c.l.*
28.053	2,3,5 SSE	$(1.07 - 3.69) \times 10^{25}$	(0.25 - 0.47)	68% *c.l.*
28.053	2,3,5 SSE	1.61×10^{25}	0.38	Best Value

Table 1: Half-life for the neutrinoless decay mode and deduced effective neutrino mass from the HEIDELBERG-MOSCOW experiment.

We derive from the data taken with 46.502 kg y the half-life $T^{0\nu}_{1/2} = (0.8 - 18.3) \times 10^{25}$ y (95% c.l.). The analysis of the other data sets, shown in Table 1, and in particular of the single site events data, confirm this result.

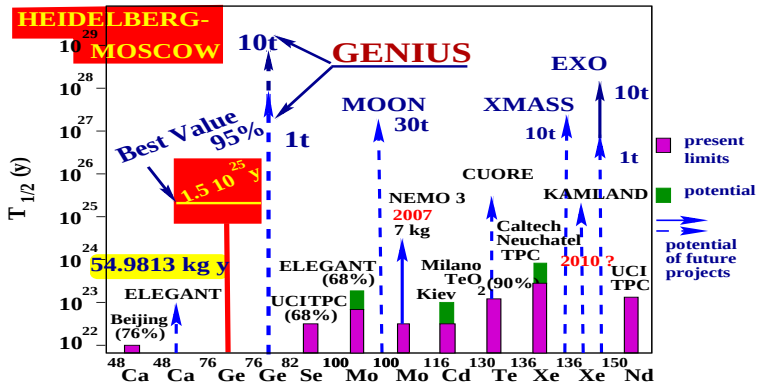

Figure 1: Present evidence for $0\nu\beta\beta$ decay from data of the HEIDELBERG-MOSCOW experiment and the potential of present and future $\beta\beta$ experiments. Vertical axis - half life in years, horizontal - isotopes used in the various experiments. Fall bars: present sensitivity, dashed lines: expectations for future projects.

The result obtained is consistent with the limit given earlier by the HEIDELBERG-MOSCOW experiment [5]. It is also consistent with all other double beta experiments - which still reach less sensitivity (see Figs. 2,1). A second Ge-experiment, which has stopped operation in 1999 after reaching a significance of 9 kg y yields (if one believes their method of 'visual inspection' in their data analysis) in a conservative analysis a limit of $T^{0\nu}_{1/2} > 0.55 \times 10^{25}$ y (90% c.l.). The ^{128}Te geochemical experiment yields $\langle m_\nu \rangle <$ 1.1 eV (68% c.l.), the ^{130}Te cryogenic experiment yields $\langle m_\nu \rangle < 1.8$ eV and the $CdWO_4$

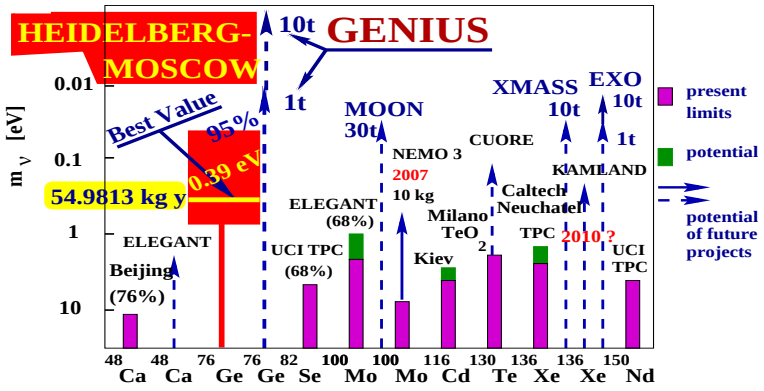

Figure 2: Present evidence for $0\nu\beta\beta$ decay from data of the HEIDELBERG-MOSCOW experiment and the potential of present and future $\beta\beta$ experiments. Vertical axis - effective neutrino mass in eV, horizontal - isotopes used in the various experiments.

experiment $\langle m_\nu \rangle < 2.6\,\mathrm{eV}$, all derived with the matrix elements of [2] to make the results comparable to the present value (for references see [6]).

Concluding we obtain, with more than 95% probability, first evidence for the neutrinoless double beta decay mode.

As a consequence, on the same confidence level, lepton number is not conserved. Further the neutrino is a Majorana particle. We conclude from the various analyses given above the effective mass $\langle m \rangle$ to be $\langle m \rangle = (0.11 - 0.56)\,\mathrm{eV}$ (95% c.l.), with best value of $0.39\,\mathrm{eV}$. Allowing conservatively for an uncertainty of the nuclear matrix elements of $\pm$ 50% (for detailed discussions of the status of nuclear matrix elements we refer to [6, 16]) this range may widen to $\langle m \rangle = (0.05 - 0.84)\,\mathrm{eV}$ (95% c.l.).

In this conclusion, it is assumed that contributions to $0\nu\beta\beta$ decay from processes other than the exchange of a Majorana neutrino (see, e.g. [17, 6]) are negligible.

With the limit deduced for the effective neutrino mass, the HEIDELBERG-MOSCOW experiment excludes several of the neutrino mass scenarios allowed from present neutrino oscillation experiments (see Fig. 3) - allowing mainly only for degenerate and partially degenerate mass scenarios and an inverse hierarchy 3ν - scenario (the latter being, however, strongly disfavored by a recent analysis of SN1987A. In particular hierarchical mass schemes are excluded at the present level of accuracy.

Assuming the degenerate scenarios to be realized in nature we fix - according to the formulae derived in [3] - the common mass eigenvalue of the degenerate neutrinos to m $= (0.05 - 3.4)\,\mathrm{eV}$. Part of the upper range is already excluded by tritium experiments, which give a limit of m $< 2.2\,\mathrm{eV}$ (95% c.l.). The full range can only partly (down to $\sim$ $0.5\,\mathrm{eV}$) be checked by future tritium decay experiments, but could be checked by some future $\beta\beta$ experiments (see, e.g. [6, 18]). The deduced best value for the mass lies in a range of interest also for Z-burst models recently discussed as explanation for super-high energy cosmic ray events beyond the GKZ-cutoff [19].

The neutrino mass deduced allows neutrinos to still play an important role as hot dark matter in the Universe.

New approaches and considerably enlarged experiments (as discussed, e.g. in [6, 18]) will be required in future to fix the neutrino mass with higher accuracy.

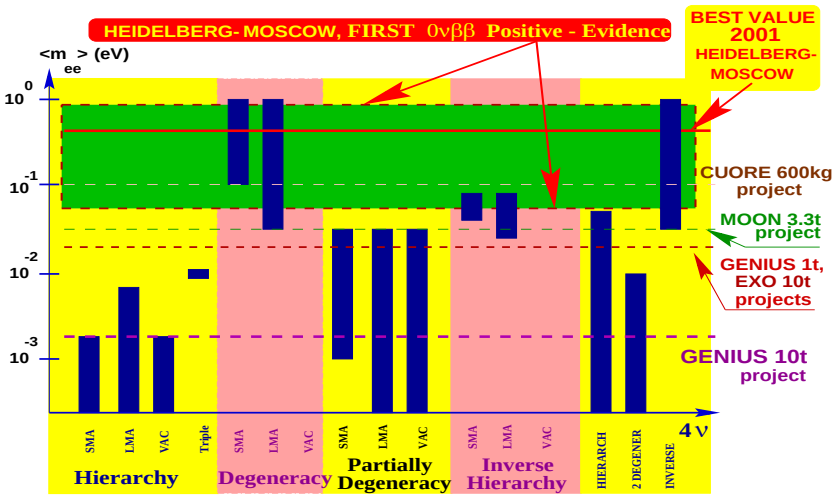

Figure 3: The impact of the evidence obtained for neutrinoless double beta decay in this paper (best value of the effective neutrino mass $\langle m \rangle = 0.39\,\mathrm{eV}$, 95% confidence range (0.05 - 0.84) eV - allowing already for an uncertainty of the nuclear matrix element of a factor of $\pm$ 50% on possible neutrino mass schemes. The bars denote allowed ranges of $\langle m \rangle$ in different neutrino mass scenarios, still allowed by neutrino oscillation experiments (see [4]). Hierarchical models are excluded by the new $0\nu\beta\beta$ decay result. Also shown are the expected sensitivities for the future potential double beta experiments CUORE, MOON, EXO and the 1 ton and 10 ton project of GENIUS [18].

Acknowledgments

One of the authors - H.V. Klapdor-Kleingrothaus - would like to thank all colleagues who have contributed to the experiment over the last decade of operation. Particular thanks go to Dr. A. Müller, and Dr. F. Petry, Dr. B. Maier, Dr. J. Hellmig and Dr. B. Majorovits who have developed the pulse shape discrimination methods and set up the VME electronics applied in the experiment since 1995. We thank Dr. T. Kihm for supporting us in highly efficient way in the field of electronics, and we thank Dr. G. Heusser for his important contributions in the field of low-level techniques. We also thank Mr. H. Strecker for his permanent invaluable technical contributions. We are indebted to Prof. D. Schwalm, director at MPI Heidelberg, for his scientific interest and his efficient support of this project. The whole collaboration thanks to the director of the Gran Sasso Underground Laboratory, Prof. E. Bettini and also the former directors of Gran Sasso Profs. P. Monacelli and E. Bellotti, for invaluable support. Our thanks extend also to the technical staff of the Max-Planck Institut für Kernphysik and of the Gran Sasso Underground Laboratory. We thank Perkin Elmer (former ORTEC) Company, and in particular Dr. M. Martini, and Dr. R. Collatz for the fruitful cooperation. We are grateful to Dr. G. Sawitzki and Prof. W. Beiglböck from the Institute for Applied Mathematics of the University of Heidelberg for encouraging discussions. We acknowledge the invaluable support from Gran-Sasso (INFN, Italy), BMBF (Germany) and DFG (Germany) of this project. We are grateful to the former State Committee of Atomic Energy of the USSR

for providing the enriched material used in this experiment.

1 List of Books

1. H.V. Klapdor-Kleingrothaus, Sixty Years of Double Beta Decay: From Nuclear Physics to Beyond Standard Model Particle Physics, World Scientific, Singapore (2001) 1235p.

2 List of Publications

1. H.V. Klapdor-Kleingrothaus, A. Dietz, H.L. Harney, I.V. Krivosheina, Mod. Phys. Lett. A 16 (2002) 2409-2420 and hep-ph/0201231.

2. H.V. Klapdor-Kleingrothaus, U. Sarkar. Mod. Phys. Lett. A 17 (2002) 2469-2482 and hep-ph/0201224.

3. H.V. Klapdor-Kleingrothaus, A. Dietz, L. Baudis, G. Heusser, I.V. Krivosheina, S. Kolb, B. Majorovits, H. Paes, H. Strecker, V. Alexeev, A. Balysh, A. Bakalyarov, S.T. Belyaev, V.I. Lebedev, S. Zhukov, Eur. Phys. J. A 12 (2001) 147-154, and in Proc. of DARK2000, Springer, Heidelberg (2001) 520-533 and hep-ph/0103062.

4. H.V. Klapdor-Kleingrothaus, H. Päs, A.Y. Smirnov, Phys. Rev. D 63 (2001) 073005 and hep-ph/0003219.

5. S. Stoica and H.V. Klapdor-Kleingrothaus, Nucl. Phys. A 694 (2001) 269-294.

6. S. Stoica and H.V. Klapdor-Kleingrothaus, Phys. Rev. C 63 (2001) 064304.

7. H.V. Klapdor-Kleingrothaus, in Proc. of NANPino, Dubna, Russia, July 19-22, 2000, Particles and Nuclei, Letters, issues 1/2 (2001) 20-39 and and Preprint: hep-ph/0103319.

8. H.V. Klapdor-Kleingrothaus in Proc. of NOW2000, Conca Specchiulla (Otranto, Italy), September 9-16, 2000, Nucl. Phys. Proc. Suppl. 100, : (2001) 309-313 and hep-ph/0102276.

3 List of Conference Contributions (2001)

1. H.V. Klapdor-Kleingrothaus, H. Pas and A.Y. Smirnov, in Proc. of DARK2000, Springer, Heidelberg (2001) Springer, Heidelberg (2001) 420-434 and hep-ph/0103076.

2. H. Päs, M. Hirsch, H.V. Klapdor-Kleingrothaus, S.G. Kovalenko, Phys. Lett. B 498 (2001) 35-39 and hep-ph/0008182.

3. H.V. Klapdor-Kleingrothaus, in Proc. of LowNu2, December 4 and 5, 2000, Tokyo, Japan, to be published in World Scientific (2001) (eds) Y. Suzuki et al., and Preprint: hep-ph/0104028.

4. H.V. Klapdor-Kleingrothaus, in Proc. of NOON 2000, Tokyo, Japan, 6-18 Dec. 2000, World Scientific (2001) (eds) Y. Suzuki et al. and hep-ph/0103074.

5. B. Majorovits, L. Baudis, A. Dietz, F. Schwamm, H. Strecker, H.V. Klapdor-Kleingrothaus in Proc. of DM 2000, Marina del Rey, California, 23-25 Feb 2000, Springer 2001, edited by D. Cline, (2001) 387-398

6. H.V. Klapdor-Kleingrothaus, B. Majorovits in Proc. of IDM2000, England, September 18-22, 2000, World Scientific (2001) 593-602 and Preprint:hep-ph/0103079.

References

[1] H.V. Klapdor-Kleingrothaus, A. Dietz, H.L. Harney and I.V. Krivosheina, Modern Phys. Letters **A 16** (2001) 2409 - 2420.

[2] A. Staudt, K. Muto and H.V. Klapdor-Kleingrothaus, Europh. Lett. **13** (1990) 31.

[3] H.V. Klapdor-Kleingrothaus, H. Päs and A.Yu. Smirnov, Phys. Rev. **D 63** (2001) 073005, and hep-ph/0103076.

[4] H.V. Klapdor-Kleingrothaus and U. Sarkar, Mod. Phys. Lett. **A 17** (2001) 2469-2482.

[5] H.V. Klapdor-Kleingrothaus et al.,(HEIDELBERG-MOSCOW Collaboration), Eur. Phys. J. **A 12** (2001) 147 and hep-ph/0103062.

[6] H.V. Klapdor-Kleingrothaus, "60 Years of Double Beta Decay - From Nuclear Physics to Beyond the Standard Model", World Scientific, Singapore (2001) 1281 pp.

[7] M. Günther et al. (HEIDELBERG-MOSCOW Coll.), Phys. Rev. **D 55** (1997) 54.

[8] G. Douysset et al., Phys. Rev. Lett. **86** (2001) 4259 - 4262.

[9] J. Hellmig and H.V. Klapdor-Kleingrothaus, Nucl. Instrum. Meth. **A 455** (2000) 638 - 644 and J. Hellmig, F. Petry and H.V. Klapdor-Kleingrothaus, Patent **DE19721323A**.

[10] B. Majorovits and H.V. Klapdor-Kleingrothaus. Eur. Phys. J. **A 6** (1999) 463.

[11] B. Maier, Dissertation, November 1995, MPI-Heidelberg; F. Petry, Dissertation, November 1995, MPI-Heidelberg; J. Hellmig, Dissertation, November 1996, MPI-Heidelberg; B. Majorovits, Dissertation, December 2000, MPI-Heidelberg; A. Dietz, Dipl. Thesis, Univ. Heidelberg, 2000 (unpublished), and Dissertation, in preparation.

[12] G. D'Agostini, hep-ex/0002055, W. von der Linden and V. Dose, Phys. Rev. **E 59** 6527 (1999), and F.H. Fröhner, JEFF Report **18** NEA OECD (2000) and Nucl. Sci. a. Engineering **126** (1997) 1.

[13] H.L. Harney, "Bayesian Inference. Data Evaluation and Decisions", Monograph in preparation, Springer Verlag, Heidelberg 2002.

[14] R.B. Firestone and V.S. Shirley, Table of Isotopes, Eighth Edition, John Wiley and Sons, Incorp., N.Y. (1998).

[15] J.G. Hykawy et al., Phys. Rev. Lett. **67** (1991) 1708.

[16] A. Faessler and F. Simkovic, J. Phys. **G 24** (1998) 2139 - 2178 and Preprint hep-ph/9901215 (1999) 1 - 32.

[17] R.N. Mohapatra and P.B. Pal, "Massive Neutrinos in Physics and Astrophysics", Singapore: World Scientific, World Sc. lecture notes in physics, **41** (1991) 318 pp.

[18] H.V. Klapdor-Kleingrothaus, hep-ph/0103074 and in Proc. of NOON 2000, Tokyo, Japan, 6-18 Dec. 2000, ed: Y. Suzuki et al., World Scientific (2001), Nucl. Phys. Proc. Suppl. **100** (2001) 309 - 313 (hep-ph/0102276), Part. Nucl. Lett. **104** (2001) 20 - 39 (hep-ph/0102319).

[19] T.J. Weiler, in Proc. Beyond the Desert 1999, edited by H.V. Klapdor–Kleingrothaus and I.V. Krivosheina, IOP Bristol, (2000) 1085 - 1106; H. Päs and T.J. Weiler, Phys. Rev. **D 63** (2001) 113015.

ICARUS T600. Imaging Cosmic and Rare Underground Signals

F. Arneodo[a], B. Babussinov[b], B. Badełek[c], A. Badertscher[d], M. Baldo Ceolin[b], G. Battistoni[e], B. Bekman[f], P. Benetti[g], E. Bernardini[a], M. Bischofberger[d], A. Borio di Tigliole[g], R. Brunetti[g], A. Bueno[d], E. Calligarich[g], D. Cavalli[e], F. Cavanna[h], P. Cennini[i], S. Centro[b], A. Cesana[j], C. Chen[k], Y. Chen[k], D. Cline[l], D. Corti[b], P. Crivelli[g], A. Dabrowska[m], M. Daszkiewicz[n], C. De Vecchi[g], R. Dolfini[g], M. Felcini[d], A. Ferrari[i,e], F. Ferri[a], S. Galli[h], A. Gigli Berzolari[g], I. Gil-Botella[g], L. Grandi[g], K. Graczyk[n], K. He[k], J. Holeczek[f], X. Huang[k], C. Juszczak[n], D. Kiełczewska[c], J. Kisiel[f], L. Knecht[d], T. Kozłowski[o], H. Kuna-Ciska[p], M. Laffranchi[d], J. Łagoda[c], Z. Li[k], B. Lisowski[d], F. Lu[k], J. Ma[k], S. Marchini[b], M. Markiewicz[q], C. Matthey[l], F. Mauri[g], D. Mazza[h] G. Meng[b], C. Montanari[g], S. Muraro[e], G. Natterer[d], S. Navas-Concha[d], M. Nicoletto[b], G. Nurzia[h], S. Otwinowski[l], O. Palamara[a], D. Pascoli[b], L. Periale[r], G. Piano Mortari[h], A. Piazzoli[g], P. Picchi[r,*] F. Pietropaolo[b], W. Półchłopek[b,q], T. Rancati[e], A. Rappoldi[g], G.L. Raselli[g], J. Rico[d], E. Rondio[o,†] M. Rossella[g], A. Rubbia[d], **C. Rubbia**[g,‡], P. Sala[d,e], D. Scannicchio[g], E. Segreto[h], F. Sergiampietri[s,l], Y. Seo[l], J. Sobczyk[n], J. Stepaniak[o], M. Stodulski[m], M. Szarska[m], M. Szeptycka[o], M. Terrani[j], S. Ventura[b], C. Vignoli[g], H. Wang[l], M. Wójcik[t], G. Xu[k], Z. Xu[k], X. Yang[l], A. Zalewska[m], J. Zalipska[o], C. Zhang[k], Q. Zhang[k], S. Zhen[k], W. Zipper[f],

[a] Laboratori Nazionali del Gran Sasso, INFN, s.s. 17bis km 18+910, Assergi (AQ), Italy
[b] Dipartimento di Fisica e INFN, Università di Padova, via Marzolo 8, Padova, Italy
[c] Institute of Experimental Physics†, Warsaw University, Warszawa, Poland
[d] Institute for Particle Physics, ETH Hönggerberg, Zürich, Switzerland
[e] Dipartimento di Fisica e INFN, Università di Milano, via Celoria 16, Milano, Italy
[f] Institute of Physics†, University of Silesia, Katowice, Poland
[g] Dipartimento di Fisica e INFN, Università di Pavia, via Bassi 6, Pavia, Italy
[h] Dipartimento d Fisica e INFN, Università dell'Aquila, via Vetoio, L'Aquila, Italy
[i] CERN, CH-1211 Geneva 23, Switzerland
[j] Politecnico di Milano (CESNF), Università di Milano, via Ponzio 34/3, Milano, Italy
[k] IHEP – Academia Sinica, 19 Yuqnan Road, Beijing, People's Republic of China
[l] Department of Physics, UCLA, Los Angeles, CA 90024, USA
[m] H.Niewodniczański Institute of Nuclear Physics†, Kraków, Poland
[n] Institute of Theoretical Physics†, Wrocław University, Wrocław, Poland
[o] A.Sołtan Institute for Nuclear Studies†, Warszawa, Poland
[p] Institute of Mechanics and Machine Design, Cracow University of Technology, Kraków, Poland
[q] Faculty of Physics and Nuclear Techniques, University of Mining and Metallurgy, Kraków, Poland
[r] University of Torino, Via Giuria 1, Torino, Italy
[s] INFN Pisa, via Livornese 1291, San Piero a Grado (PI), Italy
[t] Institute of Physics, Jagellonian University, Kraków, Poland

[*] Also at Laboratori Nazionali di Frascati, INFN, Frascati, Italy and ICG-CNR, Torino, Italy

[†] Research activity in ICARUS partially supported by NATO Grant ref. PST.CLG.977410

[‡] **Spokesman of the ICARUS Collaboration**

Abstract

The ICARUS T600 is a self-contained experimental programme, with significant physics potentialities, though with a strong connotation of technological development in view of the operability of a large mass liquid Argon "electronic bubble chamber" inside the Gran Sasso underground laboratory.
After the completion of the detector construction in 2000, the major achievement of the experimental activity during the year 2001 is represented by the full test of the T600 set-up, from the cryogenics and electronics performance up to detection of cosmic ray tracks, carried out in an external site in Pavia.
The test, extended over about 100 days of continuous operation, has been fully successful. It showed that the ICARUS technology, providing high reconstruction capability for events even at low energy deposition level, as for the solar neutrino case, is now fully operational at real experimental level.
The way for the installation of the T600 detector at the Gran Sasso Laboratory is thus open and landing at the underground site is expected by the end of the year 2002.

1 Introduction

The "ICARUS technology", first proposed by C. Rubbia [1] in 1977, combines the characteristics of a bubble chamber with the advantages of the electronic read-out. The detector is essentially a large ionisation chamber filled with ultra-pure liquid Argon (LAr) and equipped with a sophisticated electronic readout system. It is an ideal device to study neutrino interactions: it is continuously sensitive, self-triggerable, relatively cost effective and simple to build in modular form, sufficiently safe to be located underground (no pressure, no flammable gas, etc.). This detector acts also as a superb calorimeter of very fine granularity and high accuracy.
After the original proposal, the feasibility of the technology has been amply demonstrated by an extensive R&D programme, which included ten years of studies on small LAr volumes (proof of principle, LAr purification methods, readout schemes, electronics) and five years of studies with several prototypes of increasing mass at CERN (purification technology, collection of real events, pattern recognition, long duration tests, readout technology). The largest of these devices had a mass of 3 tons of LAr and has been continuously operating for more than four years, collecting a wide sample of cosmic ray and gamma source events. Furthermore, a smaller device (50 litres of LAr) has been exposed to the CERN neutrino beam, demonstrating the technique's high recognition capability for neutrino interaction events. [A complete list of references can be found in the ICARUS Web page] [2].
Thereafter, the ICARUS project has entered an industrial phase, a necessary path to proceed toward the realization of large volume detectors for physics. The first step was the realization of a large cryogenic prototype (14 t of liquid Argon), for testing the final industrial solutions adopted, successively transformed into a detector module operated at the INFN Gran Sasso Laboratory (LNGS, 1999-2000). The second step is represented by the construction of the "T600 module": a 600 t detector for physics at LNGS.

The ICARUS T600 project [3] has been fully approved and financed during the years 1996-97. The realisation (project+construction) lasted about four years. After completion, a full test of the experimental set-up has been carried out in a dedicated INFN facility in Pavia (Italy) during 2001. All technical aspects of the system, cryogenics, LAr purification, read-out chambers, detection of LAr scintillation light, electronics and DAQ have been tested and performed as expected. A large statistics of cosmic ray events (long-penetrating muons and spectacular, high multiplicity muon bundles, el.m. and hadronic showers, low energy events) have been recorded.
In this report the T600 detector is briefly described and some images of events collected during the recent Pavia test are reported.
The ICARUS T600 successful test was the proof that this technology we have been developing for many years has finally reached maturity. The T600 module, once operated at Gran Sasso, will act as the necessary demonstrational premise for larger scale detectors with a considerable experimental impact, commensurate with the potentialities of such a novel technology, in which both high visual resolution and accurate calorimetry are combined.
The initial physics program with the T600 module at Gran Sasso has been reviewed at the beginning of 2001 and it is reported in [4]: in this phase the available mass is limited, however the higher efficiency and the much more detailed information which can be collected for each event will allow to address some of the fundamental issues of modern underground physics: (1) the study of neutrino physics, with solar and atmospheric neutrinos, can provide additional hints to the present neutrino oscillation schemes, (2) the study of nucleon decay will allow to access unexplored lifetime regions for some exotic channels considered in GUT's and (3), in case of Supernova event, detection of ν_e burst may provide fundamental information both in diagnostic features of SN core collapse and in possible MSW oscillation mechanisms through the SN mantle.
In order to reach the originally foreseen sensitive mass, within the framework of the 1997 proposal, and on the basis of the experience of the T600 module, we propose [5] the design and assembly of "clones" of the present "prototype" module in a series of units. This is inevitably a graded programme for the next few years, in which the mass will be increased in a number of successive steps.

2 The ICARUS T600 Detector

The ICARUS T600 detector has been extensively described in various papers; among these we may refer in particular to the *LNGS Annual Report 2000* [6]. In the following we only recall the basic information.

ICARUS T600 is a large cryostat splitted in two identical, adjacent half-modules ($3.6 \times 3.9 \times 19.9$ m^3 each, of internal dimensions) each one housing an internal detector (composed by two Time Projection Chambers - TPC, the field shaping system, monitors and probes, and by a system for the LAr scintillation light detection) and externally surrounded by a set of thermal insulation layers. Outside the detector are located (1) the read-out electronics, on the top side, (2) the cryogenic plant made of a liquid Nitrogen cooling circuit to maintain uniform the LAr temperature, and of a system of LAr pu-

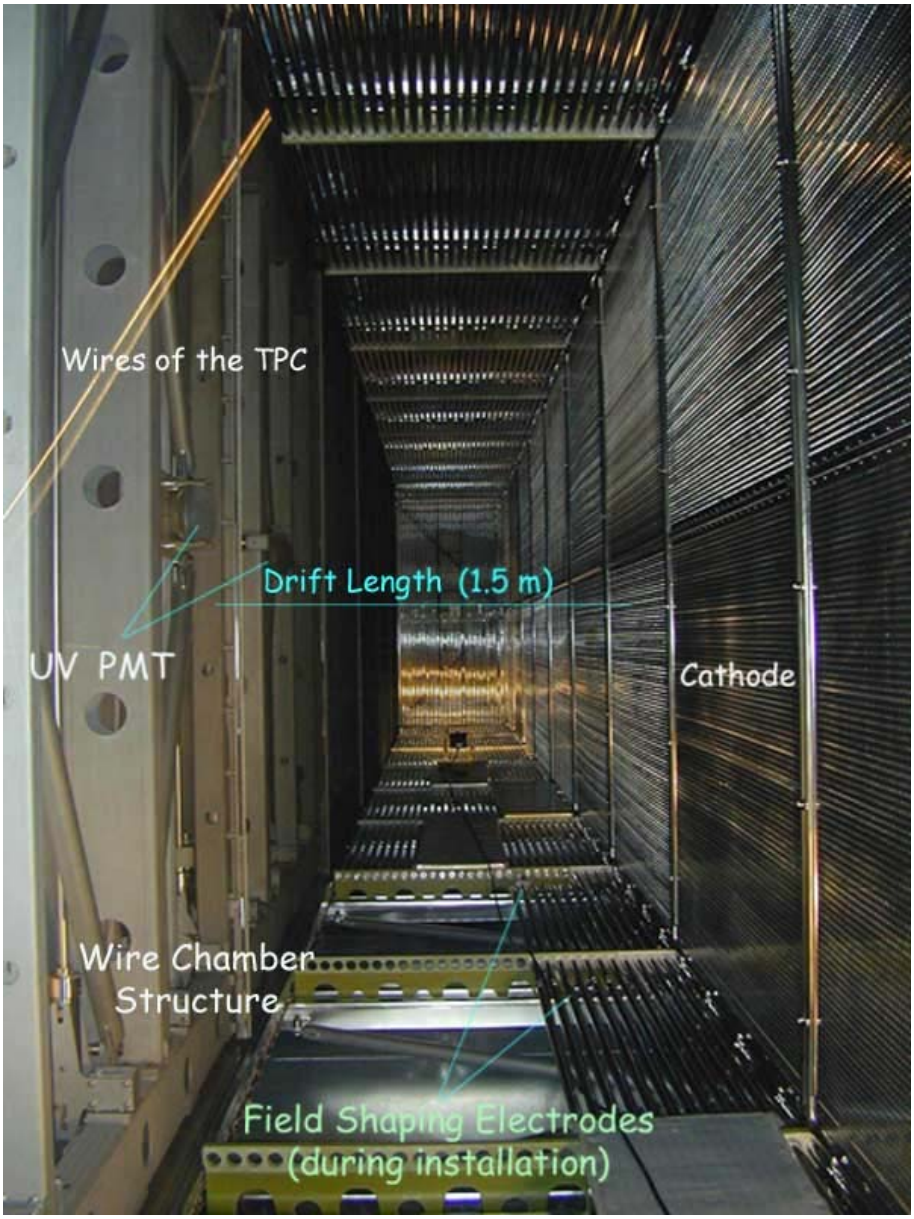

Figure 1: *Picture of the internal detector layout inside the first half-module: the cathode divides the volume in two symmetric sectors. The picture refers to the left sector where wires and mechanical structure of the TPC and some PMTs are visible.*

rifiers, to keep the LAr purity at a sufficiently high level, (3) a neutron shield around the detector, made of arrays of polyethylene tubes filled with boric acid, to moderate and capture neutrons from natural underground radioactivity (this shield is necessary to allow background reduction in the solar neutrino experiment).

The structure of the internal detector consists of two TPC's per half-module. Each TPC

Figure 2: *Top side of the T600 module during installation of the electronics racks.*

is formed by three parallel planes of wires, 3 mm apart, oriented at 60^0 angle, with 3 mm of pitch between adjacent wires [(1) *Induction*-plane (wires oriented at 0^o), (2) *Induction*-plane (wires oriented at $+60^o$), (3) *Collection*-plane (wires oriented at -60^o)]. The three planes of wires of each TPC are hold by a sustaining frame, see Fig. 1, positioned onto the longest walls of the half-module. The total number of wires in the T600 detector is about 55,000. The read-out of the signals, induced by ionising events in LAr on the wires of the TPC's, provides means for a full 3D-image reconstruction of the event topology and for an accurate measurement of the energy deposited.

An uniform electric field, perpendicular to the wire planes to allow the drift of the ionisation tracks, is established in the LAr volume of each half-module by means of a high voltage system. This is composed by a cathode plane, parallel to the wire planes, placed in the middle of the LAr volume of each half-module at a distance of about 1.5 m from the wires from both sides, setting to this length the maximum drift path. The HV system is completed by field shaping electrodes, to guarantee the uniformity of the field along the drift direction, and by a HV feed-trough to set the required voltage on the cathode (at a nominal voltage of 75 kV, corresponding to 500 V/cm of electric field, the maximum drift time is about 1 ms).

The top side of the cryostat, Fig. 2, hosts the exit flanges equipped with cryogenic feed-throughs for the electrical connection of the wires with the read-out electronics and for all the internal instrumentation (PMT's, LAr purity monitors, level and temperature probes, etc.).

The ICARUS electronics is designed to allow continuous read-out, digitization and wave-

form recording of signals from each wire of the TPC. The electronics chain is composed by three basic units: 1) the "Decoupling Board", which receives analogue signals from the TPC wires, via the vacuum tight feed-through flanges, and passes them to the "Analogue Board". It also provides biasing of the wires and distribution of calibration signals. 2) The "Analogue Board" [7] houses the signal amplifiers and provides the data conversion (10 bit) at 40MHz rate. 3) The "Digital Board" [8], employs two DAEDALUS chips, implementing a hit finding algorithm. Each board serves 32 channels (one channel per wire) and receives the digital data (multiplexed) via an external cable from the "Analogue Board".

Ionisation events in LAr are accompanied by scintillation light emission. Detection of

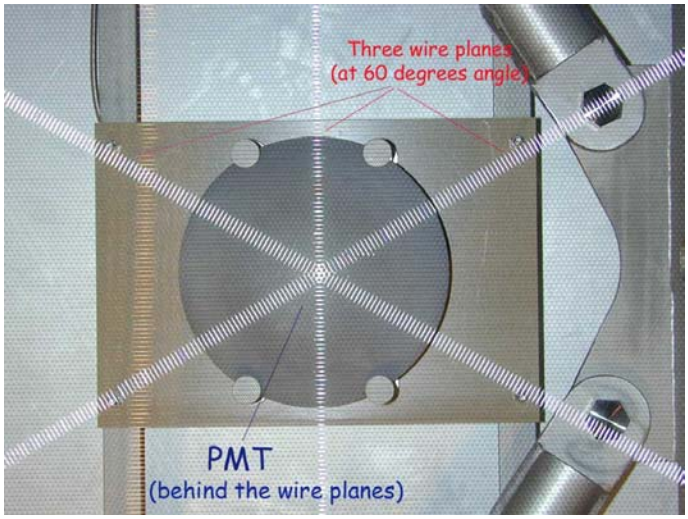

Figure 3: *Picture of a PMT in its final mounting behind the three wire planes (appearing by light reflection from the camera flash.*

this light can be used to provide an effective method for absolute time measurement (T_0) of the event and a useful internal trigger signal.

As a completion of the internal detector furniture, a system to detect light from LAr scintillation has been implemented.

The LAr scintillation light is a monochromatic radiation in the VUV spectrum, with $\lambda = 128$ nm. The scintillation provides a large, prompt ($< 1\mu$s) photon emission ($\sim 2\times10^4$ photons per MeV at 500 V/cm, typical electric field used in LAr TPCs). The attenuation length of the 128 nm light in LAr is about 0.9 m, as measured in a dedicated test by the ICARUS Collaboration [9].

After an intense R&D study, a system based on large-surface (8") PMT's immersed directly in the LAr has been adopted to detect the LAr scintillation light. These are equipped with blue sensitive bialkali photocathode on a platinum under-layer especially designed to operate at low temperature.

The PMT's have been made sensitive to the LAr VUV photons coating the glass window with a proper fluorescent wavelength shifter (TPB). The global quantum efficiency (PMT+wavelength shifter) has been measured: $\approx 10\%$ at LAr temperature.

The result of detailed simulations suggested the use of 60 PMT's per half-module placed

in the region behind the wire planes and mounted in rows with a distance of 2 m between two consecutive PMT's. This system should allow detection with high efficiency also of those events for which the light production is low (i.e. 5 MeV solar neutrino interactions). In Fig. 3 a picture showing the PMT assembling and its final mounting behind the three wires planes is presented.
The "imaging" of ionising events inside the LAr active volume is made possible from the simultaneous exploitation of the charge and of the light release occurring in ionization processes: (1) electrons, belonging to ionization tracks, during their drift motion toward and across the wire planes of the TPC induce detectable signals from the wires, (2) UV photons from scintillation provide a prompt signal (T_0 determination) from the PMT system; this allows measurement of the absolute drift time, hence of the distance travelled by the drifting electrons.
Each of the wire planes of the TPC thus provides a two-dimensional projection of the event image, where one co-ordinate is given by the wire position and the other by the drift distance. The various projections have a common co-ordinate (the drift distance); a full 3-D reconstruction of the event is obtained by correlation of signals from two different planes (x and y coordinates) and drift distance (z coordinate).

3 The T600 module test in Pavia

One T600 half-module has been fully instrumented during 2000, including all electrical connections and cabling to the outside electronics and DAQ, for allow a complete test in real experimental condition.
The full test (limited to this half-module) took place in Pavia during the period April-August 2001. The test included monitoring of the start-up operations (vacuum pumping for out-gassing of the internal surfaces, cooling-down and LAr filling) and optimisation of the electronics and DAQ system performances, up to cosmic ray events reconstruction. To this extent the experience from the ICARUS $10m^3$ prototype [10] operated at LNGS during the year 2000, represented an important forerunner input.
The above-ground location of the experimental site in Pavia allowed the collection of a large sample of cosmic ray events recorded with different configurations of dedicated trigger systems. An external scintillator system provided trigger for the long-awaited, almost horizontal muon tracks crossing up to the entire length (18 m) of the detector, see Fig. 4, allowing an overall check of the wire chambers performance and of the event builder capability. The external trigger system also allowed the acquisition of a large sample of almost vertical muon tracks for a wire-to-wire response comparison and calibration. The internal PMT's system, suitably arranged in a number of different trigger logic, provided trigger signal for events characterised by large energy deposition in LAr, like high multiplicity muon bundles belonging to extensive air showers in atmosphere, and spectacular broad electro-magnetic and hadronic showers. Combined trigger logic between internal and external systems enabled the collection of a large statistics of stopping muon events with muon decay in electron, to be used for absolute energy calibration, and the recording of low energy events like isolated electron tracks in the few MeV energy range. This sample provides a first insight of the ICARUS capability to detect solar neutrino-like events.

All the technical aspects of the performed test, like the outcomes of the cryogenics con-

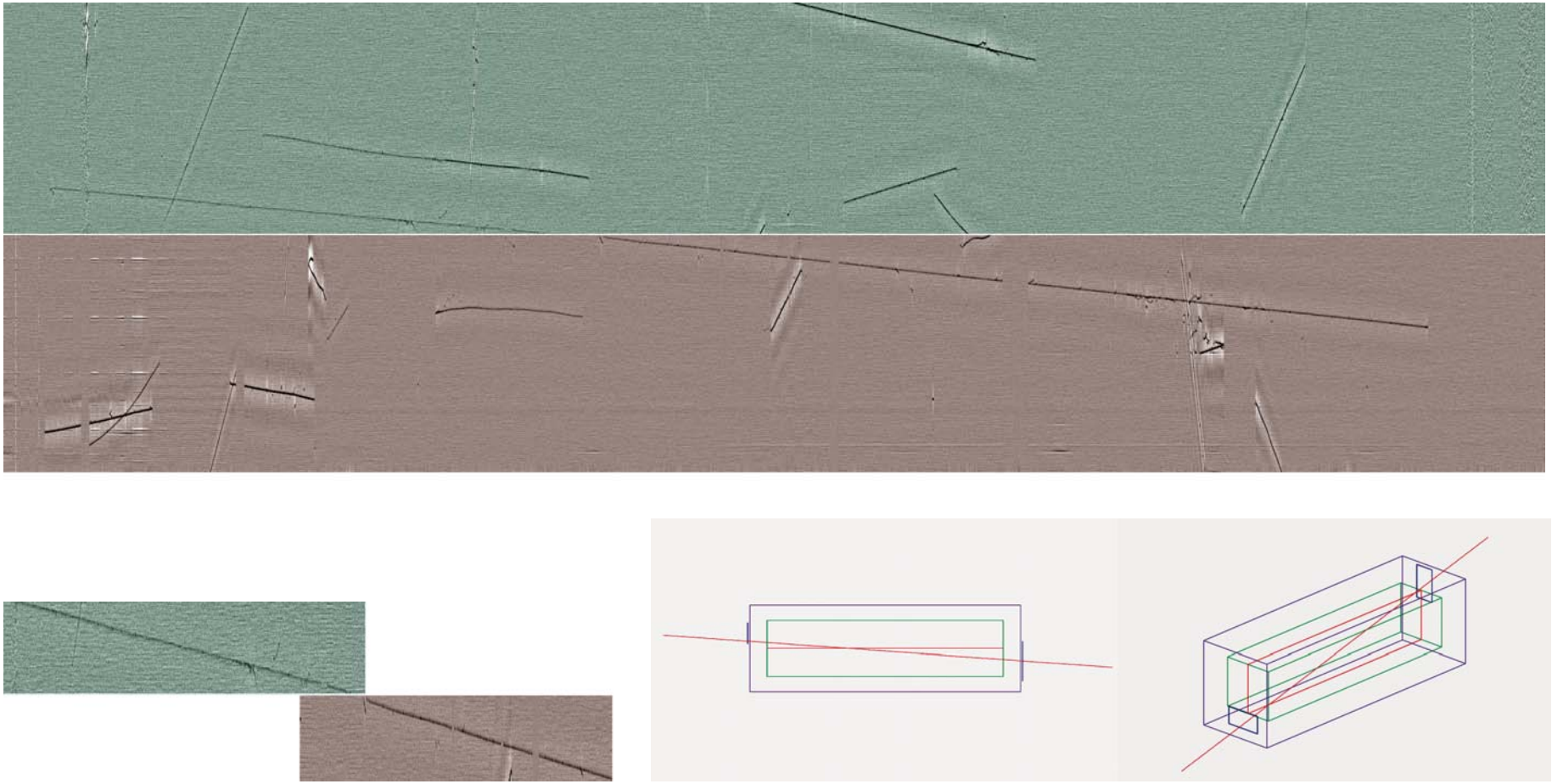

Figure 4: Run 893, Event 4, *[Top] Image of a long-penetrating muon [full (18 m × 1.5 m) Collection-Left and -Right views): the muon track, triggered by the external scintillator system, is detected first in the Right Chamber (above) and, after crossing the central cathode, is detected in the Left Chamber (below). [Bottom-Left] Detail of the muon track around the point of crossing the cathode. From off-line analysis the event has been reconstructed in space (track length, in sensitive LAr volume, 18.2 m, absolute orientation* $\theta_{Zenith} = 80.94^o$, $\phi_{Azimuth} = 92.85^o$, *deposited energy about 3.7 GeV): [Bottom-Centre] Top View of the T600 detector and the 2 scintillator planes providing the coincidence trigger, [Bottom-Right] 3D view of the reconstructed muon track.*

trol system, of the LAr purification and recirculation devices, of the signal-to-noise level from the electronics chain and of the data reduction and recording of the DAQ system, are subjects of an in-depth on-going analysis. These will be matter of a dedicated publication presently in preparation. Here, we only mention that all functioning parameters of the ICARUS T600 detector have been investigated and found to be satisfactorily in agreement with expectations. As a proof of this statement, we show in the next subsections some impressive events selected by visual scanning of the on-line event-display. These events are examples of the various classes of topologies mentioned above and selected by suitable trigger logic.

The off-line analysis of the collected data for a full 3D reconstruction and event topology study (energy deposition, particle identification, ..) is on going (see Fig. .4).
The run was stopped in August 2001, after about 100 days of continuous operation.

3.1 Atmospheric showers

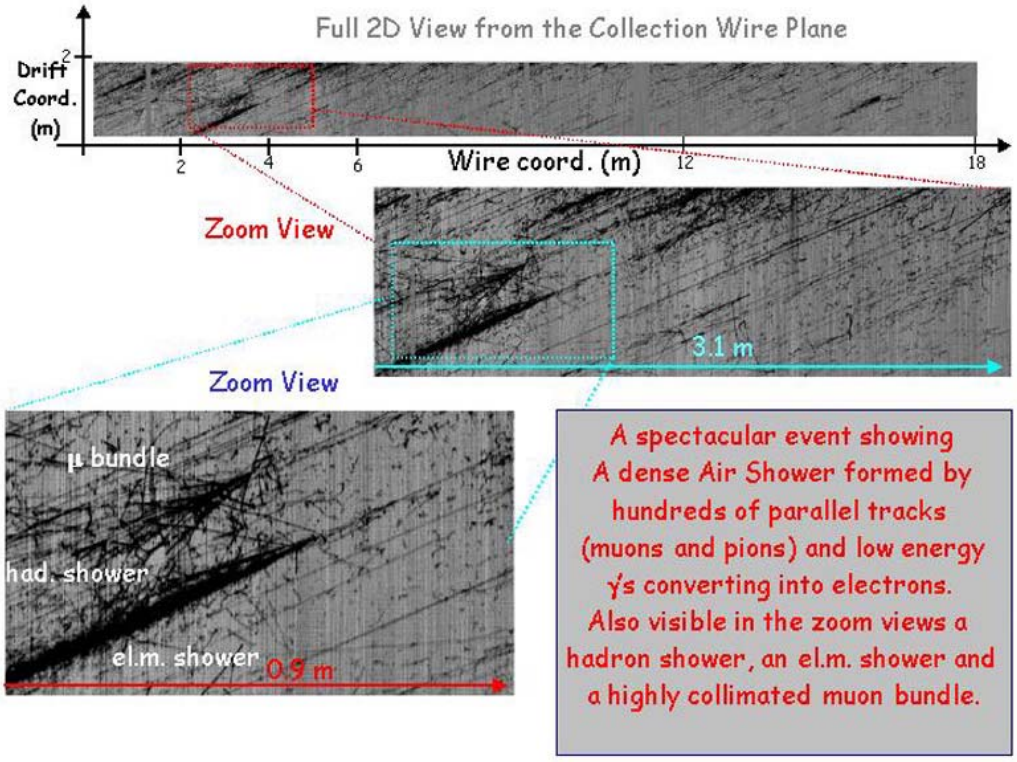

Figure 5: Run 313, Event 154, *Collection*-view: *Example of Air-shower event.*

In Fig. 5 is reported the 2D *Collection* view (i.e. the *Collection*-wire Coordinate vs. the *Drift Time* Coordinate) of an impressive cosmic event composed by hundreds of parallel tracks. The event is presumably an extended air-shower initiated by a very high energy cosmic ray interacting in atmosphere. The recorded image extends to the full length (about 18 m) and drift (1.5 m) of the detector, as shown in the upper picture, and provides a snapshot of a portion of the air-shower. The zoomed regions in the figure

contain visible details of the event, like several electromagnetic and hadronic showers, narrow muon bundles and low energy electrons from photon convertion.

Another cosmic event, consisting of a muon bundle with more than 30 parallel muon

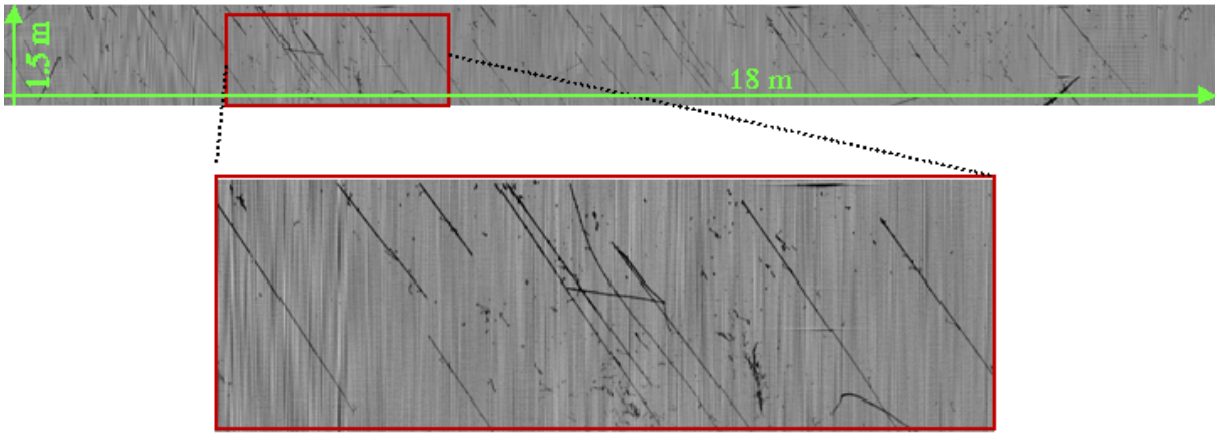

Figure 6: Run 313, Event 239, *Collection*-view: *Example of muon bundle event.*

tracks detected over the full length of the the detector is shown in Fig. 6. The upper view shows the *Collection* image, the other image refer to a zoomed region of the same event with some details of the image.

3.2 Stopping muons

Low momentum muons entering the detector may deposit all their energy, stop and decay in the LAr active volume. These kind of events are easily recognized by the presence of a muon track accompanied by an electron emitted nearby the end of the muon track. The muon track, due to the low momentum, undergoes large angle multiple scattering, and the ionization increases rapidly near the end point. Since the muon decays at rest in the detector, producing one electron plus two undetected neutrinos, the directions of the electron and muon are uncorrelated. The electron energy ranges up to half of the muon mass (i.e. to about 53 MeV).

An event matching the previous pattern is shown in Fig. 7. The muon extends about 60 cm in the increasing *Collection*-wire coordinate (top image). The track is visibly darker approaching one end: it indicates an increasing energy deposition pattern along the track, thus showing that the muon stopped rather than decayed in flight. The small track nearby corresponds to the emitted electron. The track presents many direction changes, due to multiple Coulomb scattering. The estimated energy deposition of the electron is about 20 MeV. The same event is shown as detected by the other two available views: the *Induction*-wire Coordinate (0^0) vs. *Drift Time* view and *Induction*-wire Coordinate (60^0) vs. *Drift Time* view.

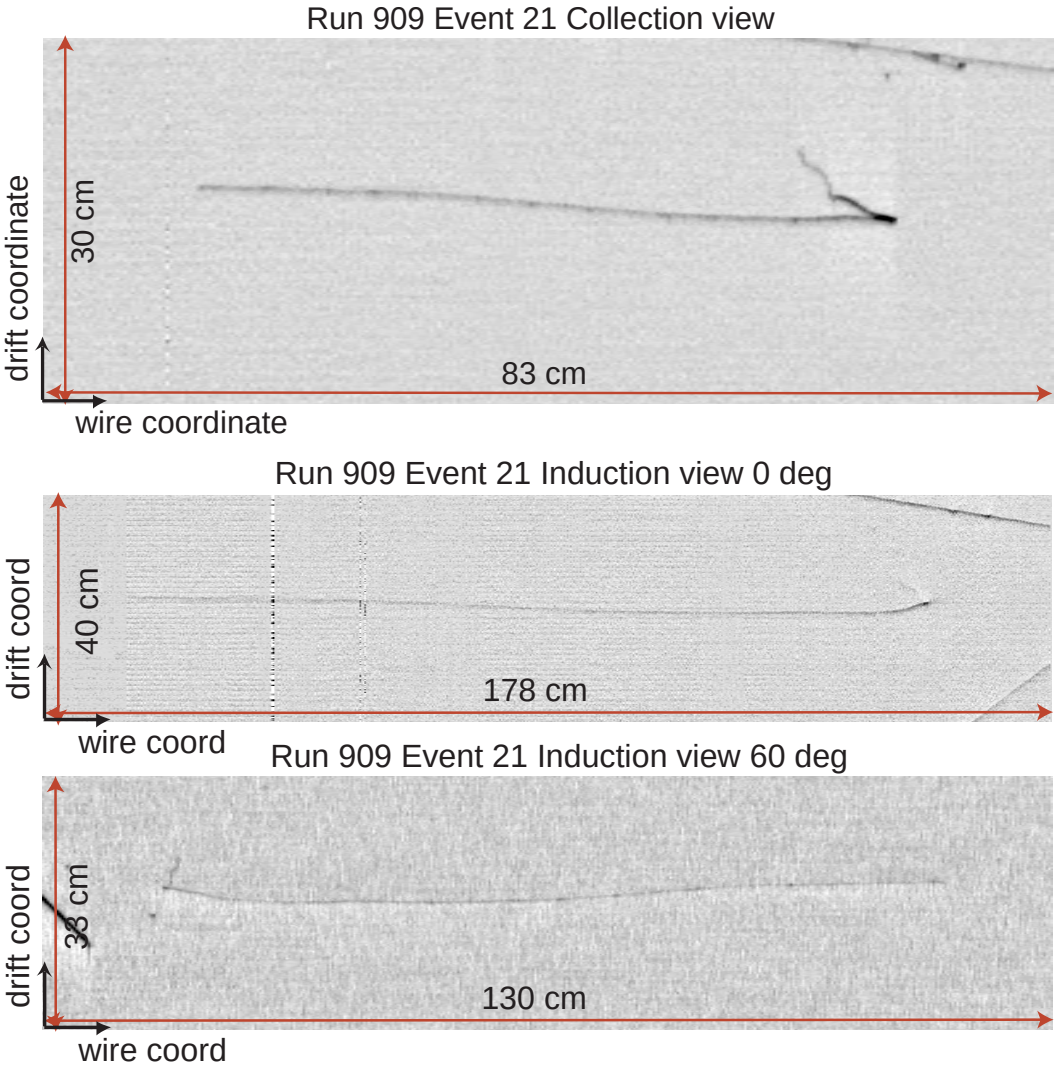

Figure 7: Run 909, Event 21, [Top] *Collection*-view (60^o), [Centre] *Induction*-view (0^o) and [Bottom] *Induction*-view (60^o). *Stopping muon with decay in electron.*

Another example of a stopping muon event is shown in Fig. 8 from all three available

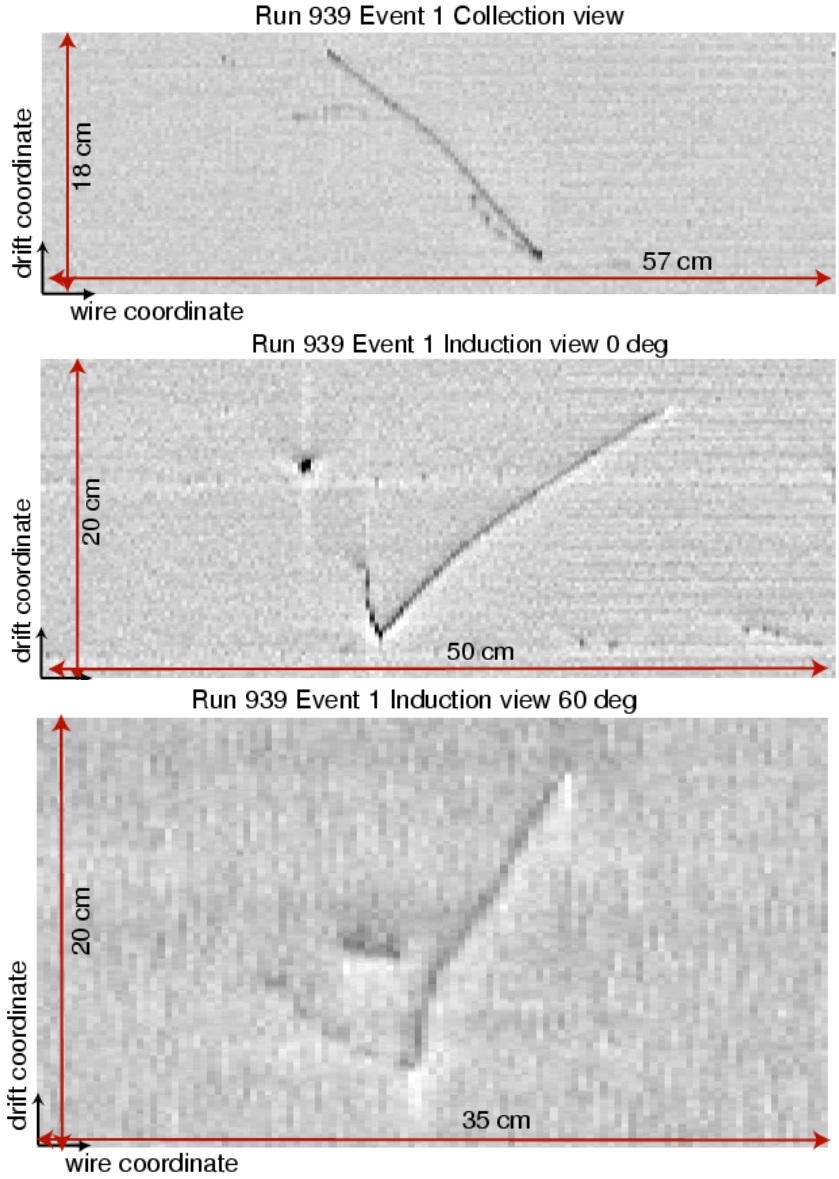

Figure 8: Run 939, Event 1, [Top] *Collection*-view (60^o), [Centre] *Induction*-view (0^o) and [Bottom] *Induction*-view (60^o). *Another stopping muon with decay in electron.*

views. Again, the muon shows large angle multiple scattering, and produces an increased energy deposition in the region close to the end point. The energy of the electron is estimated to be about 15 MeV.

3.3 Hadronic interactions

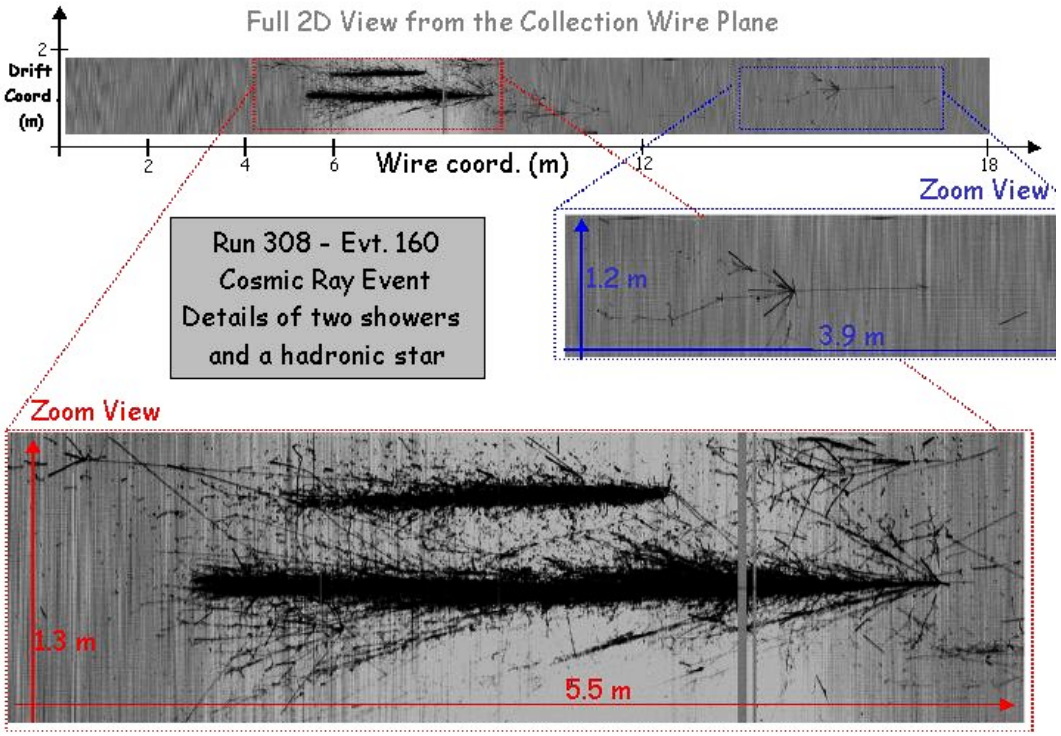

Figure 9: *Run 308, Event 160: Full Collection-view [Top],* zoomed view of a hadron interaction [Centre] and zoomed view of energetic showers [Bottom].

A very interesting event is shown in Fig. 9. Besides two energetic showers, visible near to the centre of the *Collection* view (and reported in one of the zoomed views), the most interesting part of the recorded event is shown in the other zoomed image: it shows a charged hadron entering the detector from the top and traveling around 1 m in LAr before interacting. Then, several secondary particles are produced and undergo different interactions. All three views of the hadronic interaction region are reported in Fig. 10. The cleanest image of the interaction is from the *Collection*-view, bottom image of Fig. 10: a δ ray is produced at the beginning of the hadron track. Among the secondary particles, it is possible to distinguish in the bottom part of the picture the conversion of a pair of photons, most likely coming from the decay of a π^0. A neutral particle (possibly a neutron) could also be produced, giving an additional hadronic interaction in the upper part of the figure. One of the charged hadrons coming from the main interaction vertex travels around 1.7 m undergoing secondary hadronic interactions along its path. Soft secondary heavily ionizing nuclear debris are also visible.

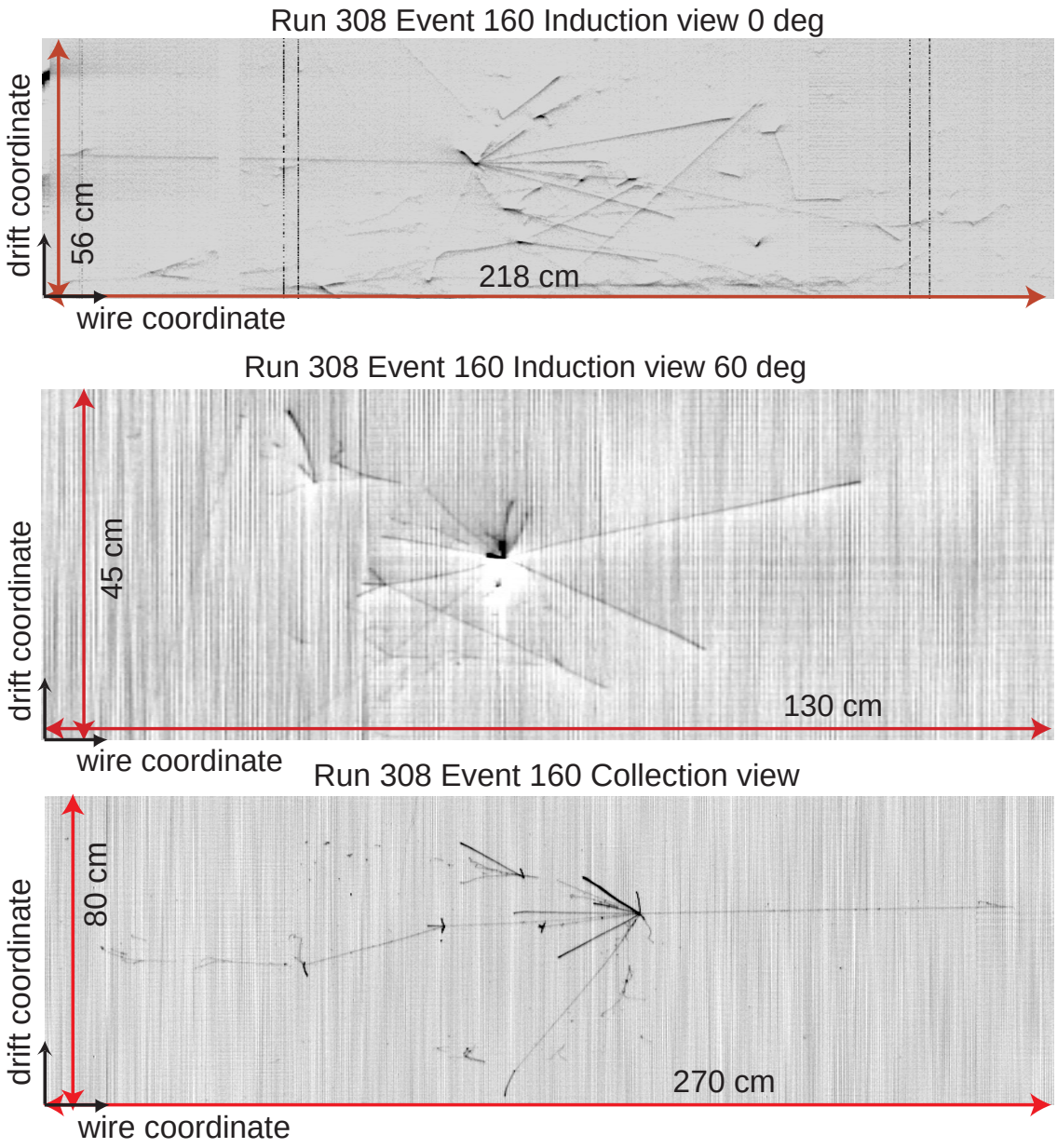

Figure 10: Run 308, Event 160, [Top] *Induction*-view (0^o), [Centre] *Induction*-view (60^o) and [Bottom] *Collection*-view (60^o). *Hadronic interaction (detail).*

3.4 V0 events

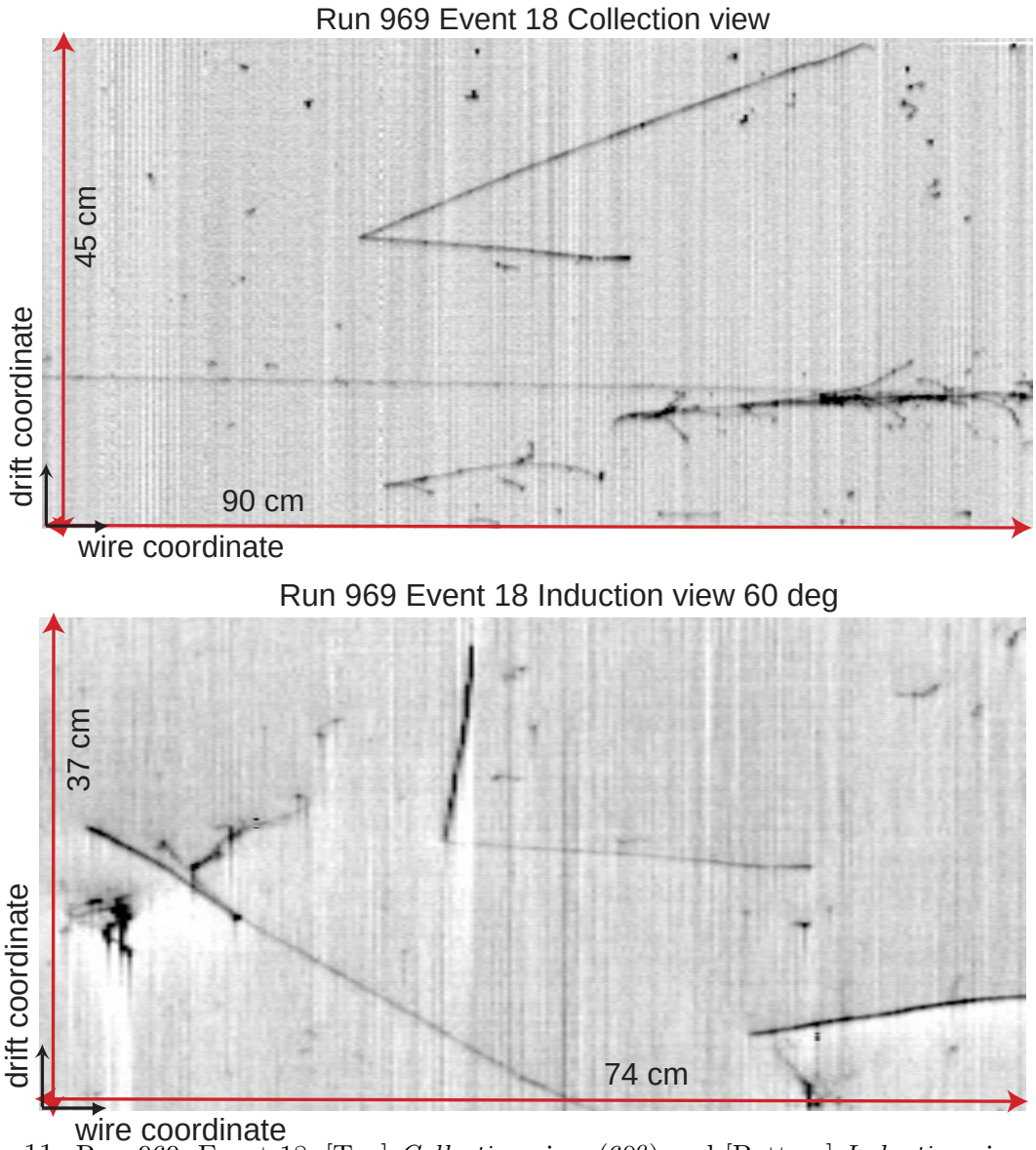

Figure 11: Run 969, Event 18, [Top] *Collection*-view (60^o) and [Bottom] *Induction*-view (60^o). *V0 event.*

A typical signature of a V0 event is shown in Fig. 11. This event can be associated to the decay of a K^0 into a pair of pions ($K^0 \rightarrow \pi^+ + \pi^-$) or a Λ particle flying a few centimeters and decaying into a pion and a proton ($\Lambda \rightarrow p + \pi^-$).
Two tracks are coming from the same interaction vertex and they are traveling towards the right part of the detector. Since there is not any other track in the opposite direction, the two tracks should be produced by the disintegration of a neutral particle.
From the analysis of the *Collection*-view (Fig. 11 [Top]), the longest track deposits an energy of about 85 MeV and escapes the detector. The other track has a total associated energy of about 50 MeV and stops inside the detector, depositing the maximal energy at the end point. The same pattern is visible in Fig.11 [Bottom] from the *Induction*-view.

3.5 Electromagnetic showers

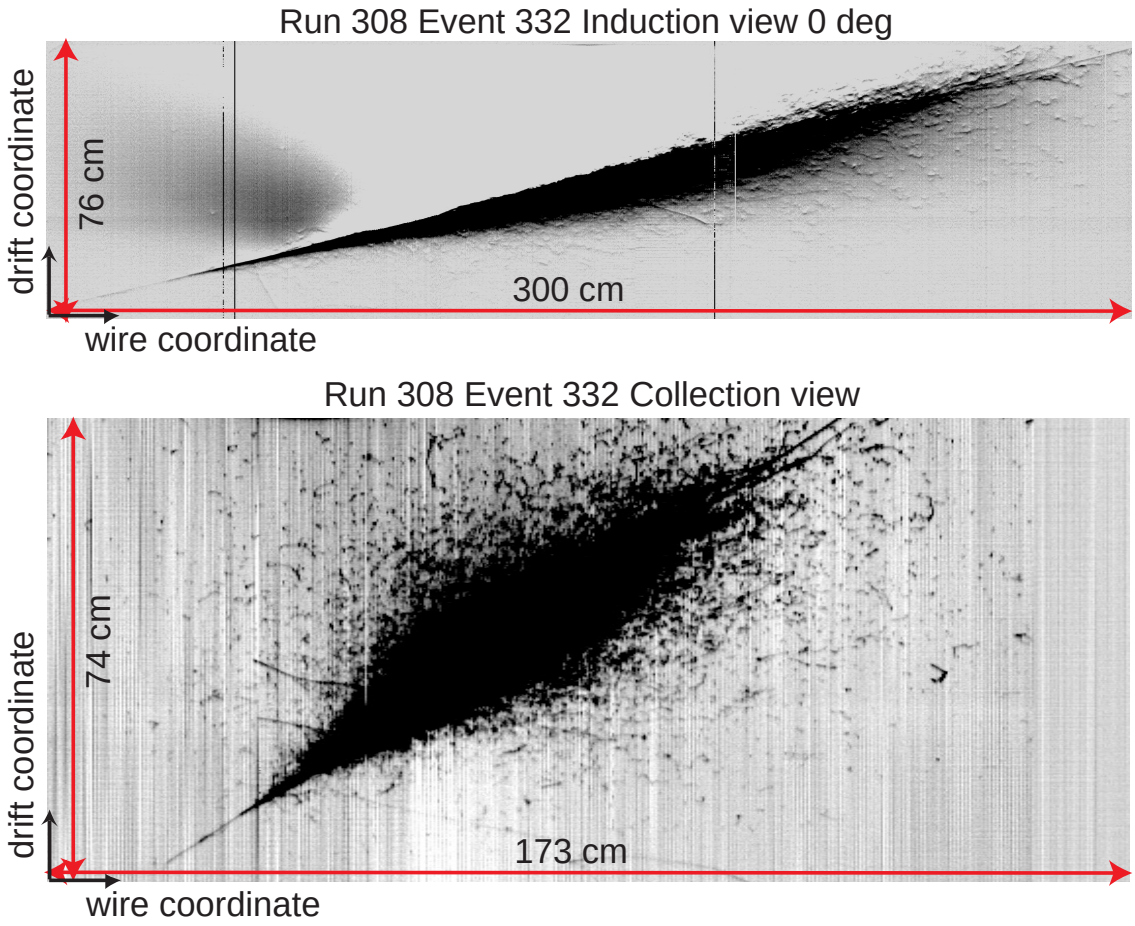

Figure 12: Run 308, Event 332, [Top] *Induction*-view (0^o) and [Bottom] *Collection*-view (60^o). *Electromagnetic shower.*

A good example of the imaging capabilities of the LAr TPC is given by the electromagnetic shower shown in Fig. 12. The image is about 75×170 cm^2 wide. The electron initiates an electromagnetic cascade (bottom-left corner of the figure) as pair production and bremsstrahlung generate more electrons and photons with lower energy. The grey level of the pixels codes the electronics pulse height, proportional to the collected charge, so that the longitudinal and transverse developments of the cascade can be easily studied. The overall drift time (vertical axis) corresponds to about 75 cm of drift distance, while the shower spreads over $\sim$15 radiation lengths.

3.6 Hadronic showers

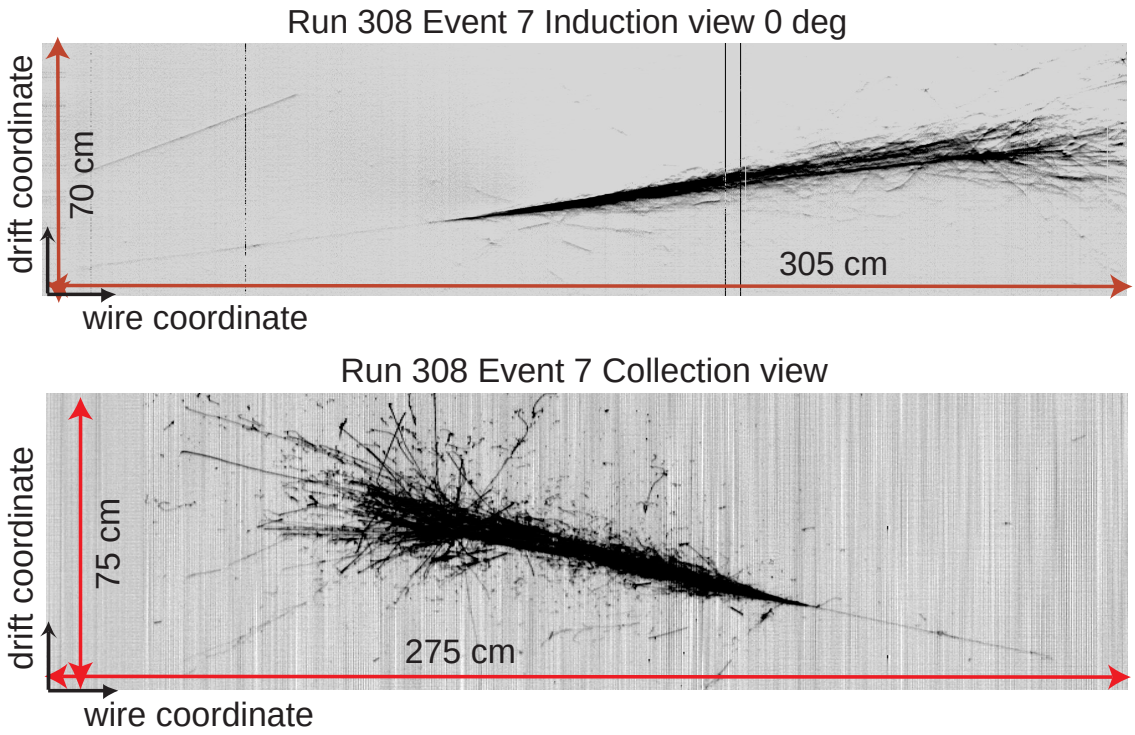

Figure 13: Run 308, Event 7, [Top] *Induction*-view (0^o) and [Bottom] *Collection*-view. *Hadronic interaction candidate.*

A nice example of an interaction producing a hadronic shower is shown in Fig. 13. In there, a high energetic charged hadron enters the detector from the top, flying to the bottom for more than 1 meter (from left to right in Figure 13). The interaction generates a spectacular shower where one can identify some secondary hadronic interactions accompanied by a high electromagnetic activity. The projection of the event in this view (*Induction I*) [Top], reveals a ∼2 meters long shower, quite collimated and almost fully contained in the detector. In addition, the hadron enters near the anode (small drift distances) flying in the direction of the cathode (from bottom to top in Figure 13), the maximum drift distance being ∼70 cm.
The beauty of the event is also shown in Fig. 13 [Bottom] (*Collection*-view), where one can appreciate that it extends for more than 2 meters in both projections.

4 Conclusions

The study of very rare nuclear reactions signals, like those related to the neutrino interactions or to nucleon decays, requires the use of very massive detectors, characterized by a granularity as thin as possible. The liquid Argon "Time Projection Chamber" (TPC) technology gives an answer to this problem. Since 1985, the ICARUS Collaboration has been developing the LAr-TPC innovative technique for nuclear particle detection. The first Proposal of Experiment, presented in 1985, described a very big monolithic detector ($4500\ m^3$) to be installed at LNGS. After a long R&D activity, in 1994 an upgraded version for a $4000\ m^3$ detector was published and later, in 1997, a Revised Version was presented, introducing the concept of "modularity", where the total mas is splitted into independent modules.. A number of test devices with rising dimensions have been successfully tested over the years.

In 2001 a milestone achievment has been reached: a first module, the ICARUS T600 detector, has been completed and tested, with fully satisfactory results. ICARUS can thus be considered ready for the experimental applications.
The ICARUS Collaboration in the near future is focusing the activity along two main parallel lines:

1. the transport of the first T600 module to the LNGS: the first part of the physics programme will include the collection of a substantial number of atmospheric neutrino events, a first search for proton decay with a background-free technique, and the detection of ^{8}B solar neutrinos. This work is essential in order to better understand the performance of this type of detector with actual physics events, including background, and to bring to maturity the LAr technology in an underground laboratory, real event signatures and, very important, all the specific operational and safety aspects.

2. Within the framework of the 1997 proposal, and on the basis of the experience of the T600 module, the design and assembly of "clones" of the present prototype module in a series of units, in order to reach the originally foreseen sensitive mass. This is inevitably a graded programme, in which the mass will be increased in a number of successive steps.

References

[1] C. Rubbia, "The Liquid-Argon Time projection Chamber: a new concept for Neutrino Detector", **CERN-EP/77-08**, (1977).

[2] The ICARUS Web Page: *http://www.aquila.infn.it/icarus*.
See also *http://www.cern.ch/icarus*

[3] ICARUS Collaboration, "A first 600 ton ICARUS detector installed at the Gran Sasso Laboratory", Addendum to Proposal by the ICARUS Collaboration, **LNGS - 95/10**, (1995).

[4] ICARUS Collaboration, "A second-Generation Proton Decay Experiment and Neutrino Observatory at the Gran Sasso Laboratory (The Initial Physics Program)", **LNGS-P28/2001**.

[5] ICARUS Collaboration, "A second-Generation Proton Decay Experiment and Neutrino Observatory at the Gran Sasso Laboratory", **LNGS-EXP 13/89 add.2/01, (November,2001)**.

[6] ICARUS Collaboration, "The ICARUS T600 Experiment", **LNGS Annual Report 2000**, (2000), 89.

[7] S.Centro et al., "Low-Noise BiCMOS Front-End and Fast Analogue Multiplexer for Ionisation Chamber", *Nucl. Instrum. and Methods* A **409**, 300 (1998).

[8] C. Carpanese et al., "DAEDALUS: a hardware signal analyser for ICARUS", *Nucl. Instrum. and Methods* A **409**, 294 (1998).

[9] ICARUS Collaboration, "Detection of scintillation light in coincidence with ionizing tracks in a LAr TPC", *Nucl. Instrum. and Methods* A **432**, 240 (1999).

[10] ICARUS Collaboration, "Operation of a 10m^3 ICARUS detector Module", Proceedings of the "Frontiers Detectors for Frontier Physics" Conference I.la d'Elba (Italy, May 2000), *Nucl. Instrum. and Methods* A **461**, 286 (2001).

5 List of Publications

1. ICARUS Collaboration, "Operation of a $10m^3$ ICARUS Detector Module", Proceedings of the "Frontiers Detectors for Frontier Physics" Conference (I.la d'Elba-Italy, May 2000), *Nucl. Instrum. and Methods* A **461**, 286 (2001).

2. ICARUS Collaboration, "The ICARUS Liquid Argon Time Projection Chamber", Proceedings of the "Imaging 2000" Conference (Stockholm-Sweden, July 2000), *Nucl. Instrum. and Methods* A **471**, 272 (2001).

3. ICARUS Collaboration, "The ICARUS Experiment", Proceedings of the "SNOW 200"1 International Conference, (Uppsala-Sweden, February 2001), submitted to *Nucl. Phys.* B.

4. ICARUS Collaboration, "ICARUS T600 and the Solar Neutrino Experiment", Proceedings of the "NO-VE International Workshop" (Venice-Italy), July 2001), Ed. M. Baldo-Ceolin, 91.

5. ICARUS Collaboration, "The Atmospheric and Solar Neutrino Experiment with the ICARUS T600 detector at Gran Sasso Laboratory", Proceedings of the "TAUP 2001" International Conference, (LNGS-Italy, September 2001), submitted to *Nucl. Phys.* B.

6. ICARUS Collaboration, "The Initial Physics Program", **LNGS-P28/2001**.

7. ICARUS Collaboration, "A second-Generation Proton Decay Experiment and Neutrino Observatory at the Gran Sasso Laboratory", **LNGS-EXP 13/89 add.2/01, (November,2001)**.

LUNA and LUNA2. Laboratory for Underground Nuclear Astrophysics

R.Bonetti[1], C.Broggini[2], L.Campajola[3], C.Casella[1], P.Corvisiero[4], H.Costantini[4], J.Cruz[11], A.D'Onofrio[5], A.Formicola[6], Z.Fülöp[7], G.Gervino[8], L.Gialanella[3], U.Greife[9], A.Guglielmetti[1], C.Gustavino[10], G.Gyürky[7] G.Imbriani[3,12], A.P.Jesus[11], M.Junker[10], A.Lemut[4], B.Limata[3], A.Ordine[3], J.V.Pinto[11], P.G.Prada Moroni[4], P.Prati[4], J.P.Ribeiro[11], V.Roca[3], D.Rogalla[6], C.Rolfs[6], M.Romano[3], C.Rossi-Alvarez[2], F.Schümann[6], E.Somorjai[7], O.Straniero[12], F.Strieder[6], F.Terrasi[5], H.P.Trautvetter[6], S.Zavatarelli[4]

[1] Università di Milano, Dipartimento Di Fisica and INFN, Milano, Italy
[2] INFN, Padova, Italy
[3] Università di Napoli, Dipartimento di Fisica and INFN, Napoli, Italy
[4] Università di Genova, Dipartimento di Fisica and INFN, Genova, Italy
[5] Seconda Università di Napoli, Dipartimento di Scienze Ambientali, Caserta and INFN, Napoli, Italy
[6] Institut für Experimentalphysik III, Ruhr-Univerität Bochum, Germany
[7] ATOMKY, Debrecen, Hungary
[8] Politecnico di Torino, Dipartimento di Fisica and INFN, Torino, Italy
[9] Colorado School of Mines, Golden, USA
[10] Laboratori Nazionali del Gran Sasso, Assergi, Italy
[11] Centro de Fisica Nuclear da Universidade de Lisboa, Lisboa (Portugal)
[12] Osservatorio Astronomico di Collurania, Teramo, Italy

Abstract

The underground accelerator facilities LUNA 50 kV and LUNA 400 kV installed at the Laboratori Nazionali del Gran Sasso have been used for studies of low cross section nuclear reactions of astrophysical interest, exploiting the strong suppression of cosmic background. At the 50 kV facility the $D(p,\gamma)^3He$ reaction has been investigated, using the gas target plus BGO detector system recently setup, down to 2.5 keV center-of-mass energy, thus covering the full Gamow peak. The new 400 kV accelerator has been tested and an excellent resolution and stability was found. The

study of the $^{14}N(p,\gamma)^{15}O$ reaction started with investigation of solid targets purity and stability and runs at selected energies below the 278 keV resonance have been performed.

Introduction

One of the challenges of experimental nuclear astrophysics is the attempt to obtain accurate determinations of S-factor values at the Gamow energy E_0 for all the reactions involved in stellar evolution. The astrophysical S(E) factor and the Gamow energy are related to the reaction cross section $\sigma(E)$ and to the stellar temperature T_6 (in units of 10^6 K), respectively, by the expressions:

$$\mathrm{S(E)} = \sigma(\mathrm{E})\mathrm{E}\exp\left(31.29\mathrm{Z_1Z_2}\sqrt{\frac{\mu}{\mathrm{E}}}\right) \;\; ; \qquad E_0 = 1.22(Z_1^2 Z_2^2 \mu T_6^2)^{1/3} \tag{1}$$

In equation (1) μ is the reduced mass in units of amu, Z_1 and Z_2 are the nuclear charges of the interacting particles in the entrance channel and E is the center of mass energy in units of keV [1] . Since E_0 is in all cases much smaller than the Coulomb barrier height, the measurement of the very small $\sigma(E_0)$ values is a very difficult - actually, in many cases, impossible at present - task for the experimentalist. Several problems - related to the extremely low reaction rates, target purity and stability, energy loss of the beam in the target, the presence of atomic electrons, etc. - demand the development of sophisticated experimental methods to optmize the signal-to-noise ratio [2]. As cosmic background is one of the main noise sources, experiments installed in the Gran Sasso underground laboratory have been proved to be an excellent solution [3, 4, 5, 6]: exploiting the strong background suppression, reactions between light nuclei could be studied in the Gamow region using the 50 kV accelerator facility in conjunction with a windowless gas target and a charged particle detector system. In the following we report on a study of the $D(p,\gamma)^3He$ reaction performed by a renewed gas target and a large solid angle segmented BGO crystal for γ-ray detection.

The investigation of reactions taking place at higher energy in astrophysical environments has been undertaken using the new 400 kV accelerator. In section 2 we give an account of the operation of the machine during the first year together with the tests performed to assess its performances and to achieve the proper tuning and calibrations. First results on the investigation of the $^{14}N(p,\gamma)^{15}O$ reaction are presented in the last section.

1 The $D(p,\gamma)^3He$ reaction

The $D(p,\gamma)^3He$ reaction, the second step of the pp chain, only affects the equilibrium abundance of deuterium in an H-burning low mass star. However, well before the onset of the H-burning (during the so called pre-main sequence phase), an important d-burning takes place [7]. Reliable proto-star models predict that a star forms by accretion of interstellar material onto a small contracting core. Until the temperature remains lower than about 10^6 K, the main source of energy is the gravitational contraction. On the basis of the virial theorem, one half of the gravitational energy is spent to supply the

surface energy loss, while the other half goes into heat. When the temperature approaches 10^6 K, the original deuterium (a mass fraction of about 2×10^{-5}) is converted in to ^{3}He via D(p,γ)^{3}He, thus providing 5.5 MeV for each reaction. The total amount of nuclear energy generated by this d-burning is comparable with the whole gravitational binding energy of the star. The main effect of the onset of d-burning is to slow down the contraction and, in turn, the heating. As a consequence, the lifetime of the star increases and its observational properties (surface luminosity and temperature) are frozen until the original deuterium is fully consumed. Due to the slow evolutionary timescale, a large fraction of the proto-stars is actually observed during this d-burning phase and only a negligible amount is expected in the previous, more rapid, evolutionary phase. A reliable knowledge of the rate of D(p,γ)^{3}He down to a few keV (the Gamow peak in a proto-star) is a fundamental prerequisite for these stellar models.

Because of the relatively low height of the d+p Coulomb barrier, several experiments have been performed on this reaction which is believed to be dominated by the direct capture mechanism [1]. The reaction Q value is 5.5 MeV: with proton beams with energy E_p of few tens of keV, the energy of the emitted photon is $E_\gamma = Q + 0.67\ E_p$ and can be considered constant at $5.5MeV$ within the typical energy resolution of scintillation detectors. Previous measurements [8, 9] do not overlap with the relevant Gamow peak in proto-stars and in the Sun (which extends from 3 to 10 keV); moreover, when extrapolated to zero energy, the astrophysical $S(0)$ factors deduced by the two groups exhibit a 40% discrepancy.

Using the 50 kV LUNA accelerator facility at the Gran Sasso underground laboratory we measured, with a precision of the order of 10%, the D(p,γ)^{3}He cross section from 22 down to 2.5 keV c.m. energy, well below the solar Gamow peak. We used a differentially pumped gas-target system designed to fit the characteristics of a large BGO gamma detector. The BGO detector has been designed to serve for several experiments scheduled at the LUNA underground facility [10]. It is shaped as a 28 cm long cylinder with a coaxial hole of 6 cm diameter. The radial thickness of the BGO is 7 cm. The crystal is optically divided into six sectors, each covering an azimuthal angle of 60 degrees. Two Hamamatsu R1847-07 photomultipliers (PMTs) are coupled to the opposite faces of each sector and can be read in coincidence reducing the electronic noise. The target chamber and the beam calorimeter are hosted inside the BGO hole, where the center of the 10 cm long target cell is placed at the middle of the detector. This arrangement allows the detector to cover a large fraction of solid angle but heavily constrains the dimensions of the calorimeter itself. The detection efficiency for 5.5 MeV γ-rays is about 70% with an energy resolution in the total absorption peak of 8%. Details on the experimental apparatus and procedure, as well as on data analysis, are given in [11].

The D(p,γ)^{3}He cross section was measured varying the extraction beam energy between 32 and 4 keV in fine steps. The results are represented in figure 1 where the astrophysical S-factor is shown as a function of the c.m. energy. During the experiment we changed the target pressures and we used different molecular beams (H_1^+, H_2^+, H_3^+): no systematic effects due to these parameters could be observed in the data. At the center of the solar Gamow peak ($E = 6.5\ keV$) the S-factor turned out to be $0.26 \pm 0.01\ (acc) \pm 0.01\ (sys)\ eV\ b$. The S-factor data show a linear trend with the interaction energy as expected since both s-wave and p-wave captures contribute to the

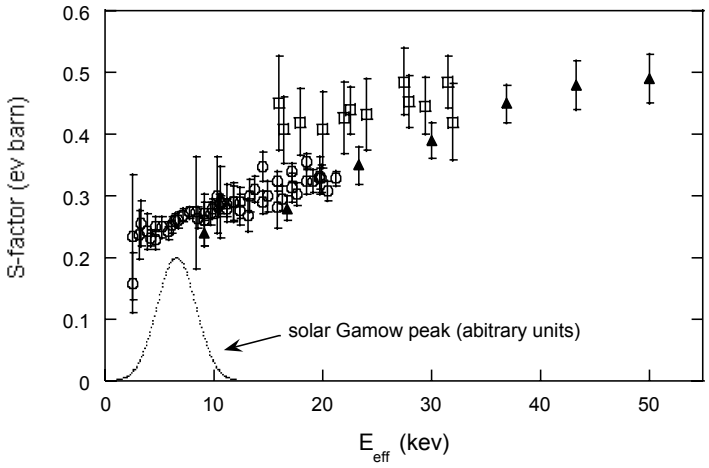

Figure 1: S -factor data for the D(p,γ)^{3}He reaction from [8] (squares), [9](full triangles) and present work (circles). The position of the solar Gamow peak is also shown schematically.

cross section value [8, 9]. LUNA data can be compared with those obtained in previous experiments as shown in fig. 1: it turns out that the measured S-factor in the Gamow peak region is in agreement with the extrapolation from higher energy data reported in [9]. The older experiment [8] found, in its measured energy range, a 40% higher S-factor. The S-factor at zero energy, S_0, can also be compared with the prediction of a recent model [12] and its extrapolation reported in [8, 9]. The LUNA data extrapolation is again in agreement with [9] and also, at a 3σ level, with the model [12] but it should be noted that for the LUNA data the extrapolation to zero energy region is 2.5 keV only. Electron screening effects can be estimated for this reaction assuming standard approaches: in the adiabatic approximation [13] the expected enhancement of the S-factor at 2.5 keV (c.m) is about 6% and it increases to 20% for interaction energies around 1 keV. The precision of our data prevents any estimation, even qualitative, of the effect. Moreover, an experiment addressed to this study should improve the luminosity by about 2 orders of magnitude and this seems not achievable in the near future.

2 Perfomances of the 400 kV accelerator facility

In 2001 the 400 kV accelerator has delivered proton beams in the energy range between 50 keV and 400 keV for an overall time of five months. During these runs stable beams of up to 750 μA have been transported on the target station mounted at the 45^0 extension. It should be noted that no beam could be delivered in the first three months of 2001, due to technical problems related to the power supply and the tank pressure of the machine. As these problems happened during the warranty period of the facility they have been solved in collaboration with High Voltage Engineering B.V. (The Netherlands). Afterwards the facility has proven to be extremely reliable and easy to handle by selected members of the collaboration after a short training period.

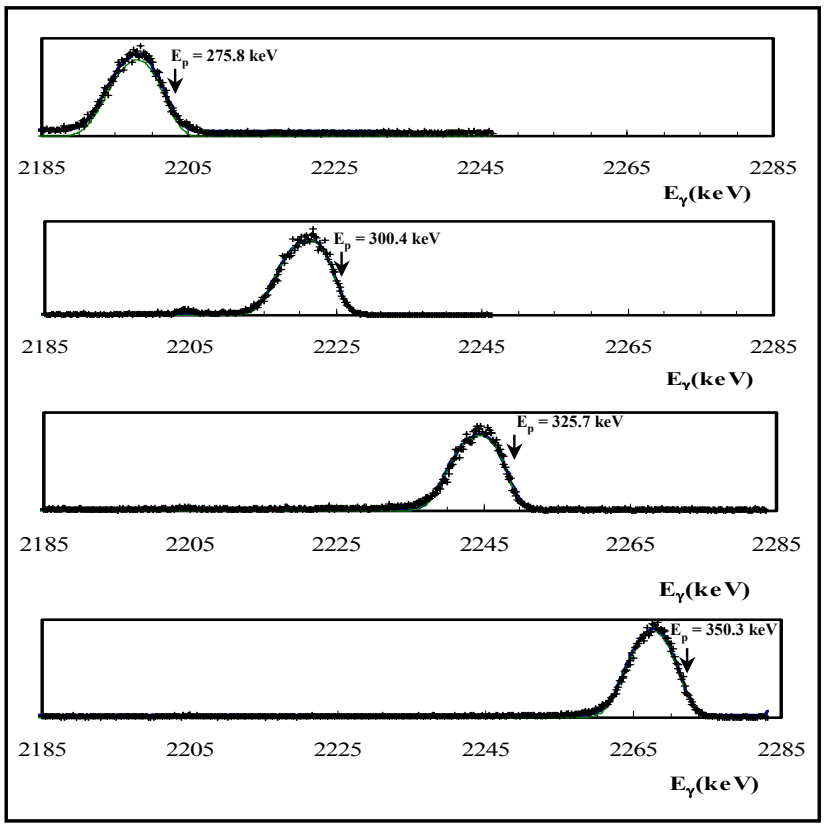

Figure 2: γ-ray spectra showing the transition to the ^{13}N ground state for the $^{12}\mathrm{C}(\mathrm{p},\gamma)^{13}\mathrm{N}$ reaction at four different incident energies.

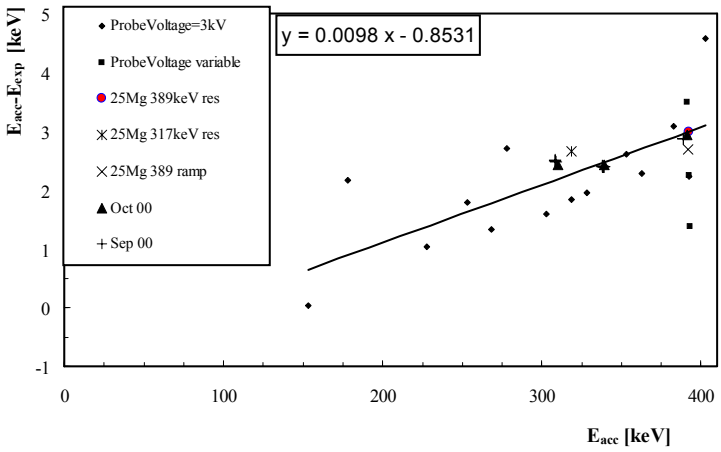

Figure 3: Plot of the beam energy "error" vs. the nominal accelerator voltage.

The uptime of the machine has been increased by implementing an emergency shutdown system, which protects the operators as well as equipment in case of technical problems in the accelerator and target system. After commissioning the protection systems equipment damages have been reliably avoided.

In order to provide maximum security to the personnel present near the experiment a radiation monitoring system has been installed in collaboration with the relevant services of LNGS. The system is based on a Berthold LB111 with two proportional counters (Type 1236, X-Ray threshold 30kV), one of which is mounted at 50 cm from the 0^0 port of the accelerator while the other is mounted outside the accelerator room. The system shuts down the accelerator in the case of a radiation level of more than 1μSv/h at one of the two sensors. After installation of the detection system the radiation has never reached values larger than 0.05μSv/h, corresponding to the sensitivity threshold of the detector. It should be pointed out that this value lies well below the limit of exposure imposed by law for the population of 1mSv/y.

Thanks to these improvements the accelerator is now operating without personnel on site, if the experimental conditions allow for that.

The characterization of the energy resolution and stability of the machine has been completed and checked after the above maintenance interventions. The energy spread of the beam was measured [15] using the resonance at $E_p = 389\ keV$ in the ^{25}Mg(p,γ)^{26}Al reaction, which has a very small natural width ($\Gamma < 20\ eV$). The experimental slope in the excitation function is then determined essentially by the energy resolution of the accelerator and by the Doppler broadening due to the thermal motion of target nuclei. An accurate analysis of the yield of the reaction as a function of the voltage applied to the target (in order to vary the beam energy in very small steps) yielded a total experimental width of 72 eV. This figure, which has been substantially confirmed in a recent run, is well within the specifications, and determines the accuracy achievable in S-factor measurements, due to the steep energy dependence of the cross section at astrophysical energies (see eq. 1).

For the same reason it is of outmost importance a precise knowledge of the energy

calibration of the accelerator. This has been accomplished combining the precise energy determination given by the position of two narrow resonances in the ^{25}Mg(p,γ)^{26}Al reaction, at $E_p = 389\ keV$ and E$_p$ = 309 keV with the information arising from the direct capture process ^{12}C(p,γ)^{13}N. This reaction has a smooth energy dependence in a wide incident energy range and its Q-value ($Q = 1.94\ MeV$) is such that the γ-ray transition to the ^{13}N ground state falls in a region of the γ-spectrum which can be precisely energy-calibrated by source and background lines. Taking into account the average Doppler correction due to the large angle subtended by the detector, the upper edge of the line provides, by subtraction of the Q-value, the c.m. energy of the protons impinging on the target surface, and then the laboratory energy of the beam. A fit to the line shape has been performed which takes into account the energy dependence of the cross section in the energy interval corresponding to the target thickness, as well as the detector response function; a sample of such an analysis is reported in fig. 2. A plot of the beam energy "error" vs. the nominal accelerator voltage is shown in fig 3, in which also the effect of the probe voltage on the beam energy at the exit of the ion source is visible.

3 The ^{14}N(p,γ)^{15}O reaction

Since the pioneering papers [14] on the subject it was immediately understood that Globular Clusters are among the oldest components of the Milky Way. Their ages may be derived by comparing the observed Color-Magnitude diagrams with theoretical isochrones (see fig. 4 a)). The location in the HR diagram of both the Main Sequence and the Red Giant Branch do not change with Age. On the contrary the Turn Off and the Subgiant Branch substantially depend on the Age (see fig. 4 b)).

During most of its life, a low mass star burns H in the center via the pp chain. However, when the central H mass fraction reduces down to 0.1, the nuclear energy produced by the H-burning becomes not sufficient and the stellar core must contract to extract some energy from its gravitational field. Then, the central temperature (and the density) increases and the H-burning switches from the pp-chain to the more effcient CNO-burning (see again fig. 4). Thus the escape from the Main Sequence is powered by the onset of the CNO burning, whose bottleneck is the ^{14}N(p,γ)^{15}O reaction. A modification of the rate of this reaction alters the turn off luminosity, but leaves almost unchanged the stellar lifetime, which is mainly determined by the rate of the pp reaction.

The minimum energy explored in nuclear physics laboratories for this reaction is $\simeq 200\ keV$, well above the region of interest for the CNO burning in astrophysical condition ($20 - 80\ keV$), so that the values used in stellar model computations are largely extrapolated. The most recent stellar models of low mass stars have been obtained by using the compilation of the nuclear reaction rates by Caughlan and Fowler ([16]). The ^{14}N(p,γ)^{15}O rate reported by the most recent compilation (NACRE collaboration [17]) does not substantially differ from the one tabulated by CF88.

At solar energies the cross section of ^{14}N(p,γ)^{15}O is dominated by a subthreshold resonance at -504 keV. Recently some indirect measurements of this subthreshold resonance have been performed employing the Doppler Shift Attenuation Method [18] and there are also some new calculations about its influence at solar energies [19]. Thus direct

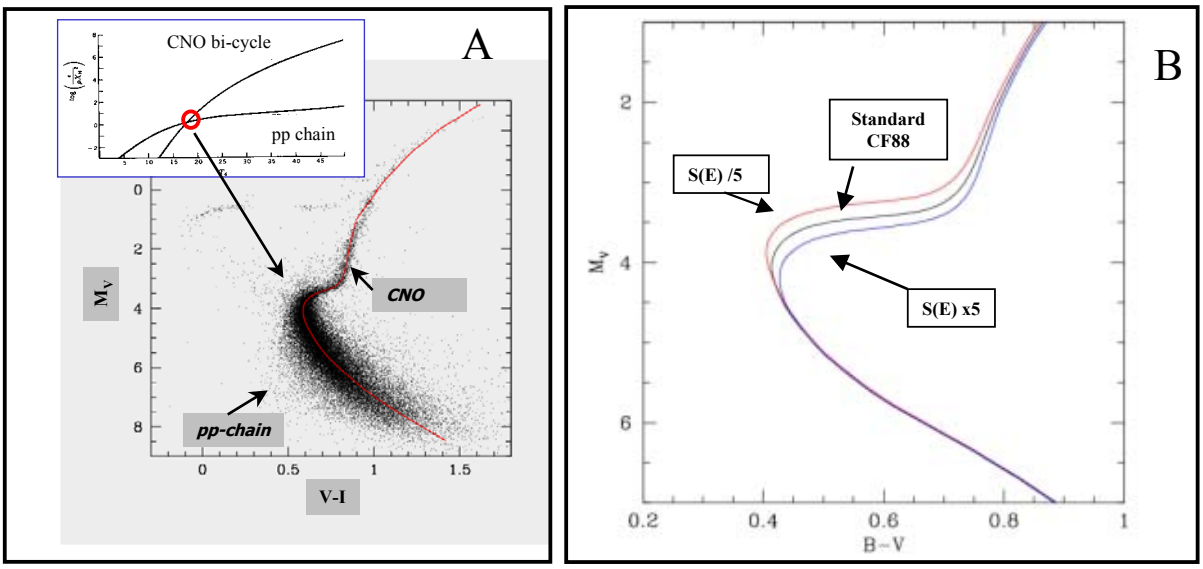

Figure 4: Model of a typical Globular Cluster observational diagram, superimposed on calculated isocrone (pannel A). Influence of a change of the $^{14}\mathrm{N}(\mathrm{p},\gamma)^{15}\mathrm{O}$ reaction rate: the turn off variation mimics an age effect (pannel B).

measurements of the $^{14}\mathrm{N}(\mathrm{p},\gamma)^{15}\mathrm{O}$ reaction at very low energies are needed.

The peculiarities of the 400 kV facility are particularly well suited for this study, where reaction γ-ray lines up to $\simeq$ 7.5 MeV have to be measured with very low intensities. High beam intensities and high detection resolutions have to be coupled to high target stability and purity, and thus low beam-induced background, as cosmic background is strongly suppressed and low intrinsic activity detectors are employed. An extensive study of the quality of N targets has then been performed, using implanted, evaporated and sputtered targets. The first ones were produced at the accelerator of the Centro de Fisica Nuclear da Universidade de Lisboa, bombarding with an isotopically pure ^{14}N low energy beam Ti, Cu and Ta backings. Evaporated targets were prepared evaporating a thin layer of Ti on Ta backings in N atmosphere. Sputtered targets were obtained by the RF magnetron sputtering technique at the Laboratori Nazionali di Legnaro [20].

In all cases during the experiments targets were water-cooled directly on the backing. In the target chamber the target ladder was shadowed by a collimator, so that a uniform circular beam spot (Φ = 4 cm) was obtained within the target area by magnetic wobbling of the beam. In order to prevent build-up of impurities of the target, a LN-cooled copper cold finger was used. For each run beam current was monitored by a digital current integrator. A Pb-shielded 120 % efficiency Ge detector was used in close geometry at 0° with respect to the beam direction.

Using targets prepared by the three above procedures and with different thicknesses, the excitation function of the $^{14}\mathrm{N}(\mathrm{p},\gamma)$ reaction (Q = 7.297 MeV) to four final states in $^{15}\mathrm{O}$ (g.s., 5.18 MeV, 6.18 MeV and 6.79 MeV) was measured in the region of the 1.2 keV broad resonance at E_p = 278 keV. Moreover, γ-ray spectra were recorded at several incident energies below the resonance energy, where the yields from the reaction

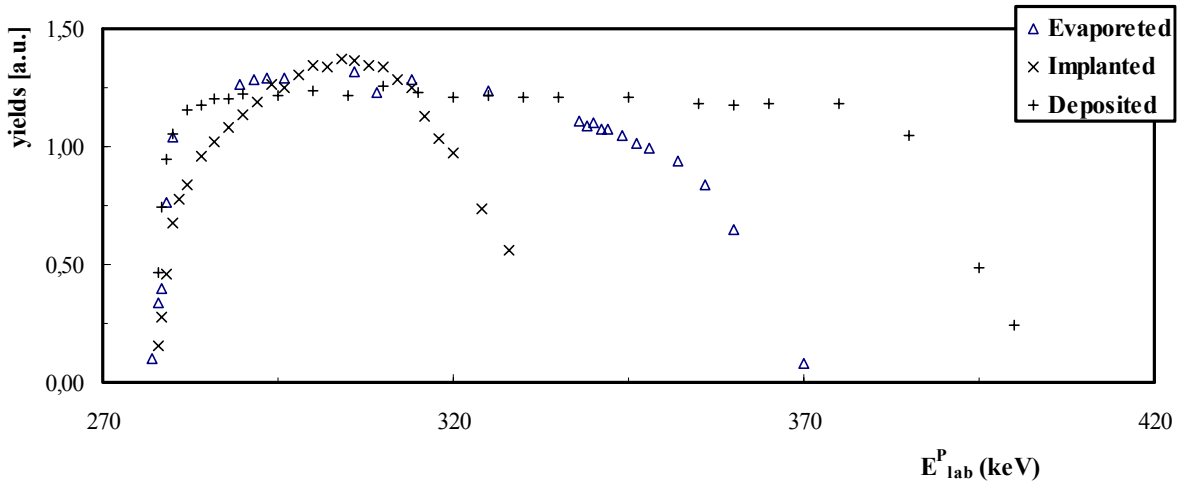

Figure 5: Excitation function of the ^{14}N(p, γ)^{15}O reaction measured using different targets.

drop by more than three orders of magnitude and the presence of lines produced by the interaction of the beam with target impurities critically influences the detection sensitivity. For this reason an extensive study of the background lines was performed, also analyzing spectra taken with the beam on target backings.

3.1 Target stability and beam induced background

A precise knowledge of target composition, stoichiometry and density profile vs depth is an essential ingredient of cross section determinations. Moreover these properties have to be stable under beam bombardment during the experiment. For a thick target of uniform density and stoichiomentry on the whole thickness, the excitation function of a reaction induced by a charged particle beam on one of the elements of target compound (Ti_xN_y or Ta_zN_w in our cases) in the region of a resonance is given, for increasing beam energy, by a more or less steep rise at the resonance energy (whose slope is determined by the convolution of beam resolution and natural width) followed by a constant plateau. The step height is proportional to the inverse of the compound stopping power, depending in turn on the stoichiometry) and its constance reflects the target uniformity. The high-energy decrease is determined by the target thickness and its slope is affected by the energy straggling. Repeated measurements of the resonance profile during long-term high-power beam bombardments allow monitoring of target quality and stability. Fig 5 shows a sample of the results obtained with implanted, evaporated and sputtered targets, out of a large number of tests performed with different backings and thicknesses. These allowed to conclude that sputtered targets of TiN on Ta backings have the most uniform number density profile and withstand many days of beam bombardment with several hundreds of μA without any significant deterioration.

Another critical property of targets employed in low-cross section measurements is the purity of the target itself, of the backing and of the material surrounding the target, which can be hit by the halo of the beam. The presence of light-element impurities

can produce, due to the relatively low Coulomb barrier, γ-ray lines which give rise an interfering background; in particular γ-lines from reactions on ^{11}B, ^{12}C, ^{16}O and ^{19}F have been investigated and their intensity in the spectra has been minimized by a proper choice of the target backing and preparation procedures.

3.2 Preliminary results on $^{14}\mathrm{N}(\mathrm{p},\gamma)^{15}\mathrm{O}$

The yield of a radiative capture reaction is proportional to the integral of the cross section over the target thickness. If the yield is measured in an energy region where no narrow resonances are present and with a steep energy-depence of the cross section, the major contribution arises from the surface part of the target to an extent which depends on the actual slope of $\sigma(E)$. Figure 6 shows the excitation functions of the $^{14}\mathrm{N}(\mathrm{p},\gamma)^{15}\mathrm{O}$ reaction to four different final states, as measured by the intensity per unit beam charge of the primary γ-rays exciting a given state as a function of incident energy. It can be seen that the yield, in the continuous part at energies lower than the $E_p = 278\ keV$ resonance, is independent on target thickness, indicating that, at all energies, the contribution to the yield of the target layers beyond the first 25 keV is negligible. As mentioned above, the precise determination of the effective energy (weighted average of the interaction energies) associated to any measured effective cross section is very critical for the S-factor determination. For this reason a simulation program has been written which calculates the γ-ray line shape as a function of the cross section, expressed as in equation 1 and including the direct capture process and the low energy tail of the $E_p = 278\ keV$ resonance. The energy dependence of the cross section is folded with the density distribution of target atoms and the response function of the Ge detector. Due to the close geometry the angle-dependent Doppler shift and the summing effect of cascade γ-ray transitions, as well as their angular distribution, have to be taken into account. A detailed investigation of all these elements is under course.

4 Publications and Conferences

1. M. Aliotta, F. Raiola, G. Gyürky, A. Formicola, R. Bonetti, C. Broggini, L. Campajola, P. Corvisiero, H. Costantini, A. D'Onofrio, S. Fülöp, G. Gervino, L. Gialanella, A. Guglielmetti, C. Gustavino, G. Imbriani, M. Junker, P.G. Moroni, A. Ordine, P. Prati, V. Roca, D. Rogalla, C. Rolfs, M. Romano, F. Schümann, E. Samorjai, O. Straniero, F. Strieder, F. Terrasi, H.P. Trautvetter, S. Zavatarelli; *Electron screening effect in the reactions ^{3}He(d,p)^{4}He and d(^{3}He,p)^{4}He*, Nuclear Physics A690(2001)790-800.

2. F. Raiola, G. Gyürky, M. Aliotta, A. Formicola, R. Bonetti, C. Broggini, L. Campajola, P. Corvisiero, H. Costantini, A. D'Onofrio, S. Fülöp, G. Gervino, L. Gialanella, A. Guglielmetti, C. Gustavino, G. Imbriani, M. Junker, R.W. Kavanagh, A. Ordine, P. Prati, V. Roca, D. Rogalla, C. Rolfs, M. Romano, F. Schümann, E. Samorjai, O. Straniero, F. Strieder, F. Terrasi, H.P. Trautvetter, S. Zavatarelli; *Stopping power of low-energy deuterons in ^{3}He gas: a threshold effect.* European Physical Journal A10(2001)487-491.

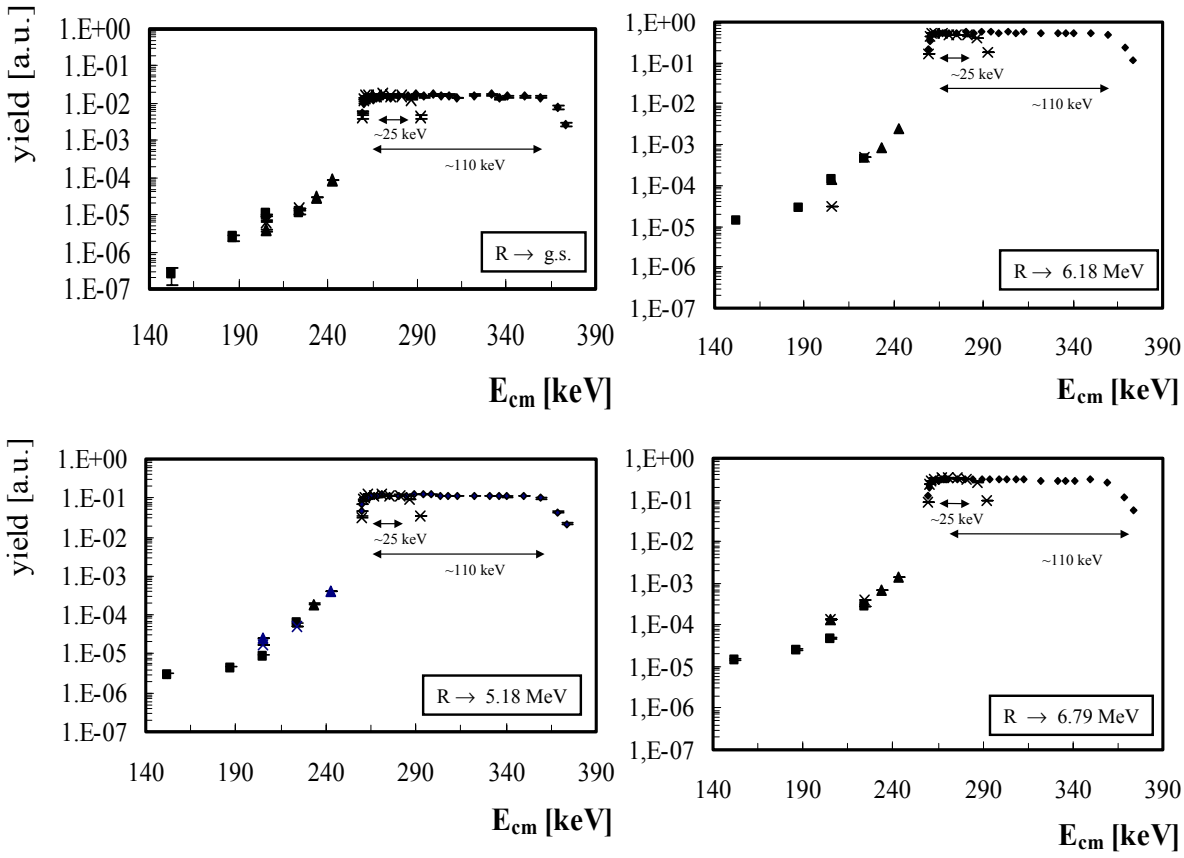

Figure 6: Excitation function of primary γ-rays from the $^{14}\mathrm{N}(\mathrm{p},\gamma)^{15}\mathrm{O}$ measured with three different targets identified by stars, triangles and squares. On the horizontal axis the beam incident energy in the center of mass system is reported.

3. S. Zavatarelli, P. Corvisiero, H. Costantini, P.G. Prada Moroni, P. Prati, R. Bonetti, A. Guglielmetti, C. Broggini, L. Campajola, A. Formicola, L. Gialanella, G. Imbriani, A. Ordine, V. Roca, M. Romano, A. D'Onofrio, F. Terrasi, G. Gervino, C. Gustavino, M. Junker, D. Rogalla, C. Rolfs, F. Schumann, F. Strieder and H.P. Trautvetter; *The $D(^3He,p)^4He$ fusion reaction: electron screening effect and astrophysical S(E) factor at low energies.* Nucl. Phys. A688(2001)514.

4. F. Strieder, L. Gialanella, G. Gyürky, F. Schümann, R. Bonetti, C. Broggini, L. Campajola, P. Corvisiero, H.Costantini, A. D'Onofrio, A. Formicola, S. Fülöp, G. Gervino, U. Greife, A. Guglielmetti, C.Gustavino, G. Imbriani, M. Junker, P.G.P. Moroni, A. Ordine, P. Prati, V.Roca, D.Rogalla, C.Rolfs, M.Romano, E.Somorjai, O.Straniero, F.Terrasi, H.P. Trautvetter and S. Zavatarelli. *Absolute cross section of $^7Be(p,\gamma)^8B$.* Nucl. Phys. A696(2001)219S.

5. C. Rolfs; *Nuclear reactions in stars.* Progress in Particle and Nuclear Physics 46(2001)23.

6. F. Strieder, C. Rolfs; *Key reactions in stellar burning: LUNA and other new approaches.* NUPECC report 11, No3(2001)5.

7. F. Strieder, C. Rolfs, C. Spitaleri, P. Corvisiero; *Electron screening effects on fusion reactions.* Naturwissenschaften 88(2001)461.

8. C. Rolfs; *Nuclear reactions in the static burning of stars.* Tours Symposium on Nuclear Physics 2000, eds. Arnould et al. (American Institute of Physics 2001, Vol. 561) p.145.

9. L. Gialanella, U. Greife, A. D'Onofrio, M. Romano, L. Campajola, A. Formicola, S. Fülöp, G. Gyürky, G. Imbriani, C. Lubritto, A. Ordine, V. Roca, D. Rogalla, C. Rolfs, M. Russo, C. Sabbarese, E. Somorjai, F. Strieder, F. Terrasi, H.P. Trautvetter; *Off-line production of a ^7Be ion beam.* Nucl.Instr.Meth. (submitted 2001).

10. C. Casella, H. Costantini, A. Lemut, B. Limita, R. Bonetti, C. Broggini, L. Campajola, P. Corvisiero, J. Cruz, A. D'Onofrio, A. Formicola, S. Fülöp, G. Gervino, L. Gialanella, A. Guglielmetti, C. Gustavino, G. Gyürky, G. Imbriani, A.P. Jesus, M. Junker, A. Ordine, J.V. Pinto, P. Prati, J.P. Ribeiro, V. Roca, D. Rogalla, C. Rolfs, M. Romano, C. Rossi-Alvarez, F. Schümann, E. Somorjai, O. Straniero, F. Strieder, F. Terrasi, H.P. Trautvetter, S. Zavatarelli; *First measurement of the $d(p,\gamma)^3He$ cross section down to the solar Gamow peak.* Nucl.Phys. (submitted 2001)

11. F. Raiola, P. Migliardi, G. Gyürky, M. Aliotta, A. Formicola, H. Costantini, R. Bonetti, C. Broggini, L. Campajola, P. Corvisiero, J. Cruz, A. D'Onofrio, Z. Fülöp, G. Gervino, L. Gialanella, A. Guglielmetti, C. Gustavino, G. Imbriani, A.P. Jesus, M. Junker, R.W. Kavanagh, P.G.P. Moroni, A. Ordine, J.V. Pinto, P. Prati, J.P. Ribeiro, V. Roca, J.P. Ribeiro, D. Rogalla, C. Rolfs, M. Romano, C. Rossi-Alvarez, F. Schümann, D. Schürmann, E. Somorjai, F. Strieder, F. Terrasi, H.P. Trautvetter, S. Zavatarelli; *Electron screening in d(d,p)t for deuterated Ta.* Eur.Phys.J.(submitted 2001)

12. C. Casella, H. Costantini, A. Lemut, B. Limata, D. Bemmerer, R. Bonetti, C. Broggini, L. Campajola, P. Cocconi, P. Corvisiero, J. Cruz, A. D'Onofrio, A. Formicola, S. Fülöp, G. Gervino, L. Gialanella, A. Guglielmetti, C. Gustavino, G. Gyürky, G. Imbriani, A.P. Jesus, M. Junker, P. Musico, A. Ordine, F. Parodi, M. Parolin, J.V. Pinto, P. Prati, J.P. Ribeiro, V. Roca, D. Rogalla, C. Rolfs, M. Romano, C. Rossi-Alvarez, F. Schümann, E. Somorjai, O. Straniero, F. Strieder, F. Terrasi, H.P. Trautvetter, S. Zavatarelli; *A new setup for the underground study of capture reactions.* Nucl.Instr.Meth. (submitted 2002)

13. M. Junker; *Underground Accelerator Laboratory LUNA.* Invitited plenary talk at the Spring meeting of the German Physical Society, 19.-23.3.2001, Erlangen, Germany.

14. M. Junker; *Thermonuclear Cross Sections.* Invited Talk at TAUP2001, 7th topical meeting workshop on Toppics in Astroparticle and Underground Physics, Italy, 8-12 settembre 2001, Assergi,Italy.

15. H. Costantini; *First measurement of the $d(p,\gamma)^3He$ cross section down to the solar Gamow peak.* 18th meeting between astrophysicist and nuclear physicist, Bruxelles, 10-11 - dec 2001.

16. P. Corvisiero; *LUNA, the First Underground Laboratory for Nuclear Astrophysics: recent results and future perspectives.* 4th Italy-Japan Symposium on Heavy Ion Physics Settembrr 26 - 29, 2001.

17. S. Zavatarelli; *Present status of the LUNA facility at the Underground Gran Sasso laboratory.* INPC 2001 Berkeley California Agosto 30 settembre 5, 2001

18. M. Aliotta; *Measurements of low-energy nuclear cross-sections.* NAP2001 Symposium, GSI - Darmstadt 3-4 Mai 2001, Germany.

19. G. Imbriani; *New Measurement of the $^7Be(p,\gamma)^8B$ Nuclear Cross Section and Impact on the Solar Neutrino Fluxes.* 5th International Topical Workshop at the Gran Sasso Laboratory "Solar Neutrinos: Where are the Oscillations?", Marzo 12-14, 2001.

References

[1] C. Rolfs and W.S. Rodney, Cauldrons in the cosmos (University of Chicago Press, 1988)

[2] G. Fiorentini, R. W. Kavanagh and C.Rolfs, Z.Phys. A350 (1995) 289

[3] U. Greife *et al.*, Nucl. instr. Meth. A350(1994) 327

[4] R. Bonetti *et al.*, Phys. Rev. Lett., 82(1999)5205

[5] H. Costantini *et al.*, Phys.Lett. B482(2000)43

[6] A. Formicola *et al.*, Eur.Phys.J. A8(2000)443

[7] S.W. Stahler, Astrophys. J. 332 (1988) 804

[8] G.M. Griffits, M. Lal and C.D. Scarf, Can. J. Phys. Lett. 41,724 (1963)

[9] G.J. Schmid et al., Phys. Rev. Lett. 76,17(1996)

[10] P. Prati *et al.*, Nucl. Phys. A654 (1999)920c

[11] C. Casella *et al.*, Nucl.Phys. (submitted 2001)

[12] R. Schiavilla, M. Viviani and A. Kievsky, Phys. Rev. C 54 (1996) 553

[13] H. J. Assenbaum et al., Z. Phys. A327 (1989) 461

[14] A. Sandage, ApJ 135(1962)349

[15] R. Bonetti *et al.*, Annual Report LNGS 2000, 107

[16] Caughlan, G.R. & Fowler, W.A., 1988, Atomic and nuclear data tables, 40, 283

[17] C. Angulo *et al.*, Nucl. Phys. A656(1999)3

[18] P.F. Bertone *et al.*, PRL, 87(2001)

[19] C. Angulo and P. Descouvemont, Nucl. Phys. A 690(2001)755.

[20] G. Della Mea, private comunication

LVD. Large Volume Detector

M.Aglietta[14], E.D.Alyea[7], P.Antonioli[1], G.Badino[14], G.Bari[1], M.Basile[1], V.S.Berezinsky[9], F.Bersani[1], M.Bertaina[14], R.Bertoni[14], G.Bruni[1], G.Cara Romeo[1], C.Castagnoli[14], A.Castellina[14], A.Chiavassa[14], J.A.Chinellato[3], L.Cifarelli[1,†], F.Cindolo[1], A.Contin[1], V.L.Dadykin[9], L.G.Dos Santos[3], R.I.Enikeev[9], W.Fulgione[14], P.Galeotti[14], P.Ghia[14], P.Giusti[1], F.Gomez[14], F.Grianti[1], G.Iacobucci[1], E.Kemp[3], F.F.Khalchukov[9], E.V.Korolkova[9], P.V.Korchaguin[9], V.B.Korchaguin[9], V.A.Kudryavtsev[9], M.Luvisetto[1], A.S.Malguin[9], T.Massam[1], N.Mengotti Silva[3], C.Morello[14], R.Nania[1], G.Navarra[14],K.Okei[10], L.Periale[14], A.Pesci[1], P.Picchi[14], I.A.Pless[8], A.Romero[14], V.G.Ryasny[9], O.G.Ryazhskaya[9], O.Saavedra[14], K.Saitoh[13], G.Sartorelli[1], M.Selvi[1], N.Taborgna[5], N.Takahashi[12], V.P.Talochkin[9], G.C.Trinchero[14], S.Tsuji[11], A.Turtelli[3], P.Vallania[14], S.Vernetto[14], C.Vigorito[14], L.Votano[4], T.Wada[10], R.Weinstein[6], M.Widgoff[2], V.F.Yakushev[9], G.T.Zatsepin[9], A.Zichichi[1]

[1] *University of Bologna and INFN-Bologna, Italy*
[2] *Brown University, Providence, USA*
[3] *University of Campinas, Campinas, Brazil*
[4] *INFN-LNF, Frascati, Italy*
[5] *INFN-LNGS, Assergi, Italy*
[6] *University of Houston, Houston, USA*
[7] *Indiana University, Bloomington, USA*
[8] *Massachusetts Institute of Technology, Cambridge, USA*
[9] *Institute for Nuclear Research, Russian Academy of Sciences, Moscow, Russia*
[10] *Okayama University, Okayama, Japan*
[11] *Kawasaki Medical School*
[12] *Hirosaki University, Hirosaki, Japan*
[13] *Ashikaga Institute of Technology, Ashikaga, Japan*
[14] *Institute of Cosmo-Geophysics, CNR, Torino, University of Torino and INFN-Torino, Italy*
[†] *now at University of Salerno and INFN-Salerno, Italy*

Abstract

The Large Volume Detector (LVD) in the INFN Gran Sasso National Laboratory, Italy, is a ν observatory mainly designed to study low energy neutrinos from the gravitational collapse of galactic objects.

The experiment has been monitoring the Galaxy since June 1992, under different larger configurations: in January 2001 it has reached its final active mass $M = 1$ kt.

1 Introduction

LVD, located in Hall A of the INFN Gran Sasso National Laboratory, is a multipurpose detector consisting of a large volume of liquid scintillator interleaved with limited streamer tubes in a compact geometry. The major purpose of the LVD experiment is the search for neutrinos from Gravitational Stellar Collapses (GSC) in our Galaxy [1].

In spite of the lack of a "standard" model of the gravitational collapse of a massive star, some features of its dynamics and, in particular, of the correlated neutrino emission appear to be well established. At the end of its burning phase a massive star ($M > 8M_{\odot}$) explodes into a supernova (SN), originating a neutron star which cools emitting its binding energy $E_B \sim 3 \cdot 10^{53}$ erg mostly in neutrinos.

The largest part of this energy, almost equipartitioned among neutrino and antineutrino species, is emitted in the cooling phase: $E_{\bar{\nu}_e} \sim E_{\nu_e} \sim E_{\nu_x} \sim E_B/6$ (where ν_x denotes generically $\nu_\mu, \bar{\nu}_\mu, \nu_\tau, \bar{\nu}_\tau$ flavors). The energy spectra are approximatively a Fermi-Dirac distribution, but with different mean temperatures, since ν_e, $\bar{\nu}_e$ and ν_x have different couplings (cross section values) with the stellar matter: $T_{\nu_e} < T_{\bar{\nu}_e} < T_{\nu_x}$.

LVD is able to detect $\bar{\nu}_e$ interactions with protons, which give the main signal of supernova neutrinos, with a very good signature. Moreover, it can detect ν_e through the elastic scattering reactions with electrons, and it is also sensitive to neutrinos of all flavors detectable through neutral and charged currents interactions with carbon nuclei of the scintillator.

The described features of stellar collapses are in fact common to all existing models and lead to rather model independent expectations for supernova neutrinos. Thus, the signal observable in LVD, in different reactions and due to different kinds of neutrinos, besides providing astrophysical informations on the nature of the collapse, is sensitive to intrinsic ν properties, as oscillation of massive neutrinos.

2 The LVD experiment

2.1 The detector and its upgrades

The LVD experiment has been in operation since 1992, under different larger configurations. During 2001 the final upgrade took place: LVD became fully operational, with an active scintillator mass $M = 1000$ t.

LVD now consists of an array of 840 scintillator counters, 1.5 m^3 each. These are interleaved by streamer tubes, and arranged in a compact and modular geometry. There

are two subsets of counters: the external ones (43%), operated at energy threshold $\mathcal{E}_h \simeq 7$ MeV, and inner ones (57%), better shielded from rock radioactivity and operated at $\mathcal{E}_h \simeq 4$ MeV. In order to tag the delayed γ pulse due to n-capture, all counters are equipped with an additional discrimination channel, set at a lower threshold, $\mathcal{E}_l \simeq 1$ MeV.

During 2001, a further upgrade took place, concerning the shielding against the local radioactivity. The top level counters, more exposed to the tunnel walls, and thus characterized by a higher background counting rate and a minor capability to disentangle $\bar{\nu}_e$ interactions, have been shielded by a 2 cm thick iron layer. With respect to the neutron background, the 72 counters which belonged to the Mont Blanc LSD telescope, have been placed as a shield on the top of LVD. In figure 1 you can see the top view of the ν telescope.

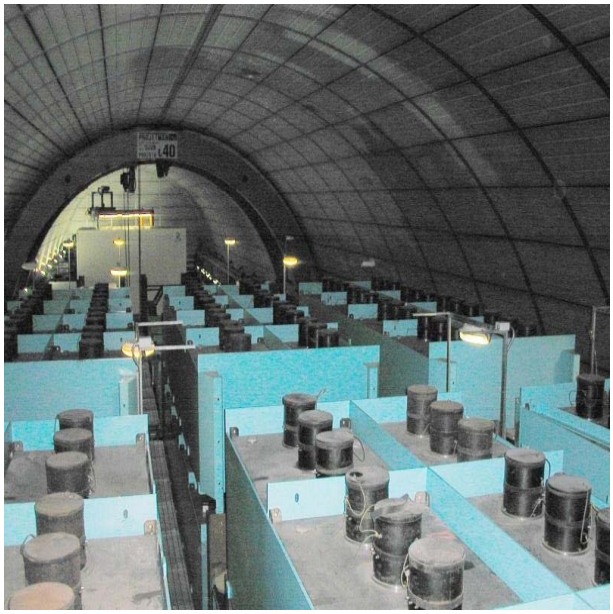

Figure 1: LVD top view

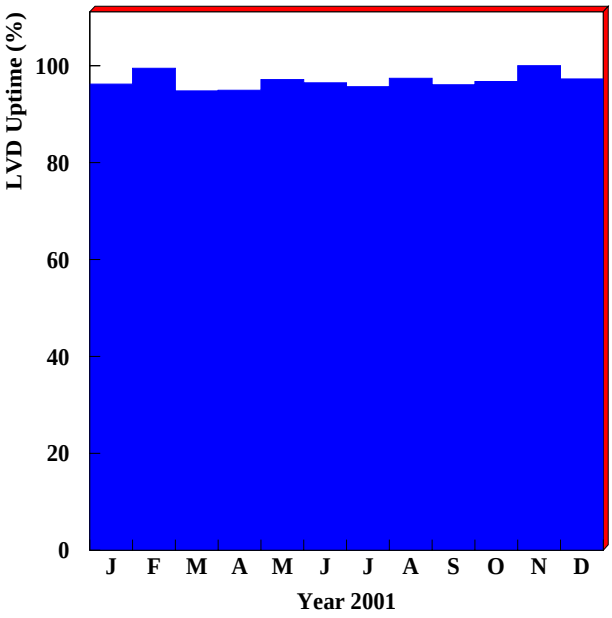

Figure 2: LVD duty cycle.

The tracking system consists of L-shaped detectors for each module. Each element contains two staggered layers of 6.3 m long limited streamer tubes. The bidimensional read-out is made by means of 4 cm strips, parallel and perpendicular to the tubes, providing high detection efficiency and an angular resolution better than 4 mrad.

Relevant features of the detector are:

- (i) good event localization and moun tagging;
- (ii) accurate absolute and relative timing: $\Delta t_{abs} = 1\,\mu s$, $\Delta t_{rel} = 12.5\,ns$;
- (iii) energy resolution: $\sigma_E/E = 0.07 + 0.23 \cdot (E/\mathrm{MeV})^{-0.5}$;
- (iv) very high duty cycle, i.e. 99.7% in the last year (see Fig.2);
- (v) fast event recognition.

2.2 SN neutrino interactions

The observable neutrino reactions are:

- *(1)* $\bar{\nu}_e p, e^+ n$, observed through a prompt signal from e^+ above threshold $\mathcal{E}_h$ (detectable energy $E_d \simeq E_{\bar{\nu}_e} - 1.8$ MeV $+2m_e c^2$), followed by the signal from the $np, d\gamma$ capture ($E_\gamma = 2.2$ MeV), above $\mathcal{E}_l$ and with a mean delay $\Delta t \simeq 180$ μs.
- *(2)* ν_e ^{12}C,^{12}N e^-, observed through two signals: the prompt one due to the e^- above $\mathcal{E}_h$ (detectable energy $E_d \simeq E_{\nu_e} - 17.8$ MeV) followed by the signal, above $\mathcal{E}_h$, from the β^+ decay of ^{12}N (mean life time $\tau = 15.9$ ms).
- *(3)* $\bar{\nu}_e$ ^{12}C,^{12}B e$^+$, observed through two signals: the prompt one due to the e^+ (detectable energy $E_d \simeq E_{\nu_e} - 13.9\,\mathrm{MeV} + 2m_e c^2$) followed by the signal from the β^- decay of ^{12}B (mean life time $\tau = 29.4$ ms). As for reaction *(2)*, the second signal is detected above the threshold $\mathcal{E}_h$.
- *(4)* $\overset{(-)}{\nu}_\ell$ ^{12}C, $\overset{(-)}{\nu}_\ell$ ^{12}C* ($\ell = e, \mu, \tau$), whose signature is the monochromatic photon from carbon de-excitation ($E_\gamma = 15.1$ MeV), above $\mathcal{E}_h$.
- *(5)* $\overset{(-)}{\nu}_\ell$ e^-, $\overset{(-)}{\nu}_\ell$ e^-, which yields a single signal, above $\mathcal{E}_h$, due to the recoil electron.

3 Supernova search

3.1 Monitoring

LVD has been continuously monitoring the Galaxy in the search for neutrino burst from GSC since 1992. The results of this search have been periodically updated and published[5, 6, 7, 8]. The latest update includes the time interval between January 1999 and December 2000: it has been presented at the XXVII ICRC Conference and published on the Proceedings volume[9]. During this period the LVD active mass was $M = 573$ t and its duty cycle reached 99.7%. The monthly averaged duty cycle and active mass in this period are shown in Fig.3 and 4, respectively. Counters showing malfunction problems have not been included on the basis of a run by run screaning (LVD Global Data Base). 4278282 pulses in the energy range $7 \div 100$ MeV have been recorded: their time sequence has been compared with the expected one. The multiplicity, m, distributions of clusters versus their time duration ($\Delta t \leq 200s$) are shown in Fig.5, compared with the expectations from Poissonian fluctuations of the background. The active mass shown in Fig.4 guarantees the detector sensitivity to GSC up to distances $d = 20$ kpc from the Earth, even for the lowest ν-sphere temperature (we expect on the average 25 events from a GSC at 20 kpc with a $\bar{\nu}_e$ temperature of 2 MeV, for an active scintillator mass of 500 t). In the scatter plot of Fig.6 each detected cluster is represented in the plane $(\Delta t, m)$, the dashed line showing the detector sensitivity at the level of 1 event every 100 years.

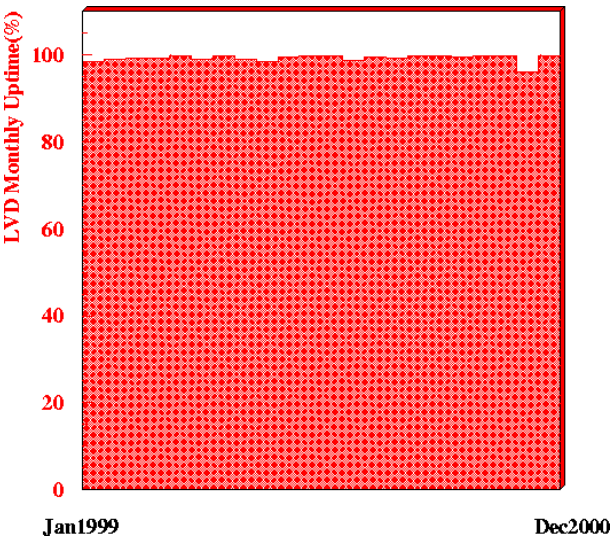

Figure 3: LVD duty cycle.

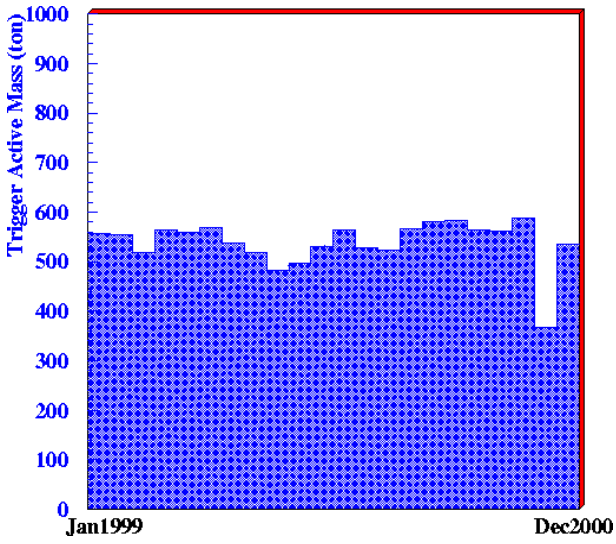

Figure 4: LVD active mass.

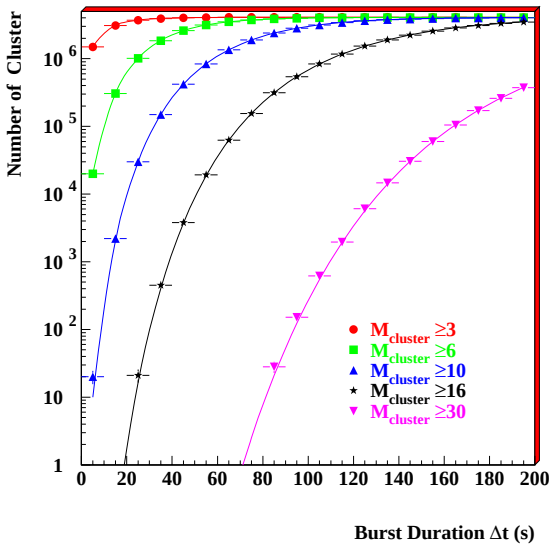

Figure 5: LVD cluster analysis.

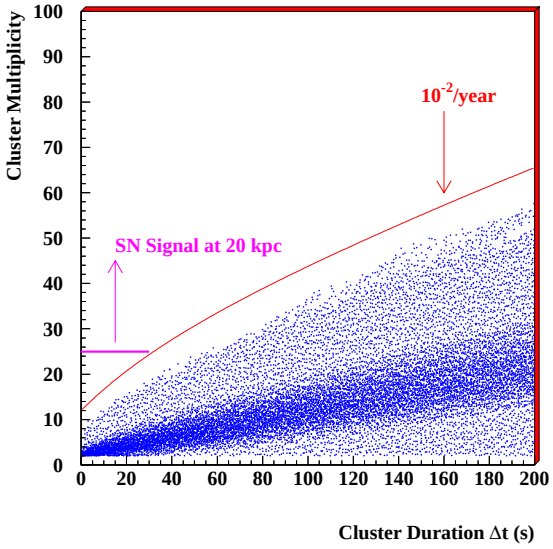

Figure 6: LVD sensitivity.

3.2 Test of supernova recognition

With the aim of studying the reliability of LVD to detect and recognize ν-bursts with different characteristics, we have performed a test simulating a clusters of signals in different counters. The cluster simulator which injects light pulses in a number of counters has been realized during 2001. In May 2001 the test has been performed through the simulation of clusters of pulses having different multiplicity and duration. We plan to evaluate the system efficiency to detect these signals, and to disentangle them from the background (simulating different background conditions). Results of the test have been analyzed and will be published soon[11].

4 SNEWS

The SNEWS (SuperNova Early Warning System) collaboration is an international group of experimenters from several major neutrino experiments with supernova neutrino sensitivity. The primary goal of SNEWS is to provide the astronomical community with a completely automated alert[10].

Two coicidence machines are currently on line, at Kamioka site and at Gran Sasso. These machines continuously run coincidence server programs, which wait for alarm datagrams from each experiment's client, and provide an alert if there is a coincidence within a specified time window. At present day the SNEWS network is in a test phase, to ensure the continued reliability of operations.

During an approximately two-month period in April-June of 2001, Super-K, SNO and LVD performed a "high rate test" of the coincidence software. The purpose was twofold: first, to check the robustness of the software and work out any remaining bugs, and second, to increase confidence in our understanding of the predicted coincidence rates. The analysis of the combined data is in progerss.

Furthermore, we plan to repeat the test of supernova recognition in connection with the others detectors of the SNEWS network, in order to test the full system.

5 Effects of neutrino oscillations on the SN signal

The signal at LVD from a SN exploding at $D = 10$ kpc for 3-flavor ν oscillation, assuming the LMA-MSW solution for solar ν and normal mass hierarchy has been calculated [2] in the cases of no-oscillation and oscillation, under the following hypotheses:

$\star$ We assumed a supernova exploding at $D = 10$ kpc, with an energy release $E_{\rm tot} = 3 \cdot 10^{53}$ erg, pure Fermi-Dirac time integrated spectrum, energy equipartition, and neutrinospheres temperatures as $T_{\nu_e} = T_{\bar{\nu}_e} = T_{\nu_x}/2$.

$\star$ We included the active mass of the detector and the energy thresholds. We used the following values of detection efficiencies above threshold: $\epsilon_{\bar{\nu}_e\, p,e^+\, n} = 95\%$ and $\epsilon_{n\, p,d\, \gamma_{2.2}} = 50\%$; $\epsilon_{\nu_e\, \mathrm{C,N}\, e^-} = 85\%$; $\epsilon_{\bar{\nu}_e\, \mathrm{C,B}\, e^+} = 70\%$; $\epsilon_{\nu_\ell\, \mathrm{C},\nu_\ell\, \mathrm{C}} = 55\%$.

$\star$ In the oscillation case, we used two extreme values for U^2_{e3}: $U^2_{e3} = 10^{-2}$ and $U^2_{e3} = 10^{-6}$, and the following numerical values: $\Delta m^2_{\rm sol} = 5 \cdot 10^{-5}\mathrm{eV}^2$, $\Delta m^2_{\rm atm} = 2.5 \cdot 10^{-3}\mathrm{eV}^2$, $U^2_{e2} = 0.33$; the selected solar parameters $(\Delta m^2_{\rm sol}, U^2_{e2})$ describe a LMA solution, favored by recent analyses [3].

$\star$ We did not include Earth matter effects ("open sky" neutrino burst). However,

Figure 7 shows the number of expected events versus T_{ν_e} in the inverse β decay $\bar{\nu}_e$ reaction: a large increase due to ν mixing is clearly visible, with respect to the no-oscillation case. It should be noted that the number of $\bar{\nu}_e p$ events is practically the same both for adiabatic and non-adiabatic conditions, since, for normal mass hierarchy, MSW effect takes place in the neutrino sector only. Quite a different picture would appear, if we were to assume inverse mass hierarchy.

Figure 8 shows the expected total number of c.c. interactions with ^{12}C, due to both ν_e and $\bar{\nu}_e$. The mixing results in an increase of the number of events, either for adiabatic or for non adiabatic conditions: in case of adiabaticity the increase is larger, and this is solely due to ν_e interactions.

Finally, the expected number of events in neutral currents (n.c.) interactions with ^{12}C is shown in figure 9: they are of course insensitive to ν mixing.

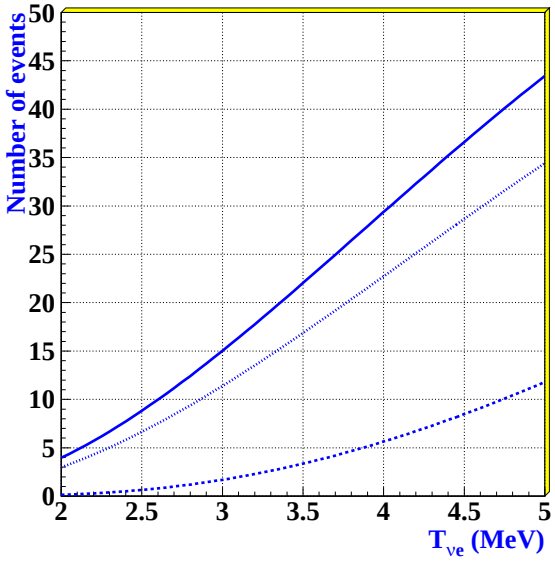

Figure 8: Number of events expected in LVD, in c.c. interactions with ^{12}C as a function of $T_{\bar{\nu}_e} \equiv T_{\nu_e}$: the dashed line represents the no-oscillation case, while full and dotted lines represent the oscillation case, adiabatic and non adiabatic, respectively.

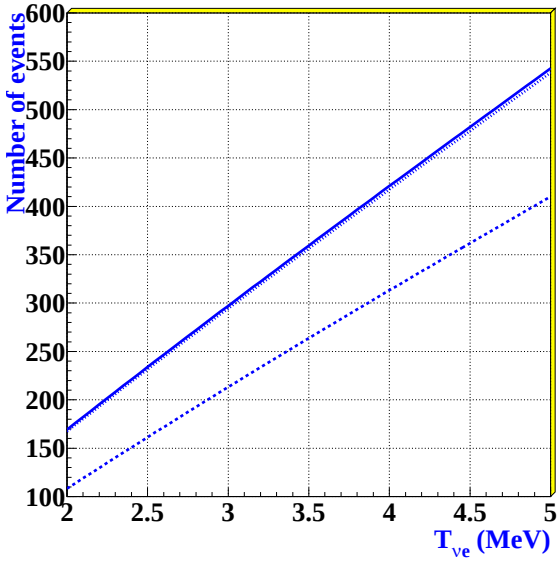

Figure 7: Number of events expected in LVD, in the reaction $\bar{\nu}_e p, ne^+$, as a function of $T_{\bar{\nu}_e} \equiv T_{\nu_e}$: the dashed line represents the no-oscillation case, while full and dotted lines represent the oscillation case, adiabatic and non adiabatic, respectively.

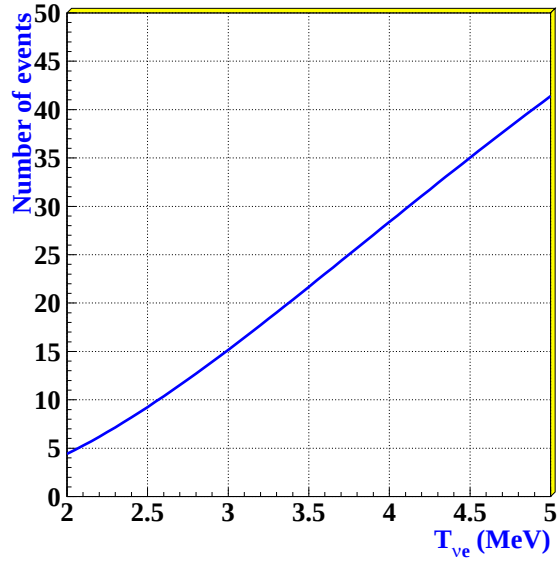

Figure 9: Number of events expected in LVD, in n.c. interactions with ^{12}C as a function of T_{ν_e}.

the number of carbon de-excitations can test the temperature of neutrinospheres at the source, and therefore could be used in combination with c.c. data to overcome theoretical uncertainties on the temperature.

The observation of a neutrino burst due to the explosion of a galactic supernova can add precious information about neutrino mass and mixing scenarios, in a complementary way with respect to solar, atmospheric and terrestrial ν experiments. The combination of well separated classes of events, namely those due to charged and neutral current interactions on carbon and those due to inverse β decay, can help to distinguish between different scenarios of massive neutrinos and astrophysical parameters. In addition, as recently discussed [4], the comparison of the results of a *network* of detectors could permit us to fully exploit the supernova neutrino signal, thus learning on neutrino intrinsic properties.

References

[1] LVD Collaboration, Il Nuovo Cimento **A105** (1992) 1793

[2] LVD Collaboration, Taup2001 Conf.Proc., astro-ph/0112312

[3] G.L.Fogli et al., hep-ph/0106247

[4] C.Lunardini and A.Yu.Smirnov, hep-ph/0106149

[5] LVD Collaboration, 23th ICRC Conf.Proc., HE 5.1.1,Vol.4,468,1993

[6] LVD Collaboration, 24th ICRC Conf.Proc., HE 5.3.6,Vol.1,1035,1995

[7] LVD Collaboration, 25th ICRC Conf.Proc., HE 4.1.12,1997

[8] LVD Collaboration, 26th ICRC Conf.Proc., HE 4.2.08,Vol.2,223,1999

[9] LVD Collaboration, 27th ICRC Conf.Proc., HE230,1093,2001

[10] http://hep.bu.edu/ snnet/

[11] LVD Collaboration, Nuclear Instruments and Methods -in preparation

MACRO. Monopole Astrophysics Cosmic Ray Observatory

Laboratori Nazionali del Gran Sasso, Assergi(AQ)

M. Ambrosio[12], R. Antolini[7], G. Auriemma[14,a], D. Bakari[2,17], A. Baldini[13], G. C. Barbarino[12], B. C. Barish[4], G. Battistoni[6,b], Y. Becherini[2], R. Bellotti[1], C. Bemporad[13], P. Bernardini[10], H. Bilokon[6], C. Bloise[6], C. Bower[8], M. Brigida[1], S. Bussino[18], F. Cafagna[1], M. Calicchio[1], D. Campana[12], M. Carboni[6], R. Caruso[9], S. Cecchini[2,c], F. Cei[13], V. Chiarella[6], B. C. Choudhary[4], S. Coutu[11,i], M. Cozzi[2], G. De Cataldo[1], H. Dekhissi[2,17], C. De Marzo[1], I. De Mitri[10], J. Derkaoui[2,17], M. De Vincenzi[18], A. Di Credico[7], O. Erriquez[1], C. Favuzzi[1], C. Forti[6], P. Fusco[1], G. Giacomelli[2], G. Giannini[13,d], N. Giglietto[1], M. Giorgini[2], M. Grassi[13], L. Gray[7], A. Grillo[7], F. Guarino[12], C. Gustavino[7], A. Habig[3,p], K. Hanson[11], R. Heinz[8], E. Iarocci[6,e], E. Katsavounidis[4,q], I. Katsavounidis[4,r], E. Kearns[3], H. Kim[4], S. Kyriazopoulou[4], E. Lamanna[14,l], C. Lane[5], D. S. Levin[11], P. Lipari[14], N. P. Longley[4,h], M. J. Longo[11], F. Loparco[1], F. Maaroufi[2,17], G. Mancarella[10], G. Mandrioli[2], S. Manzoor[2,n], A. Margiotta[2], A. Marini[6], D. Martello[10], A. Marzari-Chiesa[16], P. Matteuzzi[2], M. N. Mazziotta[1], D. G. Michael[4], S. Mikheyev[4,7,f], L. Miller[8,m], P. Monacelli[9], T. Montaruli[1], M. Monteno[16], S. Mufson[8], J. Musser[8], D. Nicolò[13], R. Nolty[4], C. Orth[3], G. Osteria[12], O. Palamara[7], V. Patera[6,e], L. Patrizii[2], R. Pazzi[13], C. W. Peck[4], L. Perrone[10], S. Petrera[9], P. Pistilli[18], V. Popa[2,g], A. Rainò[1], J. Reynoldson[7], F. Ronga[6], A. Rrhioua[2,17], C. Satriano[14,a], E. Scapparone[7], K. Scholberg[3,q], A. Sciubba[6,e], P. Serra[2], M. Sioli[2], G. Sirri[2], M. Sitta[16,o], P. Spinelli[1], M. Spinetti[6], M. Spurio[2], R. Steinberg[5], J. L. Stone[3], L. R. Sulak[3], A. Surdo[10], G. Tarlè[11], V. Togo[2], M. Vakili[15,s], C. W. Walter[3] and R. Webb[15].

1. Dipartimento di Fisica dell'Università di Bari and INFN, 70126 Bari, Italy
2. Dipartimento di Fisica dell'Università di Bologna and INFN, 40126 Bologna, Italy
3. Physics Department, Boston University, Boston, MA 02215, USA
4. California Institute of Technology, Pasadena, CA 91125, USA
5. Department of Physics, Drexel University, Philadelphia, PA 19104, USA
6. Laboratori Nazionali di Frascati dell'INFN, 00044 Frascati (Roma), Italy
7. Laboratori Nazionali del Gran Sasso dell'INFN, 67010 Assergi (L'Aquila), Italy
8. Depts. of Physics and of Astronomy, Indiana University, Bloomington, IN 47405, USA
9. Dipartimento di Fisica dell'Università dell'Aquila and INFN, 67100 L'Aquila, Italy
10. Dipartimento di Fisica dell'Università di Lecce and INFN, 73100 Lecce, Italy
11. Department of Physics, University of Michigan, Ann Arbor, MI 48109, USA
12. Dipartimento di Fisica dell'Università di Napoli and INFN, 80125 Napoli, Italy
13. Dipartimento di Fisica dell'Università di Pisa and INFN, 56010 Pisa, Italy
14. Dipartimento di Fisica dell'Università di Roma "La Sapienza" and INFN, 00185 Roma, Italy
15. Physics Department, Texas A&M University, College Station, TX 77843, USA
16. Dipartimento di Fisica Sperimentale dell'Università di Torino and INFN, 10125 Torino, Italy
17. L.P.T.P, Faculty of Sciences, University Mohamed I, B.P. 524 Oujda, Morocco
18. Dipartimento di Fisica dell'Università di Roma Tre and INFN Sezione Roma Tre, 00146 Roma, Italy
a Also Università della Basilicata, 85100 Potenza, Italy
b Also INFN Milano, 20133 Milano, Italy
c Also Istituto TESRE/CNR, 40129 Bologna, Italy
d Also Università di Trieste and INFN, 34100 Trieste, Italy
e Also Dipartimento di Energetica, Università di Roma, 00185 Roma, Italy
f Also Institute for Nuclear Research, Russian Academy of Science, 117312 Moscow, Russia
g Also Institute for Space Sciences, 76900 Bucharest, Romania
h Macalester College, Dept. of Physics and Astr., St. Paul, MN 55105
i Also Department of Physics, Pennsylvania State University, University Park, PA 16801, USA
l Also Dipartimento di Fisica dell'Università della Calabria, Rende (Cosenza), Italy
m Also Department of Physics, James Madison University, Harrisonburg, VA 22807, USA
n Also RPD, PINSTECH, P.O. Nilore, Islamabad, Pakistan
o Also Dipartimento di Scienze e Tecnologie Avanzate, Università del Piemonte Orientale, Alessandria, Italy
p Also U. Minn. Duluth Physics Dept., Duluth, MN 55812
q Also Dept. of Physics, MIT, Cambridge, MA 02139
r Also Intervideo Inc., Torrance CA 90505 USA
s Also Resonance Photonics, Markham, Ontario, Canada

Abstract

In this final status report of the MACRO experiment, results are presented on atmospheric neutrinos and neutrino oscillations, high energy neutrino astronomy, searches for WIMPs, search for low energy stellar gravitational collapse neutrinos, stringent upper limits on GUT magnetic monopoles, nuclearites and lightly ionizing particles, high energy downgoing muons, primary cosmic ray composition and shadowing of primary cosmic rays by the Moon and the Sun.

1 Introduction

MACRO was a large area multipurpose underground detector designed to search for rare events in the cosmic radiation. It was optimized to look for the supermassive magnetic monopoles predicted by Grand Unified Theories (GUT) of the electroweak and strong interactions; it could also perform measurements in areas of astrophysics, nuclear, particle and cosmic ray physics. These include the study of atmospheric neutrinos and neutrino oscillations, high energy ($E_\nu \gtrsim 1$ GeV) neutrino astronomy, indirect searches for WIMPs, search for low energy ($E_\nu \gtrsim 7$ MeV) stellar collapse neutrinos, studies of various aspects of the high energy underground muon flux (which is an indirect tool to study the primary cosmic ray composition, origin and interactions), searches for fractionally charged particles and other rare particles that may exist in the cosmic radiation.

The mean rock depth of the overburden is $\simeq 3700$ m.w.e., while the minimum is 3150 m.w.e. This defines the minimum muon energy at the surface at $\sim 1.3\,\mathrm{TeV}$ in order to reach MACRO. The average residual energy and the muon flux at the MACRO depth are $\sim 320\,\mathrm{GeV}$ and $\sim 1\,\mathrm{m^{-2}h^{-1}}$, respectively.

The detector was built and equipped with electronics during the years $1988-1995$. It started data taking with part of the apparatus in 1989; it was completed in 1995 and it was running in its final configuration until December 19, 2000. It may be worth pointing out that all the physics and astrophysics items proposed in the 1984 Proposal were covered and good results were obtained on each of them, even beyond the most rosy anticipations.

The highlights of the new results have been presented at the 2001 summer conferences (in particular at the Int. Cosmic Ray Conf. (ICRC) in Hamburg, at the 2001 European HEP in Budapest, at TAUP 2001 at Gran Sasso and at the NATO Advanced Research Workshop in Oujda, Morocco). One of the main results is the evidence for anomalies in the atmospheric ν_μ flux, which are well interpreted in terms of $\nu_\mu \to \nu_\tau$ oscillations.

We shall give a short summary of the detector and of its performances; this will be followed by an overview of the main physics and astrophysics results obtained by MACRO. A complete list of MACRO papers is given in [1]-[36]; other information may be found in http://www.df.unibo.it/macro/pub1.htm.

In the year 2001 four papers were published on refereed journals; they concerned high energy neutrino astronomy with the MACRO detector [33], the preference for $\nu_\mu \to \nu_\tau$ oscillations over $\nu_\mu \to \nu_s$ [34], a technical paper on the MACRO detector [35] and a combined analysis for a search for magnetic monopoles [36]. Several results appeared in preliminary form in 14 paper contributions that were published in various physics conference proceedings [37]-[57]. They concerned the study of high and low energy atmospheric neutrinos, the use of multiple Coulomb scattering for determining neutrino energies, high energy muon neutrino astronomy, several rare particle searches, the observation of the moon and sun shadow of high energy primary cosmic rays and several aspects of "muon astronomy".

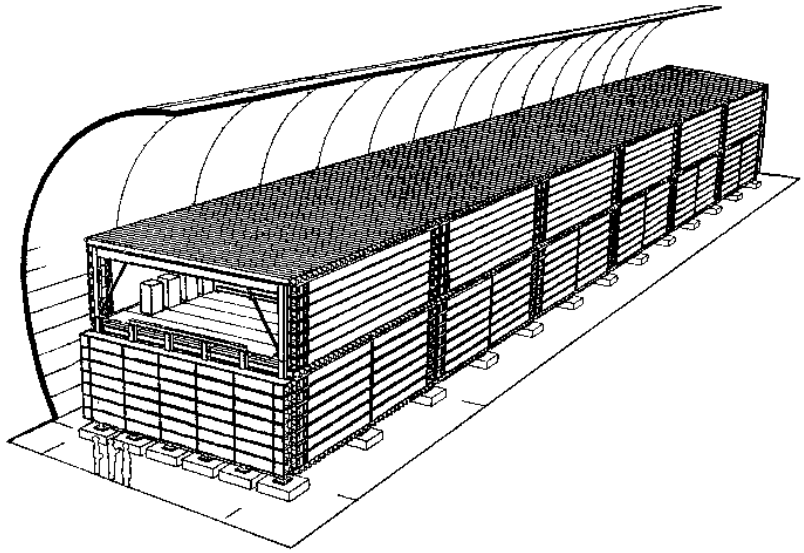

Figure 1: General layout of the MACRO detector which was installed in Hall B of the LNGS. Overall dimensions of the active part were $76.5 \times 12 \times 9.3$ m^3. [35]

2 The Detector

The MACRO detector had a modular structure: it was divided into six sections referred to as supermodules. Each active part of one supermodule had a size of $12.6 \times 12 \times 9.3\,\mathrm{m}^3$ and had a separate mechanical structure and electronics readout. The full detector had global dimensions of $76.5 \times 12 \times 9.3\,\mathrm{m}^3$ and provided a total acceptance to an isotropic flux of particles of $\sim 10,000\,\mathrm{m}^2\,\mathrm{sr}$. The total mass was $\simeq 5300$ t.

Redundancy and complementarity have been the primary goals in designing the experiment. Since no more than few magnetic monopoles could be expected, multiple signatures and ability to perform cross checks among various parts of the apparatus were important.

The detector was composed of three sub-detectors: liquid scintillation counters, limited streamer tubes and nuclear track detectors. Each one of them could be used in "stand-alone" and in "combined" mode. A general layout of the experiment is shown in Fig. 1. Notice the division in the *lower* MACRO and in the *upper* part, often referred to as the *Attico*; the inner part of the *Attico* was empty and lodged the electronics. The mass of the *lower* MACRO was $\simeq 4200$ t, mainly in the form of boxes filled with crushed Gran Sasso rock. Fig. 2 shows a cross section of the apparatus.

The scintillation subdetector. Each supermodule contained 77 scintillation counters, divided into three horizontal planes (bottom, center, and top) and two vertical planes (east and west). In the lower part, the bottom and center horizontal planes had 16 scintillation counters, the east and west vertical planes had 7 counters each. In the *Attico*, the top plane had 17 scintillation counters, the east and west vertical planes had 7 counters each. The lower part of the north and south faces of the detector were covered by vertical walls with seven scintillation counters each. The upper parts of these faces were left open

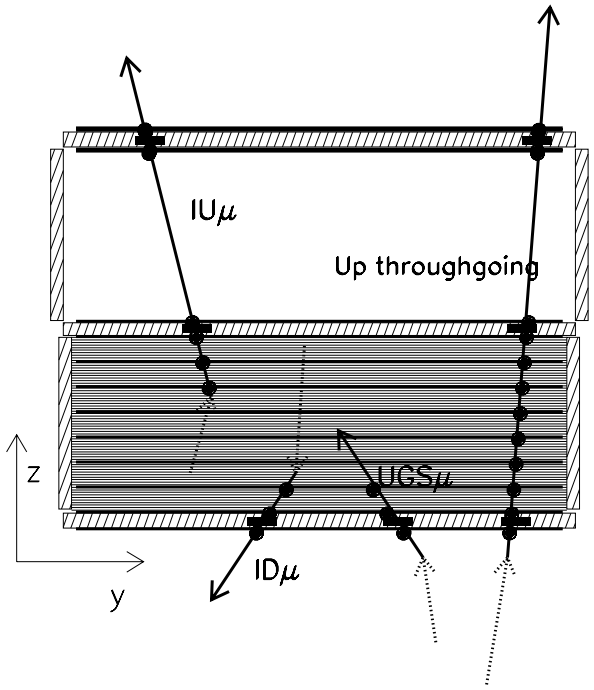

Figure 2: Vertical cross section of the detector and sketch of different event topologies induced by ν_μ interactions in or around MACRO. The black points and the black rectangles represent streamer tubes and scintillator hits, respectively. Tracking was performed by the streamer tubes; the time-of-flight of the muons was measured by the scintillators for *Up Semicontained* (Internal upgoing - IU μ) and *Upthroughgoing* events (and also for downgoing muons).

in order to allow access to the readout electronics.

The active volume of each horizontal scintillation counter was $11.2 \times 0.73 \times 0.19\,\mathrm{m}^3$, while for the vertical ones it was $11.1 \times 0.22 \times 0.46\,\mathrm{m}^3$. All scintillator boxes were filled with a mixture of high purity mineral oil (96.4 %) and pseudocumene (3.6 %), with an additional 1.44 g/l of PPO and 1.44 mg/l of bis-MSB as wavelength shifters. The horizontal counters were seen by two 8″ photomultipliers (PMTs) and the vertical counters by one 8″ PMT at each end. Each PMT housing was equipped with a light collecting mirror. The total number of scintillators was 476 (294 horizontal and 182 vertical) with a total active mass of almost 600 tons. Minimum ionizing muons when crossing vertically the 19 cm of scintillator in a counter release an average energy of $\simeq 34$ MeV and were measured with a timing and longitudinal position resolution of $\simeq 500$ ps and $\simeq 10$ cm, respectively.

The scintillation counters were equipped with specific triggers for rare particles, muons and low energy neutrinos from stellar gravitational collapses. The Slow Monopole Trigger (SMT) was sensitive to magnetic monopoles with velocities from about $10^{-4}c$ to $10^{-2}c$, the Fast Monopole Trigger (FMT) was sensitive to monopoles with velocities from about $5 \times 10^{-3}c$ to $5 \times 10^{-2}c$, the Lightly Ionizing Particle trigger was sensitive to fractionally charged particles, the Energy Reconstruction Processor (ERP) and "CSPAM" were primarily muon triggers (but used also for relativistic monopoles) and the gravitational collapse neutrino triggers (the Pulse Height Recorder and Synchronous Encoder –PHRASE– and the ERP) were optimized to trigger on bursts of low energy events in the liquid scintillator. The scintillator system was complemented by a 200 MHz waveform digitizing (WFD) system used in rare particle searches, and in any occasion where knowledge of the PMT waveform was useful.

The streamer tube subsystem. *The lower part* of the detector contained ten horizontal planes of limited streamer tubes, the middle eight of which were interleaved by seven rock absorbers (total thickness $\simeq 360\,\mathrm{g\,cm^{-2}}$). This sets a $\simeq 1\,\mathrm{GeV}$ energy threshold for muons vertically crossing the lower part of the detector. At the top of the *Attico* there were four horizontal streamer tube planes, two above and two below the top scintillator layer. On each lateral wall six streamer tube planes sandwiched the corresponding vertical scintillator plane (three streamer planes on each side). Each tube had a $3 \times 3\,\mathrm{cm^2}$ cross section and was 12 m long. The total number of tubes was 50304, all filled with a gas mixture of He (73 %) and n-pentane (27 %). They were equipped with 100μ Cu/Be wires and stereo pickup strips at an angle of 26.5°. The tracking resolution of the streamer tube system was $\simeq 1\,\mathrm{cm}$, corresponding to an angular accuracy of $\simeq 0.2°$ over the 9.3 m height of MACRO. The real angular resolution was limited to $\simeq 1°$ by the multiple Coulomb scattering of muons in the rock above the detector. The streamer tubes were read by 8-channel cards (one channel for each wire) which discriminated the signals and sent the analog information (time development and total charge) to an ADC/TDC system (the QTP). The signals were used to form two different chains (Fast and Slow) of TTL pulses, which were the inputs for the streamer tube Fast and Slow Particle Triggers. In the 11 years of operation only 50 wires were lost.

The nuclear track subdetector was deployed in three planes, horizontally in the center of the lower section and vertically on the East and North faces. The detector was divided in 18126 modules, which could be individually extracted and substituted. Each module ($\sim 24.5 \times 24.5 \times 0.65\,\mathrm{cm^3}$) was composed of three layers of CR39, three layers of Lexan and 1 mm Aluminium absorber to stop nuclear fragments.

The Transition Radiation Detector (TRD). A TRD was installed in part of the *Attico*, right above the central horizontal scintillator plane of the main detector. It was composed of three individual modules (overall dimensions $6 \times 6 \times 2\,\mathrm{m^3}$) and it was made of 10 cm thick polyethylene foam radiators and proportional counters; each counter measured $6 \times 6 \times 600\,\mathrm{cm^3}$ and was filled with Ar (90 %) and CO_2 (10 %). The TRD provided a measurement of the muon energy in the range of $100\,\mathrm{GeV} < E < 930\,\mathrm{GeV}$; muons of higher energies could also be detected and counted.

Fig. 3 shows four photographs of the Hall B taken from its south side: (a) 1987: before starting construction; (b) 1990: the 1st lower supermodule was taking data, while the second and the third were under construction; (c) the full MACRO detector in 1995 (a safety stairs and a ventilation system were added later in front of the apparatus); (d) Hall B empty again in 2001.

Fig. 4 shows a "group" of 11 downgoing muons as seen in the lateral view (wire view) by the MACRO Event Display (which also included a strip view and side views).

3 Atmospheric neutrino oscillations

Upward going muons are identified using the streamer tube system (for tracking) and the scintillator system (for time-of-flight measurement). A rejection factor of at least 10^7 is needed, and was reached, in order to separate upgoing muons from the background due to the downgoing muons. Fig. 2 shows a sketch of the different neutrino event topologies

(a) (b)

(c) (d)

Figure 3: Photographs of Hall B taken from its south side: (a) In 1987 just before starting construction; (b) in 1990 when the first lower supermodule was taking data while the second and the third were under construction; (c) in 1995 when the completed MACRO detector started data taking (notice that safety stairs and a ventilation system were added later in front of the apparatus; (d) Hall B empty in 2001.

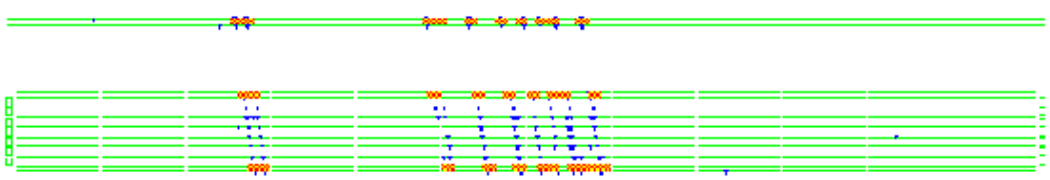

Figure 4: MACRO Event Display. A group of 11 downgoing muons as observed by part of the lateral view.

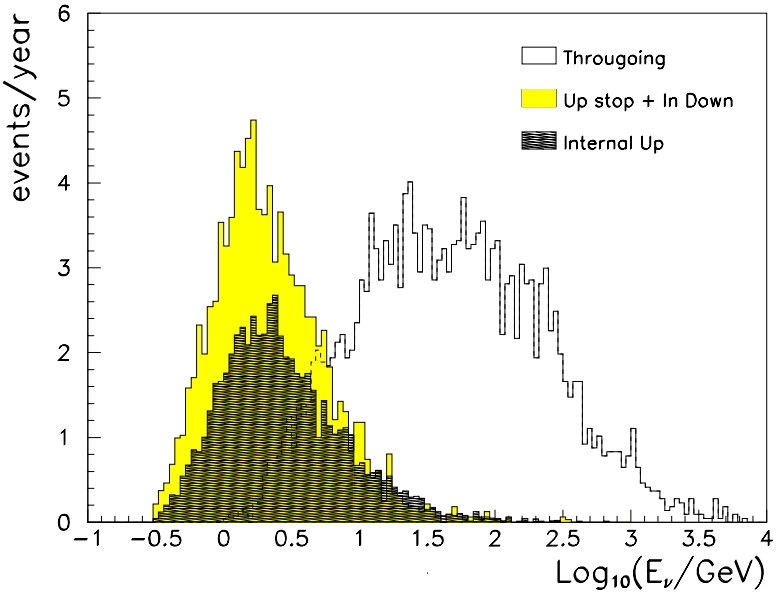

Figure 5: Distributions of the parent muon neutrino energies giving rise to the different event topologies, upthroughgoing, upsemicontained and upstopping plus downsemicontained, with median neutrino energies of approximately 50, 4.2 and 3.5 GeV, respectively.

analyzed: Upthroughgoing muons, Upsemicontained (also called Internal Upgoing muons, IU), Upgoing Stopping muons (UGS), Internal Downgoing muons (ID). Fig. 5 shows the parent ν_μ energy spectra for the three event topologies, computed by Monte Carlo methods. The number of events measured and expected for the three topologies are given in Table 1. All the data samples deviate from the MC expectations; the deviations point out to the same $\nu_\mu \rightarrow \nu_\tau$ oscillation scenario.

The background on upgoing muons arising from downgoing muons interacting in the rock around MACRO and giving an upward going charged particle was studied in detail for upthroughgoing muons in [24]. The selection cuts reduce this background to $< 1\%$.

3.1 Upthroughgoing muons

The *upthroughgoing muons* come from ν_μ interactions in the rock below the detector; the ν_μ's have a median energy $\overline{E}_\nu \sim$ 50 GeV. The upthroughgoing muons with $E_\mu > 1\,\mathrm{GeV}$ cross the whole detector. The time information provided by the scintillation counters allows the determination of the direction (versus) by the time-of-flight (T.o.F.) method. The data of Fig. 6 refer to the running period 3/1989 - 4/1994 with the detector under construction, and with the full detector till 12/2000; the total livetime was 6.16 years (full detector equivalent) [17, 25, 43, 52]. The data deviate in absolute value and in shape from the MC predictions. This was first pointed at TAUP 1993 and in [17] in 1995.

We studied a large number of possible systematic effects that could affect our measurements: no significant systematic problems exist in the detector or in the data analyses. One of the most significant checks was performed using only the scintillator system with the PHRASE Wave Form Digitizers, completely independent of the ERP system.

The measured data have been compared with Monte Carlo simulations. For the upthroughgoing muon simulation, the neutrino flux computed by the Bartol group is used

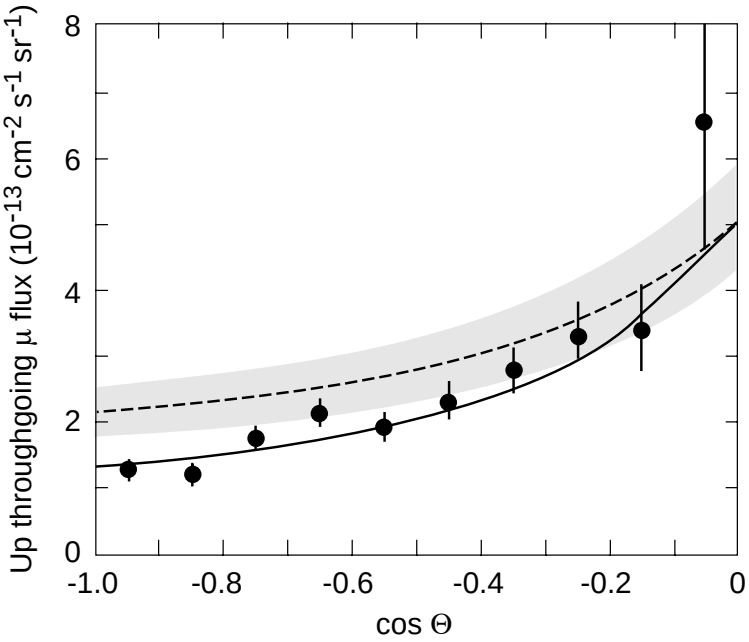

Figure 6: Zenith angle distribution of upthroughgoing muons (black points). The dashed line is the expectation for no oscillations (with a 17 % scale uncertainty band). The solid line is the fit for an oscillated muon flux with maximum mixing and $\Delta m^2 = 2.5 \cdot 10^{-3}$ eV^2.

[58]. The cross sections for the neutrino interactions were calculated using the deep inelastic parton distributions of ref. [59] The muon propagation to the detector was done using the energy loss calculation in standard rock [60]. The total systematic uncertainty on the expected muon flux, obtained adding in quadrature the errors from neutrino flux, cross section and muon propagation, is estimated to be 17 %. This uncertainty is mainly a scale error; the error on the shape of the angular distribution is $\sim 5\%$. Fig. 6 shows the zenith angle distribution of the measured flux of upthroughgoing muons. The Monte Carlo expectation for no oscillations is shown as a dashed line.

To test the oscillation hypothesis, the independent probabilities for obtaining the observed number of events and the shape of the angular distribution have been calculated for various parameter values. The value of Δm^2 obtained from the shape of the angular distribution is equal to the value obtained from the observed reduction in the number of events. For $\nu_\mu \rightarrow \nu_\tau$ oscillations, combining the probabilities from the two independent tests on the shape of the zenith angle distribution and on the total number of events, the maximum probability is 66%; the best parameters are $\Delta m^2 = 2.5 \cdot 10^{-3}$ eV^2 and maximal mixing; the result of the fit is the solid line in Fig. 6. The probability for no-oscillations is 0.4 %.

Fig. 7a shows the allowed regions for the $\nu_\mu \rightarrow \nu_\tau$ oscillation parameters in the $sin^2 2\theta - \Delta m^2$ plane, computed according to ref. [61] for the upthroughgoing muons and for the low energy events. The MACRO 90% c.l. allowed region for $\nu_\mu \rightarrow \nu_\tau$ is compared in Fig. 7b with those obtained by the SuperKamiokande (SK) [63] and Soudan 2 experiments [64].

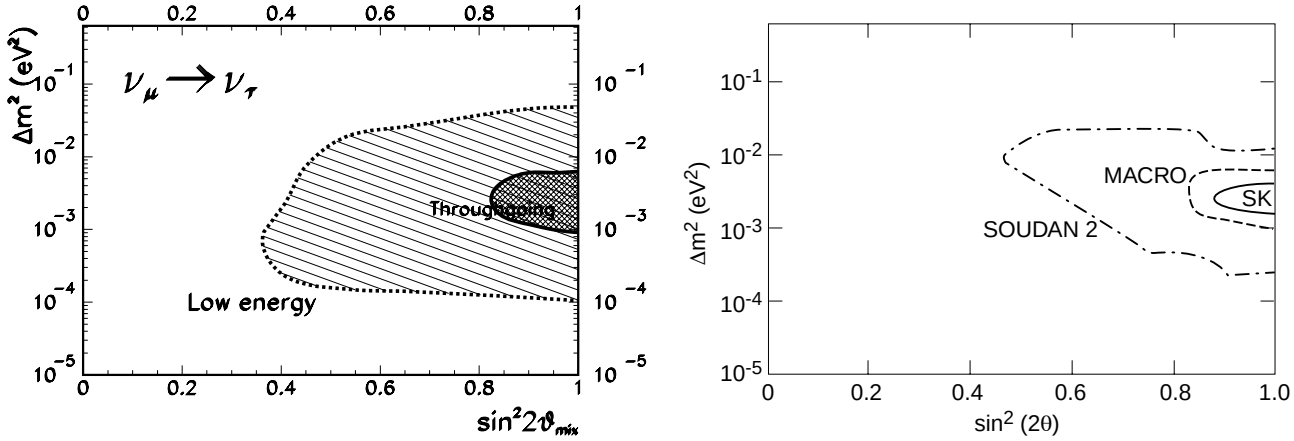

(a) (b)

Figure 7: (a) Allowed regions, at 90 % c.l., for $\nu_\mu \rightarrow \nu_\tau$ oscillations from the MACRO upthroughgoing muon sample and from the low energy events. (b) Comparison with the Soudan 2 [64] and SuperK [63] allowed regions.

3.2 Matter effects. $\nu_\mu \rightarrow \nu_\tau$ against $\nu_\mu \rightarrow \nu_{sterile}$

Matter effects due to the difference between the weak interaction effective potential for muon neutrinos with respect to sterile neutrinos (which have null potential) would produce a different total number and a different zenith distribution of upthroughgoing muons [34].

In Fig. 8 the measured ratio between the events with $-1 < cos\theta < -0.7$ and the events with $-0.4 < cos\theta < 0$ is shown as a black point. In this ratio most of the theoretical uncertainties on neutrino flux and cross section cancel. The remaining theoretical error is estimated at $\leq 5\%$. The systematic experimental error on the ratio, due to analysis cuts and detector efficiencies, is 4.6%. Combining the experimental and theoretical errors in quadrature, a global estimate of 7% is obtained. MACRO measured 305 events with $-1 < cos\theta < -0.7$ and 206 with $-0.4 < cos\theta < 0$; the ratio is R = $1.48 \pm 0.13_{stat} \pm 0.10_{sys}$. For $\Delta m^2 = 2.5 \cdot 10^{-3}$ eV^2 and maximal mixing, the minimum expected value of the ratio for $\nu_\mu \rightarrow \nu_\tau$ is $R_\tau = 1.72$ while for $\nu_\mu \rightarrow \nu_s$ is $R_{sterile} = 2.16$. The maximum probabilities P_{best} to find a value of R_τ and of $R_{sterile}$ smaller than the expected ones are 9.4 % and 0.06 % respectively. Hence the ratio of the maximum probabilities is $P_{best_\tau}/P_{best_{sterile}} = 157$, so that $\nu_\mu \rightarrow \nu_s$ oscillations are disfavoured at 99% c.l. compared to the $\nu_\mu \rightarrow \nu_\tau$ channel with maximal mixing and $\Delta m^2 = 2.5 \cdot 10^{-3}$ eV^2.

3.3 ν_μ energy estimates by multiple Coulomb scattering of upthroughgoing muons

The oscillation probability is a function of the ratio L/E_ν. E_ν may be estimated by measuring the muon energy E_μ, which was done using their Multiple Coulomb Scattering (MCS) in the absorbers.

The r.m.s. of the lateral displacement for a muon crossing the whole apparatus on

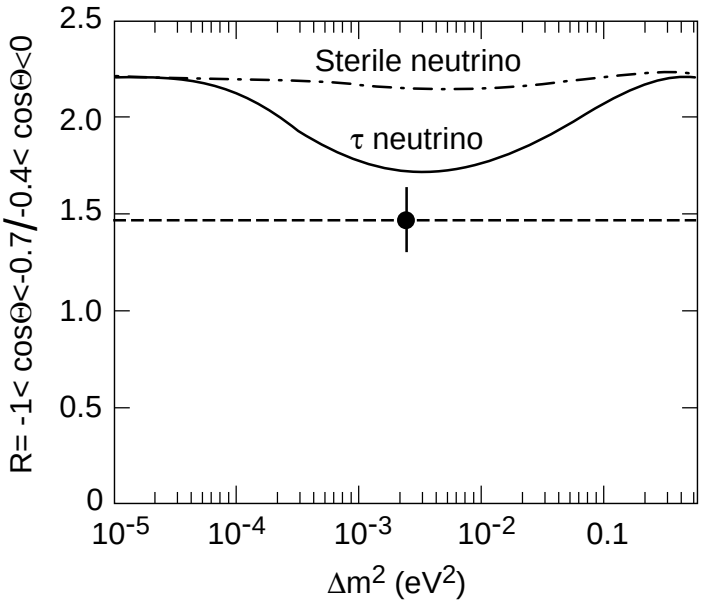

Figure 8: Ratio of events with $-1 < cos\theta < -0.7$ to events with $-0.4 < cos\theta < 0$ as a function of Δm^2 for maximal mixing. The black point with error bar is the measured value, the solid line is the prediction for $\nu_\mu \rightarrow \nu_\tau$ oscillations, the dash-dotted line is the prediction for $\nu_\mu \rightarrow \nu_{sterile}$ oscillations.

the vertical is $\sigma_{MCS} \simeq 10\,\mathrm{cm/E}_\mu(\,\mathrm{GeV})$. The muon energy E_μ estimate can be performed up to a saturation point, occurring when σ_{MCS} is comparable with the detector space resolution.

Two MCS analyses were performed.

The first analysis was made studying the deflection of upthroughgoing muons with the streamer tubes in digital mode. Using MC methods to estimate the muon energy from its scattering angle, the data were divided into 3 subsamples with different average energies, in 2 samples in zenith angle θ and finally in 5 subsamples with different average values of L/E_ν. This method could reach a spatial resolution of $\sim 1\,\mathrm{cm}$; it yielded an L/E_ν distribution quite compatible with neutrino oscillations with the parameters of Section 3.1 [38].

As the interesting energy region for atmospheric neutrino oscillations spans from $\sim$ 1 GeV to some tens of GeV, it is important to improve the spatial resolution of the detector to push the saturation point as high as possible. For this purpose, a second analysis was performed with the streamer tubes in "drift mode", using the TDC's included in the QTP system, originally designed for the search for magnetic monopoles. To check the electronics and the feasibility of the analysis, two tests were performed at the CERN PS-T9 and SPS-X7 beams [53]. The space resolution achieved is $\simeq 3\,\mathrm{mm}$, a factor 3.5 better than in the first analysis. For each muon, seven MCS sensitive variables were given in input to a Neural Network (NN) previously trained to estimate the muon energy with MC events of known input energy crossing the detector at different zenith angles. The NN output allowed to separate the upthroughgoing muons in 4 subsamples with average

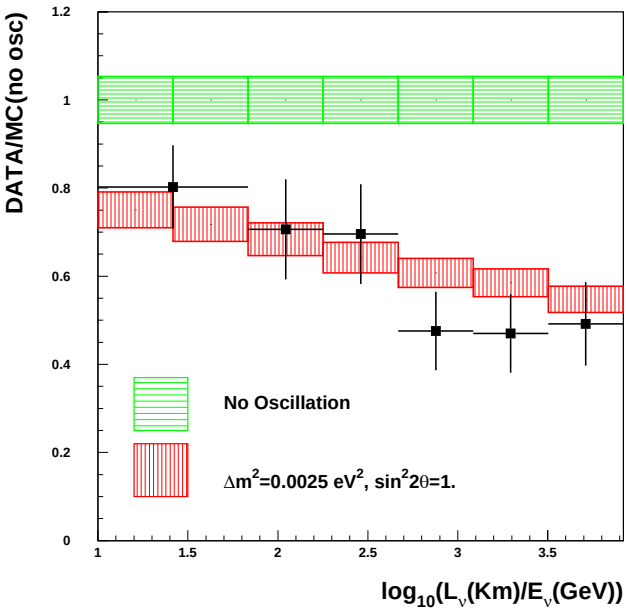

Figure 9: $R = (Data/MC_{noosc})$ as a function of $log_{10}(L/E_\nu)$ obtained using the streamer tubes in "drift mode". The data are the points with error bars, the vertical extent of the shaded regions represents the statistical uncertainties on the MC predictions for $\nu_\mu \rightarrow \nu_\tau$ oscillations and for no oscillations.

energies of 12, 20, 50 and 102 GeV, respectively. The comparison of their zenith angle distributions with the predictions of the no oscillations MC shows a disagreement at low energies (where there is a deficit of vertical events), while the agreement is restored at increasing neutrino energies. The distribution of the ratio $R = (Data/MC_{noosc})$ obtained by this analysis is plotted in Fig. 9 as a function of $log_{10}(L/E_\nu)$ [45, 57, 62]. The black points with error bars are the data; the vertical extent of the shaded areas represents the statistical uncertainties on the MC predictions (i) for $\nu_\mu \rightarrow \nu_\tau$ oscillations with maximal mixing and $\Delta m^2 = 2.5 \cdot 10^{-3}$ eV^2 and (ii) for no oscillations. Another data point can be obtained from the low energy IU sample: the value at $L/E_\nu \simeq 3$ is about 0.6, consistent with the points of Fig. 9.

3.4 Low energy data.

The *Internal Upgoing* (IU) muons come from ν_μ interactions in the lower apparatus [31]. Since two scintillation counters are intercepted, the T.o.F. is applied to identify the upward going muons (Fig. 2). The average parent neutrino energy for these events is 4.2 GeV (Fig. 5). If the atmospheric neutrino anomalies were the results of $\nu_\mu \rightarrow \nu_\tau$ oscillations with maximal mixing and Δm^2 between 10^{-3} and 10^{-2} eV^2, one would expect a reduction by about a factor of two in the flux of these events, without any distortion in the shape of the angular distribution. This is what is observed in Fig. 10a.

The *upstopping muons* (UGS) are due to external ν_μ interactions yielding upgoing muons stopping in the detector. The data correspond to an effective livetime of 5.6

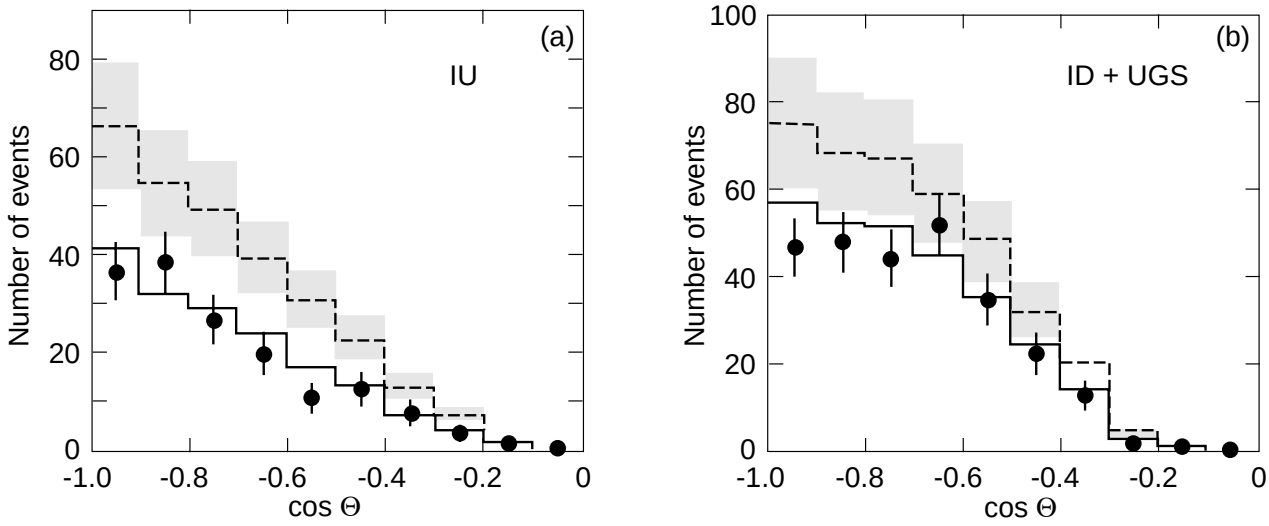

(a) (b)

Figure 10: Measured zenith distributions (a) for the upsemicontained (IU) events and (b) for the upstopping plus the downsemicontained (ID+UGD) events. The black points are the data, the dashed line at the center of the shaded regions correspond to MC predictions assuming no oscillations. The full line is the expectation for $\nu_\mu \to \nu_\tau$ oscillations with maximal mixing and $\Delta m^2 = 2.5 \cdot 10^{-3}\,\mathrm{eV}^2$.

y. The *semicontained downgoing muons* (ID) are due to ν_μ-induced downgoing tracks with vertex in the lower MACRO (Fig. 2). The two types of events are identified by means of topological criteria; the lack of time information prevents to distinguish the two sub-samples. An almost equal number of UGS and ID events is expected. In case of oscillations with the quoted parameters, the flux of the UGS should be reduced by 50%, the same amount of the ID muons at $cos\theta \simeq -1$. No reduction is instead expected for the semicontained downgoing events (coming from neutrinos having path lengths of $\sim 20\,\mathrm{km}$).

MC simulations for the low energy data use the Bartol neutrino flux and the neutrino low energy cross sections of ref. [65]. The number of events and the angular distributions are compared with MC predictions in Table 1 and Figs. 10a,b. The low energy data show a uniform deficit of the measured number of events for the whole angular distribution with respect to predictions, $\sim 50\%$ for IU, 75% for ID + UGS; there is good agreement with the predictions based on neutrino oscillations with the parameters obtained from the upthroughgoing muons.

The average value of the double ratio $R = (Data/MC)_{IU}/(Data/MC)_{ID+UGS}$ over the measured zenith angle range is $R \simeq 0.77 \pm 0.07$; the error includes statistical and theoretical uncertainties; $R = 1$ is expected in case of no oscillations [50].

	Events	MC-No oscillations	$R = (Data/MC_{noosc})$
Up throughgoing	809	1122 ± 191	$(0.721 \pm 0.026_{stat} \pm 0.043_{sys} \pm 0.123_{th})$
Internal Up	154	$285 \pm 28_{sys} \pm 71_{th}$	$(0.54 \pm 0.04_{stat} \pm 0.05_{sys} \pm 0.13_{th})$
Up Stop + In Down	262	$375 \pm 37_{sys} \pm 94_{th}$	$(0.70 \pm 0.04_{stat} \pm 0.07_{sys} \pm 0.17_{th})$

Table 1: Summary of the MACRO $\nu_\mu \to \mu$ events in $-1 < cos\theta < 0$ after background subtraction. For each topology (see Fig. 2) the number of measured events, the MC prediction for no-oscillations and the ratio (Data/MC-no osc) are given.

4 Search for Astrophysical Point Sources of High Energy Muon Neutrinos

High energy ν_μ are expected to come from a large class of galactic and extragalactic sources. Neutrino production requires astrophysical accelerators of charged particles and some kind of astrophysical beam dumps. The excellent angular resolution of our detector allowed a sensitive search for upgoing muons produced by neutrinos coming from celestial sources, with a negligible atmospheric neutrino background. An excess of events was searched for around the positions of known sources in 3° (half width) angular bins. This value was chosen so as to take into account the angular smearing produced by the multiple muon scattering in the rock below the detector and by the energy-integrated angular distribution of the scattered muon, with respect to the neutrino direction. Using a total livetime of 6.16 y (normalized to the complete configuration) we obtained a total of 1356 events, see Fig. 11. No excess was observed and the 90 % c.l. upper limits on the muon fluxes from specific celestial sources lay in the range $10^{-15} - 10^{-14}\,\mathrm{cm}^{-2}\,\mathrm{s}^{-1}$, see Fig. 11b; preliminary data were reported at the 2001 conferences [37, 43, 55].

We searched for time coincidences of our upgoing muons with γ-ray bursts as given in the BATSE 3B and 4B catalogues, for the period from April 91 to December 2000 [33]. No statistically significant time correlation was found.

We have also searched for a diffuse astrophysical neutrino flux for which we establish a flux upper limit at the level of $1.5 \cdot 10^{-14}\,\mathrm{cm}^{-2}\,\mathrm{s}^{-1}$ [55].

5 Indirect Searches for WIMPs

Weakly Interacting Massive Particles (WIMPs) could be part of the galactic dark matter; WIMPs could be intercepted by celestial bodies, slowed down and trapped in their centers, where WIMPs and anti-WIMPs could annihilate and yield upthroughgoing muons. The annihilations in these celestial bodies would yield neutrinos of GeV or TeV energy, in small angular windows from their centers.

For the Earth we have chosen a 15^o cone around the vertical: we find 863 events. The MC expectation for atmospheric ν_μ without oscillations gives a larger number of events. We set a conservative flux upper limit assuming that the measured number of events equals the expected ones. We obtain the 90 % c.l. MACRO limits for the flux of upgoing muons as shown in Fig. 12a (it varies from about 0.8 to 0.5 $10^{-14}\,\mathrm{cm}^{-2}\,\mathrm{s}^{-1}$). If

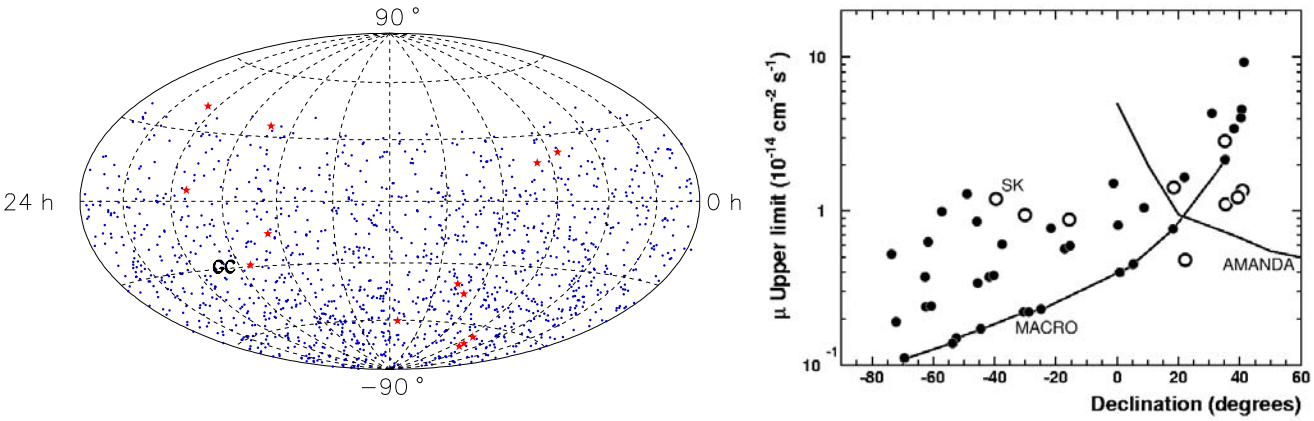

(a) (b)

Figure 11: High energy neutrino astronomy. (a) Upgoing muon distribution in equatorial coordinates (1356 events). (b) The black points are the MACRO 90 % c.l. upwardgoing muon flux limits as a function of the declination for 42 selected sources. The solid line refers to the MACRO limits obtained for those cases for which the atmospheric neutrino background was zero. The limits from the SK (open circles) and AMANDA (thin line) experiments are quoted; these last limits refer to much higher energy neutrinos.

the WIMPs are identified with the smallest mass neutralino, the MACRO limit may be used to constrain the stable neutralino mass, following the model of Bottino et al. [66], see Figure 12a.

A similar procedure was used to search for muon neutrinos from the Sun, using 10 search cones from 3^o to 30^o. In the absence of statistically significant excesses the muon upper limits are at the level of about $1.5 - 2 \cdot 10^{-14}\,\mathrm{cm}^{-2}\,\mathrm{s}^{-1}$ are established. The limits are shown in Fig. 12b as a function of the WIMP (neutralino) mass.

6 Magnetic Monopoles and Nuclearites

The search for magnetic monopoles (MM) was one of the main objectives of our experiment. Supermassive monopoles predicted by Grand Unified Theories (GUT) of the electroweak and strong interactions should have masses of the order of $m_M \sim 10^{17}\,\mathrm{GeV}$.

These monopoles could be present in the penetrating cosmic radiation and are expected to have typical galactic velocities, $\sim 10^{-3}c$, if trapped in our Galaxy. MMs trapped in our solar system or in the supercluster of galaxies may travel with typical velocities of the order of $\sim 10^{-4}c$ and $\sim 10^{-2}c$, respectively. Monopoles in the presence of strong magnetic fields may reach higher velocities. Possible intermediate mass monopoles could reach relativistic velocities.

The reference sensitivity level for a significant MM search is the Parker bound [68], the maximum monopole flux compatible with the survival of the galactic magnetic field. This limit is of the order of $\Phi \lesssim 10^{-15}\,\mathrm{cm}^{-2}\,\mathrm{s}^{-1}\,\mathrm{sr}^{-1}$, but it could be reduced by almost an order of magnitude when considering the survival of a small galactic magnetic field seed [68]. Our experiment was designed to reach a flux sensitivity well below the Parker bound, in the MM velocity range of $4 \times 10^{-5} < \beta < 1$. The three MACRO sub-detectors

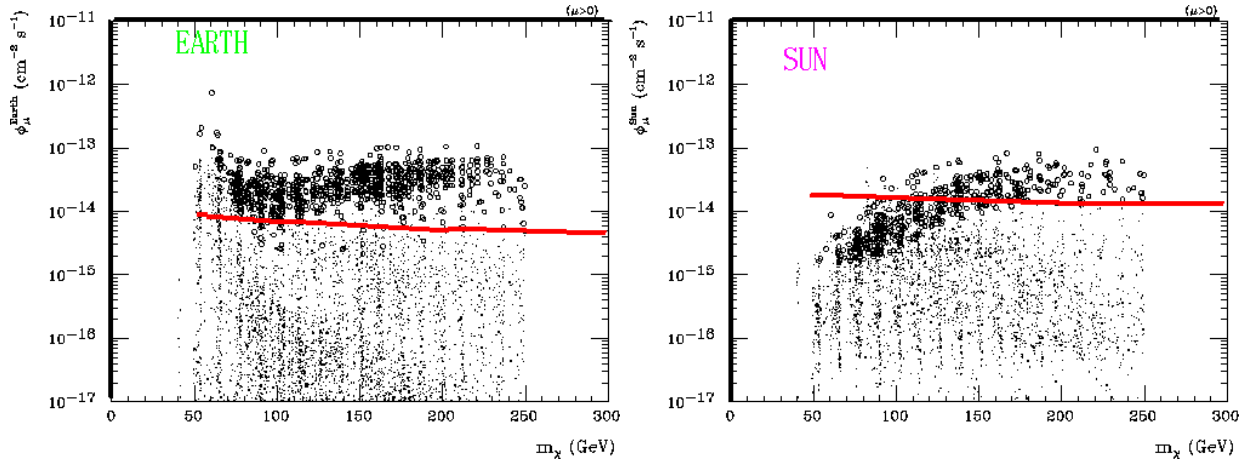

(a) (b)

Figure 12: (a) The solid line is the MACRO upwardgoing muon flux upper limit (90%c.l.) from the Earth plotted vs. neutralino mass m_χ for ${E_\mu}^{th} = 1\,\mathrm{GeV}$. (b) The same as in (a) but for upwardgoing muons from the Sun [28]. Each dot is obtained varying model parameters. The open circles indicate models *excluded* by direct measurements (in particular the DAMA/NaI experiment [67]) and assume a local dark matter density of about $0.5\,\mathrm{GeVcm}^{-3}$.

have sensitivities in wide β-ranges, with overlapping regions; thus they allow multiple signatures of the same rare event candidate. No candidates were found in several years of data taking by any of the three subdetectors.

The MM flux limits set by several different analyses using the three subdetectors over different β-range were combined to obtain a global MACRO limit. For each β value, the global time integrated acceptance was computed as the sum of the independent portions of each analysis. Our limits are shown in Fig. 13 versus β together with the limits set by other experiments [68, 70, 71]; other limits are quoted in [36, 40, 44, 56, 72]. Our MM limits are the best existing over a wide range of β , $4 \times 10^{-5} < \beta < 1$.

A specific search for monopole catalysis of nucleon decay was made with the streamer tube system [54]. Since no event was found, we can place a monopole flux upper limit at the level of $\sim 3 \cdot 10^{-16}\, cm^{-2} s^{-1} sr^{-1}$ for $10^{-4} \lesssim \beta \lesssim 5 \cdot 10^{-3}$, valid for a large catalysis cross section, $5 \cdot 10^2 < \sigma_{cat} < 10^3\, mb$. The flux limit for the standard direct MM search with streamer tubes is valid for $\sigma_{cat} < 100\, mb$.

The MM searches based on the scintillator and on the nuclear track subdetectors were also used to set new upper limits on the flux of cosmic ray nuclearites (strange quark matter), over the same β range, Fig. 14. If nuclearites are part of the dark matter in our galaxy, the most interesting β is of the order of $\sim 10^{-3}$. Fig. 14 shows our limit plotted vs nuclearite mass for $\beta = 2 \times 10^{-3}$ (at ground level). Other experimental limits are also shown.

Some of the nuclearite limits apply also to Q-balls (agglomerates of squarks, sleptons and Higgs fields) [54, 56].

The energy losses of MMs, dyons and of other heavy particles in the Earth and in different detectors for various particle masses and velocities were computed in [69].

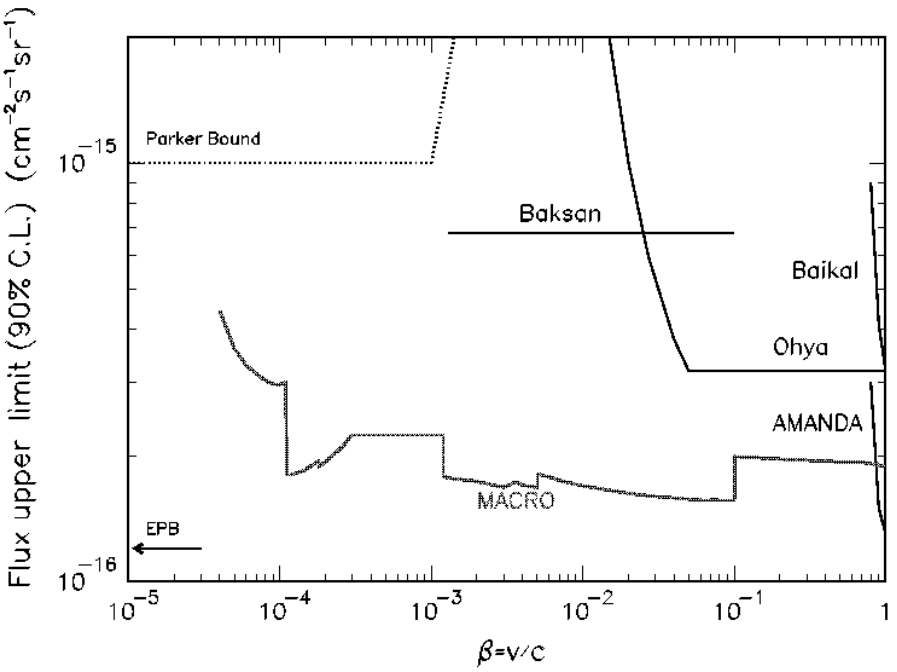

Figure 13: Magnetic monopole flux upper limits at the 90% c.l. obtained by MACRO and by other experiments [68, 70, 71]. The limits apply to singly charged ($g = g_D$) monopoles assuming that catalysis cross sections are smaller than a few mb.

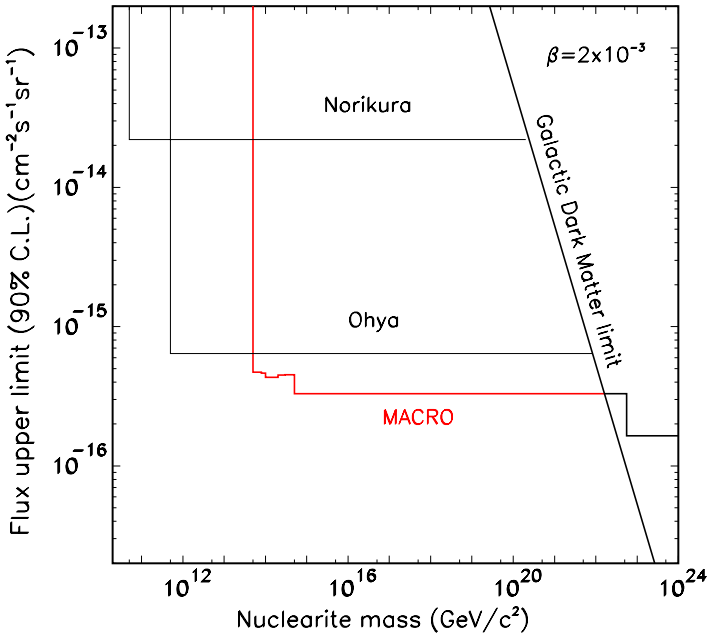

Figure 14: 90% c.l. flux upper limits vs. mass for nuclearites with $\beta = 2 \cdot 10^{-3}$ at ground level. Nuclearites of such velocity could have galactic or extragalactic origin. The MACRO direct limit (solid line) is shown along with the other direct limits [70, 71]; the indirect mica limits of [73, 74] are at the level of $2 \cdot 10^{-20} cm^{-2} s^{-1} sr^{-1}$. The limits for nuclearite masses larger than $5 \cdot 10^{22}$ GeVc^{-2} correspond to an isotropic flux.

7 Neutrinos from Stellar Gravitational Collapses

A stellar gravitational collapse (GC) of the core of a massive star is expected to produce a large burst of all types of neutrinos and antineutrinos with energies of $7 - 30$ MeV and with a duration of $\sim 10\,$s. The $\bar{\nu}_e$'s can be detected via the process $\bar{\nu}_e + p \rightarrow n + e^+$ in the liquid scintillator. About $100 \div 150$ $\bar{\nu}_e$ events should be detected in our 580 t scintillator for a stellar collapse at the center of our Galaxy.

We used two electronic systems for detecting $\bar{\nu}_e$'s from stellar gravitational collapses. The first system was based on the dedicated PHRASE trigger, the second one was based on the ERP trigger. Both systems had an energy threshold of $\sim 7\,$MeV and recorded pulse shape, charge and timing informations. Immediately after a $> 7\,$MeV trigger, the PHRASE system lowered its threshold to about 1 MeV, for a duration of 800μs, in order to detect (with a $\simeq 25\,\%$ efficiency) the $2.2\,$MeV γ released in the reaction $n + p \rightarrow d + \gamma_{2.2\,\mathrm{MeV}}$ induced by the neutron produced in the primary process.

A redundant supernova alarm system was in operation, alerting immediately the physicists on shift. We defined a general procedure to alert the physics and astrophysics communities in case of an interesting alarm. Finally, a procedure to link the various supernova observatories around the world was set up [23].

The effective MACRO active mass was ~ 580 t; the live-time fraction in the last four years was $\simeq 97.5\,\%$. No stellar gravitational collapses were observed in our Galaxy from the beginning of 1989 to the end of 2000 [39].

8 Cosmic Ray Muons

The large area and acceptance of our detector allowed the study of many aspects of physics and astrophysics of cosmic rays (CR). We recorded $\sim 6 \times 10^7$ single muons and $\sim 3.7 \times 10^6$ multiple muons at the rate of $\sim 18,000$/day.

Muon vertical intensity. The underground muon vertical intensity vs. rock thickness provides information on the high energy ($E \gtrsim 1.3\,$TeV) atmospheric muon flux and on the all-particle primary CR spectrum. The results can be used to constrain the models of cosmic ray production and interaction. The analysis performed in 1995 covered the overburden range $2200 \div 7000\,\mathrm{hg/\,cm^2}$ [16].

Analysis of high multiplicity muon bundles. The study of the **multiplicity distribution** of muon bundles provides informations on the primary CR composition model. The study of the **decoherence** function (the distribution of the distance between two muons in a muon bundle) provides informations on the hadronic interaction features at high energies; this study was performed using a large sample of data and improved Monte Carlo methods, see Fig. 15a [29]. We used different hadronic interaction models (DPMJET, QGSJET, SIBYLL, HEMAS, HDPM) interfaced to the HEMAS and CORSIKA shower propagation codes [75].

We studied *muon correlations inside a bundle* [75], using the so called correlation integral [76], to search for correlations of dynamical origin in the bundles. Since the cascade development in atmosphere is mainly determined by the number of "steps" in the "tree formation", we expect a different behaviour for cascades originated by light and

heavy CR primaries. For the same reason, the analysis should be less sensitive to the hadronic interaction model adopted in the simulations. This analysis shows that, in the energy region above 1000 TeV, the composition model derived from the analysis of the muon multiplicity distribution [19, 20] is almost independent from the interaction model.

We also searched for *substructures ("clusters") inside muon bundles* [77]. The search for clusters was performed by means of different software algorithms; the study is sensitive both to the hadronic interaction model and to the primary CR composition model. If the primary composition has been determined by the first method, a choice of the bundle topology gives interesting connections with the early hadronic interaction features in the atmosphere. The comparison between our data and Monte Carlo simulations allowed to place constraints on the used interaction models. The same Monte Carlo study has shown that muon bundles with a central core and an isolated cluster with at least two muons are the result of random associations of peripheral muons. A combined analysis with the study of the decoherence function for high multiplicity events has shown that the hadronic interaction model that better reproduces the underground observables is QGSJET.

The ratio double muons/single muons: The ratio N_2/N_1 of double muon events over single muon events is expected to decrease at increasing rock depths, unless some exotic phenomena occur. The ratio N_2/N_1 was studied in underground experiments and in phenomenological papers [78, 79]. The LVD collaboration reports that the ratio of multiple-muons to all-muons increases for rock depths $h > 7000\ hg/cm^2$.

We measured [49] the ratio N_2/N_1 as a function of the rock depth, using also multiple muon events at large zenith angles. A detailed Monte Carlo simulation was made using the HEMAS code, where the event zenith angle can be extended up to 89°. The event direction is reconstructed by the tracking system. The rock depth is provided by the Gran Sasso map function $h(\theta, \phi)$, which extends up to $\theta = 94°$. The "true" muon multiplicity is the largest value among N_{HW} and N_{VW}, the multiplicities in the horizontal and vertical planes, respectively. Monte Carlo simulations have shown that the percentage of events with mis-reconstructed multiplicity is less that 3%. Attention was devoted to the "cleaning" of the events from spurious effects (electronic noise, radioactive background, etc); in many cases, we made a visual scanning of the events. Our measured ratios N_2/N_1 as a function of the rock depth, Fig. 15, are in agreement with the expectation of a monotonic decrease of N_2/N_1 down to $h \sim 10000\ hg/cm^2$. Above this value, the low statistics does not allow to state a firm conclusion on a possible increase of N_2/N_1.

Muon Astronomy. In the past, some experiments reported excesses of modulated muons from the direction of known astrophysical sources, f.e. Cyg X-3. Our data do not indicate significant excesses above background, both for steady dc fluxes and for modulated ac fluxes. The MACRO pointing precision was checked via the shadow of the Moon and of the Sun on primary cosmic rays. The pointing resolution was checked with double muons, assuming that they are parallel. The angle containing 68% of the events in a $\Delta\theta$ bin is 0.8^o, which we take as our resolution.

All sky d.c. survey. The sky, in galactic coordinates, was divided into bins of equal solid angle, $\Delta\Omega = 2.1 \cdot 10^{-3} sr$, $\Delta\alpha = 3^o$, $\Delta sin\delta = 0.04$; they correspond to cones of 1.5^o half angles. In order to remove edge effects, three other surveys were done, by shifting the map by one-half-bin in α (map 2), by one-half bin in $\sin\delta$ (map 3) and with both α and $\sin\delta$ shifted (map 4). For each solid angle bin we computed the deviation from the average

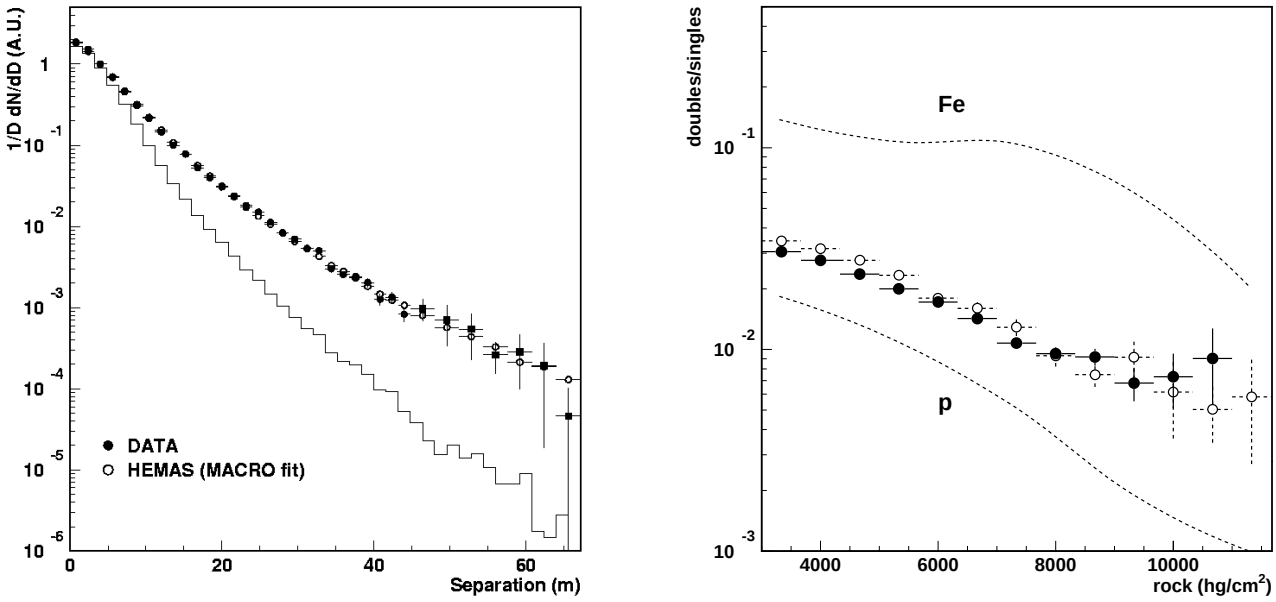

(a) (b)

Figure 15: (a) True unfolded experimental decoherence distribution for an infinite detector (black points) compared with MC expectations (open points); the measured decoherence distribution before unfolding is shown as an histogram [29]. (b) Ratio of double muon events to single muon events as a function of the rock depth. The black points are our data; the open circles are Monte Carlo predictions made using the MACRO composition model. Monte Carlo predictions using pure proton and iron primaries are shown as dashed lines.

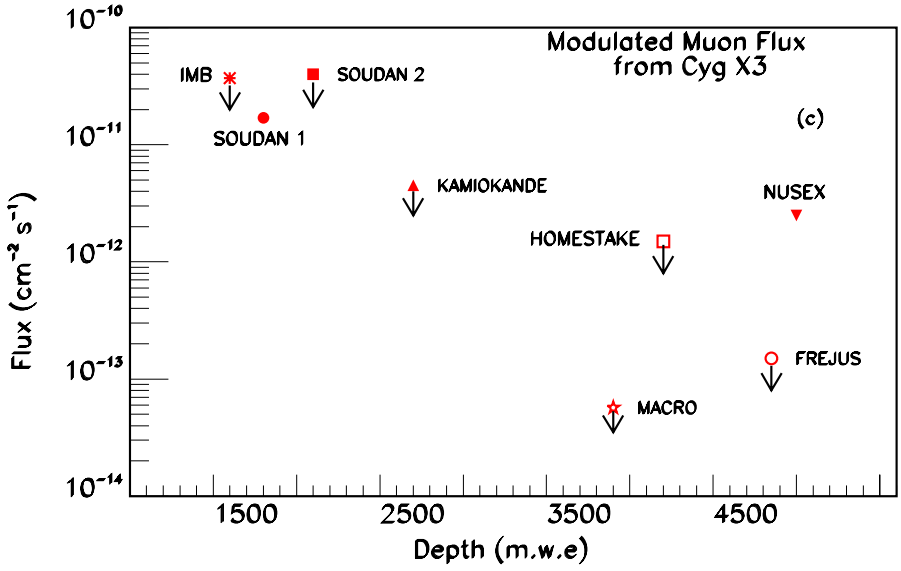

Figure 16: Present situation of the searches for a modulated muon signal from Cyg X-3. The Soudan 1 and Nusex collaborations reported positive indications, while all other experiments give flux upper limits.

measured muon intensity, after background subtraction, in units of standard deviations

$$\sigma(i) = \frac{N_{obs}(i) - N_{exp}(i)}{\sqrt{N_{exp}(i)}} \quad (1)$$

where $N_{obs}(i)$ is the observed number of events in bin i and N_{exp} is the number of events expected in that bin from the simulation. No deviation was found and for the majority of the bins we obtain flux upper limits at the level of ${\Phi_\mu}^{steady}(95\%) \leq 5 \times 10^{-13} cm^{-2} s^{-1}$.
Specific point-like d.c. sources. For Cyg X-3, Mrk421, Mrk501 we searched in a narrower cone (1^o half angle) around the source direction. We obtain flux limits at the level of $(2-4) \cdot 10^{-13} cm^{-2} s^{-1}$. There is a small excess of 2.0 σ in the direction of Mrk501.
Modulated a.c. search from Cyg X-3 and Her X-1. No evidence for an excess was observed and the limits are $\Phi < 2 \times 10^{-13} cm^{-2} s^{-1}$; see Fig. 16 .
Search for bursting episodes. We made a search for pulsed muon signals in a 1^o half angle cone around the location of possible sources of high energy photons. Bursting episodes of duration of ~ 1 day were searched for with two different methods. In the first method we searched for daily excesses of muons above the background, also plotting cumulative excesses day by day. In the second method we computed day by day the quantity $-Log_{10}P$ where P is the probability to observe a burst at least as large as N_{obs}. We find some possible excesses for Mrk421 on the days 7/1/93, 14/2/95, 27/8/97, 5/12/98.
Seasonal variations. Underground muons are produced by mesons decaying in flight in the atmosphere. The muon flux thus depends on the ratio between the decay and the interaction probability of the parent mesons, which are sensitive to the atmospheric density and to the average temperature. The flux is expected to decrease in winter, when the temperature is lower and the atmosphere more dense, and to increase in summer. We find the expected variations at the level of $\pm 2\%$ [21], see Fig. 17.
Solar daily variations. Because of variations in the day-night temperatures we expect solar daily variations similar to seasonal variations, but of considerably smaller amplitudes. Using the total MACRO data, we find these variations with an amplitude $A = (0.88 \pm 0.26) \cdot 10^{-3}$ with a significance of about 3.4 σ, see Fig. 18a.
Sidereal anisotropies are due to the motion of the solar system through the "sea" of relativistic cosmic rays in our galaxy. They are expected to yield a small effect. After a correction due to the motion of the Earth around the Sun, we observe variations with an amplitude of $8.6 \cdot 10^{-4}$ and a phase $\phi_{max} = 22.7^\circ$ with a statistical significance of 3 σ, Fig. 18b.
Moon and sun Shadows of primary cosmic rays. The pointing capability of MACRO was demonstrated by the observed "shadows" of the Moon and of the Sun, which produce a "shield" to the cosmic rays. We used a sample of $45 \cdot 10^6$ muons, looking at the bidimensional density of the events around the directions of the Moon and of the Sun [26][51]. In Fig. 19 we show two-dimensional plots of the muon deficits caused by the Moon and the Sun. For the Moon: we looked for events in a window $4.375^o \times 4.375^o$ centered on the Moon; the window was divided into 35×35 cells, each having dimensions of $0.125^o \times 0.125^o$ ($\Delta\Omega = 1.6 \cdot 10^{-2} deg^2$). In the bidimensional plot of Fig. 19a one observes a depletion of events with a statistical significance of 5.5 σ. The observed slight displacement of the maximum deficit is consistent with the displacement of the primary protons due to the geomagnetic field. We repeated the same analysis for muons in the sun

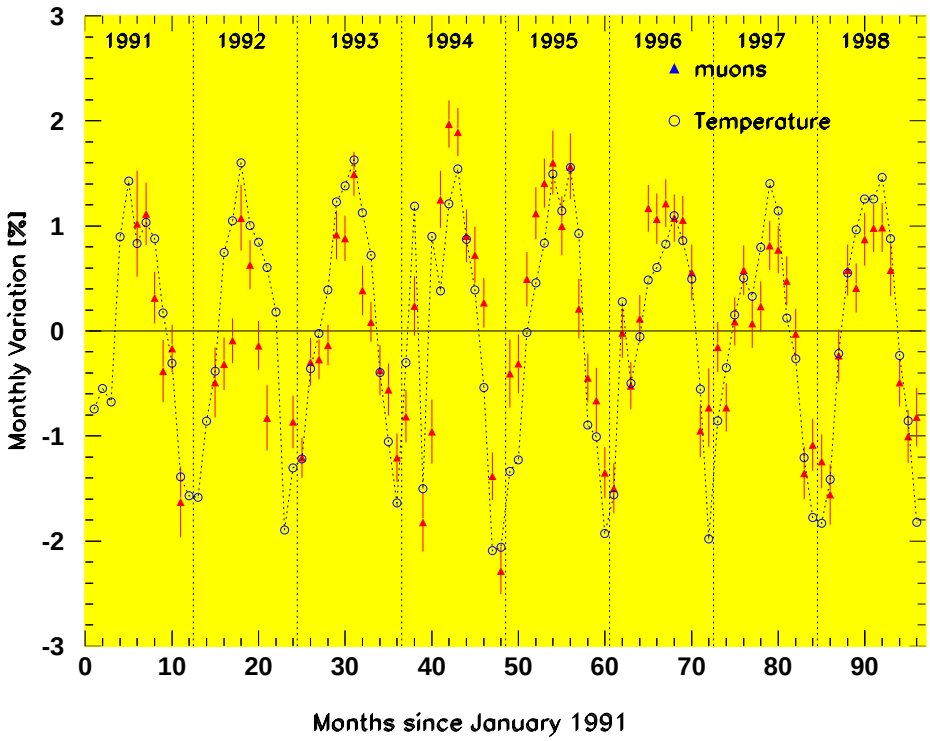

Figure 17: Seasonal variation of the muon flux from above (black triangles); the open circles are measurements of the temperature of the upper atmosphere.

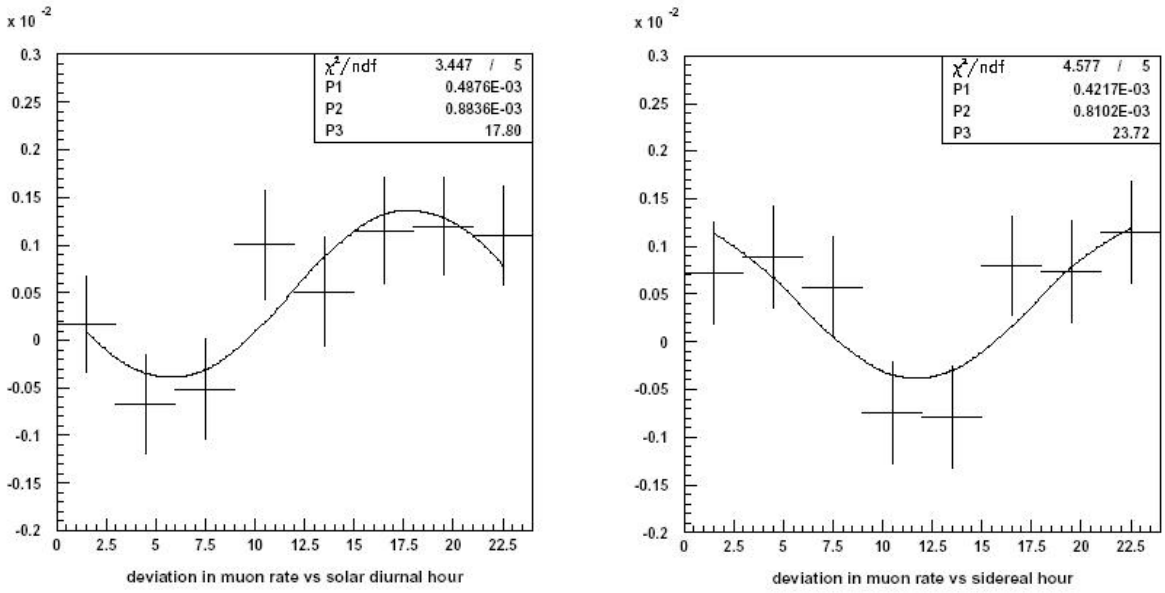

(a) (b)

Figure 18: Deviations of the muon rate from the mean muon rate (a) versus the local solar diurnal time at Gran Sasso, and (b) versus the local sidereal time.

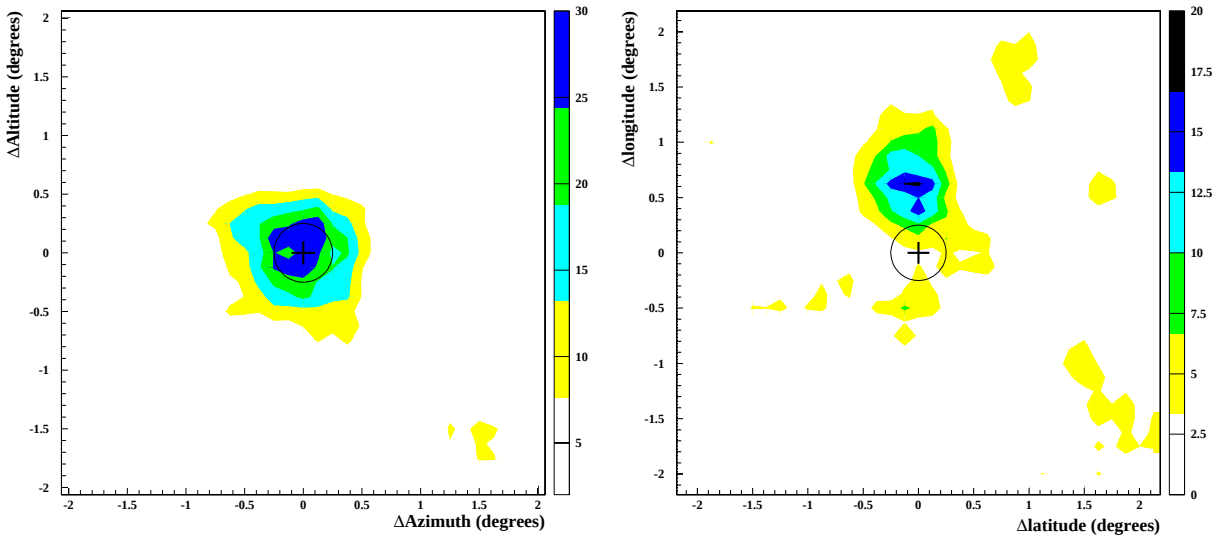

(a) (b)

Figure 19: Moon and sun shadows. (a) Two dimensional distributions of the muon event density around the moon direction. The various regions of increasing gray scale indicate various levels of deficit in percent. The darkest one corresponds to the maximum deficit. (b) Same analysis for the sun direction.

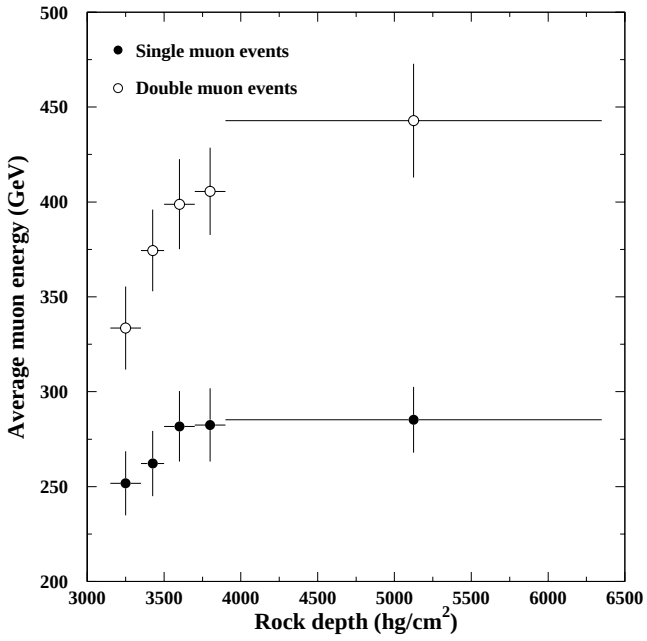

Figure 20: Residual average muon energy at the underground Gran Sasso lab versus standard rock depth for single muons and for double muons [27], see text.

window, Fig. 19b. The difference between the apparent sun position and the observed muon density is due to the combined effect of the magnetic field of the Sun and of the Earth. The observed depletion has a statistical significance of 4.5 σ.

9 Muon energy measurement with the TRD detector

The underground differential energy spectrum of muons was measured with the three TRD modules detector. We analyzed two types of events: "single muons", i.e. single events in MACRO crossing a TRD module, and "double muons", i.e. double events in MACRO with only one muon crossing the TRD detector.The measurements refer to muons with energies $0.1 < E_\mu < 1\,\mathrm{TeV}$ and for $E_\mu > 1\,\mathrm{TeV}$ [27]. In order to evaluate the local muon energy spectrum, we must take into account the TRD response function, which induces some distortion of the "true" muon spectrum distribution. The "true" distribution was extracted from the measured one by an unfolding procedure that yields good results only if the response of the detector is correctly understood. We used an unfolding technique developed according to Bayes' theorem. Fig. 20 shows the average muon energies versus standard rock thickness for single and double muons. Systematic uncertainties are included in the error bars. The average single muon energy at the Gran Sasso underground lab is 320 GeV; for double muons it is ~ 400 GeV. Double muons are more energetic than single muons; this is in agreement with the predictions of interaction models of primary CRs in the atmosphere.

10 EAS-TOP/MACRO Coincidence Experiment

For coincident events, EASTOP measured the e.m. size of the showers above the surface (at Campo Imperatore), while MACRO measured penetrating muons underground. The purpose is to study the primary cosmic ray composition versus energy reducing the dependence on the interaction and propagation models. The two completed detectors operated in coincidence for a livetime of 960.1 days. The number of coincident events is 28160, of which 3752 have shower cores inside the edges of the EASTOP array ("internal events") and shower sizes $N_e > 2 \cdot 10^5$; 409 events have $N_e > 10^{5.92}$, i.e. above the CR knee. The data have been analyzed in terms of the QGSJET interaction model as implemented in CORSIKA [84].

The e.m. detector of EASTOP is made of 35 scintillator modules, 10 m^2 each, covering an area of $\simeq 10^5\,\mathrm{m}^2$. The array is fully efficient for $N_e > 10^5$. The reconstruction capabilities of the extensive air shower (EAS) parameters for internal events are: $\frac{\Delta N_e}{N_e} \simeq 10\%$ for $N_e \gtrsim 10^5$, and $\Delta\theta \sim 0.9^o$ for the EAS arrival direction [85].

We considered in MACRO muon tracks with at least 4 aligned hits in both views of the horizontal streamer tube planes. The muon energy threshold at the surface inside the effective area of EAS-TOP, for muons reaching the MACRO depth, ranges from 1.3 TeV to 1.8 TeV. Event coincidence is made off-line, using the absolute time given by a GPS system with an accuracy of better than 1 μs. Independent analyses of the MACRO and of the EAS-TOP data are described in [20] and [86], respectively.

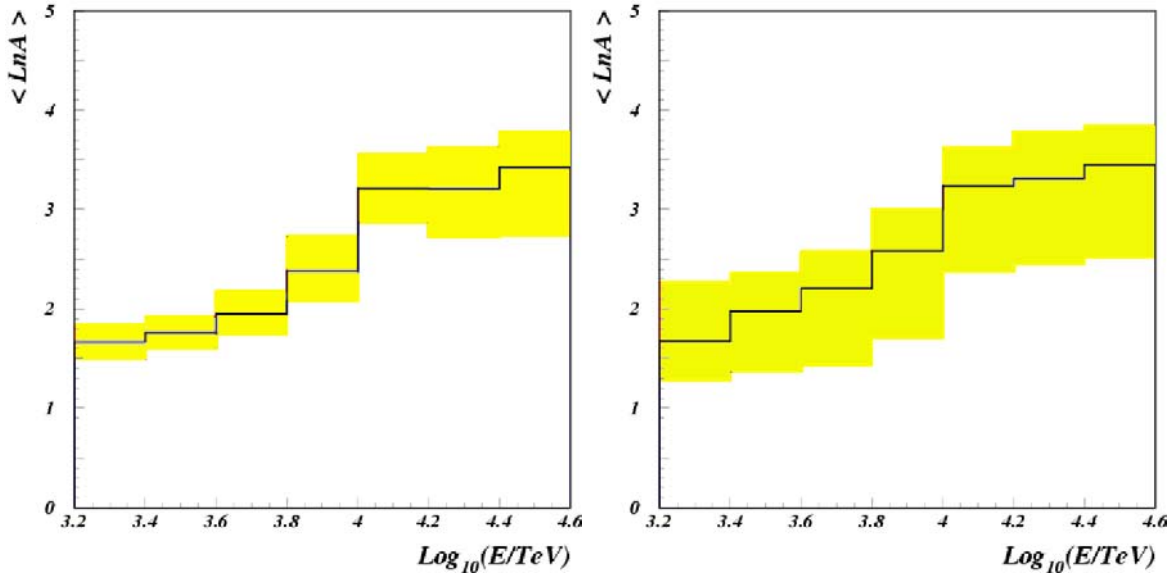

Figure 21: EASTOP-MACRO coincidences. $\langle lnA \rangle$ vs primary energy for: (a) p/Fe and (b) $Light/Heavy$ compositions. The histograms (black lines) are obtained from the data, the shaded areas include the uncertainties discussed in the text.

The main experimental features considered are the muon multiplicity distributions in six different intervals of shower sizes. For each size bin the muon multiplicity distribution was fitted with a superposition of (i) pure p and Fe components, or (ii) light (L) and heavy (H) admixtures containing equal fractions of p and He or Mg and Fe, respectively. All spectra in the simulation have slope $\gamma = 2.62$. In each of the six windows we minimized

$$\chi^2 = \sum_i \frac{(N_i^{exp} - p_1 N_i^p - p_2 N_i^{Fe})^2}{\sigma_{i,exp}^2} \tag{2}$$

where N_i^{exp} is the number of observed events in the i-th bin, N^p (N^L) and N^{Fe} (N^H) are the number of simulated events in the same bin, p_1 and p_2 are the parameters (to be fitted) defining the fraction of each mass component in the same multiplicity bin.

For each size bin we take from the simulation the $log_{10}(E)$ distributions of contributing mass groups weighted by the parameters p_1 and p_2 with weights w_k representing the relative efficiency to trigger the underground apparatus. The resulting distributions from different size bins are summed together, and we obtain the simulated energy spectra of the two basic components that reproduce the experimental data. The values of the fitting parameters p_1 and p_2 have been used to compute the average $\langle lnA \rangle$; Fig. 21 shows $\langle lnA \rangle$ versus $log_{10}E$ (E in TeV); the shaded regions include the uncertainties in the fitting parameters p_1 and p_2 for (a) the p/Fe composition model and (b) for the light/heavy model.

Fig. 21 shows the results of the fits, plotted as $\langle lnA \rangle$ versus $log_{10}E$ (E in TeV); the shaded regions include the uncertainties in the fitting parameters p_1 and p_2 for (a) the

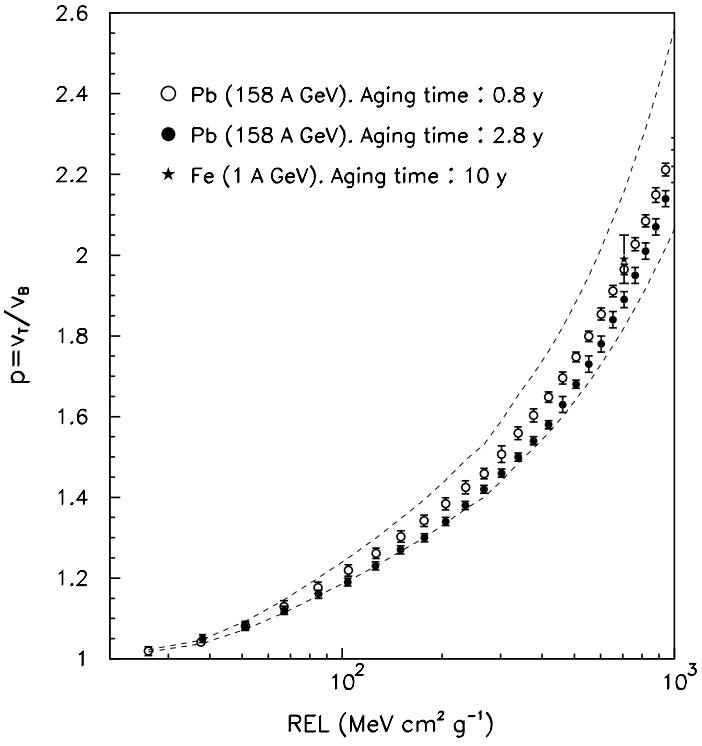

Figure 22: $p = v_T/v_B$ vs. REL for CR39 exposed to $^{2}07Pb^{8}2+$ ions of 158 A GeV and $^{5}6Fe^{2}6+$ ions of 1A GeV at different times after production. This was done to estimate possible aging effects. The dashed lines indicate the systematic uncertainty arising mainly from fluctuations of the bulk etching rate v_B.

p/Fe composition model and (b) for the light/heavy model. The results show an increase of $\langle lnA \rangle$ with energy in the CR knee region. The results are in agreement with the measurements of EAS-TOP alone at the surface using the same (QGSJET) interaction model. Our data also agree with the results of the Kascade experiment. The EAS-TOP and MACRO coincidences offered the unique opportunity of measuring the lateral distribution of Cherenkov light in the $10 \div 100$ TeV energy range by associating the Cherenkov light collected by the EAS-TOP telescopes with the TeV muon through MACRO. We compared the measured Cherenkov light lateral distribution with simulations based on the CORSIKA-QGSJET code used for the composition analysis; this check provided an experimental validation of the code [84].

11 Nuclear Track Detector Calibrations

We performed further calibrations of the nuclear track detector CR39 with both slow and fast ions. In all measurements we have seen no deviation of its response from the Restricted Energy Loss (REL) model. To complete the calibration, nuclear track detector stacks of CR39 and Lexan foils, placed before and after various targets, were exposed to 158 A GeV Pb^{82+} ions at the CERN-SPS and to 1 A GeV Fe^{26+} ions at the BNL-AGS. In traversing the target, the beam ions produce nuclear fragments with $Z < 82e$ and $Z < 26e$ for the lead and iron beams, respectively; this allows a measurement of the response of the

detector in a Z region relevant to the detection of magnetic monopoles. Previous analyses have shown that the CR39 charge resolution is about $0.19e$ in the range $72e \leq Z \leq 83e$ (obtained by measurements of the etch-cone heights); at lower Z the measurement of the cone base diameters allow to separate the different charges. Tests were made looking for a possible dependence of the CR39 response from its age, i.e. from the time elapsed between the date of production and the date of exposure ("aging effect"). Two sets of sheets, 0.8 y and 2.5 y old, were exposed in 1994 to 158 A GeV Pb^{82+} ions. For each detected nuclear fragment the reduced etch rate $p = v_T/v_B$ (v_T and v_B are the track and bulk etching rates, respectively) was computed and plotted in Fig. 22 vs REL. The dashed lines represent the systematic uncertainties coming mainly from the uncertainty on v_B. A recent test was made by exposing 10 years old CR39 samples to 1 A GeV Fe^{26+} ions; the detector response is shown as a black star in Fig. 22. Thus within experimental uncertainties, aging effects in the MACRO CR39 are negligible. Until now we etched 821 m^2 of CR39 detectors, of which 626 m^2 have been completely analyzed. As no candidates were found, the CR39 90% c.l. limit for an isotropic flux of monopoles with $\beta > 0.1$ is at the level of $2 \cdot 10^{-16}\ cm^{-2}s^{-1}sr^{-1}$ [83].

12 Search for Lightly Ionizing Particles

Fractionally charged particles could be expected in Grand Unified Theories as deconfined quarks; the expected charges range from Q=/e/ /5 to Q=e 2/3. They should release a fraction $(Q/e)^2$ of the energy deposited by a muon traversing a medium. Lightly Ionizing Particles (LIPs) have been searched for in MACRO using a four-fold coincidence between three layers of scintillators and the streamer tube system [32]. The 90 % c.l. flux upper limits for LIPs with charges $2e/3$, $e/3$ and $e/5$ are presently at the level of $1.5 \cdot 10^{-15} cm^{-2}s^{-1}sr^{-1}$.

13 Conclusions

The MACRO detector took data from 1989 to the end of year 2000. In 2001 we have extended most of our analyses and searches. We would like to stress that MACRO obtained important results in all the items listed in the proposal :

- GUT Magnetic Monopoles. We now have the best flux upper limit over the widest β range, thanks to the large acceptance and the redundancy of the different techniques employed. This limit value is a unique result and it will stand for a long time.

- Atmospheric neutrino oscillations. In this field MACRO has had its major achievements. Analyses of different event topologies, different energies, the exploitation of Coulomb multiple scattering in the detector give strong support to the hypothesis of $\nu_\mu \rightarrow \nu_\tau$ oscillations.

- High energy muon neutrino astronomy. MACRO has been highly competitive with other underground experiments thanks to its good angular accuracy. It has been limited only by its livetime and the size of the detector.

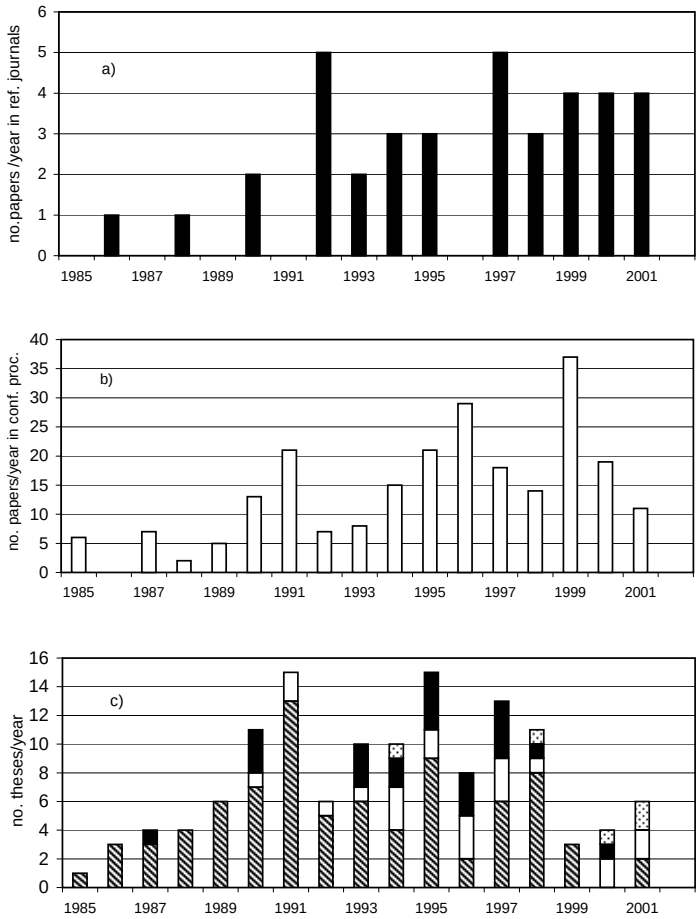

Figure 23: Time evolution of the MACRO publications: (a) in refereed journals, (b) in proceedings of conferences, (c) MACRO theses (the dashed boxes indicate Laurea theses, black boxes American PhD theses, white boxes Italian PhD theses, points theses de Doctorat Nationales).

- Search for bursts of $\bar{\nu}_e$ from stellar gravitational collapses. In this field MACRO was sensitive to supernova events in the Galaxy, it started the SN WATCH system, and for a certain time it was the only detector in operation.

- Cosmic ray downgoing muons. MACRO observed the shadows of primary cosmic rays by the Moon and the Sun; this is also a proof of our pointing capability. We observed the seasonal variation ($\sim 2\%$ amplitude) over many years. We observed solar and sidereal variations with reasonable statistical significances even if the amplitudes of the variations are small (0.08%). No excesses of secondary muons attributable to astrophysical point sources (steady, modulated or bursting) were observed. The limits obtained are the best of any underground detector.
  We used multi-parameter fits and improved Monte Carlo simulations to explore the CR composition around the "knee" of the primary CR energy spectrum.

- Results have been obtained by studying the coincidence events between MACRO and the EASTOP array. This item represents a unique occasion as no other two experiments in such configuration exist. The number of events is limited due to

the small common acceptance and short combined livetime. The data indicate an increase with increasing energy of the average Z of the primary CR nuclei.

- Sensitive searches for exotic particles have been carried out for possible Dark Matter candidates : (i) WIMPs, looking for upgoing muons from the center of the Earth and of the Sun; (ii) Nuclearites and Q-balls (obtained as byproducts of MM searches). (iii) Other limits concern possible Lightly Ionizing Particles.

Several of the above results (in particular the multiple Coulomb scattering analysis, the low energy neutrino data, etc) would have reached a greater significance if MACRO could have been granted an extension in data taking.

The dismantling of MACRO went regularly and essentially on schedule. We recuperated part of the electronics (modules, circuits, cables, etc) to be used in our Institutions, and donated the photomultipliers and part of the streamer tubes to other experiments.

The MACRO scientific and technical results have been

- published in 36 papers in refereed journals (we expect to publish 10 more)
- published in 226 contributions to conferences and in invited papers
- discussed in about 534 Internal Memos
- used for 83 italian Laurea theses
- used for 22 italian Dottorato theses
- used for 23 US PhD theses
- used for 5 moroccan theses of Doctorat Nationales

Fig. 23 shows the time evolution of the published papers, conference proceedings and of the theses (Laurea, Dottorato, PhD, Doctorat Nationale).

Acknowledgments

We acknowledge the support of the Directors and of the staff of the Gran Sasso Laboratory and of the Institutions partecipating in the experiment. We thank the Istituto Nazionale di Fisica Nucleare (INFN), the US Department of Energy and the US National Science Foundation for their support. We acknowledge the strong cooperation of our technical staff, in particular of R. Assiro, E. Barbarito, A. Boiano, E. Bottazzi, P. Calligola, A. Candela, A. Ceres, D. Cosson, P. Creti, L. Degli Esposti, U. Denni, D. Di Ferdinando, R. Diotallevi, R. Farano, E. Favero, A. Frani, M. Gebhard, R. Giuliani, M. Goretti, H. Gran, A. Hawthorne, A. Leone, D. Margherita, V. Marrelli, F. Massera, S. Mengucci, M. Mongelli, L. Mossbarger, M.Orsini, S. Parlati, G. Pellizzoni, M. Perchiazzi, C. Pinto, A. Sacchetti, P. Saggese, S. Sondergaards, S. Stalio, M. Vakili, C. Valieri and N. Zaccheo. We thank INFN-FAI, ICTP (Trieste), NATO and WorldLab for providing fellowships and grants for non-Italian citizens.

References

[1] MACRO Collaboration, C. De Marzo et al., "MACRO: a large area detector at the Gran Sasso laboratory", Nuovo Cimento 9C(1986)281.

[2] MACRO Collaboration, M.Calicchio et al., "The MACRO detector at the Gran Sasso laboratory", Nucl. Instr. Methods Phys. Res. A264(1988)18.

[3] MACRO-EASTOP Collaborations, R.Bellotti et al., M.Aglietta et al., "Simultaneous observation of the extensive air showers and deep underground muons at the Gran Sasso laboratory", Phys. Rev. D42(1990)1396.

[4] MACRO Collaboration, S.Ahlen et al., "Study of penetrating cosmic ray muons and search for large scale anisotropy at the Gran Sasso laboratory", Phys. Lett. B249(1990)149.

[5] MACRO Collaboration, S.Ahlen et al., "Arrival time distributions of very high energy cosmic ray muons in MACRO", Nucl. Phys. B370(1992)432; LNGS-91/01.

[6] MACRO Collaboration, S.Ahlen et al., "Study of the ultrahigh energy primary cosmic ray composition with the MACRO experiment", Phys. Rev. D46(1992)895.

[7] MACRO Collaboration, S.Ahlen et al., "Measurement of the decoherence function with the MACRO detector at Gran Sasso", Phys. Rev. D46(1992)4836; LNGS-92/29.

[8] MACRO Collaboration, S.Ahlen et al., "Search for neutrino bursts from collapsing stars with the MACRO detector", Astroparticle Phys. 1(1992)11; LNGS-92/32.

[9] MACRO Collaboration, S.Ahlen et al., "Search for nuclearites using the MACRO detector", Phys. Rev. Lett. 69(1992)1860.

[10] MACRO Collaboration, S.Ahlen et al., "First supermodule of the MACRO detector at Gran Sasso", Nucl. Inst. Meth. Phys. Res. A324(1993) 337; LNGS 92/34.

[11] MACRO Collaboration, S.Ahlen et al., "Muon astronomy with the MACRO detector", Astrophys. J. 412(1993)301.

[12] MACRO Collaboration, S.Ahlen et al., "Search for slow moving magnetic monopoles with the MACRO detector", Phys. Rev. Lett. 72(1994)608; LNGS 93/84.

[13] GRACE-MACRO Collaborations, M.Ambrosio et al., "Coincident observation of air Cherenkov light by a surface array and muon bundles by a deep underground detector", Phys. Rev. D50(1994)3046.

[14] EASTOP-MACRO Collaborations, M.Aglietta et al., "Study of the primary cosmic ray composition around the knee of the energy spectrum", Phys. Lett. B337(1994)376.

[15] MACRO Collaboration, M.Ambrosio et al., "Performance of the MACRO streamer tube system in the search for magnetic monopoles", Astroparticle Phys. 4(1995)33; LNGS 95/11.

[16] MACRO Collaboration, M.Ambrosio et al., "Vertical muon intensity measured with MACRO at the Gran Sasso laboratory", Phys. Rev. D52(1995)3793.

[17] MACRO Collaboration, M.Ambrosio et al., "Atmospheric neutrino flux measurements using upgoing muons", Phys. Lett. B357(1995)481.

[18] MACRO Collaboration, M.Ambrosio et al., "The performance of MACRO liquid scintillator in the search for magnetic monopoles with $10^{-3} \leq \beta \leq 1$", Astroparticle Phys. 6(1997)113; INFN-AE 96/22.

[19] MACRO Collaboration, M.Ambrosio et al. "High energy cosmic ray physics with the MACRO detector at Gran Sasso: Part I. Analysis methods and experimental results", Phys. Rev. D56(1997)1407; INFN-AE 96/28.

[20] MACRO Collaboration, M.Ambrosio et al., "High energy cosmic ray physics with the MACRO detector at Gran Sasso: Part II. Primary spectra and composition", Phys. Rev. D56(1997)1418; INFN-AE 96/29.

[21] MACRO Collaboration, M.Ambrosio et al., "Seasonal variations in the underground muon intensity as seen by MACRO", Astroparticle Phys. 7(1997)109; INFN-AE 97/05.

[22] MACRO Collaboration, M.Ambrosio et al., "Magnetic monopole search with the MACRO detector at Gran Sasso", Phys. Lett. B406(1997)249; INFN-AE 97/16.

[23] MACRO Collaboration, M.Ambrosio et al. "Real time supernova neutrino burst detection with MACRO", Astroparticle Phys. 8(1998)123; INFN-AE 97/44.

[24] MACRO Collaboration, M.Ambrosio et al., "The observation of upgoing charged particles produced by high energy muons in underground detectors", Astroparticle Phys. 9(1998)105; INFN-AE 97/55; hep-ex/9807032.

[25] MACRO Collaboration, M.Ambrosio et al. "Measurement of the atmospheric neutrino-induced upgoing muon flux using MACRO", Phys. Lett. B434(1998)451; INFN-AE 98/13; hep-ex/9807005.

[26] MACRO Collaboration, M.Ambrosio et al., "Observation of the shadowing of cosmic rays by the Moon using a deep underground detector", Phys. Rev. D 59(1999)012003; INFN-AE 98/14; hep-ex/9807006.

[27] MACRO Collaboration, M.Ambrosio et al., "Measurement of the energy spectrum of underground muons at Gran Sasso with a transition radiation detector", Astroparticle Phys. 10(1999)11; INFN-AE 98/15; hep-ex/9807009.

[28] MACRO Collaboration, M.Ambrosio et al., "Limits on dark matter WIMPs using upward-going muons in the MACRO detector", Phys. Rev. D60(1999)082002; hep-ex/9812020.

[29] MACRO Collaboration, M.Ambrosio et al., "High statistics measurement of the underground muon pair separation at Gran Sasso", Phys. Rev. D60(1999)032001; hep-ex/9901027; INFN-AE 99/04 (1999).

[30] MACRO Collaboration, M.Ambrosio et al., "Nuclearite search with the MACRO DETECTOR at Gran Sasso", Eur. Phys. J. C13(2000)453; hep-ex/9904031.

[31] MACRO Collaboration, M.Ambrosio et al., "Low energy atmospheric muon neutrinos in MACRO", Phys. Lett. B478(2000)5; hep-ex/0001044.

[32] MACRO Collaboration, M. Ambrosio et al., "A search for lightly ionizing particles with the MACRO detector", Phys. Rev. D62(2000)052003; hep-ex/0002029.

[33] MACRO Collaboration, M. Ambrosio et al., "Neutrino astronomy with the MACRO detector" Astrophys. J. 546(2001)1038; astro-ph/0002492.

[34] MACRO Collaboration, M.Ambrosio et al., "Matter effects in upward-going muons and sterile neutrino oscillations", Phys. Lett. B517(2001)59; hep-ex/0106049.

[35] MACRO Collaboration, M.Ambrosio et al., "The MACRO detector at Gran Sasso", accepted for publication on NIM A.

[36] MACRO Collaboration, M.Ambrosio et al., "A combined analysis technique for the search for fast magnetic monopoles with the MACRO detector", hep-ex/0110083; accepted for publication on Astroparticle Physics.

[37] P. Bernardini, "Neutrino astronomy using upward-travelling muons in MACRO", Invited Talk at "Very High Energy Phenomena in the Universe", XXXVI Rencontres de Moriond, Les Arcs (2001).

[38] D. Bakari for the MACRO Collaboration, "Estimate of the energy of upgoing muons with multiple Coulomb scattering", Proceedings of the NATO ARW on Cosmic Radiations: from Astronomy to Particle Physics, Oujda (Morocco), 21-23 March 2001.

[39] M. Grassi for the MACRO Collaboration, "A search for gravitational stellar collapses", Proceedings of the NATO ARW on Cosmic Radiations: from Astronomy to Particle Physics, Oujda (Morocco), 21-23 March 2001.

[40] S. Kyriazopoulou for the MACRO Collaboration, "Search for slow magnetic monopoles with the MACRO scintillation detector", Proceedings of the NATO ARW on Cosmic Radiations: from Astronomy to Particle Physics, Oujda (Morocco), 21-23 March 2001.

[41] M. Sitta for the MACRO Collaboration, "Monopole catalysis of nucleon decay: theory and experimental results", Proceedings of the NATO ARW on Cosmic Radiations: from Astronomy to Particle Physics, Oujda (Morocco), 21-23 March 2001.

[42] M. Cozzi and L. Patrizii for the MACRO Collaboration, "Nuclear track detectors. Searches for magnetic monopoles and for nuclearites", Proceedings of the NATO ARW on Cosmic Radiations: from Astronomy to Particle Physics, Oujda (Morocco), 21-23 March 2001.

[43] F. Ronga for the MACRO Collaboration, "Atmospheric neutrinos and neutrino oscillations in the MACRO experiment", Proceedings of the NATO ARW on Cosmic Radiations: from Astronomy to Particle Physics, Oujda (Morocco), 21-23 March 2001.

[44] I. De Mitri for the MACRO Collaboration, "Search for magnetic monopoles in the cosmic radiation with the MACRO detector at Gran Sasso ", International Europhysics Conference on High Energy Physics, Budapest, July 12-18 (2001).

[45] E. Scapparone et al. for the MACRO Collaboration, "Study of neutrino induced upgoing muon energy", International Europhysics Conference on High Energy Physics, Budapest, July 12-18 (2001).

[46] F. Cei for the MACRO Collaboration, "Search for lightly ionizing particles with the MACRO detector", ICRC (2001), Hamburg, Germany, 7-15 August 2001.

[47] S. Mufson for the MACRO Collaboration, "Measurement of the Solar Diurnal and Sidereal Muon Waves with MACRO", ICRC (2001), Hamburg, Germany, 7-15 August 2001.

[48] P. Vallania for the EASTOP-MACRO Collaboration, "The primary CR composition around the knee from EAS e.m., GeV and TeV muon data", ICRC 2001, Hamburg, Germany, 7-15 August (2001).

[49] M. Sioli for the MACRO Collaboration, "Measurement of the ratio double/single muon events as a function of rock depth with MACRO", ICRC 2001, Hamburg, Germany, 7-15 August (2001).

[50] M. Spurio for the MACRO Collaboration, " Low energy atmospheric ν_μ measurements", ICRC 2001, Hamburg, Germany, 7-15 August (2001).

[51] N. Giglietto for the MACRO Collaboration, "Moon and Sun shadowing effect on the MACRO apparatus", ICRC 2001, Hamburg, Germany, 7-15 August (2001).

[52] T. Montaruli for the MACRO Collaboration, "Final results on atmospheric neutrino oscillations with MACRO", ICRC 2001, Hamburg, Germany 7-15 August (2001).

[53] M. Giorgini for the MACRO Collaboration, "Performance of the MACRO limited streamer tubes for estimates of muon energies ", 7th Int. Conf. on Advanced Technology and Particle Physics, Como, Italy (2001).

[54] M. Sitta for the MACRO Collaboration, "Rare particle searches with MACRO", ICRC 2001, Hamburg, Germany, 7-15 August (2001).

[55] L. Perrone for the MACRO Collaboration, "Neutrino astronomy with MACRO", ICRC 2001, Hamburg, Germany, 7-15 August (2001).

[56] I. De Mitri for the MACRO Collaboration, "Search for massive rare particles in MACRO", TAUP 2001, Laboratori Nazionali del Gran Sasso, September 8-12 (2001).

[57] E. Scapparone for the MACRO Collaboration, "Study of neutrino induced upgoing muon energy with MACRO", TAUP 2001, LNGS, September 8-12, 2001.

[58] V. Agrawal et al., Phys. Rev. D53(1996)1314.

[59] M. Gluck et al., Z. Phys. C67(1995)433.

[60] W. Lohmann et al., "Energy loss of muons in the energy range 1 - 10000 GeV" CERN 85-03.

[61] G. Feldman and R. Cousins, Phys. Rev. D57(1998)3873.

[62] M. Giorgini, "Study of atmospheric neutrino oscillations by energy estimates of upgoing muons in MACRO", Tesi di Dottorato, Università di Bologna (2002).

[63] SuperKamiokande Coll., Y.Fukuda et al., Phys. Rev. Lett. 81(1998)1562; Phys. Lett. B433(1998)9; Phys. Rev. Lett. 85(2000)3999; Nucl. Phys. B Proc. Suppl. 91(2001)127; T. Toshito, hep-ex/0105023 (2001).

[64] Soudan 2 Coll., W.W.M. Allison et al., Phys. Lett. B391 (1997) 491; Phys. Lett. B449 (1999) 137; W. Anthony Mann, hep-ex/0007031 (2000); T. Mann et al., Nucl. Phys. B Proc. Suppl. 91 (2001) 134.

[65] P. Lipari et al., Phys. Rev. Lett. 74(1995)384.

[66] A. Bottino, N. Fornengo, F. Donato and S. Scopel (private communication). N. Fornengo, in Proceedings of the Ringberg Euroconference "New Trends in Neutrino Physics", Ringberg Castle, Tegernsee, Germany, 1998, edited by B. Kniel, World Scientific, Singapore.

[67] R. Bernabei et al., Phys. Lett. B389(1996)757.

[68] G. Giacomelli and L. Patrizii, "Magnetic monopoles", Lecture at the Fifth School on Particle Astrophysics, Trieste 29 June-10 July 1998, hep-ex/0002032.
G. Giacomelli et al. (Magnetic Monopole Bibliography) hep-ex/0005041.

[69] J. Derkaoui et al., Astropart. Phys. 9(1998)173; Astropart. Phys. 10(1999)339.

[70] S. Nakamura et al., Phys. Lett. B263(1991)529.

[71] S. Orito et al., Phys. Rev. Lett. 66(1991)1951.

[72] D. Bakari et al., "Magnetic monopoles, nuclearites, Q-balls: a qualitative picture", hep-ex/0004019.

[73] P. B. Price, Phys. Rev. D38(1988) 3813.

[74] D. Ghosh and S. Chatterjea, Europhys. Lett. 12(1990)25.

[75] M. Sioli, "A new approach to the study of high energy muon bundles with the MACRO detector at Gran Sasso", Tesi di Dottorato, Università di Bologna (2000).

[76] P. Lipa, P. Carruthers, H.C. Eggers and B. Buschbeck, Phys. Lett. 285B(1992)300.

[77] G. Battistoni et al., LNGS-95-09 (1995); Proceedings of the XXIV Int. Cosmic Ray Conf., Roma, 1995, ed. N. Iucci et al., Arti Grafiche Editoriali, Urbino, (1995), Vol. 1, p. 508.

[78] J. W. Elbert et al, XVII ICRC (Paris, 1981) Vol. 7, p.42.

[79] O. G. Ryazhskaya for the LVD Collaboration, Nucl. Phys. (Proc. Suppl.) B87(2000)423.

[80] P. Antonioli et al., Astrop. Phys. 7(1997)357.

[81] J.N. Capdevielle et al., KFK Report (1992)4998; FZKA (1998)6019.

[82] EAS-TOP Collaboration, M. Aglietta et al., Nucl. Phys. B54B(1997)263.

[83] P. Serra et al., "Total charge changing cross section of 158 A GeV *Pb* ions in different targets with nuclear track detectors" , proceedings of the XXV ICRC Conference, Durban (South Africa), (1997).

[84] J. Knapp and D. Heck, Extensive Air Shower Simulation with CORSIKA 5.61 (1998).

[85] M. Aglietta et al., Nucl. Instr. & Meth. A336(1993)310.

[86] EAS-TOP Coll., Astroparticle Physics, 10, 1, 1999 and Proc. 26th ICRC, 1, 230, (1999).

MIBETA and CUORICINO. A cryogenic experiment on double beta decay and search for rare events

C. Arnaboldi[a,b], C. Brofferio[a,b], C. Bucci[c], S. Capelli[a,b], O. Cremonesi[a,b], E. Fiorini[a,b], A. Giuliani[b,d], P. Gorla[a,b], L. Martensson[a,b], A. Nucciotti[a,b], M. Pavan[a,b], M. Pedretti[b,d], E. Previtali[a,b], G. Pessina[a,b], S. Pirro[a,b], C. Pobes[c], M. Sisti[a,b], M. Vanzini[a,b], L. Zanotti[a,b]

[a] Dipartimento di Fisica G. Occhialini dell'Università di Milano-Bicocca
Piazza della Scienza, 3, I-20126 Milan, Italy
[b] Sezione di Milano dell'INFN, via Celoria 16, I-20133 Milan, Italy
[c] Laboratori Nazionali del Gran Sasso, I-67010, Assergi (AQ), Italy
[d] Dipartimento di Scienze CC. FF. e MM. dell'Università dell'Insubria
Via Valleggio 11, I-22100 Como, Italy

Abstract

The progress achieved during 2001 by the MIBETA and CUORICINO experiments at Laboratori Nazionali del Gran Sasso is reported.

1 Introduction

Neutrinoless Double Beta Decay searches represent a unique tool to assess the Dirac/Majorana nature of neutrino and to check the Lepton Number Conservation law. The experimental approach is usually based on the observation of a large number of nuclei, stable in normal beta decay but for which a double weak interaction process, changing the nuclear charge by two units, is allowed. The decay involving the simultaneous emission of two electrons and two neutrinos is allowed by the Standard Model of Electroweak Interactions. However, if neutrinos have a Majorana nature (and mass), a process withouth the emission of any neutrino is possible. A neutrinoless double beta decay ($0\nu\beta\beta$) is an unambiguous signal of a Majorana mass and of a violation of the lepton number conservation. Most sensitive experiments are presently based on the uniform approach in which the nuclei under observation (decay source) act at the same time as detector for the occurrence of a decay. The sensitivity of such experiments scales with the square root of their masses and

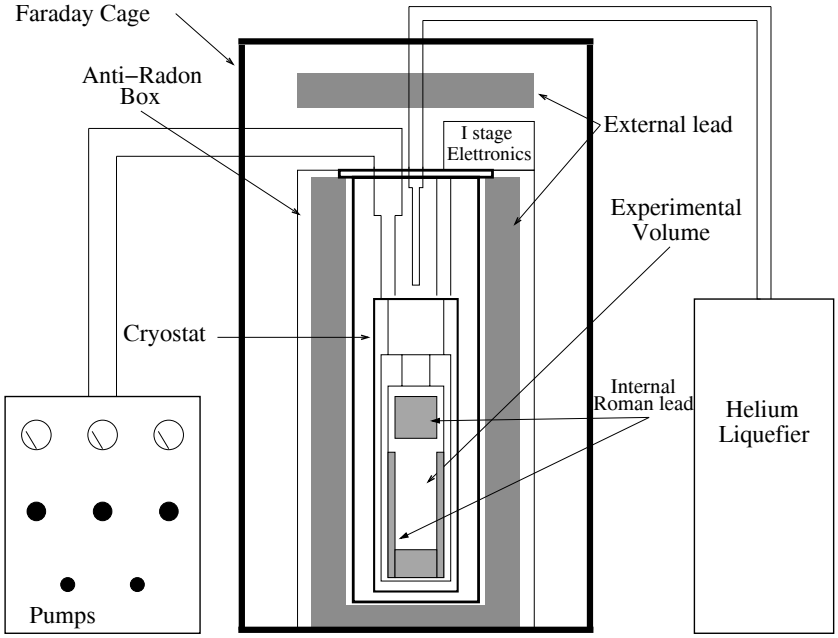

Figure 1: Schematic view of the LNGS cryogenic setups.

the inverse of the observed background rate (Eq. 1); they are therefore usually indicated also for many searches of rare events.

Because of their very good intrinsic energy resolution and the quite absolute absence of any limitation on the choice of the detector material, low temperature detectors (LTD) represent an ideal experimental approach for such searches. Proposed almost 20 years ago [1] they are finally becoming a competitive approach also with respect to Germanium diodes.

2 Experimental setup

Two low temperature experimental setups have been installed at LNGS by the Milano group. The first is used for the presently running experiment MIBETA on neutrinoless DBD of ^{130}Te (Hall A), while the second (Hall C) is strictly connected to the research and development for the already approved experiment CUORICINO in view of the larger, second generation experiment CUORE [3]. Both cryogenic setups (Fig. 1) consist of a dilution refrigerator having respectively a power of 1000 μW and 200 μW at 100 mK and having the former a larger useful experimental volume than the latter. The two refrigerators are realised with preliminarly tested low radiactive materials and are surrounded by heavy Lead shields and anti-Radon boxes. They are both equipped with an "embedded" Helium liquefier, providing a substantial recovery of the Helium and preventing Helium contamination in the tunnel atmosphere.

All the materials used for the setup construction are analysed to determine their radioactive contamination levels. These measurements are carried out by means of two large Ge detectors installed by the group itself in the underground Low Radioactivity Labora-

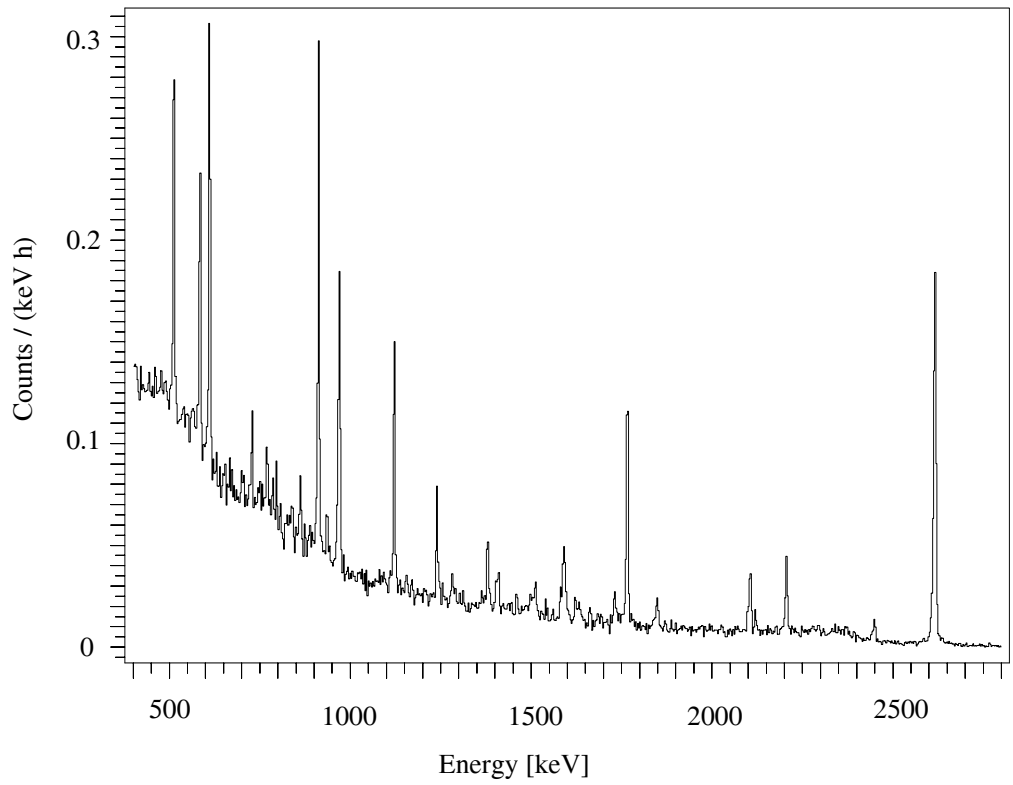

Figure 2: An U+Th calibration, sum spectrum of the 20 array detectors.

tory. The level of the radon contamination in the air of the Laboratory is continuously monitoured.

An array consisting of 20 crystals of TeO_2 of $3 \times 3 \times 6$ cm^3 each (MIBETA), for a total mass of 6.8 kg (by far the largest cryogenic mass operating underground), is presently running in the dilution refrigerator operating in Hall A. The array is held in a copper tower-like frame mounted inside the inner vacuum chamber (IVC) of the Hall A dilution refrigerator and it is maintained at a constant temperature of about 10 mK. Each detector is a $3 \times 3 \times 6$ cm^3 TeO_2 crystal of with a mass of 340 grams. A Neutron Transmutation Doped (NTD) thermistor and a Si doped resistor are glued on the surface of each crystal. The former is used to read-out the thermal signal, the latter acts as a heater to generate a reference heat pulse in the crystal in order to monitor continuously the gain of each bolometer. The electronic readout is accomplished with a room temperature low noise differential voltage-sensitive preamplifier, followed by an amplifier and an antialiasing Bessel filter. The excellent reproducibility of the detectors is shown in Fig. 2 where the total calibration spectrum obtained by summing the spectra of the 20 detectors is presented.

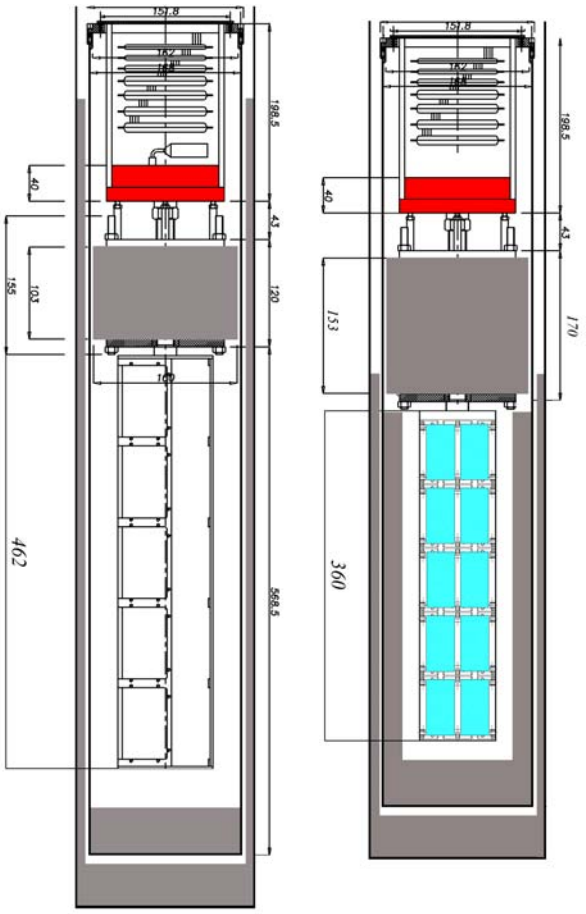

Figure 3: The old and new structure of MIBETA

The array is shielded with an internal layer of Roman lead of 1 cm minimum thickness, while the cryostat thermal shields provide a 2 cm minimum thickness of electrolytic copper. The dilution refrigerator is shielded with two layers of lead of 10 cm minimum thickness each. The outer layer is of commercial low radioactivity lead, while the internal one is made with special lead with a ^{210}Pb contamination of 16 $\pm$ 4 Bq/kg. In order to shield the detectors against the unavoidable radioactive contamination due to some fundamental components of the dilution refrigerator (as the silver powder in the heat exchangers and stainless steel tubes) a layer of 10 cm Roman lead is placed above the tower of the array inside the cryostat. A similar layer, also inside the cryostat, is placed below the tower. The external lead shield is surrounded by an air-tight box fluxed with nitrogen to avoid radon contamination of the gas contained between the cryostat and the external lead shield. The entire apparatus is inside a Faraday cage to suppress electromagnetic interference. A big effort has been carried out during 2001 in order to check both our knowledge of the background sources and the performance of the new detector mounting system proposed for CUORICINO and CUORE. The 20 detector array was in fact completely rebuilt in march, after a surface treatment of all TeO_2 crystals and

of the mounting structure and an enlargement of the internal Roman lead shields. An external neutron shield (borated polyethylene) was added in June. More details of the experimental setup can be found elsewhere [3].

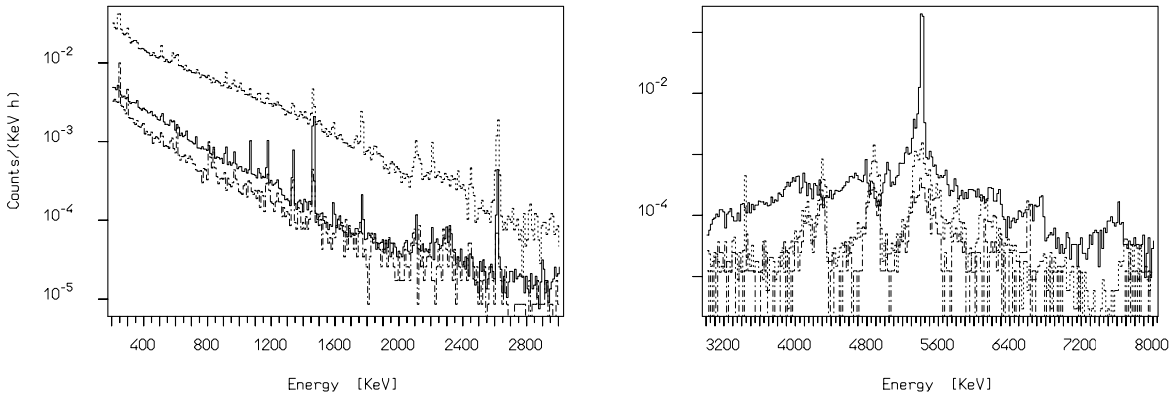

Figure 4: Comparison between the background levels obtained in the γ and α region with the different MIBETA setups: single crystal (dashed line), MIBETA 2000 (continuous line), MIBETA 2001(dotted-dashed line).

Various arrays realized with both 340 g ($3 \times 3 \times 6\ cm^3$) and 760 g ($5 \times 5 \times 5\ cm^3$) TeO_2 crystals (same as the ones used in MIBETA and proposed for CUORE/CUORICINO respectively) were operated in the dilution refrigerator installed in Hall C. Several R&D runs were carried out in order to assess both the performance of the various changes brought to the experimental setup (detector structure, suspension system, setup thermalisation, wiring, front-end electronics, etc.) and to check the effectiveness of the surface treatments (TeO_2 crystals and mounting box) aiming at a reduction of our radioactive background sources.

3 The MIBETA experiment

Main goal of this experiment is the search for ^{130}Te double beta decay both in the lepton conserving two neutrino and in the lepton non-conserving neutrinoless channel. Though allowed by the standard model of electro-weak interactions, the two neutrino channel is nevertheless attractive, since a direct result on its lifetime would solve a long standing problem arising from the data provided by geochemical experiments, in strong disagreement among themselves. For this reason four isotopically enriched TeO_2 crystals (two in ^{130}Te and two in ^{128}Te) have been installed in the dilution refrigerator operating in Hall A (together with 16 natural tellurium crystals) in order to observe the process by a direct comparison (subtraction) of the respective spectra.

Most of the interest of the group is however addressed to the neutrinoless double beta decay channel, which would unambiguously imply a non-zero Majorana neutrino

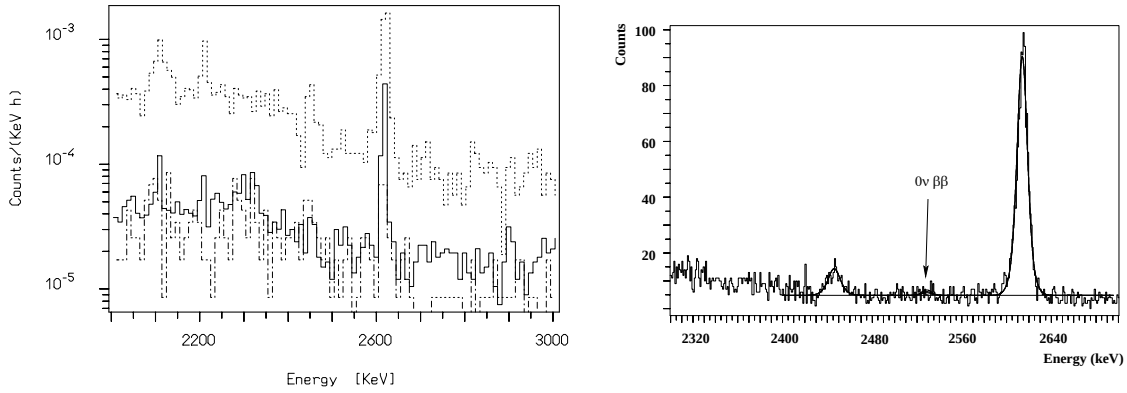

Figure 5: Comparison between the background levels obtained in the region of interest for 0ν $\beta\beta$ with the different MIBETA setups: single crystal (dashed line), MIBETA 2000 (continuous line), MIBETA 2001(dotted-dashed line). The total available statistics (4.3 kg y) in the same region is also shown.

mass. Such an interest is even more stronger in this moment, after the results of neutrino oscillation experiments which could imply a neutrino mass absolute value within the reach of the next generation of 0ν $\beta\beta$ experiments. Since the experimental sensitivity can be parametrised as

$$S = \ln(2)\ \frac{a\ N_A}{A}\ \epsilon\ \sqrt{\frac{Mt}{b\Gamma}} \tag{1}$$

(where A is the atomic mass, a is the isotopic abundance, M the detector mass (kg), b the background in counts keV^{-1} kg^{-1} y^{-1}, Γ the FWHM energy resolution (keV) and ϵ the detector efficiency) the only possibility is to select a very large amount of candidate nuclei with a high natural isotopic abundance (or isotopically enriched) with an experimental setup characterised by a very good energy resolution and the lowest background level. Thanks to their excellent energy resolution and to the possibility to select any material with very low restrictions (with its 34% natural i.a. Te is actually a very good candidate), low temperature detectors (LTD) are ideal devices for 0ν $\beta\beta$ searches, the only remaining requirements being the long term stability and the background exhaustion. Such requirements are actually characteristic of any high sensitivity search for rare events and usually WIMPS direct interaction searches are therefore another primary goal (as a matter of fact LTDs are characterised by a very high detection efficiency for nuclear recoils).

3.1 Results obtained in 2001 with the MIBETA experiment

The substantial improvements obtained during the last years for what concerns the increase of the single detector mass and the background level reduction (through the potentiation of the detector shields and the proper choice of the setup materials), brought

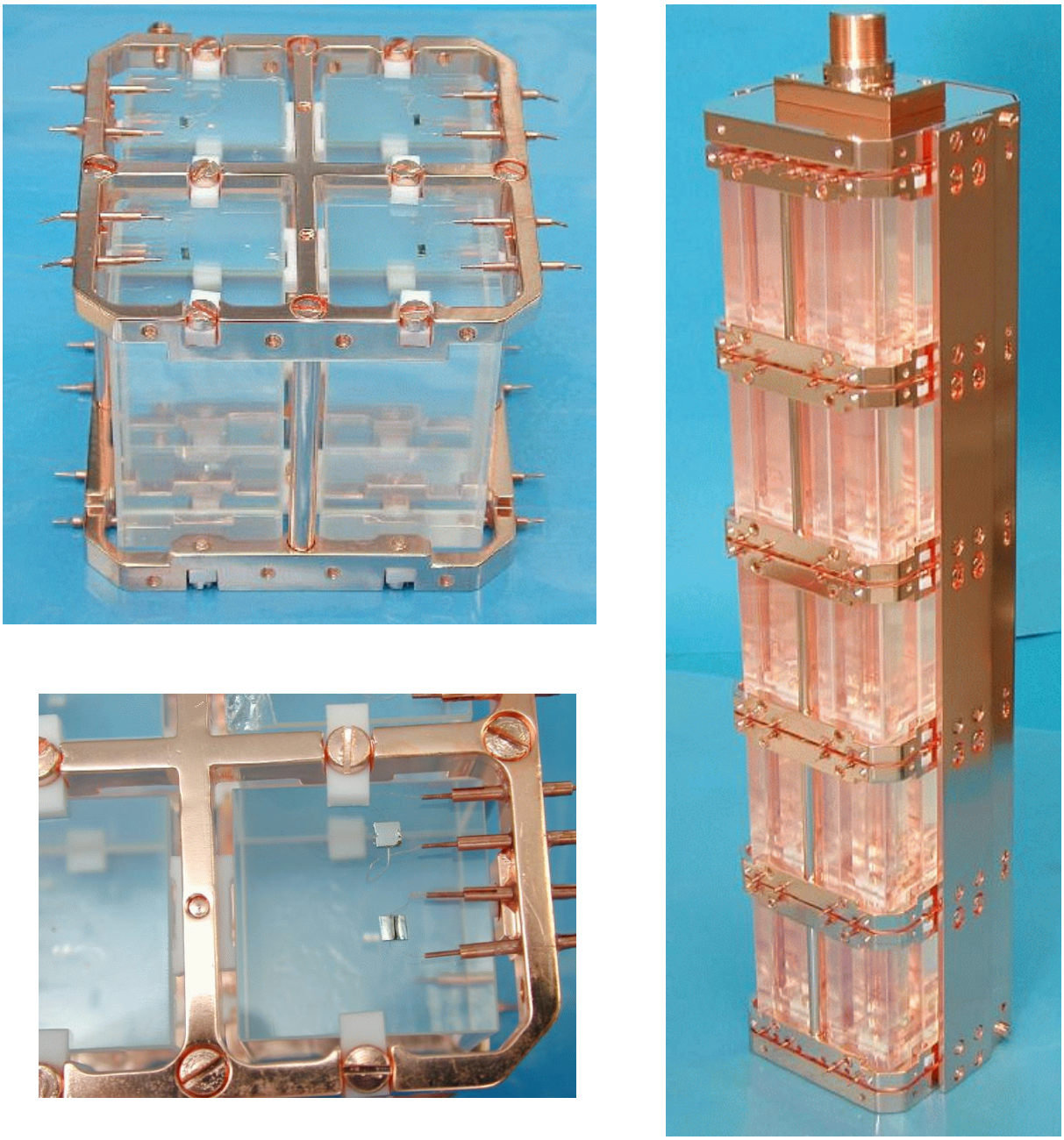

Figure 6: Details of the new structure of the MIBETA mounting system.

our group to propose the realisation of a second generation high sensitivity experiment for 0ν $\beta\beta$ named CUORE (Cryogenic Underground Observatory for Rare Events) characterised by a large mass (760 kg of TeO_2) and a low background level. After demonstrating, during 2000, the good performances (stability and energy resolution) of the single CUORE detector (charaterised by a double mass with respect to the MIBETA ones) we mainly tried, during 2001, to check our understanding of the background sources.

Data collected previously with MIBETA and with dedicated runs carried out with the

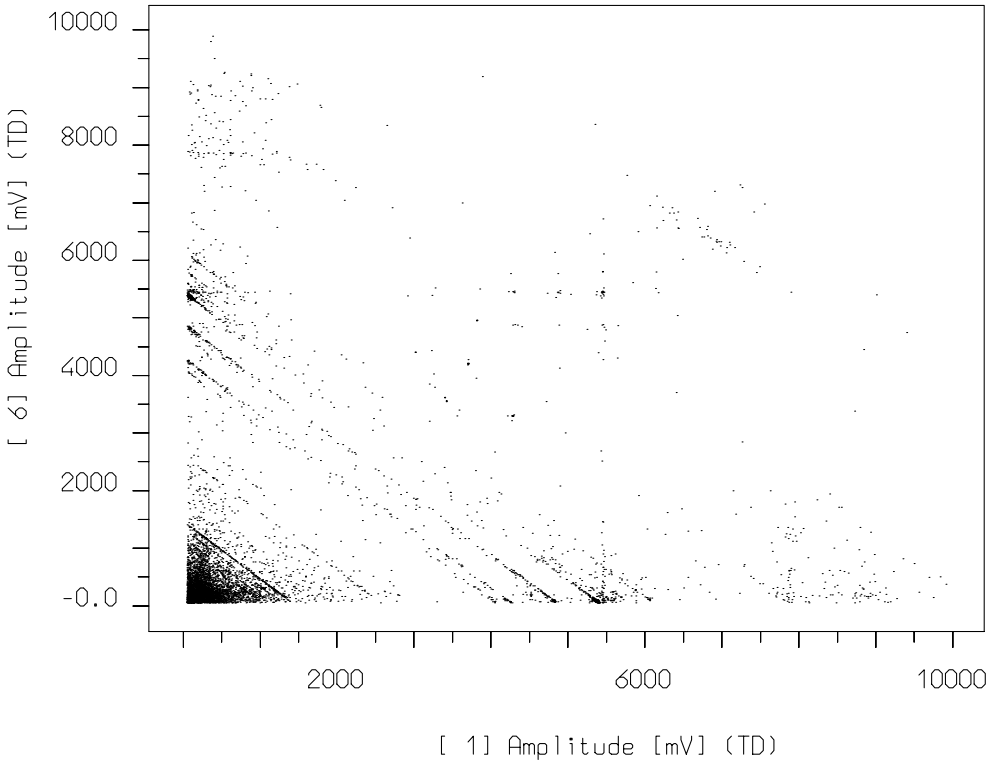

Figure 7: Coincident events in the 20 array detector. The straight lines with negative (-1) slope originates from radioactive α decays on the surface of the crystals and external γ emissions (^{40}K and ^{208}Tl).

Hall C setup, demonstrated the existence of a substantial contribution to the background in the region of interest for 0ν $\beta\beta$ arising from surface radioactive contaminations of the detector crystals and their mounting structure.

In particular, this was demonstrated by several facts: i) the analysis of the coincident events in different detectors showed the characteristic trend (Fig. 7) for α decays of surface radioactive contaminations; ii) the powders used by SICCAS to prepare our TeO_2 crystals were measured with the LNGS Germanium detectors and found heavily contaminated with ^{238}U and ^{232}Th (in particular for what concerns the CeO_2 used in the last surface treatment); iii) the characteristic breaks in the secular equilibrium of the contaminants observed in the MIBETA data analysis and in the powders measurements showed an unambiguous coincidence; iv) a strong reduction of the observed α lines was obtained in dedicated runs carried out in the Hall C setup, after a surface treatment of the TeO_2 crystals (both acid attack and polishing with radioclean powders, Fig. 8); v) a substantial reduction of the continuum in the energy region above 3 MeV was observed after a surface

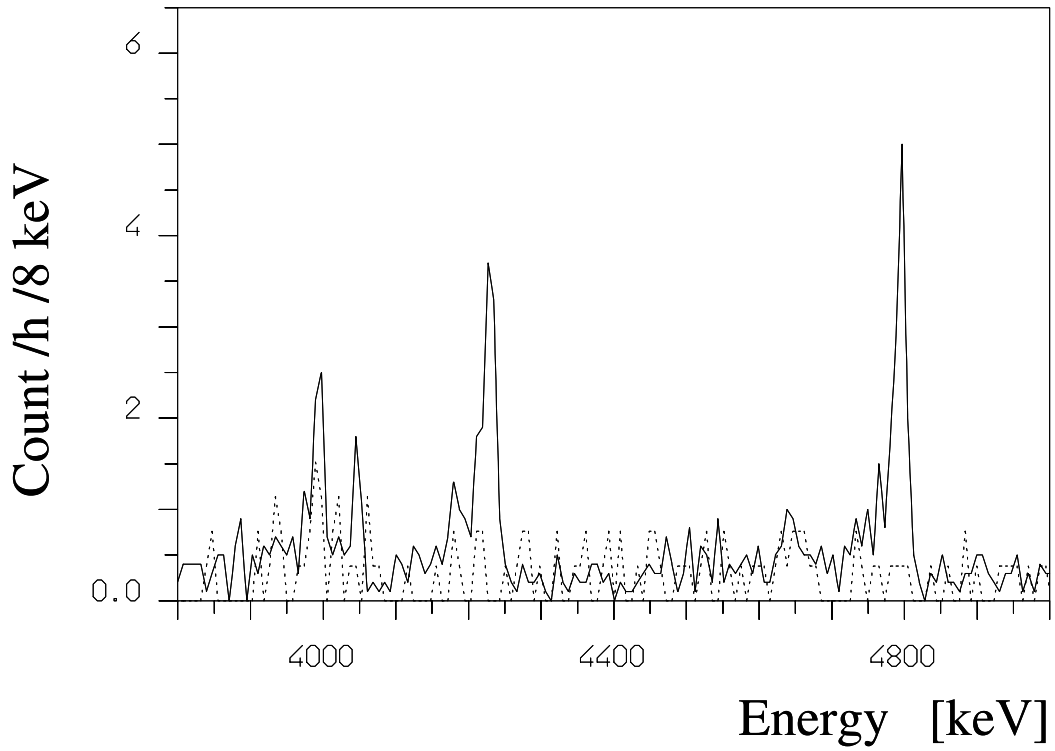

Figure 8: Comparison between background spectra (α region) collected in Hall C before and after a surface treatment of the TeO_2 crystals and of the copper mounting system. Data refers to 5x5x5 TeO_2 CUORICINO crystals.

treatment of all the mounting system copper elements (chemical etching and passivation).

We decided therefore to completely dismount the MIBETA setup and remount it only after: 1) polishing the surfaces of all TeO_2 crystals (30-40 μm) in order to completely eliminate the surface contaminants following crystal preparation (radioactive powders) and exposition to air (^{224}Rn and ^{210}Pb); 2) use a new mounting system identical to the one proposed for CUORE/CUORICINO (Fig. 9); 3) select very low activity materials for all the mounting system structure and treat all the surfaces with chemical etching and a radioclean passivating procedure. Moreover, thanks to the more compact structure proposed for CUORE/CUORICINO, a larger free vital space for improved inner shields would be available (in particular, for an additional 2 cm side and 5 cm top layer of Roman lead). A 10 cm external neutron shield realised with borated (10%) polyethylene was added in June; no notable background reduction was observed after this addition improving further on our background sources knowledge.

Such a work was started at the beginning of 2001 and carried out partly at LNGS (crystal polishing and detector remounting) and partly at LNL (mounting system cleaning procedure), for a period of about three months. The "old" and "new" structure are compared in fig. 3, while details of the new detector tower (mounting system, surface quality) are shown in fig. 6. The results can be summarised as follows:

- the background level in the region of $0\nu\ \beta\beta$ was halved (from 0.59$\pm$0.06 to 0.33$\pm$0.11

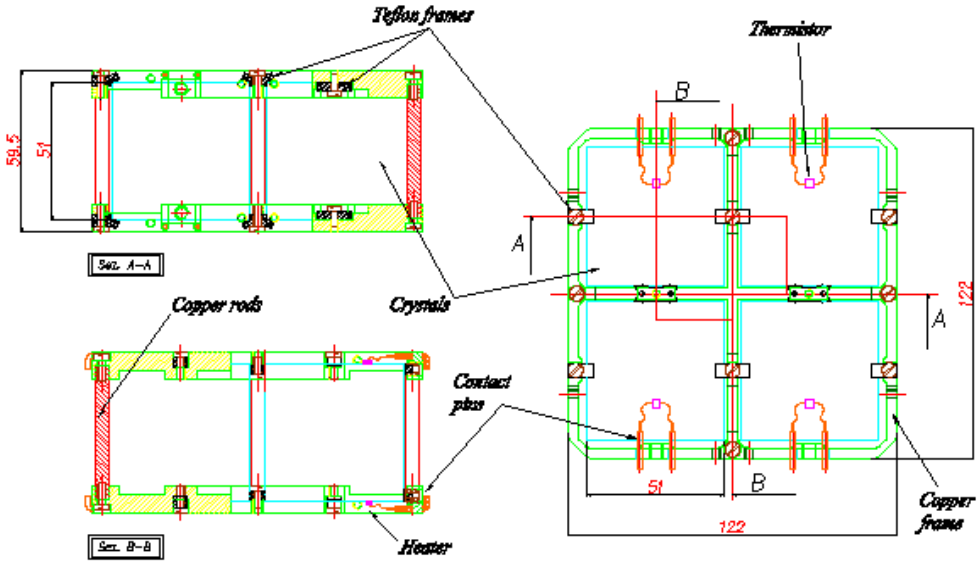

Figure 9: Scheme of the mounting system proposed for CUORICINO/CUORE and implemented in the new MIBETA setup.

counts/keV/kg/y, Figs. 4 and 5); no evidence for $0\nu\ \beta\beta$ was yet found (Fig.5, where the peaks at 2615 and 2447 keV due to ^{208}Tl and ^{214}Bi can be easily seen) and a new lower limit of 2.08×10^{23} years at 90% C.L. on the process halflifetime (total exposure: 4.3 kg y) was obtained, corresponding to upper limits in the range 0.9-2.3 eV (depending on the different nuclear matrix calculations) for the effective neutrino mass $< m_\nu >$. Such result makes MIBETA the most sensitive experiment after those based on Ge diodes. A summary of all the updated DBD results is given in Tab. 1.

- a preliminary check of our knowledge of the MIBETA background sources was carried out; in particular, the effectiveness of the surface treatments was proved while the ineffectualness of the neutron shield helped us to exclude them as a dominant contribution to our background;

- a "large scale" test of the CUORE/CUORICINO detector structure (characterised mainly by a lower passive mass per detector) was carried out; merits and defects of the new structure were identified and the collected informations will be very useful to improve the performance of CUORICINO. A suspension system based on the use of a calibrated spring (for a substantial damping the whole detector vibrations) was also adopted, while few detectors were read-out by a low temperature electronics in order to check the possibility to improve our results also in the low energy (few keV) region.

- The appreciable difference between the counting rates of the isotopically enriched TeO_2 crystals observed in the previous MIBETA measurements almost disappeared

(at least within the statistical significance of the 2001 measure) after the crystals surface treatment. No evidence for $2\nu\ \beta\beta$ can be obtained however by comparison of the enriched crystals spectra consistently with our present statistics. Enriched crystals will be probably remounted within the structure of CUORICINO in order to improve the statistical significance of the measurement.

- from the analysis of the low energy region of the background spectrum, a new limit on the occurrence of the ^{123}Te EC decay was obtained [2] ($T^K_{1/2} > 5 \times 10^{19}$ years); neutron activation was finally identified as a possible background source for the process through the production of the EC unstable ^{121}Te and ^{121m}Te isotopes.

MIBETA measurements were definitely stopped by the end of the year in order to allow the CUORICINO installation preparation phase.

^{130}Te		
Process	Counts	Limit on Half-Life [years] at 90% c.l.
$0^+ \to 0^+\ (0\nu)$	5.0 ± 7.2	2.08×10^{23}
$0^+ \to 2^+\ (0\nu)$	-19.6 ± 8.5	1.4×10^{23}
$0^+ \to 0^+\ (2\nu)$	-	6.3×10^{20}
$0^+ \to 0^+\ (1\chi)$	-	3.1×10^{21}
$0^+ \to 0^+\ (2\chi)$	-	1.1×10^{21}
^{128}Te		
$0^+ \to 0^+\ (0\nu)$	-18.7 ± 19.7	1.1×10^{23}

Table 1: Limits obtained on double beta decay of ^{130}Te and ^{128}Te.

4 CUORICINO R&D

Immediately after the approval of the experiment CUORICINO by the Gran Sasso Scientific Committee and by the National Scientific Commission (Gruppo II) of INFN, we have started an intense activity for the preparation of this experiment using our Hall C cryogenic setup. The CUORICINO detector, which will be installed in the Hall A dilution refrigerator presently housing the 20 crystal array, will consist in an array of 44 cubic crystals of natural TeO_2 of $5 \times 5 \times 5\ cm^3$, plus 18 of the 20 MIBETA crystals (arranged in two planes of 9 crystals each) for a total mass of about 40 kg. This setup will make possible not only an improved search for neutrinoless double beta decay, but also a more sensitive search for direct interactions of WIMPs. Moreover, possible subdiurnal modulations of the signal induced by electromagnetic interactions of axions coming from the sun could be observed.

Due to the larger mass of CUORICINO (both total and of the single TeO_2 crystals) a careful optimisation of the detector performance (and design) was necessary. On the other hand the critical role played by the setup materials radiopurity on the observed background level, required both a careful selection and a detailed analysis of the effects

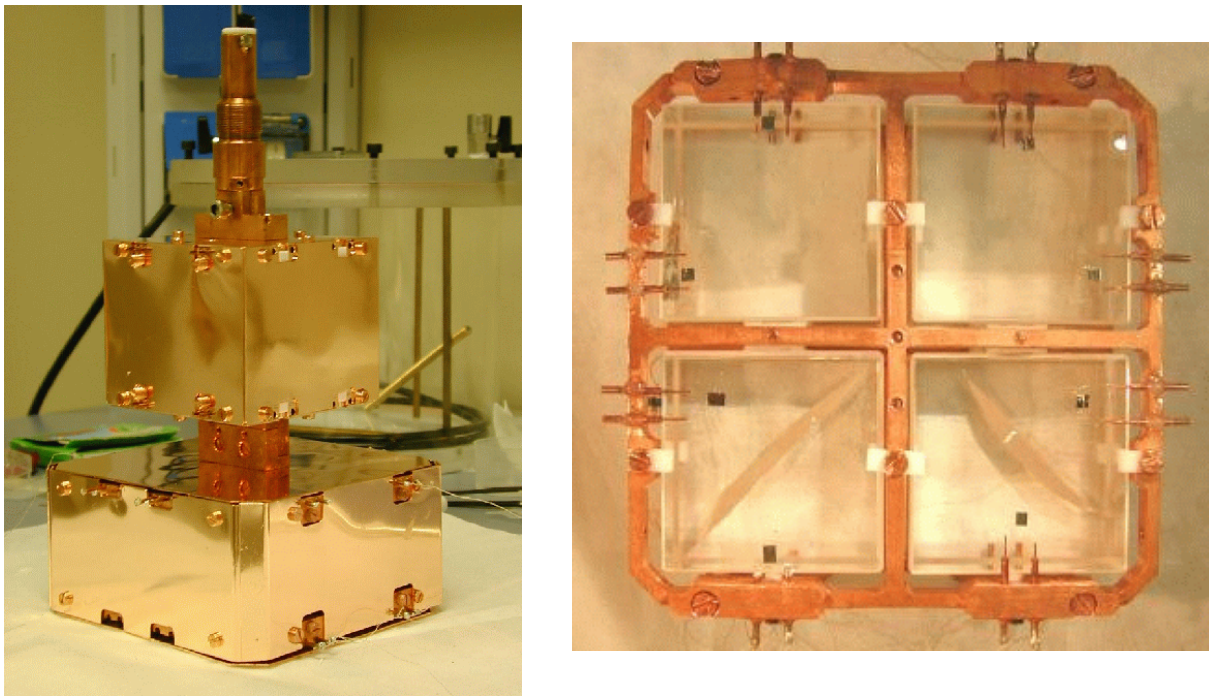

Figure 10: Side view of the cleaned Hall C R&D setup. A top view of the CUORICINO test plane (four $5 \times 5 \times 5$ cm^3 crystals) is also shown.

of the possible surface treatments. We decided therefore to develop a "hybrid" detector allowing us to carry out both R&D activities using our Hall C cryogenic setup. It consists of two 4 crystal arrays mounted in separate copper boxes as shown in Fig. 10. The upper one is made by $3 \times 3 \times 6$ cm^3 crystals (MIBETA), and is dedicated to the study of the background contributions from the radioactive contamination of the detector materials (mainly from the surface). The lower one consists of four $5 \times 5 \times 5$ cm^3 crystals (CUORICINO) and is intended to optimize the design and performance of these bolometers.

Started durind 2000, such an R&D program produced a series of results (concerning both detector design and background reduction) which convinced us of the necessity to rebuild the MIBETA setup as described above.

4.1 CUORICINO R&D results during 2001

The CUORICINO R&D program continued during 2001 mainly to fix the final details of the CUORICINO detector structure. In particular the goals and results of the series of measurements carried out in the course of the year can be summarised as follows:

- **Suspension**: the performance of different suspension systems was tested. The use of a calibrated spring showed the best results in terms of mechanical vibrations damping and will be the final choice for CUORICINO. A crytical item is then the tower thermalisation (thermal connection to the coldest cryostat structure) which

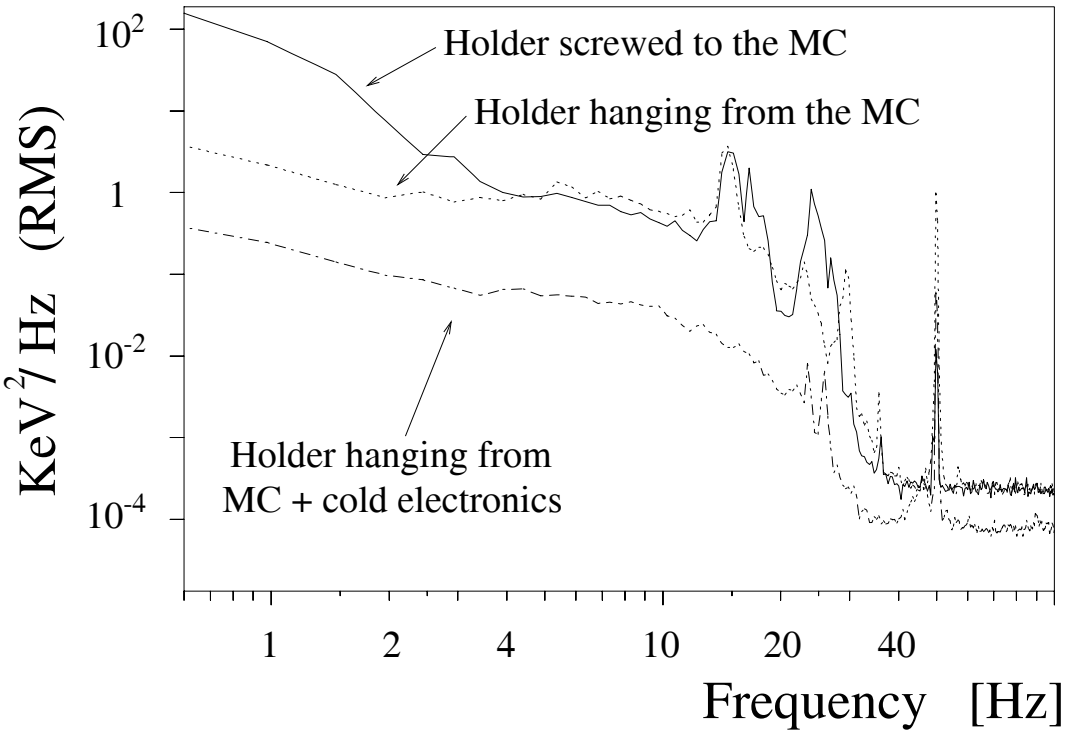

Figure 11: Comparison of the detector noise spectra obtained with different setups.

will be realised by means of calibrated copper strips. A series of dedicated measurements aiming at a best choice for the copper quality and strip geometry has recently concluded.

- **Single detector structure**: slight modifications of the originally proposed mounting system (copper frames and PTFE joints) were tested. Since similar performances were obtained, the design implying the minimum quantity of PTFE was selected. The use of brass screws was finally avoided (Fig. 10).

- **TeO_2 crystal surface polishing**: beacuse of the impossibility to use radioclean powders during the preparation of our TeO_2 crystals at SICCAS, all CUORICINO crystals were ordered with a minimal surface treatment. Since surface quality strongly affects detector performance (pulse duration and detector response), raw crystals could not be used (their performance was checked and found unsatisfactory). A careful selection of radioclean polishing powders and a development program for a surface polishing procedure was then started by the CUORICINO collaboration. After several measurement tests (including both the polishing procedure and the corresponding detector performance measurement), the use of certified 7 μm AlO_2 Sumitomo powder plus different pads (Lamplan and Ultapad) was finally selected.

- **Tower setup**: a critical contribution to the background level from passive elements of the detector structure (mechanical system) was demonstrated. Different material choices and surface cleaning processes were checked. The use of any material other

than copper for the mechanical structure and the same cleaning procedure adopted for the new MIBETA structure was finally selected.

5 Conclusions

The CUORICINO preparation phase is finally concluded. Our group is now going to install the CUORICINO setup by spring 2002 (after the due changes to the Hall A cryogenic setup), while continuing R&D measurements with the Hall C cryogenic setup for the CUORE project (a large array consisting of one thousand $5\times5\times5\ cm^3$ TeO_2 crystals). The results obtained so far with MIBETA and CUORICINO R&D make us confident to reach with the CUORICINO detector the expected background level of 0.1 conts/keV/kg/yr in the $0\nu\beta\beta$ region.

We would like to acknowledge the help of P.Gorla, S. Parmeggiano and L. Tatananni in various stages of the experiment. Special thanks are due to M. Perego for assembling the electronic read-out and to A. Rotilio for the realization of mechanical parts.

6 List of Publications

- M.Vanzini et al: High resolution bolometers for rare events detection, Nuclear Instruments and Methods in Physics Research A, vol. A461, p.293-296, 2001.
- A Alessandrello et al : New limits on naurally occurring electron capture of 123Te, Physical Review Letters (submitted)
- A. Giuliani et al: Dark matter search in the Milano double beta decay experiment and prospects for the CUORE project, TAUP, LNGS, Assergi, September 2001
- E. Fiorini : Double beta decay and neutrino mass, TAUP , LNGS, Assergi, September 2001.
- O. Cremonesi Cryogenic detectors for double beta decay, Low Temperature Detectors, Madison (Wi), July 2001.
- S. Pirro et al: The final results of the Mi-Beta Cryogenic experiment towards the CUORICINO experiment, Low Temperature Detectors, Madison (Wi), July 2001.
- C.Bucci et al: The CUORE experiment, Low Temperature Detectors, Madison (Wi), July 2001.
- C.Arnaboldi et al: CUORE: Cryogenic Underground Observatory for Rare Events, letter of intent to the Gran Sasso Scientific Committee and to the *Commissione Scientifica Nazionale II dell'INFN*, March 2001.

References

[1] E. Fiorini and T. Niinikoski, Nucl.Instrum. and Meth. In Phys.Res. 224 (1984) 83.

[2] A Alessandrello et al : New limits on naurally occurring electron capture of 123Te, Physical Review Letters (submitted)

[3] C.Arnaboldi et al: CUORE: Cryogenic Underground Observatory for Rare Events, letter of intent to the Gran Sasso Scientific Committee and to the *Commissione Scientifica Nazionale II dell'INFN*, March 2001.

The OPERA experiment

M. Serin-Zeyrek[a], P. Tolun[a], M. Zeyrek[a], A. Ereditato[b], A. Degré[c], D. Duchesneau[c], J. Favier[c], M. Lavy[c], P. Mugnier[c], H. Pessard[c], M. Ieva[d], M. Muciaccia[d], M. De Serio[d], S. Simone[d], S.L. Lu[e], J. Ren[e], S.J. Zhou[e], K. Winter[f], K. Borer[g], J. Damet[g], M. Hess[g], U. Moser[g], K. Pretzl[g], T. Wälchli[g], M. Weber[g], G. Giacomelli[h], G. Mandrioli[h], L. Patrizii[h], P. Serra[h], M. Sioli[h], G. Sirri[h], T. Kellmann[i], G. Van Beek[i], P. Vilain[i], G. Wilquet[i], D. Bardin[j], I. Boudagov[j], G. Chelkov[j], Y. Gornouchkine[j], Z. Kroumchtein[j], A. Nozdrin[j], A. Olchevski[j], A. Sadovski[j], B. Dulach[k], A. Franceschi[k], M. Spinetti[k], F. Terranova[k], L. Votano[k], S. Ogawa[l], H. Shibuya[l], D. Autiero[m], L. L. Camilleri[m], L. Di Lella[m], J. Dupraz[m], J-P. Fabre[m], F. James[m], I. Kreslo[m], R. Petti[m], A. Sharma[m], H. Schauties[n], H. Sohlbach[n], H. Woltersdorf[n], J. Goldberg[o], S. Aplin[p], I. Bagdasarova[p], C. Ballhausen[p], F.W. Büsser[p], J. Ebert[p], B. Koppitz[p], B. Naroska[p], V. Saveliev[p], W. Schmidt-Parzefall[p], R. Van Staa[p], K. Kodama[q], N. Ushida[q], S. Aoki[r], T. Hara[r], L. Chaussard[s], Y. Déclais[s], C. Heritier[s], P. Jonsson[s], S. Katsanevas[s], I. Laktineh[s], J. Marteau[s], G. Moret[s], S. Gninenko[t], N. Goloubev[t], M. Kirsanov[t], V. Matveev[t], V. Postoev[t], V. Razin[t], A. Toropine[t], A. Artamonov[u], P. Gorbounov[u], V. Khovansky[u], I. Tikhomirov[u], Y. Zaitsev[u], P. Boschan[v], N. Bruski[v], D. Frekers[v], J. Kückmann[v], K. Hoshino[z], M. Komatsu[z], M. Miyanishi[z], M. Nakamura[z], T. Nakano[z], K. Niwa[z], O. Sato[z], T. Toshito[z], S. Buontempo[x], A. Cocco[x], N. D'Ambrosio[x], F. Di Capua[x], G. De Lellis[x], G. De Rosa[x], G. Fiorillo[x], T. Kawamura[x], M. Messina[x], P. Migliozzi[x], R. Peluso[x], C. Pistillo[x], P. Strolin[x], V. Tioukov[x], J. Busto[w], G. Jonkmans[w], J-L. Vuilleumier[w], J-M. Vuilleumier[w], J. Boucrot[aa], J-E. Campagne[aa], B. Merkel[aa], J-P. Repellin[aa], J-J. Veillet[aa], R. Brugnera[bb], F. Dal Corso[bb], S. Dusini[bb], C. Fanin[bb], A. Garfagnini[bb], L. Stanco[bb], P. Righini[cc], G. Rosa[cc], M. Beyer[dd], H. Schröder[dd], R. Waldi[dd], R. Zimmermann[dd], E. Barbuto[ee], C. Bozza[ee], P. Grella[ee], G. Romano[ee], S. Sorrentino[ee], R. Arnold[ff], E. Baussan[ff], M. Dracos[ff], J-P. Engel[ff], J.L. Guyonnet[ff], C. Feng[gg], Y. Fu[gg], M. He[gg], J.Y. Li[gg], L. Xue[gg], Y. Sato[hh], I. Tezuka[hh], K. Jakovcic[ii], A. Ljubicic[ii], M. Stipcevic[ii]

[a] METU, Ankara - Turkey
[b] Laboratori Nazionali del Gran Sasso, Assergi - Italy
[c] LAPP, IN2P3-CNRS and Université de Savoie, Annecy - France
[d] Bari University and INFN - Bari
[e] IHEP, Beijing - China
[f] Humboldt University, Berlin - Germany
[g] Bern University, Bern - Switzerland
[h] Bologna University and INFN, Bologna - Italy
[i] IIHE (ULB-VUB), Bruxelles - Belgium
[j] JINR, Dubna - Russia
[k] LNF, Frascati - Italy
[l] Toho University, Funabashi - Japan
[m] CERN, Geneve - Switzerland
[n] Märkische Fachhochschule FB Elektrotechnik, Hagen - Germany
[o] Technion, Haifa - Israel
[p] Hamburg University, Hamburg - Germany
[q] Aichi University of Education, Karyia - Japan
[r] Kobe University, Kobe - Japan
[s] IPNL, IN2P3-CNRS and Université C. Bernard Lyon I, Villeurbanne, Lyon - France
[t] INR, Institute for Nuclear Research of the Russian Academy of Sciences, Moscow - Russia
[u] ITEP, Moscow - Russia
[v] Münster University, Münster - Germany
[z] Nagoya University, Nagoya - Japan
[x] Federico II University and INFN, Napoli - Italy
[w] Neuchâtel University, Neuchâtel - Switzerland
[aa] LAL, IN2P3-CNRS and Université Paris-Sud, Orsay - France
[bb] Padova University and INFN, Padova - Italy
[cc] La Sapienza University and INFN, Rome - Italy
[dd] Fachbereich Physik der Universität Rostock, Rostok - Germany
[ee] Salerno University and INFN, Salerno - Italy
[ff] IReS, IN2P3-CNRS and Université Louis Pasteur, Strasbourg - France
[gg] High Energy Physics Group Shandong University, Jinan, Shandong - China
[hh] Utsunomiya University, Utsunomiya - Japan
[ii] Rudjer Boskovic Institute (IRB), Zagreb - Croatia

Abstract

The OPERA experiment aims at the direct observation of ν_τ appearance from $\nu_\mu \rightarrow \nu_\tau$ oscillations in the CNGS long baseline beam from the CERN SPS to the Gran Sasso Laboratory. The detection of τ decays is achieved by the use of Emulsion Cloud Chamber (ECC) technology (lead - nuclear emulsion sandwitch), providing a total target mass of about 1800 t. Overall, low background levels are expected (0.75 events) for the τ search. During 2001 the detector design has been finalized with extensive tests on full scale prototypes. The experiment is now entering the final construction phase.

1 Design principles

The OPERA experiment is designed for the direct observation of ν_τ appearance from $\nu_\mu \rightarrow \nu_\tau$ oscillations in the CNGS long baseline beam from the CERN SPS to the Gran Sasso Laboratory. The measurements of atmospheric neutrino fluxes performed by the Super-Kamiokande experiment indicate a deficit of muon neutrinos and an anomaly in their zenith angle distribution, consistent with $\nu_\mu \rightarrow \nu_\tau$ oscillations with $\Delta m^2 \approx 1.2 \div 5.4 \times 10^{-3}$ eV^2 (90% CL) and full mixing. The Soudan2 and MACRO experiments also made observations compatible with this result. Therefore, the primary goal of OPERA is to obtain direct evidence for ν_τ appearance, which would confirm the oscillation hypothesis.

A long baseline of 732 km is used between the neutrino source (the CERN beam line) and the detector (located in the underground Gran Sasso laboratory) in order to be sensitive to the oscillation parameters indicated by the Super-Kamiokande data. The CNGS neutrino beam has been optimized for the detection of ν_τ charged-current (CC) interactions and provides an average ν_μ energy of about 20 GeV. For the evaluation of the performance of the experiment an integrated fluence of 2.25×10^{20} protons on target is assumed, corresponding to a 5 year SPS operation in a shared mode.

The main principle of the ν_τ search is the *direct* detection of the decay of the τ lepton produced by CC interactions. This is achieved by a massive (about 1800 t) neutrino target based on the ECC design which combines, in a sandwich-like cell, the high precision tracking capabilities of nuclear emulsions (two 50 μm layers on both sides of a 200 μm plastic base) and the large target mass provided by lead plates (1 mm thick). This technique has been recently demonstrated to be effective for τ detection by the DONUT collaboration.

The basic element of the target structure is the *brick*, composed by a consecutive series of individual cells with transverse dimensions of 10.2×12.7 cm^2. Bricks are arranged into planar structures (*walls*), which are interleaved with electronic tracker planes (Figure 1). These planes are built from vertical and horizontal strips of plastic scintillator, 2.6 cm wide. The main purpose of the electronic target tracker is to localize the particular brick in which the neutrino interaction occurred, once an interaction trigger is recorded. This brick is then extracted for the emulsion development and scanning in a quasi-online sequence. Large emulsion areas can be scanned with automatic microscopes equipped with fast track recognition processors. This allows the measurement of both track momenta from their multiple scattering in the brick and electron and gamma energies from shower development.

The target and the tracker sections are further arranged into three independent supermodules (Figure 1). Each supermodule is followed by a downstream muon spectrometer. A spectrometer consists of a dipolar magnet made of two iron walls, interleaved by pairs of vertical drift tube planes. Planes of RPC's are inserted between the magnet iron plates to allow a coarse tracking inside the magnet and a measurement of the stopping particles from the upstream supermodule.

The OPERA design is optimized to achieve low background levels for the τ appearance search. The experiment aims at the analysis of all single-prong τ decay modes (e,μ,h). Signal events are classified as *long* or *short* decays depending whether the τ track traverses an emulsion sheet or not. The main background sources are charm production in CC

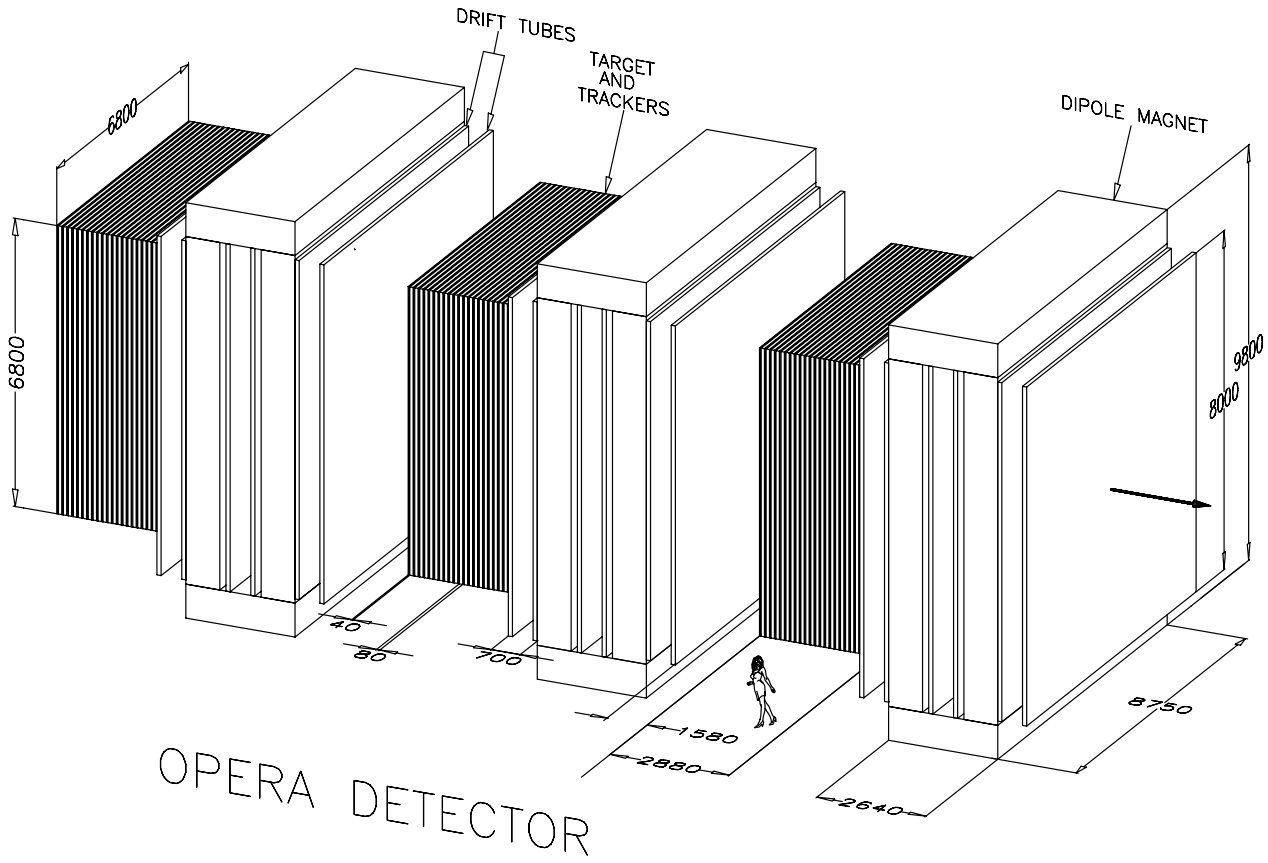

Figure 1: *Schematic view of the OPERA detector.*

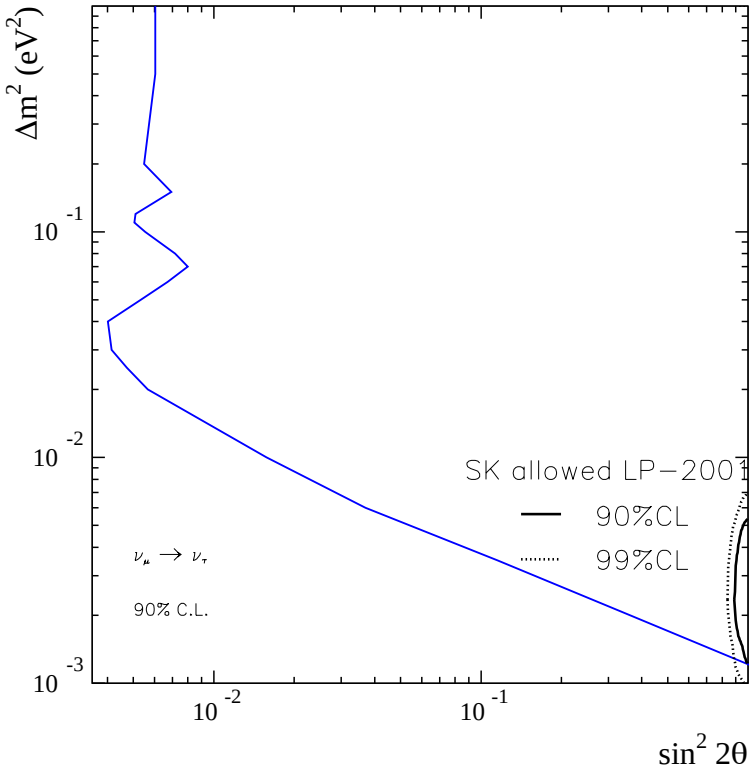

Figure 2: *Sensitivity of the OPERA experiment to $\nu_\mu \rightarrow \nu_\tau$ oscillations for 5 years of CNGS running (2.25×10^{20}pot), defined as the average 90% upper limit obtained, in the absence of a signal, by an ensemble of experiments. The region allowed by the analysis of Super-Kamiokande data (Lepton-Photon 2001) is also shown.*

interactions, hadronic interactions in lead and large angle muon scatterings. These events are rejected by the identification of the primary lepton in CC interactions and either by requiring the presence of a τ-like kink topology (long decays) or by an impact parameter method (short decays). In addition, a kinematic analysis is used to enhance the signal to background ratio. Overall, a total background of 0.75 events is expected. If $\nu_\mu \rightarrow \nu_\tau$ oscillations occur, the average number of detected signal events ranges from 2.7 at $\Delta m^2 = 1.2 \times 10^{-3}$ to 53.5 at $\Delta m^2 = 5.4 \times 10^{-3}$ (full mixing). The achieved sensitivity at 90% C.L. is shown in Figure 2 and broadly covers the region of the parameter space allowed by the Super-Kamiokande data. Within this region, the probability to obtain a statistical significance on the detected signal of at least 4σ (gaussian equiv.) is 90% after a 5 year run.

2 Milestones achieved during 2001

2.1 Emulsion target

2.1.1 Emulsion refreshing facility

Due to their continuous sensitivity, the emulsion plates will collect latent track images, mainly from cosmic-rays and ambient radioactivity, since the very beginning of their lifetime at the production firm Fuji Co. in Japan, and all along their way to the OPERA detector in the Gran Sasso cavern.

In the study of events induced by the CNGS beam, background tracks may affect the pattern recognition and may cause degradation of the measurements of the energy of electromagnetic showers. The remedy was proposed and succesfully tested at Nagoya University: a treatment of the emulsion plates at moderate temperature (see Section 2.1.2) and very high humidity for a few days will cancel out a significant fraction of the previously stored latent track images. This is known as a "refreshing" procedure and reduces the number of reconstructed track segments by more than a factor of ten.

In the strategy described in the Proposal, refreshing should be performed inside the Gran Sasso cavern soon after the delivery of the emulsion plates and just before the brick assembly. However, taking into account the limited space available underground and the need to carefully handle a huge number of individual plates in darkroom, almost synchronously with the preparation of bricks and their insertion into the apparatus, an alternative scenario is now under investigation. The idea is to perform the refreshing in Japan, possibly in the Sakashita or Tono mines. The sheets that will ultimately be part of a given brick would then be packed together but without lead. Shipment and delivery to Gran Sasso could be carefully timed. The tracks collected after this provisional packing could be recognized and rejected at the scanning stage since the segments in the emulsion sheets would appear staggered, due to the subsequent insertion of the lead sheets.

2.1.2 Preparation for production of emulsion films

After the proposal submission, ten small batch productions and one large production of emulsion films were performed in order to refine and tune the specifications for mass production of the OPERA emulsion films.

The samples also underwent a refreshing procedure designed to erase tracks accumulated between the production of the emulsion and its exposure to the neutrino beam. The procedure involves storing it for three days at 30^0C and 95% relative humidity. The characteristics of the refreshed samples are:

Initial sensitivity before refreshing	36 grains/$100\mu m$
Surviving grain density of recorded tracks after refreshing	8 grains/$100\mu m$
Sensitivity after refreshing	33 grains/$100\mu m$

These characteristics are satisfactory for OPERA.

Complete tests involving refresh-transport- ECC assembling-beam exposure- development and read-out by UTS systems are currently being analyzed. We are planning to report the results at the presentation of the Status Report.

2.1.3 Status of brick packing in Japan

Designing of the "Origami" packing system is now in its final stage. We will have a prototype packing system at the end of September in Nagoya. It will be used as a test machine to define the final specifications for OPERA. Mass treatment tests with this machine are planned this autumn. In parallel, the design of the laminated multilayered paper is also in progress. The combination of the materials constituting the multilayered paper and their thicknesses is under investigation.

2.1.4 Brick Assembly Machine (BAM)

The BAM has to perform the following tasks:

- Intake of the emulsion films, lead plates, spacer sheets, protective paper and packing material.
- Stacking and wrapping if needed (light tight).
- Packing (light and vacuum tight).
- Bar code labelling.
- Insertion of the brick on a support, if needed.
- Storage of the bricks.

In order to establish contact with potential industrial partners a BAM specification document has been produced. It gives the list of operations to be performed by the BAM, and the constraints for handling lead, emulsion and packing material. Several companies already gave a positive reaction to the submission of the BAM specification document. Different stacking and packing stategies have been suggested. The stacking can be automated or hand made. Packing materials such as multilayered paper and rubber are being considered. Welding tests on the paper have been performed. The paper packing can be either pre-formed or folded in place. Within one month one vendor, Fuji, will deliver to the Nagoya University a prototype of a packing machine based on the Origami technique. It will be used to produce prototype bricks. An alternative packaging solution based on the use of rubber pre-shaped envelopes and proposed by the French Company Jeantet is being studied. First rubber envelope prototypes have been delivered to CERN. The main rubber component, called "Butyl", is under tests in Nagoya University for emulsion compatibility.

2.1.5 Brick Manipulator System (BMS)

The OPERA bricks are moved in and out of their supporting trays in the walls by means of an automated system called Brick Manipulator System (BMS). The study of this system has made substantial progress in the past twelve months.

The principle of forming horizontal rows of bricks and sliding them collectively along their supporting trays has been assessed in full detail. In this scheme the initial operation of loading the 235,000 bricks into the detector can be performed at a rate larger than the brick production rate. Even with quite moderate speeds in the movements this operation

has been evaluated as being safe. Sliding together "trains" of bricks allows the daily exchange of the 30 bricks where a neutrino interaction occurred, in about an hour with the same moderate speeds.

The supporting structure of the bricks will be composed of two half walls which are vertically separated. This has led to the design of two symmetric manipulators, moving along either side of the detector and operating independently.

Mechanical tests have shown that the sliding friction was larger for a sliding stainless steel band supporting a train of bricks than for the same train of bricks equipped with plastic skates. Bricks with skates have then been adopted.

By means of a jack the bricks will first be pushed out of the carousel storage, onto the manipulator platform. Once the carousel is empty, the bricks will then be moved towards the detector centre by means of a special device included in the bridge connecting the platform to the supporting trays.

During the insertion of the bricks, a thin metallic band is connected to the first brick and is drawn between the brick skates. For retrieving a brick row, this band is wound by a motor to the platform where it is locked to a platform resident metallic band. An alternate scheme using suction grips to retrieve bricks back to the carousel is a possible back-up solution and will be tested experimentally in the coming months.

Recent measurements to evaluate the resistance of the lead-emulsion sandwich under vacuum to relative movements of the plates have shown that it is possible to push or pull together a full line of 26 bricks on skates, without protective bricks holders and with a significant safety factor relative to brick deformation. If these measurements are confirmed, brick holders would not be used, leading to a large reduction of the inter-brick gap within a brick plane.

In parallel, a large amount of the work on the brick manipulator has been devoted to the development of the lift structure and the platform design (precision X-Y tables, carousel storage, bridge system, winding foil system, positioning system). A full scale prototype of the platform is presently being mounted at LAPP for tests with a prototype brick supporting wall. A large effort is also underway to prepare the automation of the various movements, using different types of sensors to control the corresponding motors, including video cameras for the positioning.

2.1.6 Wall support structure

The wall support structure is made of thin stainless steel vertical bands welded to light horizontal trays where the bricks are positioned with a precision of one millimeter. Using high resistance stainless steel bands of 0.8 mm thickness, the structure weight is less than 0.4% of the total target weight. This design limits as much as possible neutrino interactions in the target area outside of the bricks themselves, ensures easy and quick removal of bricks from lateral sides and permits a minimum separation between bricks in transverse and longitudinal directions. The structure is suspended through rods and joints from the general support structure and tensioned from the bottom through a spring system.

The structure design has been accomplished and the whole system including suspensions and tensioning system checked against the effect of earthquakes in the general

support structure frame. After many destructive tests on the critical welding points, the stainless steel band material has been chosen and the welding procedure established. One prototype (full height and 1 m wide) has been assembled at the Frascati Laboratory, suspended and loaded with dummy bricks. The expected positioning precision has been achieved. Long term mechanical stability tests are underway. A second prototype (full width and 1 m high) is under construction and will be equipped with a more compact tensioning system. This prototype will be used for the brick manipulator tests.

2.2 Target Tracker

The main purpose of the Target Tracker (TT) is to identify the brick where a neutrino interaction occurred. An additional TT requirement is provided by the need to minimize the number of wrong associations between a genuine μ^-, as measured in the TT and muon spectrometers, and a hadron track in the emulsion. These wrong associations become a source of background if the hadron suffers a scattering consistent with a τ decay kink. Their rate depends on the uncertainty of the reconstructed μ^- track parameters.

2.2.1 Plastic scintillators

In the 2001 we finalzed the TT design: it consists of two orthogonal planes of plastic scintillator strips installed behind each brick wall. These strips are 2.6 cm wide, 1 cm thick, and are read out by wave-length shifting fibres. All estimates of τ^- detection efficiencies and backgrounds were based on this design, which represents the TT baseline option.

A full scale prototype module (Figure 3) was constructed and completed by March 2001 according to schedule. Very preliminary results had been presented at the March LNGS Committee meeting; since then several tests have been performed. The prototype is composed of 64 plastic scintillator strips, 670 cm in length and 2.6×1.0 cm^2 in cross section. All the strips have been scanned using an electron spectrometer (1.8 MeV electrons). An average number of 3 photoelectrons per read-out end has been observed in the middle of the strips which is the most unfavourable position for readout at both ends.

Using cosmic rays, the track detection efficiency has been found to be higher than 98% even in the middle of the strips.

Since then, efforts have been made to improve the WLS fibre gluing inside the scintillator grooves. The shape and the depth of the grooves have also been optimized. After these improvements, using the same industrially produced scintillator strips as for the prototype construction, the number of photoelectrons in the middle went up to 5 per readout end.

Extra efforts have been made by the prototype scintillator producer Pol.Hi.Tech. to improve the quality of scintillators. They made new extrusions using, as previously, PPO+POPOP but under a nitrogen atmosphere. With these new strips more than 5.5 photoelectrons have been measured in the middle of the strips. They also extruded strips under normal atmosphere but with BDB instead of POPOP (BDB is known to react less with oxygen than POPOP), also resulting in 5.5 photoelectrons in the middle of the strip.

Promising results were also obtained recently with plastic scintillator samples extruded

Figure 3: Full scale prototype of a module of the target tracker with plastic scintillators constructed and tested at Strasbourg.

at the Kharkov factory using the technology of polimerisation and extrusion in one production step (thus avoiding the contact with oxygen).

Tools are now under development for large-scale production of plastic scintillator modules. For all aspects, decisions will be also based upon compatibility with schedule.

2.3 The veto system

A veto system, required to flag events from neutrino interactions in the rock surrounding the OPERA detector, we also studied.

In a "minimal" scheme, a veto detector could be placed in front of the first supermodule. Two planes with about 10×10 m^2 cross section made of RPC chambers can be mounted attached to the so called "arch" support structure, composing a supermodule. If backscattering from the target interactions would turn out to be relevant, another similar module, placed 1-2 m upstream, would allow a TOF measurement to flag backward going tracks. A time resolution of about 1 ns seems to be adequate and achievable with RPCs. One can also accommodate similar veto detectors in front of the other supermodules. A detailed study of this veto configuration is in progress.

Another task of the veto detector is the monitoring of the neutrino beam. By counting neutrino interactions in the rock upstream of the OPERA target through the detection of muons one can obtain valuable information on the CNGS beam right at start up.

The envisaged veto system configuration includes two RPC modules each of 10×10 m^2, separated by a distance of ~ 1 m and placed in front of the first supermodule, plus

a single $\sim 7 \times 7$ m^2 RPC module in front of supermodules 2 and 3.

A Monte Carlo simulation shows that the rate of triggers from neutrino interactions in the rock is as large as that of genuine neutrino interactions. The use of VETO reduces the trigger rate from rock events by nearly 94%. The surviving rock events can be further reduced by a factor of 3 by applying pattern recognition and brick finding algorithms. However, a study of the effect of this additional rejection on the efficiency for signal events has not yet been performed.

2.4 Spectrometers

2.4.1 Magnets

A full scale prototype of part of the dipole magnet has been constructed in Frascati. It consists of two vertical walls of rectangular cross section and of top and bottom flux return path. The walls are made up of four iron layers (5 cm thick) interleaved with 2 cm of space allocated for the housing of RPC. Each iron layer is made up of two plates $50 \times 1250 \times 8200$ mm^2 (Figure 4). The final OPERA spectrometer will have the same structure but consists of seven plates instead of two (overall length 8750 mm) and 12 layers instead of 4. Studies have been made in order to understand its mechanical construction, and the performance of the final magnets, as well as to measure and monitor the magnetic field.

2.4.2 Inner trackers

The design of the Resistive Plate Chambers (RPC) inserted in the magnets has been studied and measurements have been performed.

RPC prototypes have been tested at CERN, Frascati, Gran Sasso and Padova, as well as at the T9 test beam from the CERN PS. These prototypes are RPC's of the latest generation, where the bakelite foils have more melamine content than earlier chambers, the surface of the backelite is much smoother and the plastic corners and spacers are made with LEXAN instead of PVC.

Efficiencies as well as spatial and time resolutions have been studied as a function of various parameters (high voltage, gas mixtures, etc.).

Sixteen full scale prototypes have been constructed and tested, in particular to check their performance around the 6 cm diameter holes which house the bolts of the magnet. Full scale prototypes for the layers of the x-view strips have already been produced by Pol.Hi.Tech (12 layers). They will be tested to measure the degradation of the signals over their 8 m length.

A prototype of the front end electronic card has been developed in Padova, based on the commercial disciminator LM361, double register to avoid dead time, in-line test calibration, VME controller. A second prototype with an optimized layout is under construction.

Figure 4: Full scale prototype of part of the dipole magnet constructed and tested at Frascati, as seen during construction.

2.4.3 Precision trackers

Since autumn last year progress has been made in drift tube prototype development, design and construction. Elongation tests have shown that the 45 μm gold-plated tungsten wires from the company LUMA fulfill our requirements, in a cost effective way.

Long prototype tubes in brass and in aluminum with a length of 8.1 m have been tested. A satisfactory attenuation length has been measured: $\lambda = (22.2 \pm 0.7)$ m with brass and $\lambda = (25.9 \pm 0.7)$ m with alluminium. With a $\pm 250\,\mu$m alignment no wire motion $> 40\,\mu$m has been observed up to 3.2 kV. In addition, two brass (1 m long) and one aluminum (30 cm long) tubes have been used for tests. The operation voltage range will be 2.3-2.5 kV for the current gas mixture of Ar/CO_2 (80%/20%). The gas gain was measured to $8 \cdot 10^4$ at 2.3 kV and the maximal drift time to 1.1 μs. Up to 2.5 kV no after pulsing was observed.

The optimal tube staggering in a module has been studied with MC simulations in order to minimise the loss of tracks due to left/right ambiguities.

The design of the tube end caps is almost finished. A method to fix the end caps by shrinking has been tested successfully and negotiations with industry for the mass production can start. The support of the modules is being designed and the first version of the drawings has been produced.

The production of two 1 m long OPERA drift tube prototype modules (each consisting of three layers with eight tubes per layer) with the final staggering has been started in July. These modules will allow the understanding of the resolution and the efficiency, as well as to test the electronics electronics and HV board.

2.5 Emulsion laboratories at Gran Sasso

As stated in the OPERA Proposal, facilities for emulsion handling are expected to be operational at the Gran Sasso Laboratory both during the construction of the apparatus and in the course of data taking.

During construction, the infrastructures for emulsion storage, for any pre-treatment of the plates, namely the so-called refreshing, and for hosting and operating the Brick Assembly Machine (BAM) will be needed inside the cavern. In the course of data taking, the extracted bricks will be equipped with additional veto sheets and exposed to cosmic-rays outside the cavern. The disassembly of the bricks, the development of the plates and their delivery to the scanning stations will follow.

Candidate sites to locate underground and outside Emulsion laboratories at LNGS, have been identified, with the help and advice of LNGS staff. Project designs are in progress, as will be reported below. Meanwhile, small laboratories for emulsion tests underground and cosmic ray exposures outside the cavern were set-up, in order to tune the final choice of operating conditions. Tests are in progress, as will also be reported below.

Even considering that emulsion refreshing at the production will be carried out in Japan (Section 2.1.1), a rather large and well equipped area for emulsion storage will be needed in the Gran Sasso cavern. This area must be adjacent to the BAM area. The candidate site for both functions is a 50 m long, 5 m wide tunnel connecting Hall A

and Hall B, crudely finished and presently not in use ("Bypass"). Note that the Bypass solution is the only viable hypothesis, irrespective of the Hall assigned to OPERA.

The Bypass was surveyed, and the Radon and wall radioactivity monitored by LNGS Services on request by OPERA. The access from the Hall B side must be enlarged. The floor and the walls need surface coverage and protection from water flow. A clean area of over 40 m x 5 m could be made available for the BAM, the emulsion storage and all the peripheral operations.

The specifications given to industrial companies require that the BAM fits the available space. Conveniently shaped barracks have to be placed in the Bypass to host, partly as darkrooms, the emulsion handling underground and to allow the dispatching of the target components and of the bricks ready for installation. A detailed plan will be presented in the next few months.

2.5.1 Cosmic-ray exposures and processing

During the run, the cosmic-ray exposure of bricks selected for event location and study is expected to provide enough good through-passing tracks for plate-to-plate alignment. Unwanted electromagnetic showers, still abundant at mountain sites, and the soft muon component must be minimized by installing suitable shielding (rock or metal) above the cosmic-ray exposure station.

The brick disassembly and development which follow this exposure also benefit from shielding.

In agreement with LNGS, it is planned to take advantage of a new building, that could be partly devoted to the post-trigger brick handling and processing. The request has been made by OPERA to connect this new building to a pit for cosmic-ray exposures, to be excavated nearby a few meter below-ground. The pit should be covered by an iron disk, 0.5 to 1 m thick, in order to select hard muons. We have also proposed an optimal internal subdivision of the part of the new building assigned to OPERA.

This building is expected to be constructed early enough to allow the setting-up and extensive test of the emulsion facilities before the CNGS beam starts.

2.5.2 Emulsion tests at LNGS

An extensive test program is in progress in order to study the environmental radioactivity and the cosmic-ray flux and spectrum at LNGS, and to test all steps of the emulsion handling on site.

Two small laboratories were implemented.

i) Inside the cavern, in the corridor connecting Hall B and Hall C, a darkroom was installed. It is a 12 m x 2.2 m barrack, well equipped to pour emulsion plates and to develop either locally or commercially produced plates. The two activities can operate independently. Many test plates were already succesfully produced and processed. Scanning of these plates allowed to measure the ambient radioactivity in several places underground and outside. Compared to similar measurements performed at home institutions, it was confirmed that the local radioactivity is about 1/3 of the level usually detected in conventional civil engineering sites. Indeed, low-activity concrete was adopted on purpose at

LNGS. Also, cosmic-ray exposures were already performed, and more are in progress, as explained below.

ii) A cosmic-ray station was set-up at the LNGS surface, in the parking area where the above-mentioned new building will be located. It consists of a 5m x 2.2 m barrack, hosting an iron structure designed to allow exposures to cosmics at different depths, ranging from 0 to 100 cm of iron. Gaps between the iron sheets allow the insertion of standard OPERA bricks. Scintillator counters could also be inserted inside the same gaps to perform independent and complementary tests on cosmics.

Since late June extensive tests have started. Full results are expected by the end of the year, so that the design and shielding of the exposure pit can be finalized. More complete tests with full bricks are planned in the near future. The support of the LNGS staff and of local workshops, which allowed the setting-up of these facilities in a very short time is very gratefully acknowledged.

2.6 Preparation of Scanning Stations

2.6.1 Reformed scanning lab in Nagoya

The scanning laboratory in the Nagoya F-lab has been renovated in Februrary 2001. The new scanning laboratory has enough space and infra-structures such as electricity and air conditioning to setup the new fast scanning systems for OPERA (S-UTS).

2.6.2 Plan for a Scanning Station in Europe

The brick emulsion scanning can be subdivided in three parts:

- the vertex location inside bricks, requiring a 24 hours per day scanning load with dedicated people working in shifts as in a running experiment;
- the selection of events with decay like topology;
- precision measurements on selected events.

The first part requires a Scanning Station. The last two imply a smaller scanning load but more detailed measurements. Therefore, in order to optimise the use of resources, the following scanning strategy is envisaged: the Scanning Station will perform the vertex location and distribute bricks among the measurement laboratories that will take the scientific responsibility of the event selection and/or precision measurements.

The construction of a Scanning Station, handling 15 bricks per day, is planned in Italy and its location is under investigation. It is intended to be a European facility. In 2003 the design of the scanning system will be finalized and the construction of the Scanning Station is foreseen to start. The present studies indicate the need of about 200 m^2 to host: a brick handling area, 13 automatic microscopes (assuming a scanning speed of 20 cm^2/hour) and a control room. Technicians, physicists and hardware/software experts have to be on site.

2.7 Preparation of Scanning Systems

2.7.1 S-UTS preparation

The type A scheme described in the proposal has been chosen and is being developed. A prototype of a piezo-controlled objective lens is completed. The achieved fluctuation of the microscope stage movement is below 0.5% which satisfies the requirement (better than 1%) to guarantee a stable image taking. The synchronization of the stage and of the objective lens is being tested extensively. We plan to use this system combined with the existing CCD camera and electronics for the UTS in September to scan emulsion sheets exposed for tests. A fast CCD camera is being prepared by industry and a prototype should be available soon. Then the UTS will be upgraded with this fast CCD camera and new electronics to form a complete S-UTS system.

2.7.2 Progress in automatic scanning in Europe

A scanning system (SYSAL) developed in Salerno is operational for the CHORUS experiment with a scanning speed of 1.6 cm^2/hour in the OPERA emulsions. In order to reach a scanning speed of 20 cm^2/hour as required by OPERA, Italian (Bari, Bologna, Naples, Rome and Salerno) and other European (Bern, Münster) groups are carrying out an R&D program to develop a new scanning system based on SYSAL. Also Lyon intends to participate in R&D on automated scanning. In addition, several laboratories will participate in the scanning of the emulsions.

The R&D approach is based on the use of commercial technology to profit from the continuous improvements in speed of CPUs, Image Processors and TV cameras.

Prototypes of small stage microscopes (OPERA emulsions are smaller than the CHORUS ones) are under test. and encouraging results were obtained. The small stages show better performance in terms of speed, accuracy and reproducibility with respect to the larger ones used in CHORUS. A settling time of better than 80 ms was obtained moving from one field of view to the next (350 μm). The image grabbing and processing was performed using a 1 Mpixel CCD TV camera working at 60 frames/sec with a set of 3 parallel image processors. First preliminary results show that a scanning speed of about 10 cm^2/hour is feasible. This system is ready to support CCD frame speeds up to 120 frames/sec. Studies on new CCD cameras and CMOS sensors are under way. Additional speed improvement can be obtained by faster processors being available on the market.

Tests on new optics are in progress to optimise the use of large (350x350 μm^2) fields of view (CHORUS typical field size was 100x100 μm^2 due in part to the bad planarity of the image edges). The aim is to use objectives without immersion oil and with full planar image. The present optics production on the market proposes infinity corrected optics that was adapted to the microscope prototypes. First results show good planarity and tests are in progress to evaluate their performance when connected to the image processing chain.

2.7.3 R&D on dedicated scanning systems for precise measurements

A dedicated optics of higher magnification and thinner focal depth is required to separate each grain for precise measurements such as: i) dE/dx measurement to reject the charm background to the $\tau \rightarrow \mu$ decay channel by muon identification in the emulsions of the bricks and ii) precise momentum measurement for τ candidate events. R&D for such an optics is being started in Nagoya.

2.8 Scanning strategy and related tests

2.8.1 Changeable Sheets

We are considering the possibility to use Changeable Sheets (CS) instead of the Veto sheets surrounding the brick during the cosmic ray exposure (see Proposal p. 130). A CS is an emulsion sheet which is placed downstream of a brick along the neutrino beam direction. Assuming that this CS is refreshed before its exposure in order to reduce the recorded track density, it is possible to locate the tracks produced in neutrino interactions in the CS by the "general scan" technique. These tracks are then followed back through a "scan back" procedure in order to locate the position of the primary vertex. The CS approach has been used in several experiments (E531 and E653 at FNAL, CHORUS at CERN and E176 at KEK) and it is therefore a well-established technique.

The use of CSs results in two main advantages:

- Reduction of the overall scanning load.
  The scheme foreseen in the Proposal requires the scanning of both SS and Veto sheets (4 emulsion layers in total) in order to subtract the tracks found on Veto sheets from those recorded on SS. Instead, only two emulsion layers have to be scanned with CS, thus reducing by a factor of two the scanning load for the vertex location. This would allow, in turn, an increase of the neutrino flux with respect to the Proposal without a corresponding increase in the number of S-UTS systems.

- Increase of the brick finding efficiency (if needed).
  As described in Section 2.2, one of the main sources of ambiguity to find and extract the brick where a neutrino interaction occured is related to back-scattering tracks.

  A sizable fraction of these back-scattering tracks are low momentum πs, which are not minimum ionizing particles, and electrons, which are not straight tracks even in a single emulsion layer. Moreover, their angular distribution is much wider than that of secondary particles from neutrino interactions (m.i.p.). This means that most of the back-scattering tracks could be discriminated from minimum ionizing base tracks with appropriate cuts.

  Suppose that there is an ambiguity among two bricks, one downstream of the other. This ambiguity can be resolved by extracting the CS between the two candidate bricks and by searching for a minimum ionizing track in this CS. If the actual vertex is in the downstream brick and back-scattering occurred no m.i.p. track is expected.

An increase of the brick finding efficiency would naturally reduce the number of empty bricks which are extracted and, consequently, also the scanning load.

The refreshing of CSs requires much less space than the emulsions of the bricks and should be performed in the Gran Sasso underground laboratory before their exposure.

For the second purpose, the CSs have to be extremely clean so that less than about 0.1 m.i.p. tracks are present on a CS surface. Mis-connection of a fake micro-tracks due to Compton electrons from underground environment can be a problem at such level of cleanness with the present Track Selector algorithm. However, most of such tracks can be easily rejected by eye scan since they are not straight tracks, even in a single emulsion layer. In addition, the grain information from a single emulsion layer can also be used to fit the track trajectory and eliminate Compton electrons.

The CSs are first packed in a laminated paper. They are then put into a "ribbon" like envelope made of carbon fiber sheets. Each ribbon holds all the CSs of a single row of bricks. These ribbons are then inserted into larger envelope stuck behind the wall support structure. Overall, this mechanical solution requires an additional space of $\leq 5\ mm$ along the beam direction.

2.8.2 Track erasing in emulsion analysis

Suppose that a set of emulsion sheets are unpacked and then packed again in between two different exposures. Two groups of tracks, tracks recorded before and after re-packing, can be distinguished easily, because each group of tracks can be connected or reconstructed only in the configuration in which they were recorded. In CHORUS, 1996 and 1997 exposures used this technique without any problem. Emulsion sheets exposed in 1996 were unpacked and packed again in a stack and then exposed in 1997.

Using this technique, micro tracks recorded in emulsion sheets while transportation can be "virtually" erased if a set of emulsion sheets are packed together. One should note that there is a maximum tolerable track density around $10^6/cm^2$ in emulsion sheets which should, of course, not be exceeded. An accumulation of cosmic rays during the transportation of the emulsion sheets from Japan to Europe is expected to be $10^3/cm^2$ assuming 1 month on ship. This should not be a problem.

Tests on this new scheme are planned to check the remaining isolated base-tracks after rejecting all the base-tracks recorded while emulsion sheets are packed for transportation. The emulsion sheets of a brick, used in May test exposure, were refreshed and packed in Nagoya ground lab, transported to CERN by air and then assembled as a brick at the CERN ground lab. Those sheets were analyzed and the remaining base-tracks were amounting to $176/cm^2$. This is consistent with the accumulation of cosmic rays at ground level for 3 hours.

For a complete test, we also plan to analyze emulsion sheets refreshed and packed in an underground laboratory in Japan. They will be exposed to cosmic rays on surface and then unpacked and developed underground.

2.8.3 Track reconstruction efficiency

The micro-track reconstruction efficiency of the latest emulsion sheets developed by Fuji Co. (H416-01) was evaluated using the UTS. About 98% efficiency for micro tracks was observed. The tuning of the readout chain (thickness of the emulsion layer, optics, ADC gain, etc.) is in progress and thus the final efficiency could be higher. The detailed information is contained in an OPERA internal note.

2.8.4 Momentum measurement by Angular Method

We present a test of the momentum determination in an ECC brick using a Multiple Coulomb Scattering measurement by the "angular method". The results achieved with a $3X_0$ brick exposed to 2 and 3 GeV/c π^- are shown.

The ECC used here is made of 19 cells, each of them consisting of 1 mm lead plate followed by 305 μm thick Emulsion Sheet (ES). An ES is made up of a pair of emulsion layers 60 μm thick on either side of a 185 μm plastic base. Emulsion sheets are produced by the Fomos company.

2.8.5 γ detection

The detection of γs or electron pairs is being studied in CHORUS, DONUT and in a test exposure performed in May for OPERA. The pointing accuracy and the detection efficiency are essential, since the identification of the γs originating from τ decays among the γs produced in neutrino interactions is very important to increase the sensitivity to the $\tau \rightarrow h$ decay channel.

The pointing accuracy was evaluated with CHORUS and DONUT data. We indicate with $\Delta\theta$ the difference between the average angle of an electron pair, immediately after conversion, and the angle of the line which connects the interaction point to the conversion point.

In CHORUS, all electron pairs in about 100 cm^3 emulsion volume (about 0.5 X_0 in beam direction) were first reconstructed by the NetScan method and then they were checked by eye to confirm that they are really electron pairs. In the same volume, 140 neutrino interactions were also reconstructed by NetScan. Neutrino interaction vertices are defined by requiring at least two tracks with angle less than 0.3 rad with respect to the beam direction. The average charged multiplicity for these vertices amounts to about five.

In DONUT, a search for electron pairs has been performed in a volume of 2.6 $mm \times$ 2.6 $mm \times 13$ mm (about 0.5 X_0 along the beam) around the located neutrino interactions. Up to now, 50 electron pairs were confirmed by eye check among the reconstructed down-going stopping tracks from 97 interactions. An evaluation of the reconstruction efficiency is in progress.

The energy resolution for γs and the reconstruction of the π^0 mass peak is also being studied.

3 Status of the experiment

The experiment has been approved as CNGS1 and it is now entering the construction phase after the completition of the design studies and of the tests of prototypes. An organization structure has been formed in order to fulfill the detector construction. The spokesperson is P. Strolin. The OPERA collaboration includes about 150 physicists from 32 institutes.

References

[1] An appearance experiment to search for $\nu_\mu \rightarrow \nu_\tau$ oscillations in the CNGS beam, Experiment Proposal, The OPERA Collaboration, CERN/SPSC 2000-028, SPSC/P318, LNGS P25/2000, July 10, 2000.

[2] Status Report on the OPERA experiment, The OPERA Collaboration, CERN/SPSC 2001-025, SPSC/M668, LNGS-EXP 30/2001 add. 1/01, August 21, 2001.

THEORY GROUP

Z.Berezhiani, V.Berezinsky, D. Delepine, G. Di Carlo, A. Galante, A.F.Grillo, F.Vissani.

The activity of the group in year 2001 has concerned research in three fields: Astroparticle Physics, Particle Phenomenology and Lattice Gauge Theory. The activities are more specifically reported below.

1 Astroparticle Physics

The Astroparticle group of LNGS in 2001 included V.Berezinsky, F.Vissani and visitors V.Dokuchaev (Institute for Nuclear Research, Moscow), B.Hnatyk (Lviv University, Ukraine) ,S.Grigorieva (Institute for Nuclear Research, Moscow) and O.Petruk (Lviv University, Ukraine). The group worked in close collaboration with A.Vilenkin (Tufts University, USA), M.Kachelriess (CERN), P.Blasi (Fermilab), A.Strumia (Pisa University), G.Senjanovich (ICTP, Trieste) and others

Scientific work

The main field of the work is astroparticle physics, including solar neutrinos, physics in underground detectors, massive neutrinos, ultra high energy cosmic rays, topological defects, and relativistic astrophysics. From several works finished in 2001 two following results can be mentioned

V.Berezinsky, B.Hnatyk and A.Vilenkin developed the model of GRB production by cusps of superconducting strings suggested by them in 2000. The short pulse of low frequency e-m radiation emerges during a cusp event. It produces the beam of accelerated particles, which plays a role of fireball in GRB. This model has essentially one free parameter and successfully explains the range of observed fluences, rate of GRBs, rate-fluence dependence, and the range of durations. Acceleration of particles is now studied in details. It is demonstrated how galactic GRBs can be generated. The calculated diffuse X-ray and gamma-radiation agrees with observations of EGRET. The generation of gravitational pulses in cusp events is calculated. The paper is published in Phys.Rev. D64 (2001) 034007.

A.Strumia and F.Vissani have evaluated the sensitivity of KamLAND and Borexino to the parameters of solar neutrino oscillations. The error on Δm^2 will be few per-mille in (Q)VO, a few percent in LMA, and around 10% in LOW regions; the error on $\sin^2 2\theta$ is $\sim 5\%$. KamLAND and Borexino will tell us which new measurement devoted to pp neutrinos is able to improve on these parameters. The paper is published in JHEP 0111 (2001) 48.

Conferences

V.Berezinsky and F.Vissani have organized the 5th International Topical Workshop "Solar Neutrinos: Where are the Oscillations?" (Gran Sasso, March 12 - 14, 2001. The workshop collected most active people in the field from Europe and USA. The emphasis was traditionally given to the discussions. About 100 participants attended the workshop.

V.Berezinsky was a member of the Organizing Committee of TAUP 2001 in Gran Sasso, and F.Vissani - a convener of astrophysical session at Europhysics Conference HEP 01 in Budapest in July 2001.

F.Vissani works (together with O.Palamara) as the organizer of the LNGS seminar.

V.Berezinsky participated as invited speaker in Conferences "Neutrino Telescopes" in Venice, in NANP 2001 in Dubna, in SUSY 2001 in Dubna, and in "Astroparticle workshop" in Heidelberg.

F.Vissani presented the talks at Europhysics Conference HEP-01 (Budapest), at Int. workshop "Matter, Antimatter and Dark Matter" (Trento) and at TAUP 2001 (Gran Sasso).

Journal and Proceedings publications of 2001

1. V.Berezinsky and M.Lissia, "Electron-neutrino survival probability from solar-neutrino data" Physics Letters B521 (2001) 287

2. V.Berezinsky, M.C.Gonzalez-Garcia, and C.Pena-Garay, "Status of the Gribov-Pontecorvo solution to the solar-neutrino problem" Phys. Lett. B517 (2001) 149.

3. V.Berezinsky, B.Hnatyk, and A.Vilenkin, "Gamma ray bursts from superconducting cosmic strings" Phys. Rev. D64 (2001) 043004.

4. V.Berezinsky and M.Kachelriess, "Monte Carlo simulation for jet fragmentation in SUSY-QCD". Phys. Rev. D 63 (2001) 034007.

5. V.S.Berezinsky and V.I.Dokuchaev, "Hidden source of high-energy neutrinos in collapsing galactic nuclei" Astrop.Physics, 15 (2001) 87.

6. V.Berezinsky, "Oscillation solutions to solar-neutrino problem" Nucl. Physics Proc. Suppl. B80 (2000) 17.

7. V.Berezinsky, "Puzzles in astrophysics in the past and present" Proc.9th Int. Workshop "Neutrino Telescopes",ed. Milla Baldo Ceolin, 1 (2001) 13

8. A.Strumia and F.Vissani, "Which solar neutrino experiment after Kamland and Borexino?" JHEP 0111 (2001) 048

9. D.Delepine and F.Vissani, "Indirect bounds on $Z \to \mu e$ and lepton flavor violation at future colliders" Phys.Lett. B522 (2001) 95.

10. F.Vissani, "Expected properties of massive neutrinos for mass matrices with a dominant block and random coefficients order unity" Phys.Lett. B508 (2001) 79.

11. F.Vissani, "Charm production by cosmic muons" Astropart.Phys.15 (2001) 217.

12. F.Vissani, Non-oscillation searches of neutrino mass in the age of oscillations" Nucl.Phys.Proc.Suppl.100 (2001) 273

13. F.Vissani, "The weight of neutrinos and related questions" Proceedings of 'Dark matter in astro- and particle physics, DARK 2000, Heidelberg, 435, 2001.

14. F.Vissani, "What is the standard model of elementary particles and why we have to modify it. Conference Proceeding v 73, 'Frontier Objects in Astroparticle and Particle Physics', eds. F.Giovannelli and G.Mannocchi, SIF Bologna, pages 117-135, 2000.

15. B.Bajk, G.Senjanovich and F.Vissani, "How neutrino and charged fermion masses are connected within minimal supersymmetric SO(10)" Proc. of EPS Int. Conf. on HEP, Budapest, 2001 (eds D. Horvath, P. Levai, A. Patkos), JHEP Proceedings Section, PrHEP-hep2001/198

Preprints of 2001

1. V.Berezinsky, M.Kachelriess, and S.Ostapchenko,, "Extensive air showers from ultra high energy gluinos" astro-ph/0109026

2. V.Berezinsky, "Exact analysis of the combined data of SNO and Super-Kamiokande" astro-ph/0106166

3. V.S.Berezinsky, A.Z.Gazizov and S.I.Grigorieva, "Ultra high energy cosmic rays from extragalactic astrophysical sources" astro-ph/0107306.

4. F.Vissani, "Is a coherent picture of massive neutrino emerging?" hep-ph/0102235

5. F.Vissani, "A statistical approach to leptonic mixing and neutrino masses" hep-ph/0111373

2 Particle Phenomenology

The particle phenomenology group which included Z. Berezhiani, P. Ciarcellutti, D. Delepine, L. Gianfagna and M. Giannotti worked in close collaboration with A. Rossi (Padova), D. Comelli, A. Drago, F. Villante (Ferrara), A. Kobakhidze (Helsinki), L. Bento (Lisbon) and others.

Scientific work

The main field of the groups activity is the particle phenomenology, including supersymmetry and grand unification, flavour problem, CP violation, neutrino physics, and various implications of particle physics for the Early Universe, like inflation, baryogenesis, dark matter etc. Fromseveral works done in 2001 the following results are to be mentioned.

Z. Berezhiani, D. Comelli and F. Villante have studied a cosmological evolution of the hidden mirror universe, an identical copy of the observed particle world interacting with the latter only gravitationally. Its existence can be motivated in the context of string or brane world theories, namely the epochs of the inflation, baryogenesis, nucleosynthesis and photon decoupling. The primordial nucleosynthesis bounds demand that at the Big Bang the mirror particle sector is born with a lower temperature than the ordinary one. As it was suggested by Z. Berezhiani and L. Bento, the concept of such a hidden sector offers new mechanism for the primordial baryogenesis. Namely, non-zero lepton and baryon numbers in the Universe can be generated by out-of-equilibrium scattering processes which transform ordinary leptons and Higgses into their hidden partners, while the same scatterings generate analogous asymmetry in mirror sector and thus mirror baryons can constitute dark matter, with strong implications for the large scale and galactic halo structures, CMBR angular anisotropies, microlensing, etc.

Z. Berezhiani and A. Rossi have studied the fermion mass and mixing structure in supersymmetric theories with the flavour symmetry between families. It was shown that the concept of spontaneously broken symmetry $SU(3)_H$ can allow to naturally explain the origin of the fermion mass and mixing hierachy and provide fermion mass textures with testable predictions in confront of the experimental situation concerning the quark and lepton mixing angles and CP-violation parameters.

Z. Berezhiani, L. Gianfagna and M. Giannotti have suggested a new type of axion, which emerges in the context of the mirror sector models with spontaneously broken parity. Such an axion can have mass order 1 MeV for the decay constant order $10^5 - 10^6$ GeV, in a sharp difference with the conventional axion models. It was shown that such an axion can be tested with future reactor or beam dump experiments, and various astrophysical implications have been discussed. In particular, it can explain the origin of Gamma Ray Bursts via mechanism suggested by Z. Berezhiani and A. Drago, related to emission of such axion-like particles from collapsing objects and their further decay info e^+e^- pairs.

Participation in conferences

Z. Berezhiani presented invited talks at Fifth Topical Workshop "Solar Neutrinos: Where are the Oscillations?", (Assergi, Italy, 12-14 March 2001); Int. Workshop on extra dimensions "Living on the Wall", (Minneapolis, USA, 21 May - 1 June 2001); Joint UK BSM - Cosmology Conference (Ambleside, UK, 27-28 Aug. 2001); Int. Workshop on QCD "Ioffe-fest: 75 Anniversary of B.L. Ioffe", (Gif-sur-Yvette, Paris, 3-5 Sept. 2001); 18th Symposium "100 Years of Werner Heisenberg", (Bamberg, Germany, 26-30 Sept. 2001); and delivered lectures on supersymmetry and grand unification at National Summer School on Particle Astrophysics "Astroscuola", (Conca Specchiula, Otranto, Italy, 11-16 June 2001).

Publications

1. Zurab Berezhiani, Anna Rossi, "Predictive Grand Unified textures for qaurk and neutrino masses and mixings", Nucl. Phys. B594, pp.113-168, 2001.

2. Zurab Berezhiani, Leonida Gianfagna, Maurizio Giannotti, "Strong CP problem ans Mirror World: the Weinberg-Wilczek axion revisited", Phys. Lett. B500, pp.286-296, 2001.

3. Zurab Berezhiani, Denis Comelli, Francesco L. Villante, "The early Mirror Universe: Inflation, Baryogenesys, Nucleosynthesys and Dark Matter", Phys. Lett. B503, pp.362-375, 2001.

4. Z. Berezhiani, M. Chaichian, A. Kobakhidze, Z.H. Yu, "Vanishing of Cosmological Constant and fully localized gravity in a brane world with extra time(s)", Phys. Lett. B517, pp.387-396, 2001.

5. G.C. Branco, D. Delepine, R. Gonzalez Felipe, "Dynamical CP violation and flavor changing processes", Nucl. Phys. B607, pp.268-292, 2001.

6. Z. Berezhiani, A. Mazumdar, A. Perez-Lorenzana, "Affleck-Dine Leptogenesis via right handed sneutrino fields in a supersymmetric hibrid inflation model", Phys. Lett. B518, pp.282-293, 2001.

7. Z. Berezhiani, I. Gogoladze, A. Kobakhidze, "TeV scale Unification in four-dimensions versus extra dimensions", Phys. Lett. B522, pp.107-116, 2001.

8. Zurab Berezhiani, Anna Rossi, "Flavor structure, flavor symmetry and supersymmetry", Nucl. Phys. B, Proc. Suppl. 101, pp.410-420, 2001.

9. David Delepine, Francesco Vissani, "Indirect bounds on $Z \to \mu e$ and lepton flavor violation at future colliders", Phys. Lett. B522, pp.95-101, 2001.

10. Zurab Berezhiani, Alessandro Drago, "GRB, SN and the monster Axion", Proc. Third Int. Conf. "New Worlds in Astroparticle Physics", Eds. A. Mourao et al., Singapore, World Scientific, pp. 170-176, 2001

11. Luis Bento, Zurab Berezhiani, "Blocking active-sterile neutrino oscillations in the Early Universe with a majoron field", Phys. Rev. D 64:115015, pp.1-8, 2001.

12. Luis Bento, Zurab Berezhiani, "Leptogenesis via collisions: the Lepton number leking to the hidden sector", Phys. Rev. Lett. 87:231304, pp.1-4, 2001.

13. Luis Bento, Zurab Berezhiani, "Baryogenesis: the lepton leaking mechanism", e-Print Archive: hep-ph/0111116, to be published in Proc. 11th Int. School on "Particles and Cosmology", Baksan Valley, Russia, 18-24 Apr 2001.

14. Zurab Berezhiani, Anna Rossi, "limits on non standard interactions of neutrinos from e^+e^- colliders", e-Print Archive: hep-ph/0111137, accepted in Phys. Lett. B

15. Zurab Berezhiani, R.S. Raghavan, Anna Rossi, "Probing non standard couplings of neutrinos at the Borexino detector", e-Print Archive: hep-ph/0111138, submitted to Phys. Lett. B

3 Lattice Gauge Theory

The group consisted in G. Di Carlo (also LNF), A.F. Grillo and A. Galante from the University of L'Aquila , in collaboration with V. Azcoiti (Zaragoza), V. Laliena (Zaragoza), E. Follana (Glasgow), R. Scimia (Perugia).

We have analyzed the phase diagram of SU(2) at finite baryonic density; in particular we have addressed the diquark condensation phenomenon using an original technique that elimiates the need of an explicit di-quark source in the action.

We have also studied from the point of view of numerical non perturbative renormalization the non compact formulation of lattice gauge theories proposed by F. Palumbo. We have shown that the results coincide to those in the Wilson formulation with the advantage of larger physical volume for fixed number of lattice sites without the use of improved actions with empyrical parameters. In this sense this non compact formulation is nearer to the continuum and less affected by discretization artifacts.

We have recently approached the study of QCD with a topological term in the action. This analysis is related to our work on finite density since in both cases the action is complex, and the importance sampling cannot be used in simulations. All the earlier attempts failed to reproduce the analytically known results in simple 2-dimensional models (CP(N-1) and U(1)); in particular the methods based on binning and/or reweighting introduce spurious transitions for theta smaller than pi, transitions that are pure numerical artifacts.

To address this problem we have developed an evaluation method for the free energy density as a function of theta that, using analysis methods in arbitrary precision arithmetics, allowed us to reproduce the analytical results with a precision better than one per cent. We are presently writing two papers on the argument describing the numerical scheme and the continuum limit of the CP(3) model. These results will be extended to other statistical models with complex actions like the Hubbard model and to gauge theories (e.g. SU(2)) with a topological term.

Publications

1. G. Di Carlo, R, Scimia, "Numerical study of the scaling properties of SU(2) lattice gauge theory in Palumbo non-compact regularization", Phys.Rev. D63 (2001) 094501.

2. R. Aloisio, V. Azcoiti, G. Di Carlo, A. Galante, A.F. Grillo, "Probability Distribution Function of the Diquark Condensate in Two Colours QCD", Nucl. Phys. B (2001) (in press)

Conference Proceedings

1. Giuseppe Di Carlo, Fabrizio Palumbo, Roberto Scimia, "Larger physical volume with a noncompact lattice regularization of SU(N) theories",hep-lat/0110133

TRIS

E.Battistelli[a], G.Boella[a], F.Cavaliere[b], A.De Lucia[a],
M.Gervasi[a], A.Passerini[a], G.Sironi[a], A.Tartari[a], M.Zannoni[a]

[a] Dipartimento di Fisica G. Occhialini - Universita‘ degli Studi - Milano Bicocca - Italy
[b] Dipartimento di Fisica - Universita‘ degli Studi - Milano - Italy

Abstract

TRIS, a set of three absolute radiometers for measurements of the absolute temperature of the sky at 600 MHz, 820 MHz and 2.5 GHz, has been prepared by the Milano Radio Group and installed at Campo Imperatore with the aim of detecting deviations from a Planck distribution in the spectrum of the Cosmic Microwave Background, relic of the Big Bang. Observations ended in December 2000. During the first six months of 2001 we planned to carry on supplementary observations before closing the experiment. Unfortunately very bad weather conditions which affected the power supply line forced us to turn off the receivers at the end of January. In May when snow melted the experiment was definitely closed and the Campo Imperatore area cleared. Data reduction is now underway.

1 Introduction

TRIS was set up at the beginning of the ‘90 with the aim of detecting deviations from a Planck Distribution in the low frequency spectrum of the Cosmic Microwave Background (CMB), relic of the Big Bang ([1]). Observations were made with a set of three absolute radiometers at 600 MHz, 820 MHz and 2.5 GHz and included: i)absolute measurements of the sky temperature, ii)measurements of the spectral shape of the galactic diffuse background, superimposed to the CMB, iii)evaluation of undesired contribution, namely ground and atmospheric radiation.

2 2001 activity

The observational program was completed in December 2000 when the last run of absolute measurements of the sky temperatrure, made using a large cryogenic (Liquid Helium) calibrator were finished ([2], [3], [4], [5]). Because at that time moving heavy equipment from Campo Imperatore to Assergi was impossible because of snow, we planned to use the first six months of 2001 to carry on additional measurements. Unfortunately very bad weather conditions affected the power supply line and forced us to turn off the receivers at the end January. In May when the snow melted, the experiment was definitely closed and the equipment sent back to Milano. We are now reducing the data.

3 Conclusions

The data we collected in the past years are promising: we expect to be able to improve the accuracy of the meaasured values of the CMB temperature at frequencies close to 1 GHz. Detection of distortions in this region are interesting because they offer the opportunity of evaluating Ω_b the barionic density in our Universe.

4 List of Publications

1. M. Zannoni et al. 2000 : The Spectral Index of the Galactic foreground affecting CMB measurements IAU Symp. 201 on New Cosmological Data and the Values of the Fundamental Parameters : in press

References

[1] G. Bonelli, M. Gervasi, G. Giardino, G. Sironi, M. Zannoni 1995: Low frequency observations of the cosmic microwave background radiation: the Campo Imperatore Experiment Ap. Lett. Comm. 32, 15

[2] M. Zannoni, G. Boella, G. Bonelli, F. Cavaliere, M. Gervasi, A. Lagostina, A. Passerini, G. Sironi, A. Vaccari 1998: TRIS EXPERIMENT: a search for spectral distortions in the CMB spectrum close to 1 GHz AIP Conf. Proc. 476, 165

[3] R. Baselli, G. Boella, G. Bonelli, P. Buratti, F. Cavaliere, M. Gervasi, A. Lagostina, A. Passerini, G. Sironi, A. Vaccari, M. Zannoni 1999: TRIS - A search for distortion in the spectrum of the Cosmic Microwave Background INFN-LNGS Annual Report 1998, pag. 187 Second reference.

[4] R. Baselli, G. Boella, P. Buratti, F. Cavaliere, A. de Lucia, M. Gervasi, A. Passerini, D. Restifo, G. Sironi, D. Spiga, M. Zannoni 2000: TRIS: A Measurement of the Spectral Index of the Galactic Diffuse Emission INFN-LNGS Annual Report 1999, pag. 173

[5] M. Zannoni, E. Battistelli, G. Boella, F. Cavaliere, M. Gervasi, A. Passerini and G. Sironi 2000 : TRIS Experiment: Recent Measurements of Spectral Index of the Galactic Duffuse Emission SIF Conf. Proc. 68, 179

ENVRAD. Radon groundwater analysis

Francesco Bella[a] and Wolfango Plastino[a,b]

[a] Department of Physics, University of Roma Tre, via della Vasca Navale, Rome (Italy)
[b] INFN, Section Rome III, via della Vasca Navale, Rome (Italy)

Abstract

During the radon groundwater monitoring some *anomalies* have been recorded in geophysical and geochemical groundwater parameters emphasizing an high correlation with tectonic deformation processes and local seismicity [1,4]. In particular, during 2001 strong long and short time variations in pH and electrical conductivity have been recorded. These are probably related to seismic clusters located near the measurement site.

1 Introduction

The hydrological properties of the Gran Sasso aquifer are characterized by an high dynamics behaviour due to high permeability of the rocks. From May 1996, geophysical investigations by an automatic multiparametric equipment have being performed at Laboratori Nazionali del Gran Sasso-INFN to better define the hydrological setting near the overthrust fault and, particularly, to study the link between the possible radon variations and the seismic activity [1,4].

2 Results

The trends of the geochemical parameters monitored during the period from May, 1996 to December, 2001 are shown in figure 1.

The data of the groundwater temperature sensor from July, 1997 to September, 1997 are not supplied for the breakdown between the thermocouple output and the analogic input channel.

The trends of the setting parameters monitored during the period from May, 1996 to December, 2001 are shown in figure 2.

The ε Dobrovolsky's parameter [5] is computed by means of the seismic events of INGV (National Institute for Geophysics and Volcanology) catalogue recorded within a

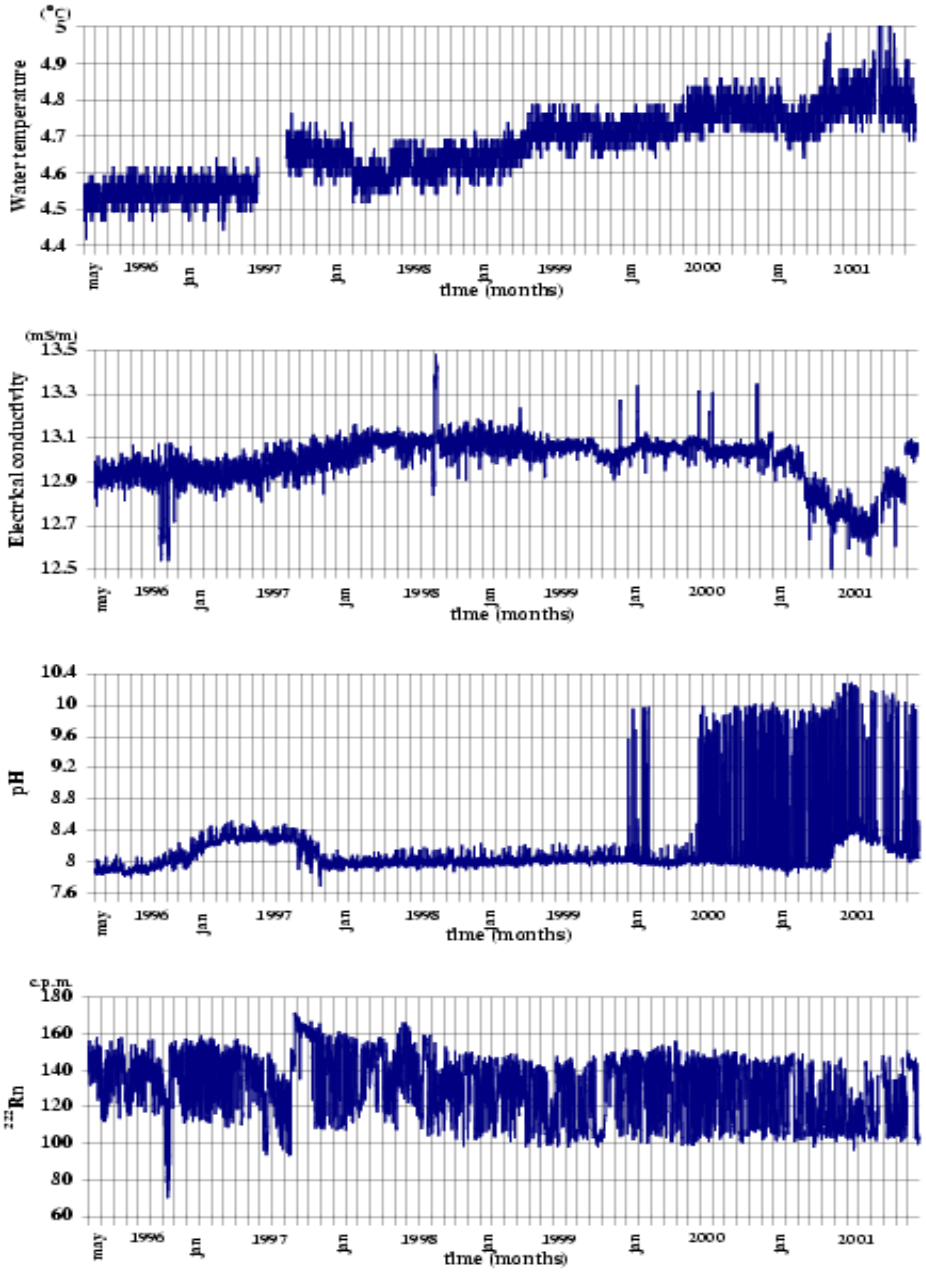

Figure 1: The trends of the geochemical parameters monitored during the period from May, 1996 to December, 2001.

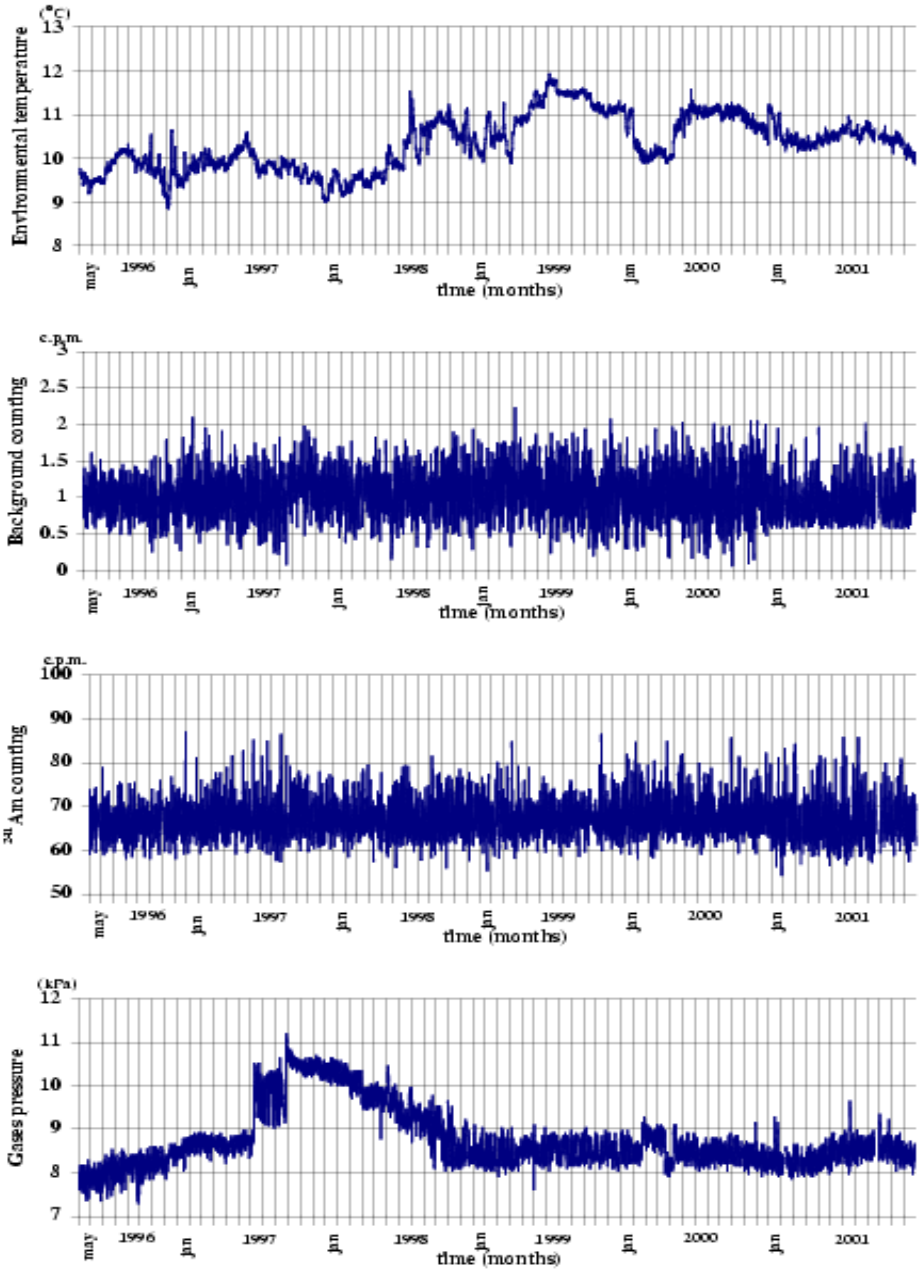

Figure 2: The trends of the setting parameters monitored during the period from May, 1996 to December, 2001.

distance of 100 km from the measurement site and available from May, 1996 to December, 2001 [6]. We have considered an inferior limit of ε equal to $0.1 \cdot 10^{-8}$.

The ε Dobrovolsky's parameter during the above mentioned period is shown in figure 3.

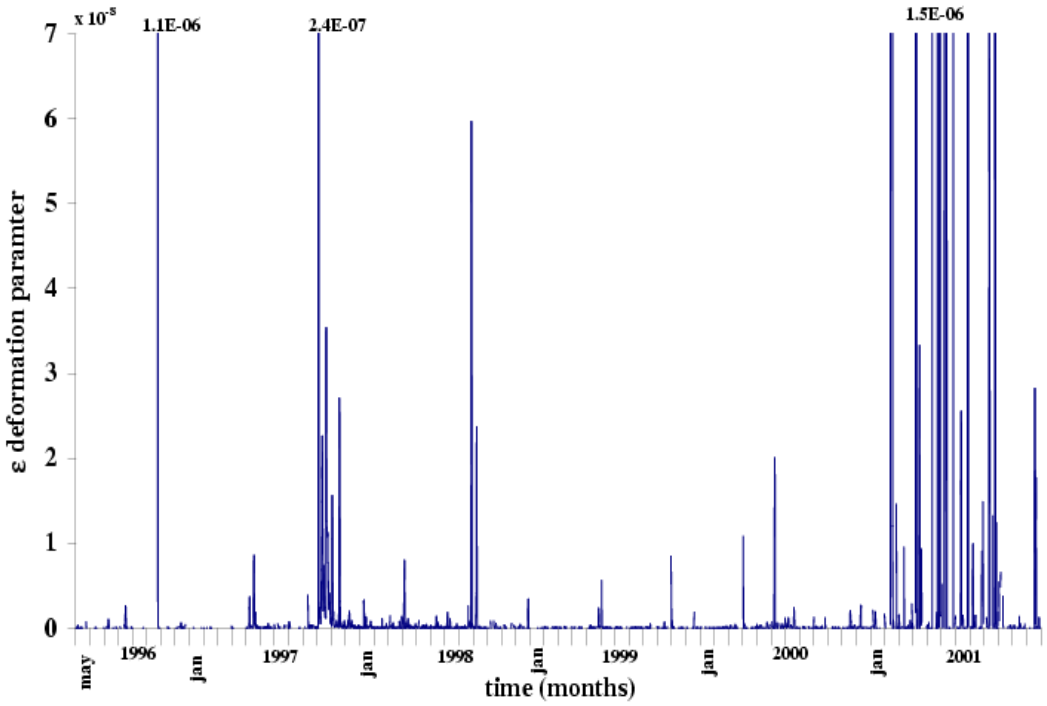

Figure 3: Dobrovolsky's parameter during the period from May, 1996 to December, 2001.

3 Discussion

The analysis of raw data shows long time variations in pH, radon and pressure of solved gases highly correlate with the Umbria-Marche seismic sequence (1997-1998) and probably due to the occurrence of transient compression phase producing a change of the carbon dioxide content in groundwater. Also, electrical conductivity spike-like *anomalies* are related to local seismic events emphasizing variations in groundwater dynamics [1,4].

During the period from January, 2000 to February, 2000 and from July, 2000 till now pH spike-like *anomalies* have been point out. Furthermore, from May, 2001 to December, 2001 a long time pH variation superimposed to the above mentioned pH anomalies has been recorded. Also, electrical conductivity spike-like *anomalies* have been point out

during the above mentioned periods and a long time variation from December, 2000 to December, 2001 has been recorded. The groundwater temperature shows during the period from June, 1998 to December, 2000 a rise trend with a maximum excursion of 0.2°C and a long time variation from February, 2001 to December, 2001. The long time temperature and pH variations are directly related and inversely related to the long time electrical conductivity variation. This phenomenology is probably due to mixing of groundwater through the tectonic discontinuities which separate dolomitic limestones from sileceous limestones emphasizing a local deformation process. Furthermore, during the above mentioned periods any radon anomalies have been recorded because these are related to strong variations of carbon dioxide content in groundwater as shown during the Umbria-Marche seismic sequence (1997-1998) [2,4].

Using the ε Dobrovolsky's parameter, seismic clusters probably related to detected pH and electrical conductivity long time and spike-like *anomalies* have been identified. This seismic activity is located in NW-W-SW direction from the measurements site.

4 Conclusion

During 2001 the analysis of the geophysical and geochemical parameters has emphasized strong *anomalies* in pH and electrical conductivity probably related to mixing of the groundwater through mylonitized faults. The occurrence of this phenomenology may be justified by local deformation process producing rock permeability variations and related to seismic clusters occurred in NW-W-SW direction respect to LNGS.

Acknwoledgments The authors wish to thank Prof. Alessandro Bettini for the his kind collaboration and the Dr. Raffaele Adinolfi Falcone, Dr. Alfredo Fulgenzi, Mr. Massimiliano De Deo, Mr. Nicola Massimiani, Mr. Nando Polidoro, Mr. Fabrizio Torelli of the LNGS and Mr. Fabio Basti, Mr. Antonio Miriametro of the University of Rome "La Sapienza" for the useful and precious assistance. The authors are grateful to Dr. Rita Di Giovambattista for the seismological data and Dr. Domenico Giambuzzi and Mr. Maurizio Faragalli of the Azienda Speciale Acquedotto del Ruzzo for tha data provided.

References

[1] Plastino, W. and F. Bella, 2001, *Radon groundwater monitoring at underground laboratories of Gran Sasso (Italy)*, Geophysical Research Letters, 28 (14), 2675-2678.

[2] Bella, F. and W. Plastino, 1999, *Radon time series analysis at LNGS, I*, LNGS Annual Report 1999, INFN, 193-198.

[3] Bella, F. and W. Plastino, 2001, *Radiocarbon and radon analysis for geophysical monitoring of Gran Sasso aquifer*, LNGS Annual Report 2000, INFN, 187-194.

[4] Plastino, W., Bella, F., Catalano, P.G. and R. Di Giovambattista, *Radon groundwater geochemistry related to seismic events in central Appenines (Italy)*, submitted to Journal of Geophysical Research.

[5] Dobrovolsky, I.P., Zubkov, S.I and V.I. Miachkin, 1979, *Estimation of the size of earthquake preparation zones*, Pure and Appl. Geophys., 117, 1025-1044.

[6] INGV, Istituto Nazionale di Geofisica e Vulcanologia, 1996-2001, *Seismological Bulletins*, Roma.

GIGS. The Interferometric Station at LNGS

Antonella Amoruso[a,c], Luca Crescentini[b,d], Roberto Scarpa[a,c]

[a] Dip.to di Fisica Univ. dell'Aquila, L'Aquila - Italy
[b] Dip.to di Scienze della Terra Univ. di Camerino, Camerino (MC) - Italy
[c] INFN - Gruppo collegato dell'Aquila, L'Aquila - Italy
[d] INFN - LNGS, L'Aquila - Italy

Abstract

During 2001 strain data have been recorded continuously, apart from an unexpected four-month interruption in summer, due to the unusually long time required for changing the laser tube. Several months of tidal records have been analyzed and modelled. As regards slow earthquakes (the main scientific results obtained so far) we have performed a detailed study of ground deformation at the interferometer site caused by slow slips on nearby capable faults. All faults but one give expected signals quite different from observations. The possibility of a slow slip diffusion has been related to the presence of a gouge layer between fault faces, with a visco-plastic rheology.

1 Introduction

The interferometric station at LNGS consists of two 90-m long laser interferometers for geophysical purposes. Their azimuth are N66E and N24W, i.e. approximately perpendicular and parallel to the Apennines. Any interferometer measures the difference in extension between two baselines. ¿From May 1994 to October 1995 we have monitored the extension of a 90-m long baseline (azimuth = N66E), using a 20-cm long reference baseline (unequal-arm configuration). Laser frequency fluctuations can give spurious signals whose amplitude depends on the difference in length between the two baselines. In order to check for the effects of fluctuations of the laser wavelength on the recorded signal from December 1995 to October 1998 both arms were 90-m long and one component of shear strain was measured (equal-arm configuration). Some instrumental changes in 1999, which caused the instrument to stop working for several months, allowed to measure extensions of the two baselines independently, so that now also areal strain can be obtained. After a few months of test runs, and several interruptions due to problems with the hard disks, from August 2000 we are routinely recording the extension of both baselines at 5 Hz, apart from an unexpected four-month interruption in summer 2001, due to the unusually

long time required for changing the laser tube. In what follows, extensions are expressed as dimensionless strain, $\Delta l/l$, where l is instrument length, and Δl is positive for an increase in length. We use the symbol nϵ, nanostrain, for $\Delta l/l = 10^{-9}$. The instruments are characterized by very high sensitivity ($\approx 3 \times 10^{-3}$nϵ), wide frequency band (from d.c. up to hundreds of Hz), large dynamic range (unbounded in principle), and good reliability. During the transit of teleseismic waves it recorded signals as large as 600 nϵ and as fast as 100 nϵ/s without any nonlinearity or abnormal behavior. The experiment has been planned for a better knowledge of crustal deformation processes, due to tectonics (strain accumulation and release, aseismic slips, coseismic steps and earthquakes - regular and slow) as well as to earth tides.

2 Earth tides

Tidal strain depends on local elastic properties. These could change during earthquake nucleation (dilatancy effects). As previously mentioned, the Gran Sasso interferometer is producing shear-strain data since 1996, apart from interruptions caused by technical works to improve the instrument. So we can search for possible changes in the local response to tidal forcing before, during, and after the slow earthquake crisis. As a first step, we have decided to analyze data recorded for several months starting from August 2000, since the knowledge of areal and shear strain gives better information about the strain field and bigger check opportunities. Records from August 2000 to March 2001 have been preliminarly analyzed and compared with theoretical predictions in the case of an elliptic rotating Earth and taking into account ocean loading effects. Theoretical predictions have been generated by using the GOTIC2 code [1] and satellite altimetric data from TOPEX/POSEIDON. The period under examination was brief and lacking any noticeable event. As expected, tidal response was constant during it. Ocean loading effects account for about 10% of total expected tidal signal, in the case of the reference layered Earth (PREM). Both areal and shear strain are about 20% smaller than predicted. Such differences could be caused by topographic effects, but the release of GOTIC2 available at that time had a severe bug which resulted in erroneous loading estimation for shear stress and further work is necessary. Difficulties in obtaining a good model of topographic effects make the retrieval of local lithospheric properties from ocean loading effects a quite hard task. Topographic effects could be estimated comparing interferometric records of long-period seismic waves with seismograms recorded by the very-broad-band seismometer of the INGV at work in L'Aquila. Work in cooperation with Andrea Morelli (INGV - Rome) is in progress.

3 Slow earthquakes

Several clustered slow earthquakes have been recorded by the geodetic interferometer from March to October 1997 (see 1999 LNGS Annual Report). Half of the events were recorded from mid March to mid April. The swarm was preceded by few events occurring since the end of 1996 and followed by other episodic events. As mentioned in the Introduction, until 1999 the interferometer measured difference in strain between one baseline oriented

N66E and another baseline oriented N24W, i. e. one shear-strain component. Sampling frequency was 0.5 Hz. Slow earthquakes appear as nearly-exponential strain changes with duration from tens to thousands of seconds and amplitudes of a few nanostrains. Three more slow earthquakes have been recorded on May 2001. The shear-strain component of the signals is very similar to that of the 1997 events, and sources are presumably on the same fault. All the 2001 signals give negative (compressive) areal strain. No strong historical earthquake has been associated with the faults of the Gran Sasso region (central Italy), despite the evidence of relevant quaternary activity. Average slip rate from paleoseismological investigations is of the order of 1 mm/year, similar to that observed in the Fucino area (about 40 km south of Gran Sasso), struck by a destructive earthquake in 1915 (moment magnitude ≈ 7). In cooperation with Andrea Morelli (INGV - Rome), we have tried to locate the fault responsible for the slow earthquake swarm. Comparison of observations with synthetic strain signals not only suggests that the slow earthquakes ruptured a single fault, but also allows to identify the fault. Synthetic seismograms are in agreement with the lack of seismometer observations at L'Aquila. These observations suggest the important role of episodic aseismic faulting throuh slow earthquakes in regions other than subduction zones, characterized by the presence of shallow, unconsolidated sediments, and would have important consequences on evaluating seismic hazard. A paper concerning the results of such researches is about to be submitted for publication. A mechanical model of slow earthquakes has been proposed in collaboration with Michele Dragoni and Antonello Piombo (Physics Department, University of Bologna). According to our model, a slow diffusion-like slip propagation can occur in the presence of an unconsolidated fault gouge imbibed with water, with a visco-plastic rheology. The model shows that when the plastic stress threshold is exceeded at a given point in the fault, a pressure gradient is produced in the gouge layer, originating the viscous flow of the gouge. This entails the slow propagation of slip along the fault. The model succeeds in predicting the observed scaling law between seismic moment and rise time of strain records, i. e. $M \propto \sqrt{t_s}$, as well as the shape of recorded straingrams. Although an extension of our model to other environments is not obvious, it might also account for other slow events characterized by a square-root scaling law between seismic moment and duration, and for tsunami earthquakes, which are characterized by larger tsunamis than expected from their seismic moments and by slow rupture velocity.

4 List of Publications

1. A. Amoruso, L. Crescentini, M. Dragoni, and A. Piombo, Fault slip controlled by gouge rheology: A model for slow earthquakes, submitted for publication.

References

[1] Matsumoto, K., T. Sato, T. Takanezawa, and M. Ooe, GOTIC2: A Program for Computation of Oceanic Tidal Loading Effect, *J. Geod. Soc. Japan*, *47*, 243-248, 2001.

LNGS-EXP 20/99. Measurement of the Radon concentration in the water from the Gran Sasso fault

D. Barbaresi[a], A. Bassignani[b], G. Colombo[b], L. Degli Esposti[a], R. Fresca Fantoni[b], G. Giacomelli[a], G. Mandrioli[a], F. Materazzi[b], D. Matteuzzi[a], L. Patrizii[a] and G. Sirri[a]

[a] Dipartimento di Fisica dell'Università di Bologna and INFN, Bologna
[b] Eni S.p.A. Agip Division, Radiation Protection Department, San Donato Milanese

Abstract

Since 1999 the Rn concentration in the groundwater from the fault in the interferometric tunnel of the underground Gran Sasso Laboratory has been monitored. The main goal of the experiment is the search for possible correlations between changes of the radon concentration in water and seismic activity.

Water is directly collected from the fractured rock and radon gas is extracted by nitrogen bubbling from samples of water. The detector is a silver activated zinc sulfide scintillator located in an electrostatic chamber.

The apparatus is remotely controlled via internet; a new software for displaying data and monitoring the acquisition has been installed. New data have been collected in 2001; during this period there was some seismic activity .

1 Introduction

Radon contents in groundwaters and in air are being monitored by several experiments with the aim of studying possible correlations between radon concentration variations and seismic phenomena [1-6].

We developed and implemented an automatic instrument for monitoring the radon concentration in groundwater. Since the middle of 1999 this apparatus is collecting data in the interferometric tunnel of the underground Gran Sasso laboratory, near the fault. The fault is one of the most important features of the Gran Sasso Massif.

The apparatus may be considered to complement other instruments that are monitoring seismic activities in the underground laboratory: a geodetic interferometer [2], tiltmeters and the apparatus for groundwater analysis of the University of Roma Tre [3].

Since year 2000 we made measurements of the radon concentration in water with a sampling rate of 2 measurements per day [7].

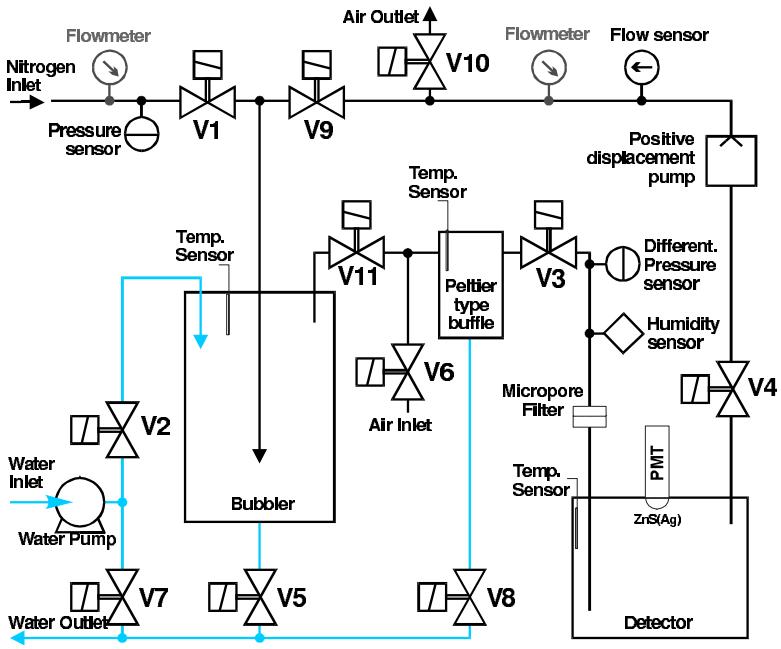

Figure 1: *Layout of the radon extraction system.*

2 The apparatus

The apparatus consists of three sections: the system for the extraction of radon from water, the detection system and the data acquisition and control system. The layout of the extraction system is shown in Fig. 1.

The process starts by flushing the radon extraction system with nitrogen gas; background counting starts immediately after this phase. Then a sample of 1.9 liters of water collected directly from the rock fault is pumped into the bubbler. Radon gas is then extracted from water by nitrogen bubbling. After radon extraction all the valves are closed and radon counting starts. At the end of each counting run, the water is pumped out, and the process restarts.

The detector is a Pylon mod. PMT-EL, which is a silver activated zinc sulfide scintillator ZnS(Ag) located in a 5 litre electrostatic chamber. The scintillator is covered by an aluminized mylar foil that acts as cathode of the electrostatic chamber and collects the positively charged radon daughters. A power supply polarizes the chamber creating a potential difference of about 1000 Volts.

Control processes and data acquisition are performed by a PC with a Pentium processor and two I/O interface boards. The temperatures of the devices, the pressure and air flow in the circuit, the water level and the environmental temperature and pressure are monitored. The computer is remotely controlled via Internet; measurements of parameters and raw data are displayed on web pages.

3 Measurements

A plot of the radon concentration in water in the period June 2001-Feb 2002 is shown in Fig. 2. Atmospheric pressure and detector and bubbling temperatures are shown in Fig. 3. During this period there was a considerable seismic activity around the Gran Sasso Laboratory, as shown by the ϵ deformation parameter in Fig. 4. The data are presently under study.

4 Conclusions

An apparatus for monitoring radon concentration in the water from the Gran Sasso fault has been designed and implemented. The extraction technique and the detector system allow to have a good reproducibility and good count ratio between radon and background.

Data have been taken from June 2001 to February 2002 (Fig. 2). The time series of the data are under study.

Several improvements are in progress. In order to improve the stability of radon extraction and of the detection efficiency, a new air-conditioning system has been installed in the hut. A new system for collecting water is being designed in order to minimize radon exchange phenomena between air and water.

References

[1] M. Noguchi and H. Wakita, A method for Continous Measurement of Radon in Groundwater for Earthquake Prediction, Jou. Geoph. Res. 82 (1977) 1353.

[2] A. Amoruso et al., GIGS. The Interferometric Station at LNGS, LNGS Annual Report (2000) 177.

[3] F. Bella and W. Plastino, Radiocarbon and Radon analysis for geophysical monitoring of Gran Sasso acquifer, LNGS Annual Report (2000) 187.

[4] Dobrovolsky et al., Estimation of the size of earthquake preparation zones, Pure and Appl. Geophys. 117 (1979) 1025.

[5] M.M. Monnin and J.L. Seidel, Physical models related to radon emission in connection with dynamic manifestations in the upper terrestrial crust: a review, Radiation Measurements 28 (1997) 703.

[6] M. Singh et al. , Radon in ground water related to seismic events, Radiation Measurements 30 (1999) 465.

[7] D. Barbaresi et al. , LNGS 20/99, LNGS Annual Report (2000) 195.

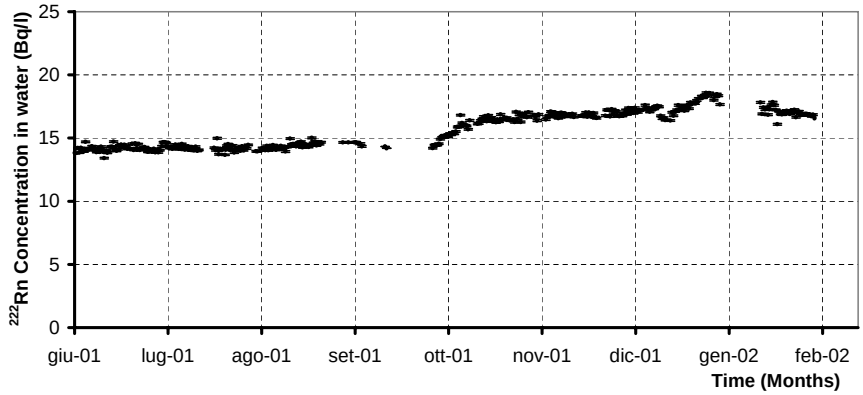

Figure 2: *Radon concentration in water during the period June 2001 - Feb 2002.*

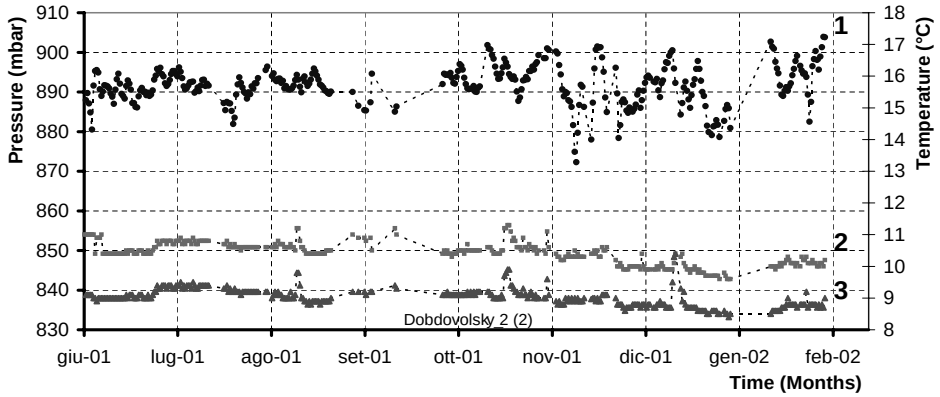

Figure 3: *Atmospheric pressure (1) and detector (2) and bubbling (3) temperatures during the period June 2001 - Feb 2002.*

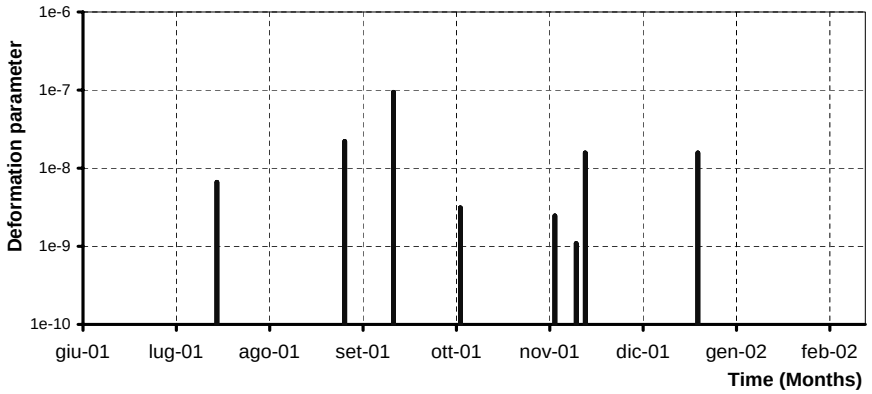

Figure 4: *Parameter of Dobrovolksy during the period June 2001 - Feb 2002.*

TELLUS. Ground deformations and their effects on the near-Earth Space

V. Sgrigna [a], L. Conti [a], V. Malvezzi[a]

[a] Dipartimento di fisica "E. Amaldi", Universitá degli Studi di Roma "Roma Tre"- Italy

Abstract

During 2001, to the tilt monitoring of local deformation processes carried out by a network of three tiltmeters installed at LNGS, has been added the study of coupling phenomena between ground emissions caused by such deformation events and perturbations and instabilities in the ionosphere-magnetosphere region. Tilt observations at LNGS as well as two scientific projects (ARINA and ESPERIA) devoted to the investigation of lithosphere-atmosphere-ionosphere-magnetosphere coupling mechanisms will be briefly reported. TELLUS (Telluric Emissions and Local Lithospheric Uppermost Strains) is the new coin for the geophysical experiment at LNGS which takes into account the above-mentioned extension in the geophysical research activities.

1 Aim of the TELLUS Experiment

The primary aim of the experiment is to carry out a continuous tilt monitoring at LNGS in order to detect aseismic creep strain episodes associated with earthquakes preparation. The observation of numerous seismic precursors and the development of theoretical models on this subject aim at seeing in perspective the phenomenon "earthquake" within the framework of a unique theory able to explain the causes of its genesis, and the dynamics, rheology, and micro-physics of its preparation, occurrence, post-seismic relaxation, and inter-seismic phases.
More in general, seismo-associated phenomena also include electromagnetic, acoustic and gas emissions from the Earth's surface which perturb the surrounding medium and can reach large distances up to the ionosphere and magnetosphere. Therefore, in our investigation of local deformation processes we also decided to include the study of possible perturbations and instabilities in the near-Earth space as a consequence of such local ground processes. In doing this, both ground monitoring, atmosphere radio-sounding and satellite observations are necessary.
At this purpose, the scientific space mission ESPERIA (Earthquake investigation by Satellite and Physics of the Environment Related to the Ionosphere and Atmosphere) based on a low-orbit micro-satellite has been proposed. On board the satellite ULF, ELF, VLF, HF electromagnetic fields, charged particle fluxes, and ionospheric plasma parameters will be detected. Simultaneous ground based measurements of mechanical and electromagnetic fields will be carried out in several test areas one of which is the Central Apennines where an instrumental network is operational. The LNGS tilt sites constitute one point of this network.

2 Experimental apparatus

The experimental apparatus consists of three bi-axial tiltmeters, of the ESPERIA satellite configuration resulting from a phase A study, and of the ARINA particle detector design.

2.1 Tiltmeters

The two-component-horizontal-pendulum tiltmeters, with Zöllner bifilar suspension and relative analog detecting and digital acquisition systems, have been described in the LNGS Annual Report 2000 [1].

2.2 The ESPERIA satellite overview

Some main elements of the ESPERIA phase A study [2] carried out during 2001 is reported in subsection 3.2. In figure 1 is shown an overview of such satellite configuration. In the same figure some instrumental allocations of the payload are also reported.

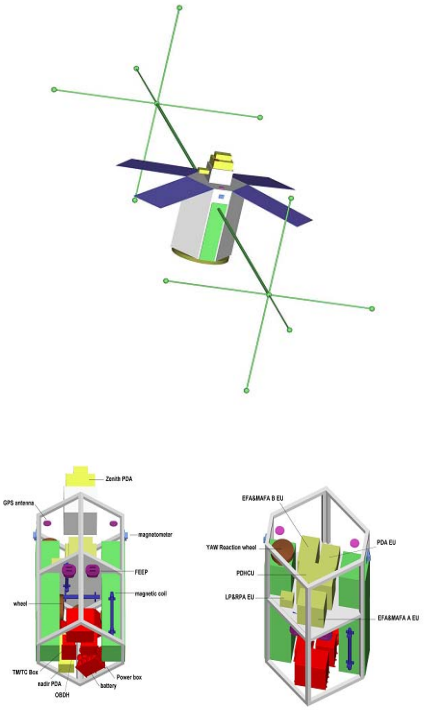

Figure 1: [top] Schematic external view of the ESPERIA satellite with deployed booms and relative systems of antennas for electric and magnetic field measurements. Particle detector (represented with a double box), and solar panels are shown at the top of the platform. Close to the particle detector the Langmuir probe & Retarding Potential Analyzer system (box on the left) is also indicated. [bottom] ESPERIA Spacecraft internal configuration including the multi-instrument payload EFA/MAFA, PDA, and LP&RPA, FEEP and other platform instruments.

In the following are schematically indicated the fundamental characteristics of the ESPERIA mission and spacecraft.

Payload Composition

- Electric Field Analyzer (EFA): frequency range: DC-10 MHz; accuracy: 300 nV/m; dynamic range: 120 dB
- Magnetic Field Analyzer (MAFA):
  FLUX-GATE: frequency range: DC-10 Hz; accuracy a few pT; resolution 24 bit
  SEARCH-COIL: frequency range: 10 Hz - 100 kHz; sensitivity $10^2 pT/(Hz)^{1/2}$ (at 1 kHz)
- Langmuir Probe and Retarding Potential Analyzer (LP&RPA)
  LP: electron temperature: 300 - 15000 K; electron density: $10^2 - 10^7 cm^{-3}$
  RPA:ionic temperature: 300 - 10000 K; ionic density: $10^2 - 10^7 cm^{-3}$

- Particle Detector Analyzer (PDA): electrons and protons with energy $E \sim 300keV - 2GeV$ (by two different detectors)

Orbit Characteristics

Ground trak repetition with an accuracy of $\leq 10km$ and $\leq 24hours$
Geo-synchronous: 14 orbits/day
Altitude: 813 km
Inclination: 11.5^0
Eccentricity: 0

Spacecraft

Platform MITA
Nadir pointing
FEEP applied

Possible Launchers: START-1, PEGASUS, SOJUZ-Fregat.

The Mission Operation and Ground Segment will be based on the ASI Scientific Data Center, the single equatorial S-Band TT&C Ground Station located at the ASI Facility in Malindi (Kenia), and the Ground Control Facility located at the Telespazio FUCINO Space Center.

2.3 The ARINA particle detector design

The ARINA particle detector has been design during 2001. It will be illustrated in subsection 3.3

3 Results obtained with regards to year 2001

3.1 Aseismic creep strain episodes revealed by tiltmeters and their numerical modeling

The primary local source of preseismic signals demonstrated to be constituted by the anelastic volumetric increase (dilatancy) caused by microfracturing processes associated with the preseismic strain accumulation during frictional locking in a fault asperity. During such preseismic dilatancy period several characteristic signals of different nature (mechanical, electromagnetic, chemical, etc.) are generated in the fault asperity (where stress concentration and dilatancy takes place) and propagate in the surrounding medium giving rise to the so-called preparation focal area. Among these typical signals (also called anomalies or earthquake precursors), intermediate-term preseismic ground tilt variations from a few weeks to several months revealed to be particularly informative within the framework of earthquake prediction studies. A number of interesting results concerning anomalous surface tilt variations observed at LNGS during earthquake preparation times

have been reported over the years.
This report deal with ground tilt investigations carried out in the seismic area of the Central Apennines of Italy where in previous studies intermediate-term tilt precursors were observed before earthquakes of moderate magnitude ([3], [4]).
LNGS tilt site constitutes (see section 1) one site of a network of four tilt stations located in the Central Apennines (fig. 2): the ancient castle of L'Aquila (AQU), the Peschiera tunnel (PES), and the Stiffe cave. Figure 2 also illustrates the discrete structures which characterise this carbonate platform area.
The general character of raw tilts shows seasonal and long-(or secular)-term systematic

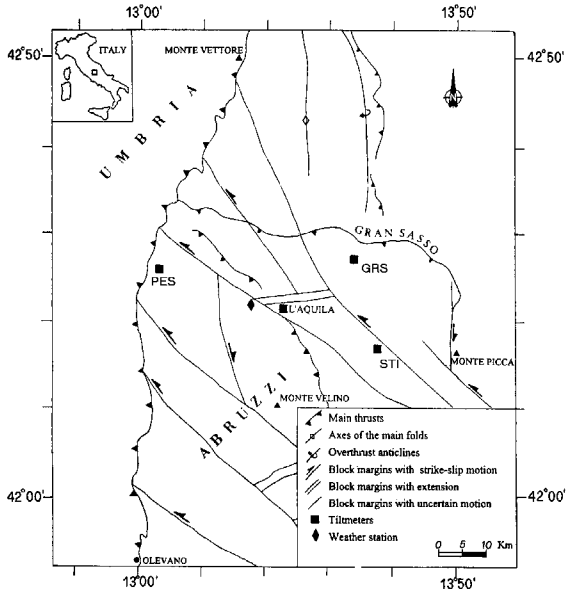

Figure 2: The Central Apennines area of Italy including the Latium-Abruzzi platform and location of tiltmeters. The crustal block structures of the platform and their motions as well as the main folds and thrust faults of the region are also shown.

tilts on which is superimposed an anomalous shorter-(or intermediate)term perturbation of a few months. The tilt signals, the monotonic linear tilt trend increasing in time is the manifestation of a well known long-term tectonic effect on the local faults. The very low-amplitude and short-term variations, which constitutes the background of tilt signals, is generally constituted by the instrumental noise with superimposed contributions of daily thermoelastic and tidal effects. The presence of tides K1 and M2 is particularly evident in the harmonic content of the hourly tilt background reported in figure 3. Finally, seasonal tilt variations demonstrated to be due to meteorological contributions. A time shift analysis for the meteorological data (atmospheric temperature, barometric pressure, and rainfall) confirms variations which seem to correlate quite well with the seasonal local tilt response. These variations are significant for atmospheric temperature and to a smaller extent for rainfall, while barometric pressure does not give relevant effects on tilt data.
In order to look for intermediate-term tilt anomalies of preseismic origin, both linear and seasonal tilt trends of tectonic and meteorological nature were removed, and the strongest

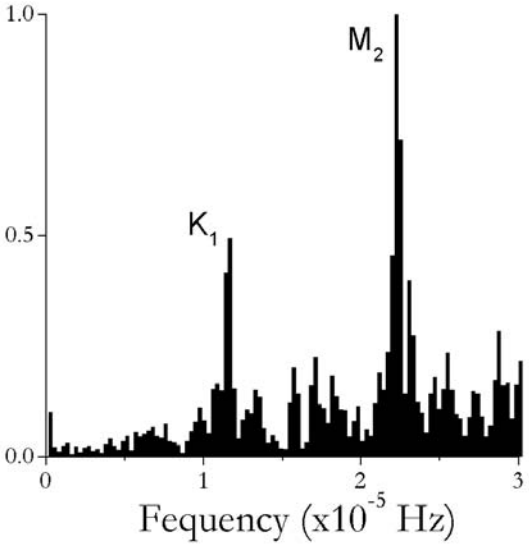

Figure 3: K1 and M2 tides appear evident in the normalised spectrum of the hourly tilt background.

earthquakes occurred during 1996-1999 in the same area under study were considered. It is very easy to remove both the linear trend and thermoelastic contributions, while the climatic effects due to rain has been eliminated by subtracting a function of rainfall from the tilt data.
The rainfall function is:

$$f_i = \sum_{k=1}^{i} r_k e^{-(t_i - t_k)/\tau}$$

for $t_i \geq t_k$.
Where r_k is the amount of rain recorded at t_k and f_i is the cumulative effect of all rain previous to t_i.
Finally, the rainfall function f_i is fit to the tilt data $\overline{\psi}$, that is, an optimal β is estimated for

$$\psi_i = \overline{\psi} + \dot{\psi} t_i + \beta[f_i - \overline{f} - \dot{f} t_i]$$

Where dots denote differentiation with respect to time and $\overline{\psi}$ and $\overline{f}$ are the average tilt and rain, respectively.
In order to look for a possible correlation between intermediate-term tilts and seismic events, the strongest earthquake were selected taking into account both magnitude, M, and tiltmeter-earthquake distance, R. According to previous results obtained in the same area ([3]) two selection criteria based on dilatancy model and dislocation theory were used.
Earthquakes selected in this way are constituted by the strongest ones belonging to the 1997 Umbria-Marche seismic sequence and by an event with $M_L = 4.4$ occurred on May 12, the peak event with $M_L = 4.4$ belonging to the seismic swarm which preceded the two

main shocks of September 26, the event with $M_L = 4.7$ of September 3, and the largest aftershocks which continued up to March 1998. All these events had epicentres in the Colfiorito area.
The selected earthquakes are reported in figure 4 (bottom) together with the residual intermediate-term tilts. These residual tilt changes (which are over the three standard deviation level of the signal background) are unaffected by any meteorological contribution over the entire period 1996-1999. The earthquake of May 12 is reported by a vertical

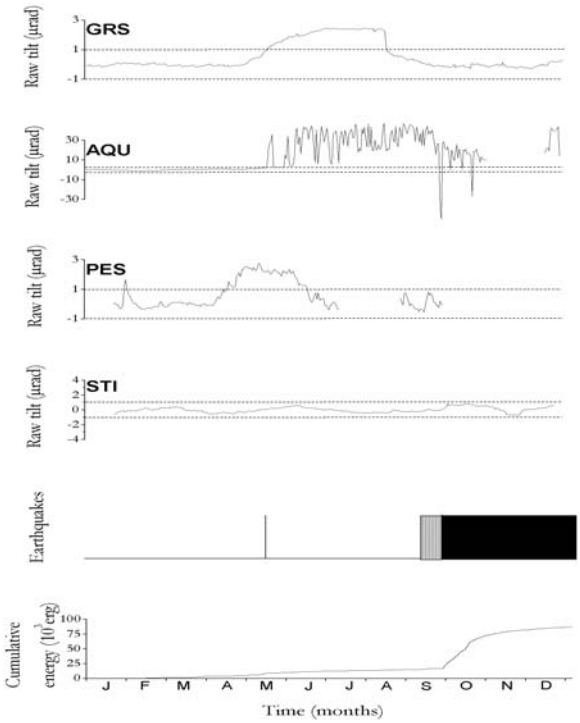

Figure 4: Residual intermediate-term tilts of 1997 obtained after meteorological and long-term tectonic effects have been subtracted from the original data. From top to bottom NS GRS, EW AQU, NS PES, and EW STI components are reported. Horizontal dashed lines indicate the 3 standard deviation level of the signal background. The last two plots at the bottom of the figure represent the selected events and the cumulative energy released by eartquakes occurred in 1997.

bar, those of the Umbria-Marche seismic sequence, including swarm and aftershocks, are indicated by black and shadow areas.
Figure 4 shows that the onset times of all such residual tilts precede the time occurrence of the selected earthquakes. Then, such anomalous intermediate-term tilts can be tentatively considered as preseismic signals. They can be associated with the deformation processes (dilatancy or dislocation) caused by local stress-strain variations which occur in the focal area during the earthquake preparation time.
Ground tilts of figure 4 also show time shifts relatively to each other. In particular, those recorded at AQU and GRS sites (that are characterise by a distance R of about 15 km

greater than that of PES) have almost the same onset times, while both of them are delayed by about 35 days with respect to that obtained at PES, indicating the existence of a slow propagating strain field from the preparation focal area with an average velocity of about 0.5 cm/s. This result is in agreement with the location of tilt sites with respect to the selected earthquakes and to the 1-D and 2-D models of tilt and strain field propagation proposed by [4], [5], [6] and mentioned in the Introduction section.
We tentatively modelled residual tilts under the hypothesis that they are the manifestation of aseismic creep episodes in faults close to the GRS, AQU, and PES tilt sites and assuming, as in previous cases [3], that rheology of the fault gouge which divides rigid crustal blocks is viscoelastic.
According to previous results obtained in the same area [3], the Kelvin-Voigt viscoelastic model has been applied.
The fit of residual ground tilts with this creep function (fig. 5) gives rigidity and dynamic viscosity values $\mu \approx 10^{11} Pa$ and $\eta \approx 10^{12} Pa \cdot s$, which are similar to those normally attributed to fault materials.

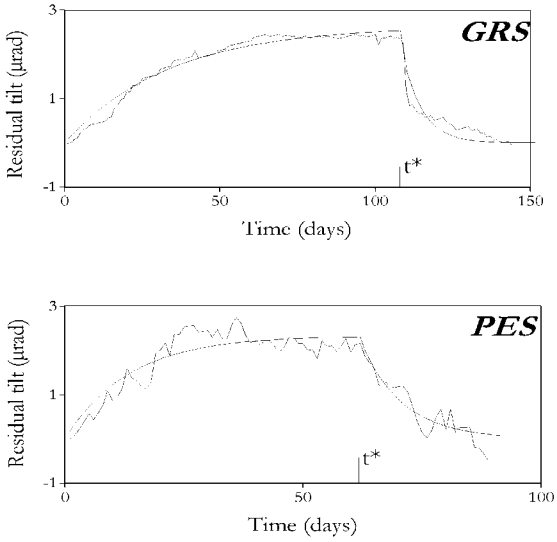

Figure 5: Data fitting of GRS and PES intermediate-term residual tilts with the creep function from the Kelvin-Voigt viscoelastic model.

Theoretical studies on tilt anomalies preceding earthquakes are rather poor. A 2-D numerical model was proposed by our team [4] to determine the tilt field during the earthquake preparation. We assume the crust to be divided into a set of trapezoidal blocks with horizontal (top and bottom) boundaries and inclined side boundaries. The geometry of the system of the blocks is shown in figure 6. The transition zones between blocks are filled by a material with Standar Linear Solid rheology.
The forces applied to each block are as follows:

1. 'tectonic' forces applied to the left and right side boundary of only the first and last block, respectively;

2. normal and tangential stresses arising within the transition zones and applied to the side boundaries;

3. friction applied to the bottom boundary;

4. gravity force applied to the centre of mass.

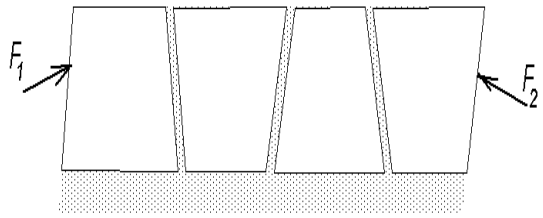

Figure 6: Geometry of four crustal blocks separated by zones with viscoelastic rheology. Arrows show directions of quasi-horizontal forces F1 and F2, applied to the side blocks

These forces move and rotate the blocks. The equations controlling their movements may be written in general form as follows:

$$m_i \ddot{U}_i = \sum_k F_{xi}^{(k)}$$

$$m_i \ddot{W}_i = \sum_k F_{zi}^{(k)}$$

$$I_i \ddot{\phi}_i = \sum_k M_{yi}^{(k)}$$

where m_i and I_i are the mass and the moment of inertia of the i-th block, ϕ_i indicates rotation, and U_i and W_i are the horizontal and vertical displacements. Summation in the right-hand sides is performed all over the horizontal and vertical forces F_{xi} and F_{zi} and over moments M_{yi} applied to the i-th block.
These equations may be solved numerically by the Runge-Kutta method.
For numerical calculations we assumed some arbitrary values for parameters, which are not associated with realistic parameters of the transition (fault) zone material, but selected in such a way that they allow to achieve a steady state of the system. All the parameters are assumed to be dimensionless.
To simulate the process of the earthquake preparation we assume that at some moment the rigidity μ drops up to a given portion of its initial value. Correspondingly the viscosity $\eta = \mu T_\varepsilon$ also drops to the same portion of its initial value. This moment may be chosen arbitrarily, because it depends on many unpredictable factors, such as the penetration of fluid into the rocks, the variation of temperature and atmospheric pressure, chemical rock

processes, etc.
The moment of the 'earthquake' is also assumed to be arbitrary, though in reality the fracture may occur when the shear stress exceeds the strength, which is proportional to the normal stress (Coulomb failure criterion). In fact, during the second stage the shear stress increases while, on the contrary, the normal stress decreases, so at some moment the failure criterion can be achieved. But instead of assuming the parameters of the Coulomb criterion, we assume the moment, at which it is achieved. At this time the deformation in the transition zone drops by a given quantity, and the parameter μ is restored to its initial value.
The behaviour of tilts in a line of seven blocks is shown in figures 7.
Anomalies of all the functions decrease with increasing distance from the fracture zone. To make clearer how the tilt anomalies in the successive blocks are shifted in time, the tilts in blocks 3-7, reduced to their initial values, are normalised to their maximum values (fig. 8).

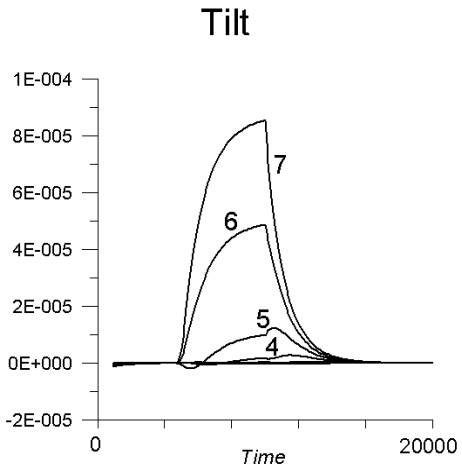

Figure 7: Tilt anomalies in a line og seven crustal blocks.

3.2 The ESPERIA project

The project ESPERIA has been selected by ASI (Italian Space Agency) for a phase A study. The final report of this study has been given to the same Agency last July 2001 and discussed during a workshop which took place in Rome last November 2001 [2] and on the occasion of other meetings [7] - [10].
The primary objective of the ESPERIA mission is to study ionospheric and magnetospheric perturbations caused by seismicity, and in particular, to develop a method to reveal short-term earthquake precursors.
The secondary objective of the project is to study the influence of electromagnetic emissions on the ionosphere caused by anthropogenic activities. These are mainly constituted by power line harmonic radiation, VLF transmitters, and HF broadcasting stations.

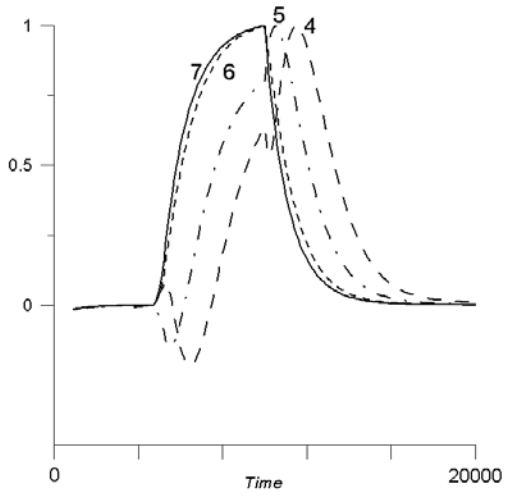

Figure 8: Normalized tilts in the blocks 4-7

Electromagnetic emissions (EME) in the ULF/ELF/VLF/HF range ($\approx DC - 10MHz$) which are related with seismic activity will be investigated. They are known since a long time, even if their generation mechanisms and interaction processes with matter or charged particles is not yet completely understood. In addition to EME, two more types of emissions which cause acoustic-gravity waves will be considered: gas exhalation and elastic (seismic) ground vibrations or acoustic emissions (AE).
A specific study based on many events is required in order to support investigations on generation mechanisms of EME waves, gas exhalation and ground vibrations, as well as on their propagation and ionospheric and magnetospheric perturbations they produce [12], [13].
As a complementary approach to ground-based investigations, satellite observations may cover most of the seismic areas and offer the possibility to increase statistics useful for the study of both preseismic effects and anthropogenic activities.
In particular, ULF EME waves emitted from the Earth's surface have shown a resonant interaction with trapped particles of the inner Van Allen radiation belt causing particle precipitation from the lower region of the magnetosphere into the upper ionosphere. The explanation of this phenomenon deals with a local disturbance of the particle fluxes inside the radiation belt caused by the ULF EME waves.
ULF EME waves may propagate upwards into the ionosphere without any significant attenuation. At certain altitude the EME can be captured by the geomagnetic field and then propagates as Alfven wave along the geomagnetic field lines. Reaching the radiation belt boundary, the Alfven wave begins to interact with trapped particles, causing particle precipitations as a result of pitch-angle diffusion. The precipitated particles drift around the Earth along the L-shell, which corresponds to the EME source location at the Earth's surface. This process creates the wave of precipitated particles, and the wave may make one or more revolutions around the Earth due to the longitudinal drift of the particles. The instrumentation on board a satellite observes these waves as particle bursts, when

satellite crosses the disturbed L-shell. It should be stressed that due to the drift around the Earth, the particle bursts may be observed not only over the source at the Earth's surface but also at any longitude, where satellite crosses the disturbed L-shell.

3.3 The ARINA project: Study of high energy charged particles bursts in the near-Earth space

Within the framework of the PAMELA mission(ASI, INFN, ROSAVIACOSMOS collaboration), which launch is scheduled for year 2003, the ARINA-PAMELA collaboration [14] consists of the:

- realization of the ARINA particle detector analyzer to detect electrons with energy from 3 MeV to 30 MeV and protons from 30 MeV to 100 MeV;
- spatialization of the ARINA instrument;
- study of high-energy particles precipitation due to the terrestrial ULF electromagnetic waves interaction with trapped particles of the inner Van Allen radiation belt;
- preliminary data from ARINA which will help in defining the better counting rate for the particle detector of the ESPERIA particle detector;
- participation of one proposer and many co-proposers of the ARINA-PAMELA experiment in the ESPERIA project.

So, the availability of preliminary data with respect to those that could be collected by ESPERIA, the complementarily between instruments and experiences, and their consequent fruitful integration, the possibility to detect long time series of data, the opportunity for the different teams to carry out common studies on similar scientific topics, will constitute some of the more relevant outputs of the collaborations between ESPERIA and PAMELA missions.
Partial funding needed to the Italian team for this experiment has been assigned by INFN (Fifth Commission) last December 11, 2001.

Method of realization of ARINA project

The ARINA particle detector will be installed on board the <<RESURS-DK1>> N1 satellite (where PAMELA spectrometer will be also placed). <<RESURS-DK1>> N1 satellite will be launched in the near-Earth orbit (altitude is about 390-600 km, inclination is about 70^0). The mission duration will be of three years.

Physical scheme of ARINA instrument

The ARINA instrument (Figs. 9, 10) consists of the set of scintillation detectors C1-C12 made on the basis of polystyrene, which are viewed by photomultipliers (PMTs), the event recording system, the data acquisition and processing system (DAPS), the power supply system (PSS), and the command unit (CU). Detectors C1-C12 are functionally combined

into three systems: the hodoscopic trigger system HTS (detectors C1-C3), the scintillation calorimeter SC (detectors C4-C9), and the anticoincidence system ACS (detectors C10-C12). Each of the detectors C1 and C2 consists of four strips directed perpendicularly and positioned just one under another. Detector C3 is situated below detectors C1 and C2 and has a mosaic structure (6 elements). Each mosaic element is viewed by its own PMT. Such detector's assembly allows to determine the angle of incident particles. The geometry and dimensions of detectors C1-C3 define the instrument aperture and the geometric factor. The scintillation calorimeter can comprise the detector C3 in addition to a set of detectors C4-C9. It provides the separation of the protons and electrons and allows to measure the particle energy by the number of detectors, passed by the particle up to its stop. That is, it is used the range of the particle in stack of detectors. The ACS consists of the detector C10 and lateral detectors C11 and C12, and it is needed to exclude from recording the particles moving in the opposite direction from the bottom to upward as well as in all directions beyond the aperture.

When the incident particle is in the aperture of instrument, the signals from detectors

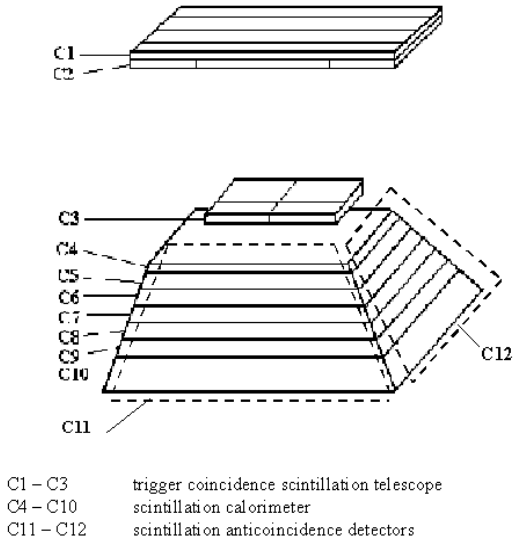

Figure 9: ARINA instrument layout.

C1, C2, and C3 coincide with each other in the HTS (i.e., when the TS signal is generated) and the HTS generates preliminary trigger signal TS entering into the controlled coincidence circuit (CCC). The CCC circuit generates the main trigger signal of the instrument MTS, if there are no signals from the anticoincidence detectors AC. Thus, the main trigger signal of the instrument is generated for the particles stopped in one of the SC detectors. The CCC resolution time is 50 ns and the duration of the formed MTS pulse is about 30 ns. During the generation of the MTS signal, the instrument is blocked automatically for the time required for recording the source data (preliminary format). Thus, the instrument records all those particles that sequentially incident its aperture with a time interval more than the time equaled to the sum of the MTS pulse duration

and the time required for data recording in the instrument electronic recording system. The fast electronics of HTS, SC systems, and ACS use the fast amplitude channel (FAC) for the particle identification. It consists of the PMT signal adapter and the dual-threshold shaper DTS. The DTS lower amplitude threshold is set to suppress the PMT noise and the upper threshold is tunable and serves for separation the electrons and protons. Amplitudes of the detector signals are separated in FAC into two ranges: the first range values are placed between the lower and upper thresholds of the shaper (this allows to detect electrons with energies of 3-30 MeV). The second range includes the values, which exceed the upper threshold (this corresponds to detection of the protons with the energies of 30-100 MeV). The main principle used for the separation of electrons and protons is based on the fact that, in the mentioned energy ranges, the protons are non-relativistic (have large energy losses in detectors) whereas the electrons are ultra relativistic (their energy deposition is much more low). This fact allows by setting an upper threshold of the shaper the identification of electrons and protons with an imitation probability of about 0.1%.

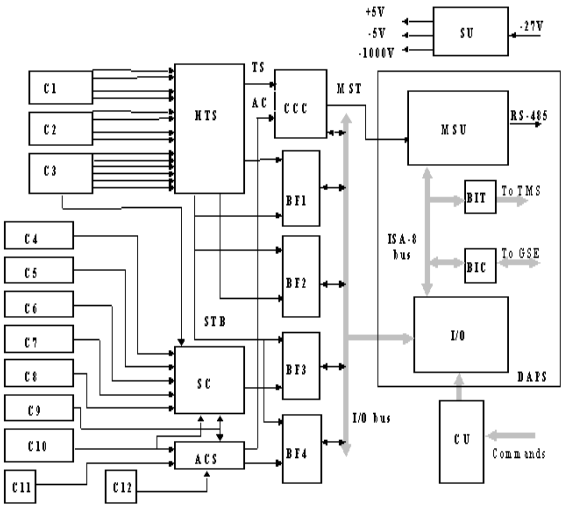

Figure 10: The block-scheme of the spectrometer-telescope ARINA for charged particle burst observation on the satellite.

Electronics of ARINA instrument

The event recording system (ERS) of the instrument operates according to the following algorithm. Generation of the preliminary trigger strobe signal STB initiates the data processing system and forms preliminary data format of the event. This format contains the following information: the elements of the triggered detectors in the HTS mosaic structure, the number of the SC detector in which the particle stopped, the particle type, counting rates of individual detectors, etc. ERS based on the fast buffer registers BF1-

BF4. The main trigger signal MST enters to the interrupt input of the microprocessor system unit MSU, which is the core of data acquisition and processing system DAPS. The input data array is read through the external bus by the input-output unit into the MSU memory. CCC is unblocked and the instrument is ready to detect new particle. The maximum event counting rate of the instrument is determined by the MSU speed and can be an order of one hundred kHz. When the spectrometer is unblocked, the MSU microprocessor returns to the background program for data processing of preliminary data up to the next interrupt. The preliminary format of the event is supplemented with a time mark, statistical data of the trigger counters, control and housekeeping data. Then, this format download into the data memory buffer for transmission to the telemetry system. The event recording system and the DAPS operate in two modes (normal and burst) depending on the frequency of the trigger signal. In the normal mode interrupts enter with an average frequency not more than 10 Hz, and the MSU executes full-scale data processing algorithm with record of maximum information for each event. For an interrupt frequency more than 10 Hz, the MSU compresses the information about events with different compression ratios depending on frequency of events. At maximum possible interrupt frequency (about 100 kHz), the compression ratio has maximum value about 100. In this case, only various histograms of the particle distributions (angular, temporal, energy) is accumulated for chosen time intervals.

General characteristics

The instrument includes a power supply system (PSS), which supports stabilized low voltages (+5 V and 5 V) for electronics and high voltage (1000 V) supplying the PMTs. The total power consumption of the instrument does not exceed 10 Watt.
The instrument physical and technical characteristics are presented in Tables 1 and 2.

1.	Geometric factor, cm^2sr	10
2.	Aperture, degrees	± 25
3.	Angular resolution, degrees	6
4.	Energy ranges, MeV: Electrons Protons	 $(3 \div 30)$ $(30 \div 100)$
5.	The probability of imitations of electrons and protons under their selection	0.1%
6.	Energy resolution	10%
7.	Trigger time resolution, ns	50

Table 1: Physical parameters of the ARINA instrument

The scientific information from the ARINA instrument is stored in the onboard memory and is transmitted to the ground-based receiving center every day. The separation of

1.	Mass, kg	6.5
2.	Dimensions, mm	$300 \times 200 \times 200$
3.	Power consumption, W	9.5
4.	Input voltage, V	24-34
5.	Number of telecommands	9
6.	Maximum counting rates, Hz	10^5
7.	Maximum dead time, μs	10
8.	Accuracy of time mark to UT, ms	10
9.	Mass memory volume, Mbytes	8
10.	Temperature range, C	5-35
11.	Total mass of materials in the field of view (g/cm^2)	1
12.	On board instalation of instrument	in hermetic vessel of satellite
13.	Orientation of instrument axis	perpendicular to the plane of orbit

Table 2: Technical parameters of the ARINA instrument

scientific data from the service information is immediately made during the data receiving, including the distinction of data concerning the satellite position and orientation.

4 List of Publications in 2001

The list of publication in 2001 is included in the following references section with numbers [2], [4], [7], [10], [11], [12], [13], [14].

References

[1] V. SGRIGNA, 2000. *Tectonic Deformation Events and Local Seismicity in the Gran Sasso Area of the Central Apennines*, Laboratori Nazionali del Gran Sasso, INFN, Annual Report 200, pp. 181-185.

[2] SGRIGNA, V., (*Principal Investigator*), 2001. *ESPERIA: Earthquake investigation by Satellite and Physics of the Environment Related to the Ionosphere and Atmosphere*, Phase A Report, Italian Space Agency (ASI), Program for Scientific Missions dedicated to Earth Sciences, Rome, July 2001, pp.194.
Participating Institutions and related Scientific Team Leaders:
University of Rome, "Roma Tre" (V. Sgrigna);
University of Rome, "Tor Vergata" and INFN Section (P. Picozza);
University of Rome, "La Sapienza" (M. Caputo);
University of Florence and INFN Section (P. Spillantini);
University and Polytechnic of Milan (V. Piuri);
University of L'Aquila (R. Scrimaglio);
National Institute of Geophysics and Volcanology (INGV) of Italy (R. Console);
IFSI and IROE of the National Council of Research (CNR) of Italy (R. Bruno and M. Bini, respectively);

National Council of the Scientific Research (CNRS) and National Space agency (CNES) of France (M. Parrot and F. Lefeuvre, respectively);
University of Athens (K. Eftaxias);
Russian Aviation and Space Agency (L. Makridenko);
Moscow Engineering Physics Institute (MEPhI) and Institute of Cosmic Physics (A. Galper);
Institute of Physics of the Earth of the Russian Academy of Sciences (RAS), (I. Shirokov);
National Institute of geophysics of the Georgian Academy of Sciences (GAS), (D. Zilpimiani);
University of St. Petersburg (T.B. Yanovskaya);
LABEN S.p.A., Italy (E. Cavazzuti);
CGS Space S.p.A., Italy (A. Della Torre);
TELESPAZIO S.p.A. Italy (A. Coletta).

[3] Bella, F., P.F., Biagi, M., Caputo, G., Della Monica, A., Ermini, P.V., Manjgaladze, V., Sgrigna and Zilpimiani, D.O., 1995. *Possible Creep-related Tilt Precursors Obtained in the Central Apennines (Italy) and in the Southern Caucasus (Geirgia)*, Pure abd Appl. Geophys., **144**, 277–299.

[4] SGRIGNA, V., and V. MALVEZZI, 2002. *Preseismic creep strains revealed by ground tilt measurements in central Italy on the occasion of the 1997 Umbria-Marche Apennines earthquake sequence*, Pure and Appl. Geophys.(PAGEOPH), in press.

[5] Bella, F., P.F. Biagi, M., Caputo, G., Della Monica, A., Ermini and Sgrigna, V., 1990. *Very slow-moving Crustal Strain Disturbances*, Tectonophysics, **179**, 131-139.

[6] Bella, F., M., Caputo, G., Della Monica, A., Lisi, W., Plastino, R., Scandone and Sgrigna, V., 1998. *Crustal Blocks and Seismicity in the Central Apennines of Italy*, Nuovo Cimento, **21C**, 597-607.

[7] SGRIGNA, V., 2001. *The ESPERIA Project*, EOS Trans., AGU, vol. **82**, S52A-15, n. 20, S272.

[8] SGRIGNA, V., 2000. *Il progetto ESPERIA*. Workshop Nazionale su "Utilizzo Scientifico e Tecnologico della ISS" , ASI, Unitá programmi Scientifici, Osservatorio di Capodimonte, Napoli, 17-19 aprile.

[9] SGRIGNA, V., 2000. *The Project ESPERIA*. International Workshop on Seismo Electromagnetics, IWSE2000, Sept. 19-22, Chofu, Tokyo.

[10] SGRIGNA, V., 2001. *ESPERIA*. NASA/ASI Workshop on "Observing Earth from Space", Venice, June 12-14.

[11] SGRIGNA, V., D'AMBROSIO, C., YANOVSKAYA, T.B., 2001. *Numerical modeling of slow movements of crustal blocks caused by quasi-horizontal tectonic forces*, Phys Earth. Planet. Int., in press.

[12] SGRIGNA, V., CONTI, L., CORSI, M., GALPER, A., MALVEZZI, V., PICOZZA, P., SCRIMAGLIO, R., STAGNI, L., ZILPIMIANI, D., 2001. *Ionospheric perturbations possibly caused by preseismic electromagnetic emissions*, EOS Trans., AGU, vol. **82**, S52A-14, n.20, S272.

[13] SGRIGNA, V., 2001. *Emissioni Elettromagnetiche presismiche e loro Possibile Interazione con le Fasce di Van Allen*, Relazione su invito all'LXXXVII Congresso Nazionale della Societá Italiana di Fisica (SIF), Milano-Bicocca, 24-29 Settembre 2001.

[14] The ARINA project. Collaboration from the Italian side:
INFN - Roma 2, Piergiorgio Picozza (Principal Investigator);
INFN - L'Aquila, R. Scrimaglio;
INGV - Roma Tre, V. Sgrigna
Collaboration from the Russian side:
MEPhI;
ROSAVIACOSMOS